

LECTURE NOTES OF STELLAR ASTROPHYSICS
Prof. Antonino Milone

Patrizia Bussatori, Fabrizio Muratore

March 2021

Premise

This book contains the notes taken from the lessons of the Stellar astrophysics course held by prof. Antonino Milone for the master degrees in Cosmology and Astrophysics, in the academic year 2020/2021. As these are not official professor approved notes, we do not guarantee the correctness of the contents. Indeed, any error reporting is welcome! Enjoy the reading!

Patrizia Bussatori & Fabrizio Muratore

Contents

1 Stellar population	2
1.1 Globular and Open Clusters	3
1.2 Color-Magnitude Diagram	4
1.2.1 Relation between theory and observations	7
1.3 What is a star?	8
1.4 Color indices	10
1.4.1 Passage from the theoretical to the observational plane	11
1.5 Extinction	11
1.5.1 Extinction law	13
1.6 The formation of the galaxy: constraints from the CMD	14
1.6.1 The lambda cold dark matter model	14
1.6.2 The missing-satellite problem	15
1.7 Metallicity and the isochrones	15
1.7.1 Metallicity indicators	15
1.8 Examples of CMD	16
1.9 Age-Metallicity relation	16
1.10 Other techniques to obtain the age of GCs	17
1.10.1 The vertical method	17
1.10.2 The horizontal method	18
1.11 Resolution of the missing-satellite problem	18
1.12 The ultra-faint dwarf	20
1.13 Binaries method	22
1.13.1 Binaries in SSP	22
1.13.2 Equal-mass binaries	22
1.13.3 Fraction of binaries	24
1.14 Imaging with Hubble	24
1.14.1 The Wide Field Planetary Camera 2 (1993-2009)	24
1.14.2 The Advanced Camera for Surveys (ACS)	25
1.14.3 Wide Field Channel (WFC) of ACS	25
1.14.4 Charge Transfer Efficiency loss	25
1.14.5 Point-Spread Function Photometry	26
2 White Dwarf	27
2.0.1 White Dwarf structure	27
2.1 The age-luminosity relations	27
2.1.1 The strange case of NGC6791	33
3 Stellar spectroscopy	35
3.1 Stellar absorption: line formation	35
3.2 Information from the spectra	36
3.3 Abundance scales	37
3.4 Line broadening	38

3.4.1	Hydrogen lines	41
3.4.2	Helium lines	41
3.4.3	Metal lines	41
3.5	Ages from the MS knee	41
3.6	Stellar parameters	44
3.6.1	Abundances	44
3.6.2	How to measure the abundances?	45
3.6.3	Determining of the effective temperature	46
3.6.4	Determining of the surface gravity	48
3.7	Spectral synthesis	49
3.7.1	The Uncertainties in parameters	49
3.7.2	Relative abundances	50
3.8	Relative abundances: An application on exoplanets	50
3.9	Stellar parameters: the photometry approach	54
3.9.1	Opacity	55
3.9.2	Balmer jump	55
3.9.3	Stroemgren photometry	56
3.9.4	Infrared flux method (IFRM)	57
3.10	The Lithium cosmological problem	57
3.10.1	The value from the model	58
3.10.2	The value observed	58
4	Differential reddening	61
4.1	Extinction	61
4.2	Schlegel reddening maps	63
4.3	The RGB bump	63
4.4	The red clump	64
4.5	The Red Clump in the Galactic Bulge CMD	67
5	Binaries, Blue Stragglers, and other exotic objects in the CMD	71
5.1	Luminosity profiles of star clusters	71
5.1.1	King profile	71
5.1.2	Core collapse	73
5.1.3	Intermediate-mass black holes	73
5.2	Binaries in star clusters	73
5.3	Blue Stragglers	78
5.3.1	Testing the theories	79
5.3.2	Blue Stragglers & dynamical evolution	82
5.4	Types of binaries	83
5.4.1	WD-MS binary system	83
5.4.2	Cataclysmic variables	83
5.4.3	X-ray variables	86
5.4.4	How to detect low mass X-ray binaries?	87
5.5	The initial Mass function	87
6	Hunting Black Holes	90
6.1	Some important reminders	90
6.2	Techniques to find Black Holes	90
7	The first stars	95
7.1	The cosmology approach	95
7.1.1	Summary	97
7.2	The astrophysics approach	98
7.2.1	The Milky Way	98

7.2.2	Hunting the first stars	99
8	Photometry of multiple populations	103
8.1	The chromosome map	103
8.2	How did multiple populations form?	106
8.2.1	SCENARIO I: Multiple Generations	106
8.2.2	SCENARIO II: Single Generation	107
8.3	Ten properties of multi stellar populations	107
8.3.1	1G-2G discreteness	107
8.3.2	Ubiquity	108
8.3.3	Variety	108
8.3.4	Two classes of Type I and Type II	109
8.3.5	Dependence on cluster mass	109
8.3.6	Maximum Helium enhancement	109
8.3.7	Dependence on GC orbit and on the host galaxy	109
8.3.8	No dependence on stellar mass	111
8.3.9	More centrally-concentrated 2G	113
8.3.10	2G stars exhibit anisotropic motions	113
8.4	Globular cluster and the missing satellite problem	113
8.4.1	The case of M54	114
8.5	Analysis of some Chromosome Map	117
8.5.1	Horizontal Branch	117
8.6	Formation scenarios of multiple stellar populations	119
8.6.1	Scenarios with multiple generations	119
8.6.2	Scenarios with a single generation	119
8.6.3	Supermassive Stars	120
9	The extended Main Sequence Turn off phenomenon	122
9.0.1	Comparison between some properties of Galactic and extra Galactic GCs	126
9.0.2	The comparison with respect to Open clusters	126
10	Galaxy: The bulge	130
10.1	How did Bulge form at high z ?	130
10.1.1	Observations of bulges at high-redshift	130
10.1.2	Bulge formation scenarios	132
10.1.3	The age of the Bulge	135
10.1.4	Other approaches	138
10.2	The structure of the Bulge	141
10.2.1	Kinematics	147
10.2.2	Optical vs. infrared observations	149
10.2.3	The X-shape component of the Galactic Bulge	150
10.2.4	The rotation of the Bulge	150
10.2.5	Study of Galactic bulge structure using RR-Lyrae	151
10.2.6	Chemical abundances in the Galactic Bulge	151
11	Galactic archaeology with the Milky Way Disk	154
11.1	The formation of the disc	155
11.2	Asteroseismology	155
11.3	New modern studies: APOGEE and GAIA data	157
11.4	GAIA and Enceladus	159
12	The second Parameter problem of the HB morphology	163
12.1	Multiple populations and the 2nd parameter of the HB morphology	166
12.2	The mass loss contribution	168

12.2.1 M4 Case	168
13 Dwarf Galaxies	173
13.1 What is a dwarf galaxy?	173
13.1.1 Dwarf Spheroidals (dSphs)	173
13.1.2 Dwarf Irregulars (dIrrs)	173
13.2 Morphological transformations	173
13.2.1 Ram pressure	174
13.2.2 Photo-evaporation	174
13.2.3 Stellar evolution	174
13.2.4 Harrassment	175
13.2.5 Star formation history	175
13.3 Ultra-compact dwarf	179
14 Dark matter and stellar streams	180
14.1 The Hunting	180
14.2 Candidates	182
14.3 Modified Newtonian Dynamics (MOND)	185
15 Summery of Marco Tailo conference	186
15.1 The position of a star on the HB	186
15.2 Breaking the degeneracy	187
15.3 Searching for correlations	189
15.3.1 Most important correlation of the 1G	190
15.3.2 Most important correlation of the 2Ge	190
15.4 Conclusions	191
16 Exam simulations	192
16.0.1 Simulation 1	192
16.0.2 Simulation 2	193
16.0.3 Simulation 3	193
16.0.4 Simulation 4	194

Introduction

Globular Cluster (GC) are a spherical collection of stars. They are formed around 400 Million yrs after the big bang. These clusters are ones of the oldest objects in the universe, so we study the clusters that we see today to get information on the primordial Universe. Astronomers use the space telescope, as HST, to investigate the properties of all stars in the GC. With the photometry they build the Colour-Magnitude diagram (CMD) a fundamental tool to study many astrophysical issues. In this course we'll study the CMD and how to read this diagram, then we'll study some elements of stellar spectroscopy, after that, we'll talk about the Milky Way. The last issues that we'll investigate are the unresolved stellar populations and the haunting of the first stars of the Universe.

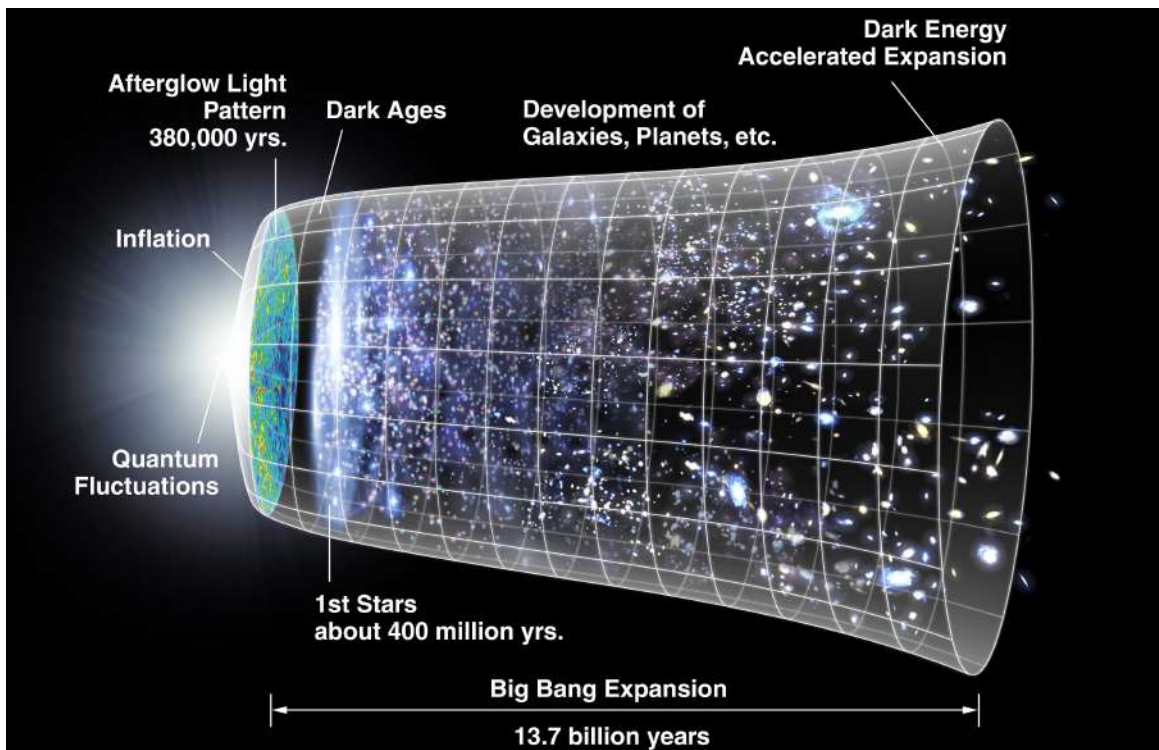


Figure 1: A cartoon that represents the history of the universe.

Chapter 1

Stellar population

A **resolved stellar population** is a stellar population whose we can measure the luminosity of single stars, using photometry¹⁾ and investigate detailed chemical abundances of single stars through spectroscopy or analyse the motion of stars along the line of sight thanks to radial velocity. On the contrary, in **unresolved stellar population** we cannot distinguish each stars from the others, so we could get the integrated luminosity or integrated spectra. Those type of structures are unresolved due to the high distance from us in terms of space and time. It is useful to get the maximum amount of information from resolved objects that are easy to observe and for which it is possible to obtain the maximum spectral resolution or the highest photometric precision. This provides fundamental information or parameters but only for few objects. On the other side, observing deep in the universe, also at high redshift, a huge variety of structures is observable.

Remainder

Here there are few important remainders useful for the course.

- Luminosity, L , (intrinsic property) is the total amount of electromagnetic energy emitted by a star per unit time (unit $J/s, W$).
- Observed flux (or apparent brightness), F , is the power per unit area that we receive from a star (unit W/m^2). It depend on distance, d , and diminishes as the inverse square of the distance. The relation between flux and luminosity is: $F = \frac{L}{4\pi d^2}$
- Apparent magnitude, logarithmic measurement of the apparent brightness. The fundamental law for magnitudes is: $m_1 - m_2 = -2.5 \log \frac{I_1}{I_2}$ **Caution:** Apparent magnitude is NOT Luminosity! A star can exhibit faint (high) apparent magnitude because it is far from us, or because its luminosity is low.

A **simple stellar population** (SSP) is an assembly of coeval, initially chemically homogeneous single stars. A SSP is described by four main parameters:

1. Age
2. Chemical abundance of helium (Y)
3. Chemical abundance of metals (Z)
4. Initial mass function

They formed in a single star formation burst, so stars have the same chemically composition and same age. This is very useful because once a SSP is identified, analysing those stars it is possible to obtain parameters and properties about stellar evolution and formation mechanism because, by definition,

¹⁾The photometry measure the entire amount of light in a given filter

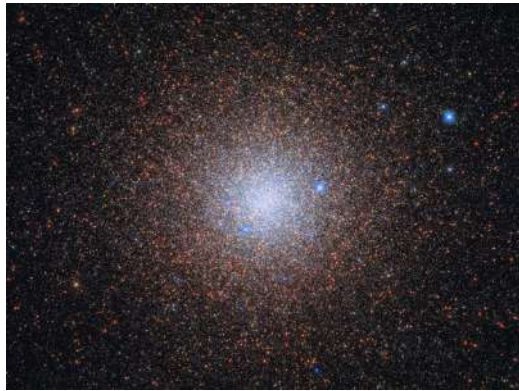


Figure 1.1: In figure we can see M4, one of the most brightness GC e the closest



Figure 1.2: Westerlund 2 is an open young cluster in the Milky Way

they are formed by same material with same mechanism. In general, SSP are ideal; they are prototypes but not real. However some structures in the universe can be approximated to SSP.

When one or more of these properties are not fulfilled, the stellar population under scrutiny is a complex stellar population and is composed by various SSPs. In this case we talk about **Multiple stellar population**. In this case stars are not born with same composition or they are not of same age.

1.1 Globular and Open Clusters

Inside the Milk Way, there are some specific regions that, in first approximation, can be considered SSP: the globular clusters. Globular clusters are populated by up to millions of old stars. Their stars are very tightly bound by gravity, which gives them their spherical shapes and relatively high stellar densities toward their centers.

Instead, an open cluster is a group of up to a few thousand stars (weakly) gravitationally bound that were formed by the same molecular cloud. They are smaller and less massive than the globular one. Open clusters are often populated by young stars. Since they are weakly gravitationally bounded, they can dissolve after few hundreds Myr. Some open cluster are single while other are double as the one in Perseus.

According to some theories, all stars (or at least the most) formed inside a cluster, including our Sun. Nowadays, using some new modern techniques, is it also possible to discover exoplanets around stars analysing chemical composition of stars.

Historically, globular were considered the best examples of old SSPs in nature (Renzini & Buzzoni 1986). The oldest GCs have the same age of the universe, while the youngest an age around 12-11 Gyrs. Instead historically, open clusters were considered the best examples of young SSPs in nature

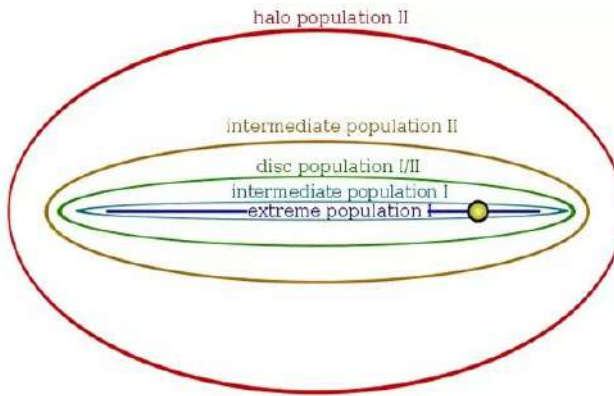


Figure 1.3: Different population in the Galaxy

(Renzini & Buzzoni 1986).

In literature there is a confusion on the difference between the definition of open and globular cluster, in same case it is difficult to say what type of cluster we are observing. The main difference is the ages: indeed in open cluster we find a young population, instead in globular cluster we find a old population.

Historically, Milky Way stars are classified as Population I and II (figure 1.3). Population I is composed of metal rich stars, relatively young and located in the disk , instead the Population-II stars are metal poor and old, located in the most external part of the galaxy.

Characteristics of stars cluster:

- Stars have different colors: some are blue and some are reddish.
- Stars have different luminosity.
- Stars share the same distance. This is a very useful approximation from physical point of view. Assuming that, it is interesting to analyse how the luminosity is correlated to the temperature of stars. This is a good and simple way from experimental point of view to create a Color-Magnitude Diagram.

1.2 Color-Magnitude Diagram

With the characteristics that we saw before (sorting stars in terms of color and then in terms of magnitude) we can build the Color-Magnitude Diagram (CMD) of clusters. This is a plot of the star's magnitude (which is indicative of the stellar luminosity) as a function of the color (which is a proxy of the temperature). The CMD is an observer's diagram! An example is shown in figure 1.4. In this type of diagram stars populate some specific regions inside the graphic and the shape tells important information about clusters (that we assumed as prototype of SSP). We are able to do this because all stars have same distance.

A problem on the derivation of the CMD is the presence of contamination by other stars in the field. In this figure 1.5 we see on the left the CMD of the center of the cluster, on the right the CMD of the edge regions of the cluster where there are mainly field stars. In the past astronomers use a statistically subtraction to delete the field stars from the CMD, observing once the cluster and once the region nearby the cluster.

Nowadays a more accurate way to resolve the problem of contamination is studying the proper motion of the star in the field. Indeed the stars of the cluster are moving all in same way. To be more specific all stars in the cluster have a component of the motion relative to the star cluster but then the entire cluster is moving around the gravity center of the galaxy so the motion of stars belonging to the cluster is clearly distinct from the motion of field stars. To do those measurements often modern satellites

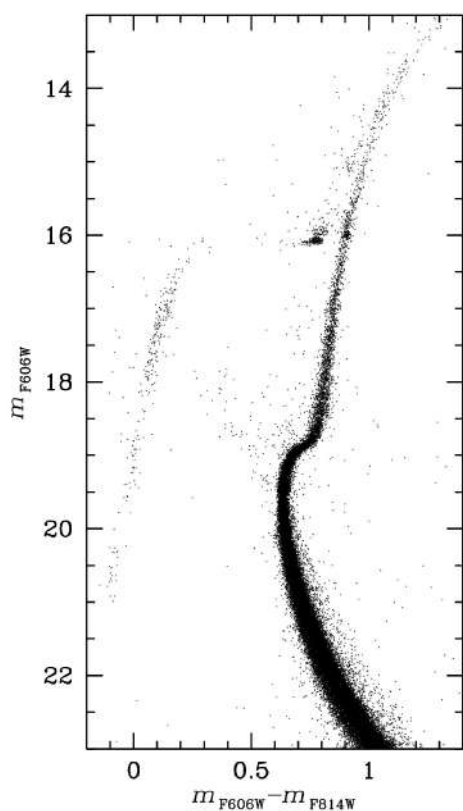


Figure 1.4: CMD of NGC2808, a cluster 12Gyrs old.

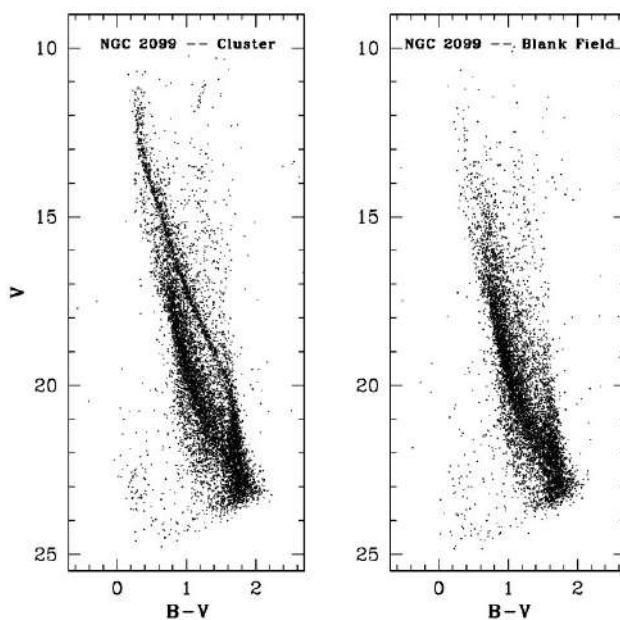


Figure 1.5: NGC2099 is a young cluster with an age around 500Myrs.

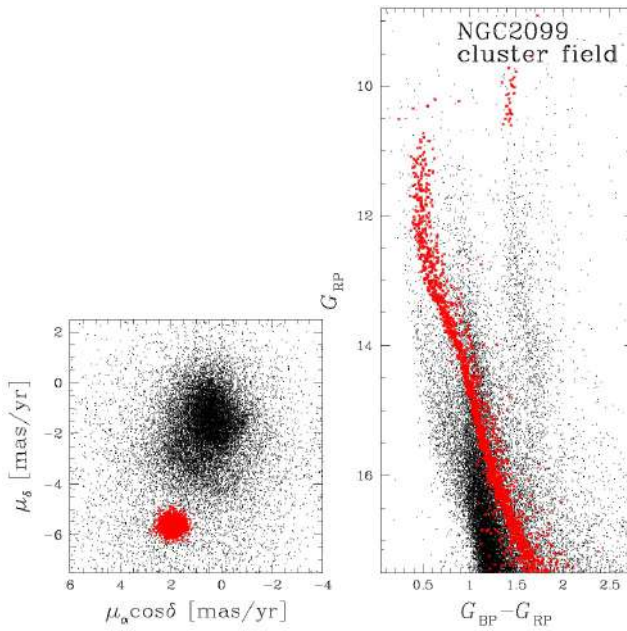


Figure 1.6: On the left we can see the diagram of the proper motion. On the right the CMD. In red era shown the cluster's stars. (Cordoni et al. 2018)

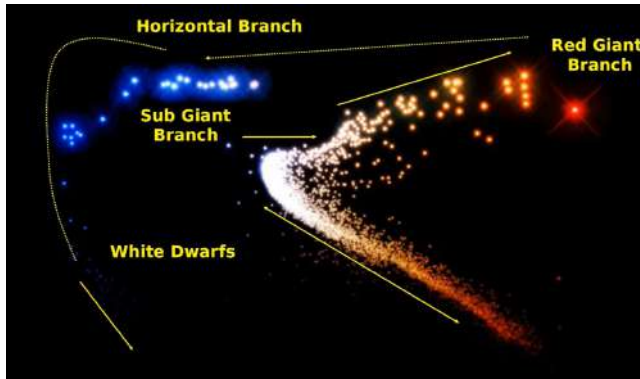


Figure 1.7: A General CMD

as Gaia are used. We can derive a diagram as that on left in figure 1.6. Using this tool we can know what star are in the cluster and what star not.

An example of CMD can be seen in figure 1.7 where are shown the main regions. The position of each star inside the diagram provides information about properties and physical configuration or evolution.

A brief overview of the stellar evolution:

- *Main sequence*: is the region where we found the most of the observed stars. In this phase stars are burning hydrogen (H) into helium (He). It is the same evolutionary phase of the Sun.
- *Turn-off point*: Stars here have exhausted the H in the central part, the core. This point is very important to investigate, indeed its position is a proxy of the age of the cluster. It is a sort of clock to analyse the age of stars and corresponds to the point where stars leave the main sequence and go to the giant branches.
- *Sub-giant Branch*: Stars are burning H in a shell around a inert He core.
- *Red-giant Branch*: the He core has reached the degeneracy.
- *Horizontal Branch*: He is burning in the core.
- *Asymptotic Giant Branch*: Stars have two burning shells: one for H and one for He .

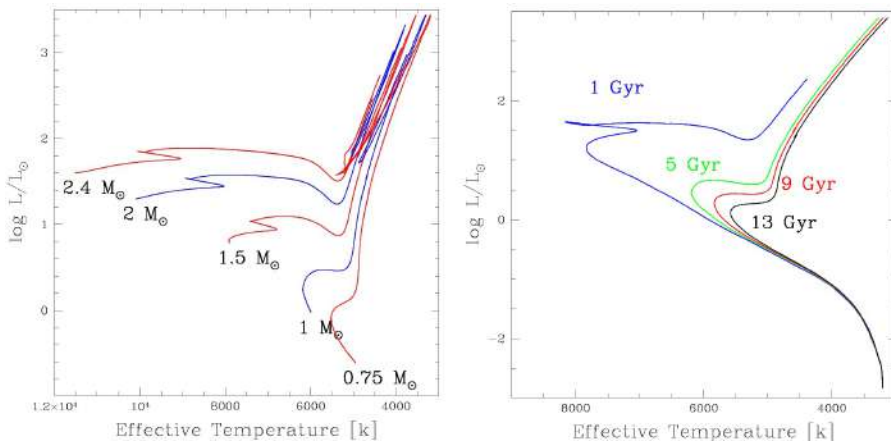


Figure 1.8: On the left the evolutionary track, on the right the isochrones

- White Dwarf: Final stage of evolution, they are composed in general of CO core. These stars are just cooling down.

In the CMD we can plot two different curve:

- **Stellar evolutionary track:** The stellar evolutionary track is the curve on the CMD representing how the color and the luminosity of a star changes over time (panel left figure 1.8). Each point corresponds to a star at different age and each line corresponds to stars of the same mass.
- **Isochrones:** The stellar isochrone is the curve on the CMD representing stars with the same age (panel right figure 1.8). By this definition, it is not necessary to take into account the mass function - that describes the number of stars in a given mass range - and, of course, if the age changes, also the isochrone changes

Focus on the isochrones and the turn-off: The brightness of the turn off depends from age. The turn off is considered as a chronometer provided by stellar evolution. In particular this point becomes redder and fainter over the years.

The diagrams in figure 1.8 are theoretical diagram, indeed we see luminosity (we are enable to get the luminosity because we cannot collect the photons at all wavelength, from all spectrum) as function of the effective temperature. From the observational point of view this diagram is translated into magnitudes versus color. From instruments we provide magnitude and colors, not luminosity and effective temperature. We need to transfer information from the theoretical to the observational plane. Then, it is important that the model fits the observations because model tell us more information and more intrinsic details.

1.2.1 Relation between theory and observations

Spectroscopy and photometry have to be related to the properties predicted by stellar models. The formula that related the magnitude to the luminosity is the following:

$$M_{bol} = M_{bol,\odot} - 2.5 \log \frac{L}{L_\odot} \quad (1.1)$$

where M_{bol} is the bolometric magnitude that measures the total radiation of a star emitted across all wavelengths of the electromagnetic spectrum. The $M_{bol,\odot} = 4.74[mag]$. We cannot observe M_{bol} , in fact we observe the magnitude in a given filter or passband. The relation between the magnitude in a given filter and the bolometric one is the following:

$$M_A = M_{bol} - BC_A \quad (1.2)$$

where M_A is the absolute magnitude² in a band A; BC_A is the bolometric correction in the A band (it is a color index) that permits to pass from M_A to M_{bol} and vice versa. So, to transfer information from the theoretical to the observational plane we need M_A and BC_A . The observed magnitude of a star, called apparent magnitude (m_A), is related to the absolute magnitude as:

$$m_A = M_A + 5 \log d - 5 + A_A \quad (1.3)$$

where d is the distance in parsec of an astronomical object, A_A is the interstellar extinction, a coefficient that describes the absorption in the interstellar medium.

In astronomy, for completeness, is used to refers to distance using the distance modulus:

$$m_A - M_A = +5 \log d - 5 + A_A \quad (1.4)$$

$$(m - M)_0 = m_A - M_A - A_A \quad (1.5)$$

$$(m - M)_A = m_A - M_A \quad (1.6)$$

where $(m - M)_0$ is the distance modulus (the intrinsic one) and $(m - M)_A$ is the apparent distance modulus. So, at 10 parsec the distance modulus is equal to zero and the apparent magnitude is equal to the absolute one. In high-redshift objects we must account for the fact that:

1. the redshifted spectrum is stretched through the bandwidth of the filter;
2. The light that we observe through the filter comes from a bluer part of the spectral energy distribution because of the redshift.

So, in the formula of distance modulus we need a new coefficient K_X , called K-correction to the filter X, that takes to account to the redshift of the light so it depends on the redshift Z but also on L , the flux coming from the source, and on T_X , the filter response. In this case the relation between magnitudes and distance is:

$$m_X = M_X + 5 \log d - 5 + A_X + K_X \quad (1.7)$$

1.3 What is a star?

The vast majority of stars appear as point-like sources. By using interferometry astronomers have resolved a few nearby stars however the vast majority of stars observable in the sky are not resolved because the are too distant and their diameter is too small to resolve those objects. The ideal target to investigate stellar structures is the Sun. It is very close and we can study it very well. A schematic structure of the Sun is visible in figure 1.9.

The light that we receive from a star has been released by the photosphere, where the optical depth, τ (the probability that a photon has an interaction with the stellar matter), is about 1. To be more specific, light emitted by stars has a black body spectrum, whose energy distribution depends only on the effective temperature. In particular blackbodies radiation is described by the **Planck law**:

$$B_\lambda(T) = \frac{2hc^2}{\lambda^5} \frac{1}{e^{hc/\lambda kT} - 1} \quad (1.8)$$

where B is the spectral radiance (units: power per unit solid angle and per unit area normal to the propagation), h is the Planck constant and k is the Boltzmann constant.

The total flux emitted in all the directions at all the wavelengths is obtained integrating the Planck law over the solid angle and the λ . The result is the following:

²The absolute magnitude is the apparent magnitude of an object located at 10 parsec from the observer

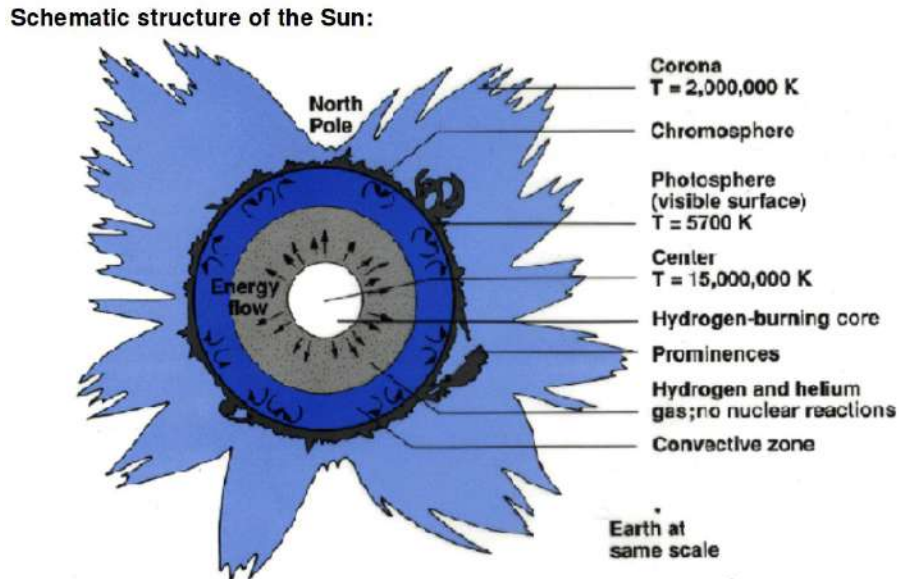


Figure 1.9: Schematic structure of Sun. The photosphere is the visible surface. Most of the structures in the spectra of the star are produced in the photosphere so the most information we obtain come from it.

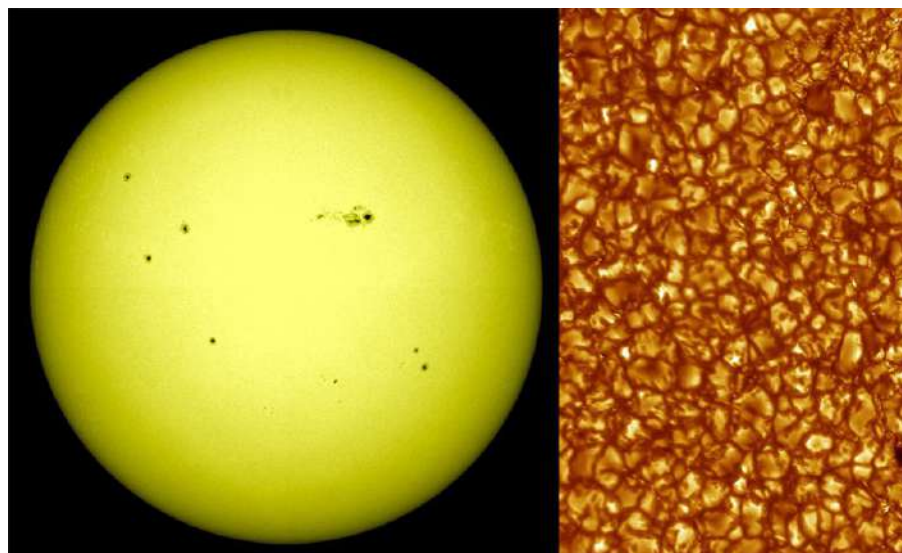


Figure 1.10: An image of the surface of Sun. On the right we can see a pattern that is similar to bubbles, in fact we see this pattern due the convection.

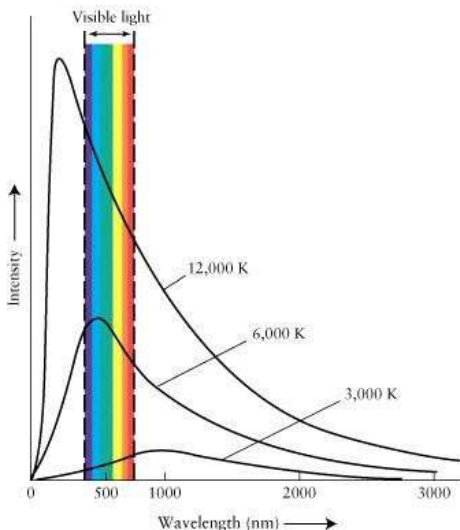


Figure 1.11: Some planckians at different temperatures

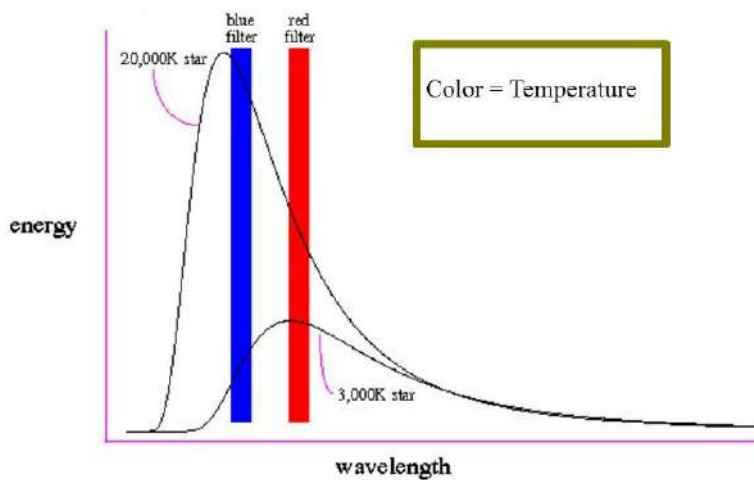


Figure 1.12: Filters intercepts the BB distributions in different point so we obtain a different measure of the slope for different distributions.

$$F = \sigma T^4 \quad (1.9)$$

where σ is the Stefan-Boltzmann constant. The energy distribution depends only on the effective temperature: for example a red star has the emission peak in the red part of the diagram, a blue star in the blue part, a yellow star in the center.

1.4 Color indices

A generic colour index (A-B) is defined as the difference of the magnitudes in two photometric filters.

$$C_{A,B} = m_A - m_B \quad (1.10)$$

Color indices provide a measure of the slope of the black body curve, therefore of the temperature.

A generic colour is independent of the stellar distance, but is affected by extinction.

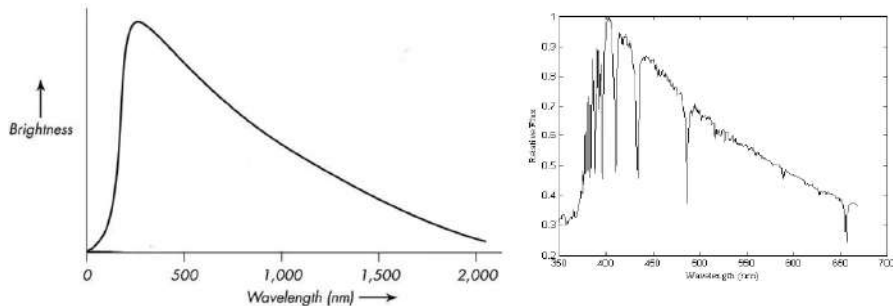


Figure 1.13: On the left the BB emission, on the right the spectrum of a star.

$$\begin{aligned}
 (A - B)_0 &= M_A - M_B = \\
 m_a - 5 \log d + 5 - A_A - m_B + 5 \log d - 5 + A_B &= \\
 m_A - m_B - (A_A - A_B) &= \\
 (A - B) - E(A - B) & \quad (1.11)
 \end{aligned}$$

where $(A - B)_0$ is the color index intrinsic, $(A - B)$ is the color index observed and $E(A - B)$ is the color excess that is defined as:

$$E(A - B) = (A_A - A_B) \text{ or } E(A - B) = (A - B) - (A - B)_0 \quad (1.12)$$

this quantity measure the excess of color that we observe due the reddening.

If stars are black bodies, two magnitudes would be enough to constrain both stellar temperature and luminosity, but stars show a deviation from the BB distribution (see figure 1.13).

Stars are blackbodies in first approximation

1.4.1 Passage from the theoretical to the observational plane

After being released by the photosphere, the photons cross the overlying stellar atmosphere, where $\tau < 1$. It is the crossing of the atmosphere that introduces a dependence of the spectral energy distribution on gravity and chemical composition, in addition to the temperature. This is an apparent limitation but constitutes an opportunity to study the gravity or the chemical composition of the star.

Theoretical models of stellar atmosphere and predictions of the spectral energy distribution of the emerging photons are mandatory to compute bolometric corrections to any given photometric band.

We have said that to pass from theoretical plane to the observational one we need to know the bolometric correction. So, if we derive it from the theory of the stellar atmosphere we can do the conversion. In figure 1.14 we can see the passage from (L, T) to (M, C) plane. Moreover it is necessary to take into account that L and T have not the same relation as M and C . Indeed cold stars have redder color than hot stars, also depending on the filter used for observations.

Comparing the isochrones to the astronomical data we derive information of the population.

1.5 Extinction

Interstellar space is permeated by interstellar medium (ISM), that is composed of gas and dust. Dust tends to scatter radiation, instead the gas tends to absorbs the radiation and radiates at different directions.

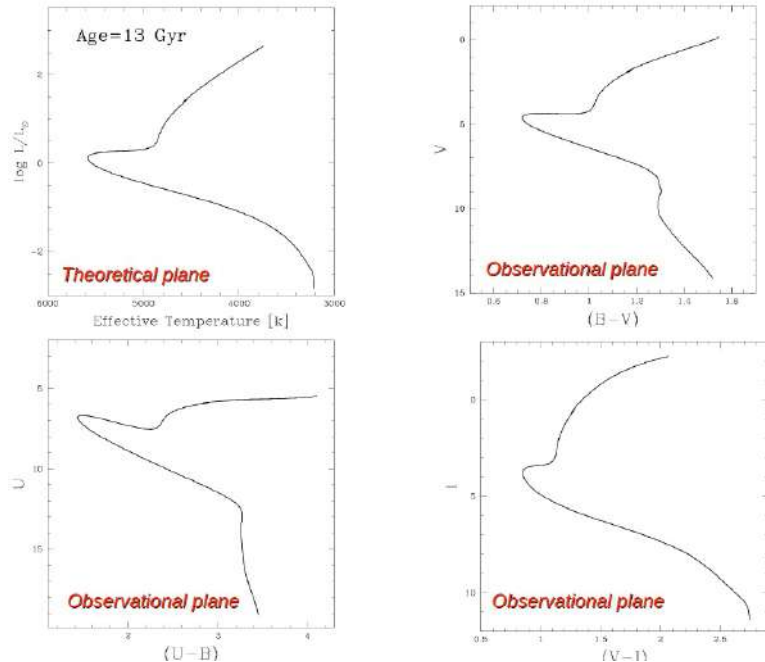


Figure 1.14: In the first panel we have the theoretical plane (L, T), then knowing the bolometric correction we can pass to the observational plane (M, C) and fit the data. In the other panels we see the observational plane in different filters.

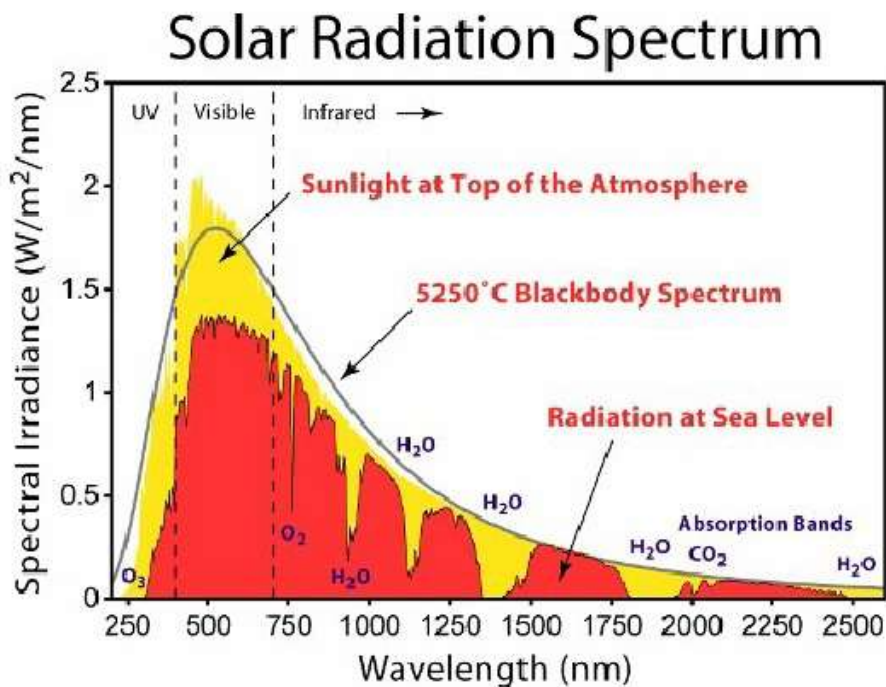


Figure 1.15: The black solid line is the BB distribution, the yellow line is the energy distribution of Sun taken outside the Earth's atmosphere, the red line is the energy distribution of the Sun taken on the ground. We can see that the Earth's atmosphere affects the spectrum too. The atmosphere absorbs radiation in particular range of wavelength. If we study the transmission (fraction of light that can reach the ground without interactions) we see that the transmission is near zero in some ranges. So, the presence of an atmosphere affects a lot a spectrum.

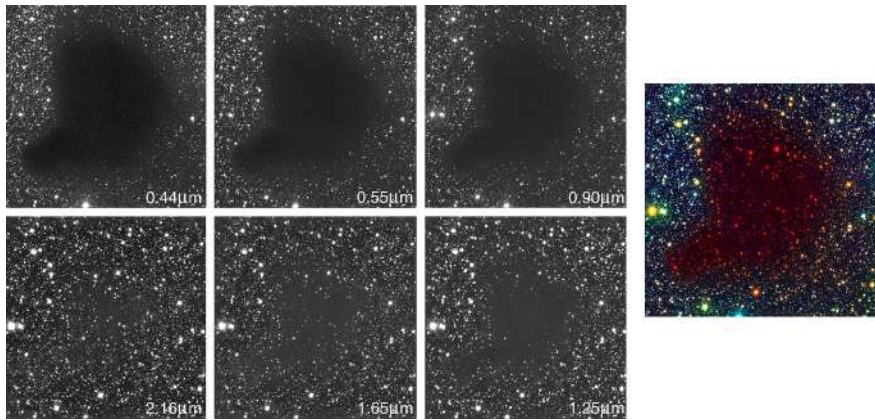


Figure 1.16: The absorption changes with wavelength; at larger λ the extinction is less. On the right we see the sum of all images, but we associated to each image a color to get an trichromy image.

The observed flux is related to the intrinsic one by:

$$f_1 = f_2 e^{-\tau_\lambda} \quad (1.13)$$

Where τ_λ is the optical depth of the ISM at the observed wavelength. The change in apparent magnitude at wavelength λ due to extinction is:

$$m_\lambda - m_{\lambda,0} = -2.5 \log e^{-\tau} = 2.5 \tau_\lambda \log e = 1.086 \tau_\lambda \quad (1.14)$$

The extinction at wavelength λ is:

$$A_\lambda = 1.086 \tau_\lambda \quad (1.15)$$

However, the extinction is not the same at all wavelength. It depends on the wavelength as shown by the **Whitford law**:

$$A_V = 1/\lambda \quad (1.16)$$

This empirical law is only a first approximation for the visible band. The first consequence of the extinction is that the sources appear redder than they really are.

In the figure 1.16 we see that from the dark nebula we collect only red photons due absorption effect.

1.5.1 Extinction law

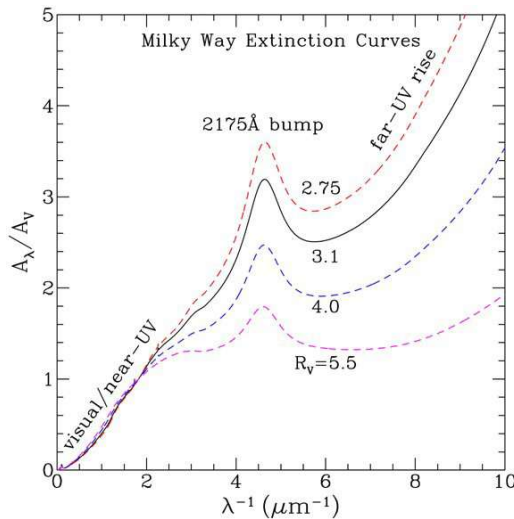
What is usually derived empirically is the so-called extinction law, that relate the ration A_{λ}/A_V , the relation between the absorption coefficient in a certain wavelength λ with respect to the absorption coefficient in visible.

In the figure 1.17 we see the graph that shows this relation. There are different curves for different values of the parameter R_V , that is defined as:

$$R_V = \frac{A_V}{E(B-V)} \quad (1.17)$$

Accepted values of R_V range from 3.1 to 3.3, although in peculiar directions it could be different. The values of R_V can vary in different galactic and extragalactic environments.

As an example, in the Johnson system the reddening law is approximated as:

Figure 1.17: Extinction law for different value of R_V coefficient

$$\begin{aligned}
 A_U &= 1.53A_V \\
 A_B &= 1.32A_V \\
 A_R &= 0.82A_V \\
 A_I &= 0.60A_V \\
 A_J &= 0.29A_V \\
 A_H &= 0.17A_V \\
 A_K &= 0.11A_V
 \end{aligned}$$

What is the physical implications? In the past astronomers were used to use a single extinction law for all universe. This assumption is wrong and the error that astronomers committed propagated into measurements of distances, and the in the property of the universe.

1.6 The formation of the galaxy: constraints from the CMD

1.6.1 The lambda cold dark matter model

According to the standard model of Big Bang, the Universe contains a cosmological constant, lambda, associated to dark energy and cold dark matter. Predictions from the Lambda-CDM model are in agreement with:

1. The existence and the structure of the cosmic microwaves background. This background is uniform indeed its anisotropy is around 1/100000, very small (it is pretty uniform). To be more specific, the model predicts that the universe at the beginning was made up by hot matter, a plasma of H and due to the high temperature, all radiation was absorbed by plasma. When the plasma cooled down, the universe became transparent to the radiation (so to the photons). Due to the expansion, the energy of those photons became lower over the time and this is the way we expect to observe radiation coming from the microwaves background.
2. The accelerating expansion of the Universe.
3. The abundances of H , He , Li .
4. Distribution of galaxies on large scale, which is almost uniform and isotropic.

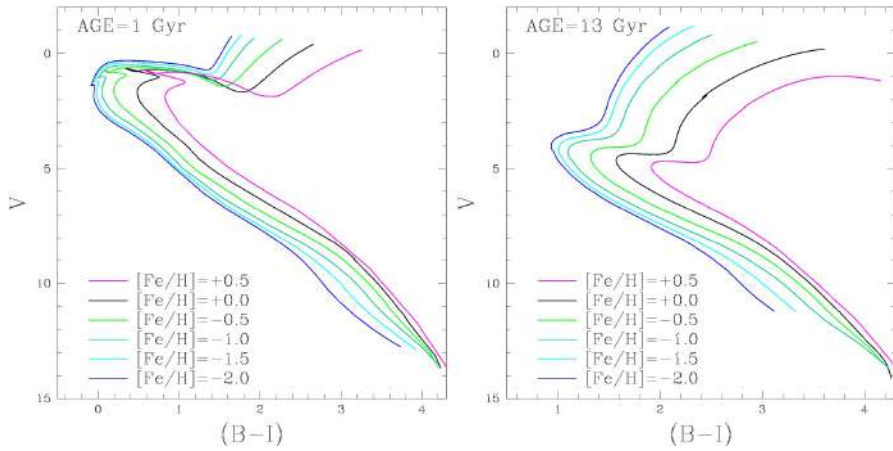


Figure 1.18: Isochrones of 1 and 13 Gyrs according to different metallicity.

1.6.2 The missing-satellite problem

Simulations based on the lambda CDM model predict that dark matter clusters form in a hierarchically way. We expect that the number of counts increasing for smaller-and-smaller sized halos. Observed normal-sized galaxies account for the predicted distribution, instead, the number of dwarf galaxies is orders of magnitude lower than expected from simulation.

Muratov & Gnedin (2010) devised a semi-analytical model of the formation of GC population in a massive host galaxy. The model is based on simulations of the cold dark matter galaxy-formation theory.

So, studying the GC population we can test the model of galaxy formation, that is our target and, for example, understand what is the contribution from dwarf galaxies to the assembly of the Milky Way and other big galaxies.

1.7 Metallicity and the isochrones

1.7.1 Metallicity indicators

If Lambda-CDM model works, then we expect that metallicity changes with the age, so let's focus on metallicity. One of the most used metallicity indicator is the quantity:

$$[Fe/H] = \log \frac{(Fe/H)}{(Fe/H)_\odot} \quad (1.18)$$

where Fe and H are the abundances respectively of iron and hydrogen. If one assumes that the solar heavy-element distribution is universal, the conversion from $[Fe/H]$ to Z is given by:

$$[Fe/H] = \log \frac{Z}{X} - \log \frac{Z}{X_\odot} \quad (1.19)$$

Using the empirical value of the solar Z/X ratio we get:

$$[Fe/H] = \log \frac{Z}{X} + 1.61 \quad (1.20)$$

A value of $[Fe/H] = -2.0$ correspond to a very metal poor star, instead a value of $+0.5$ correspond to a metal rich star.

In figure 1.18 we see how isochrones change with metallicity. In particular, going from metal poor stars to metal rich stars (increasing the metallicity) the isochrones became redder and the turn-off point becomes fainter and redder. There is a sort of degeneracy.

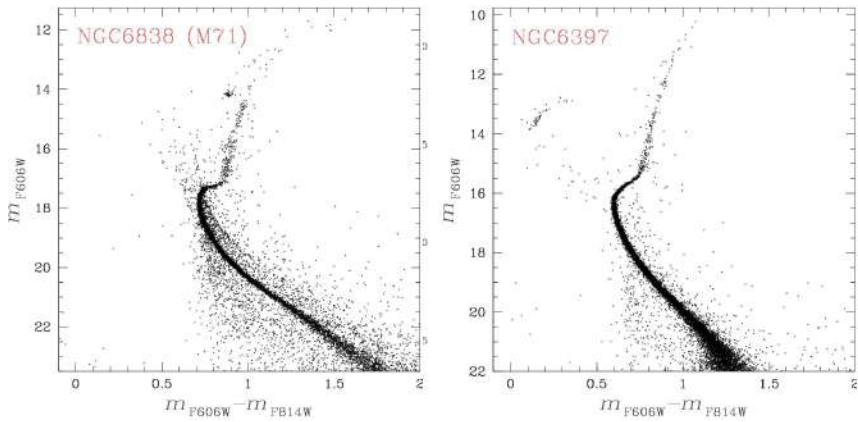


Figure 1.19: Comparison between two different CMD of clusters

Globular clusters are among the oldest objects of the Universe for which we can derive reliable age determinations. The absolute ages of globular clusters provide lower limits to the age of the Universe. Before the GCs formation there have been others stars but single stars not clusters. Dating these single stars is too difficult and not reliable, so astronomers prefer using GCs ages to obtain a lower limit for the age of universe.

1.8 Examples of CMD

In figure 1.19 we can compare the CMD for a metal rich and a metal poor cluster. On the right there is the CMD of NGC6838, on the left the CMD of NGC6397. The first shows:

- The shape of the curve: tell us how old is a cluster. In particular NGC6838's CMD is similar to an old isochrone.
- Red clump: tell us that the cluster is metal rich (indeed is not present the horizontal branch).
- A lot of stars above the MS telling us that there are many binary stars.

The second shows:

- The shape of the curve tell us how old is a cluster. In particular NGC6397's CMD is similar to an old isochrone.
- The presence of horizontal branch tell us that the cluster is metal poor.
- The slope of the main sequence is different from the previous one, in particular it is slower. Also the lower number of points above the main sequence tells us that the number of exotic and binaries objects is smaller.

1.9 Age-Metallicity relation

Precise age determinations based on high-precision Hubble-Space Telescope photometry of 68 clusters from the ACS survey of Galactic Globular Clusters reveal that Clusters with different distance from the Galactic center follow different Age-Metallicity relations, see figure 1.20.

In the outer part of the galaxy (the halo) the most of them are metal rich with a strong metallicity relation: metallicity increases very quickly with the age inside a big range of metallicity. Here there are old GC about 12 – 14 Gyr but also some about 8 – 10 Gyr, suggesting prolonged GC formation in the outer halo. In the internal part of the galaxy we have a slow increase of age with metallicity. Here there are the oldest GC (about 12 – 14 Gyr) with a significant improvement of metallicity in a short time, indicating a rapid chemical enrichment in the inner Galaxy.

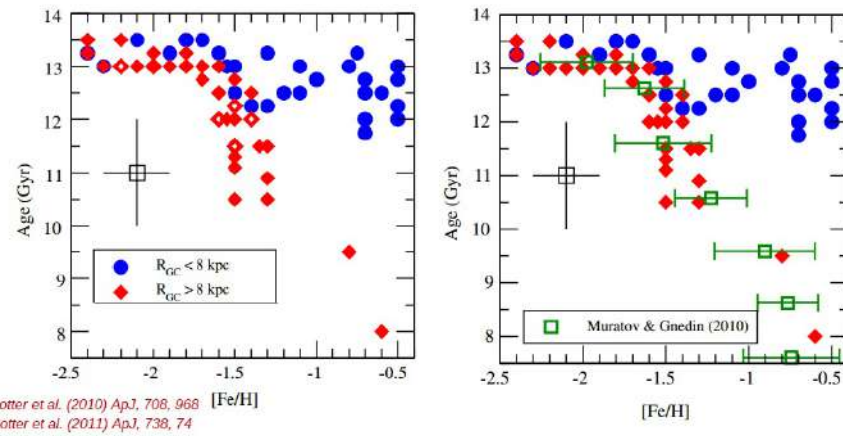


Figure 1.20: In these two panels we can see the age-metallicity relation. In red the cluster in outer part of the galaxy, instead in blue the ones in the inner part. On right: the plot with the data, on left: the comparison with the model (green) of Muratov & Gnedin that we want to test.

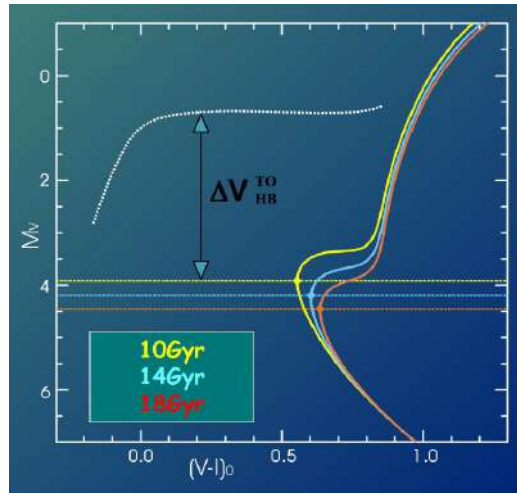


Figure 1.21: Explanation of the vertical method

So, in general, GC in the inner part are older and metal poor while GC in the outer part have a star formation prolonged over the time and they are metal rich.

The latter is consistent with the outer halo GCs forming in dwarf galaxies and later being accreted by the Milky Way.

The age-metallicity relation inferred for the inner galaxy is consistent with the predictions by Muratov and Gnedin, but there is something related to the blue points, not predicted by the model.

1.10 Other techniques to obtain the age of GCs

1.10.1 The vertical method

It is based on the magnitude difference between the Main-Sequence Turn Off and the Horizontal Branch at the level of the RR Lyrae instability strip.

Physical explanation - The helium core mass at the He-burning ignition is almost constant for stellar populations older than 5 – 6 Gyrs. For a fixed metallicity, the luminosity of the Horizontal-Branch (HB) depends on the mass of the helium core. As a consequence, the HB magnitude of (old) stellar populations with different ages is almost the same. We know that the luminosity of the turn-off decreases with time, so the difference in magnitude between the HB and the TO change with time.

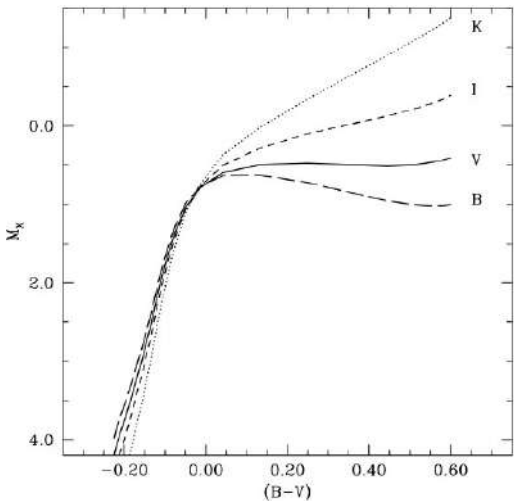


Figure 1.22: The HB is not horizontal, look at the different slope as change filters. The vertical method can be used only for V band.

Advantages:

- Not dependent on cluster distance.
- Not dependent on cluster extinction.
- Not dependent on photometric calibration.
- It is (seems) on sound theoretical footing.

Disadvantages:

- Accurate determination of the turn off luminosity can be challenging.
- Accurate determination of the HB level are challenging in clusters with few or no RR Lyrae.
- The HB luminosity depends on the helium abundance. Multiple stellar populations have different helium content.
- The ‘Horizontal branch’ is NOT horizontal. See the figure 1.22

1.10.2 The horizontal method

It is based on the measurements of the color difference between the MS turn-off and a given point along the RGB (for instance, that 2.5 mag brighter than TO).

This method is reliable if the physics that describes the MS,RGB and the HB is correct.

1.11 Resolution of the missing-satellite problem

As stated before, the problem is that the number of dwarf galaxies is orders of magnitude lower than expected from simulation of Lambda-CDM model. As one way of rectifying this problem, reionization could have suppressed star formation in the smallest dark-matter sub-halos (Bullock et al. 2000). The dearth of stars would then make these sub-halos difficult or impossible to detect. In figure 1.24 we can see in the first panel the dark matter distribution in a large scale (it is a simulation around a big spiral galaxy, we cannot see the dark matter). In the others panels are shown in green the dwarf galaxies where the star formation has continued after the reionization, in red the dwarf galaxies where this process has been interrupted.

In some dark matter halo the star forming is stopped, so there are dwarf galaxy dominated of dark matter.

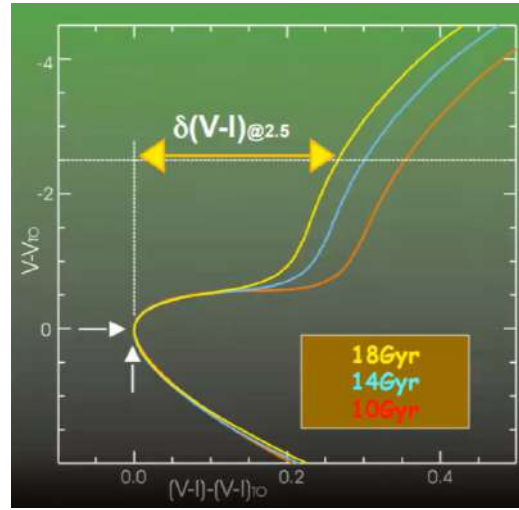


Figure 1.23: The Horizontal method.

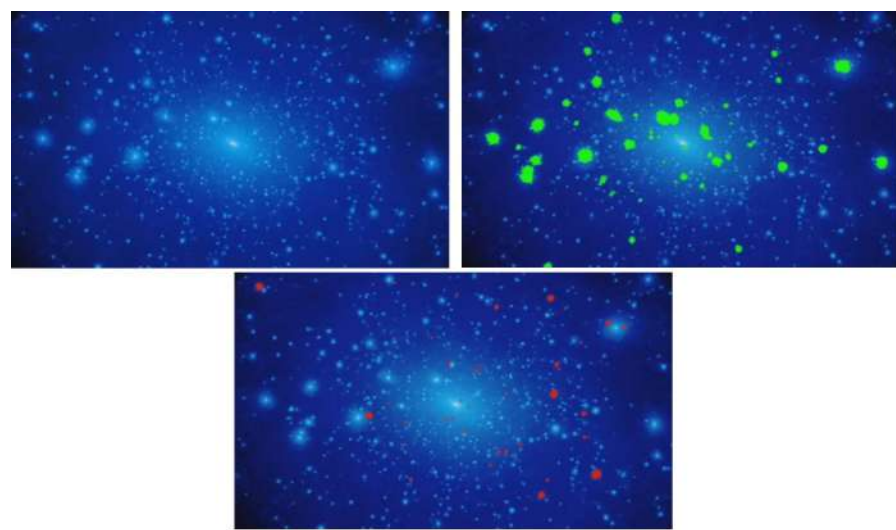


Figure 1.24: Dark Matter distribution around a large spiral galaxy. In green the Bright dwarf galaxies, where star formation continued beyond reionization, in red Low-luminosity dwarf galaxy where star-formation was shut off by reionization



Figure 1.25: On the left we have an image of a small portion of the sky, studying the proper motion of the stars we can delete the contamination, the result of the subtracting of contamination is the image on the right. There are some stars that are not of Milky way but form an ultra-faint dwarf.

If this is true, there should be faint dwarf galaxies beyond the bright dwarf galaxies that we have known from decades.

If this is correct, satellites of spiral galaxies can be divided in three different groups according to their evolutionary path (Ricotti & Gnedin (2005)):

1. **True fossils** (?), that formed most of their stars prior to reionization.
2. **Polluted fossils** with star formation continuing beyond reionization.
3. **Survivors** that largely formed their stars after reionization.

1.12 The ultra-faint dwarf

In figure 1.25 on the left we can see an image of a region of the sky. Removing all elements creating contamination, astronomers discovered an ultra-faint dwarf galaxy. The ultra-faint dwarf (UFD) galaxies were discovered recently. They have luminosity of $M_V > -7$ ($M \sim 10,000$ solar masses). They are agglomerations characterized by a very low density, about 10 thousands stars (while classical dwarf galaxies have 10 million stars and giant elliptical galaxies have 100 billion stars).

How is it possible to observe those structures? How they survived in the halo of the Milky Way? One possibility is that this is the first encounter between the UFD and the galaxy. The second possibility is that their mass is significantly bigger than it appears from their light, being dominated by dark matter.

The internal kinematics (analysis of the velocity of stars) reveal that UFD have mass to light ratio $M/L > 100$, hence they are dark-matter dominated. To make a comparison, GC are consistent with having no dark matter indeed their mass to light ratio is $M/L \sim 2$ while classical dwarfs have $M/L \sim 10$. However to have the M/L ratio we have to study the dynamics based on radial velocity so we have to take spectra of stars, analyse lines and measure how much they are shifted from expectation. This can be done only for few stars because they are too distant so, maybe, there are huge uncertainties about measurements giving a high M/L as result of low statistics.

In general, from CMD we understand that UFD are composed by very old population. The slope of giant branch (indicative of metallicity) indicates that those type of structures are metal poor. The fact that UFD are composed by very old stars demonstrates that they used to be dominated by dark matter halo and maybe star formation was stopped by reionization.

As shown in figure 1.26, ultra-faint dwarfs look like extension of dwarf galaxies, and not star clusters!

Big questions: Do true-fossil galaxies exist ? Are the ultra-faint dwarfs true-fossil galaxies?

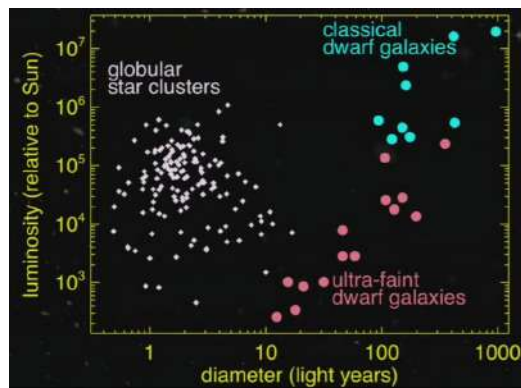


Figure 1.26: Another way to discriminate GCs, classic dwarf and UFD galaxy.

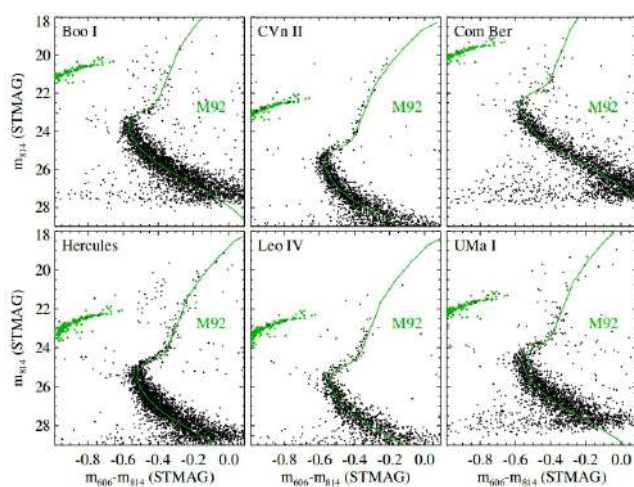


Figure 1.27: Brown et al. (2014) have studied six UDF galaxies near M92 using HST. In green the stars of these six UFD galaxies.

Using HST, Brown et al. in 2014 have studied six UFD galaxies (figure 1.27) and discovered that the 80% of stars formed by $z=6$ and 100% of stars formed by $z=3$. So, these stars are old, the vast majority were formed at $z=6$. The similarly ancient populations suggest that star formation in the smallest dark-matter sub-halos was suppressed by a global outside influence (e.g. the reionization).

1.13 Binaries method

As stated before usually dark matter quantity is measured analysing stellar dynamics (dispersion of velocity), but there are also other methods. Another method to derive the quantity of dark matter is using the binaries. Some systems are born as a binary system, other form later, after an encounter. Usually they are not the minority inside a stellar population. Sometimes they constitute the half of the stellar population. As consequence, to understand stellar population we have to understand also binaries.

If we consider the two components of an unresolved binary system and indicate with m_1 , m_2 , F_1 , and F_2 their magnitudes and fluxes, the binary system will appear as a single point-like source with magnitude:

$$m_{bin} = m_1 - 2.5 \log \left(1 + \frac{F_1}{F_2} \right) \quad (1.21)$$

Indeed:

$$\begin{aligned} m_1 &= -2.5 \log(F_1) \\ m_2 &= -2.5 \log(F_2) \\ m_{bin} &= -2.5 \log(F_1 + F_2) \\ &= -2.5 \log[F_1(1 + F_2/F_1)] \\ &= -2.5 \log(F_1) - 2.5 \log(1 + F_2/F_1) \\ &= m_1 - 2.5 \log(1 + F_2/F_1) \end{aligned}$$

1.13.1 Binaries in SSP

In the case of a simple stellar population the fluxes are related to the stellar masses M_1 , M_2 .

As a consequence, the luminosity of the binary system will depend on the mass ratio $q = M_2/M_1$. For simplicity we assume: $M_1 \geq M_2$ and $0 \leq q \leq 1$. In particular $q = 1$ in the case of two stars with same mass.

In figure 1.28 we can see a plot that shows where binary system are located for different value of masses and q ratio.

1.13.2 Equal-mass binaries

Equal-mass binaries are binary systems formed by two stars with the same mass $M_1 = M_2$. In this case $m_1 = m_2$ and $F_1 = F_2$ and, as consequence:

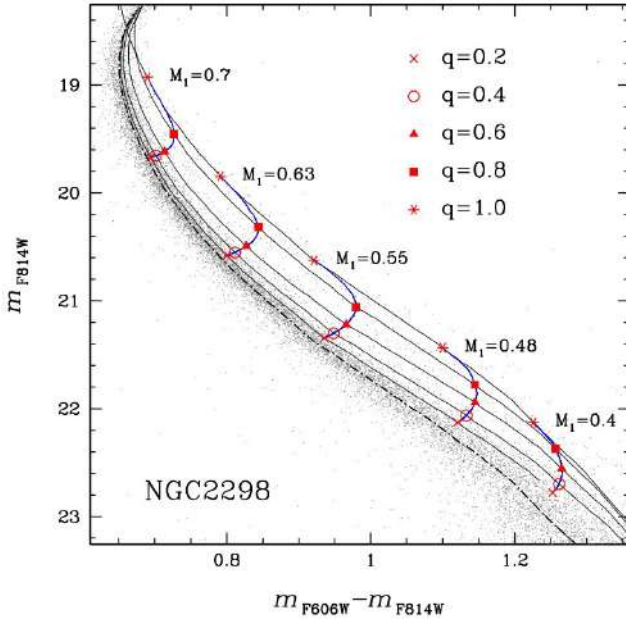


Figure 1.28: The dashed dotted line corresponds to a simple population: stars here are single stars. In blue there is the path that we generate for a simulated binary system, with different masses and thus different value of q . The black solid line represents the path of systems with same q value at different masses. In general, depending on the mass ratio q , pure binaries populate distinct sequences in the CMD. In the extreme case of $q = 1$ of equal-mass binaries, stars will move on a sequence composed of stars with same color of a single star but 0.75 magnitude brighter. For ratio from 1 to 0, for a fixed mass of primary star, binaries will go closer to the main sequence. This is a method to understand the fraction of binaries in a stellar population, including exotic ones.

$$\begin{aligned}
 m_{bin} &= m_1 - 2.5 \log(1 + F_2/F_1) \\
 &= m_1 - 2.5 \log[F1(1 + 1)] \\
 &= m_1 - 2.5 \log[F1(2)] \\
 &= m_1 - 0.752
 \end{aligned}$$

This means that the binary system will appear 0.752 *mag* brighter than each single star. As an example, the *V* and *I* magnitudes of two equal-mass binaries are:

$$V_{bin} = V_1 - 0.752 \quad (1.22)$$

$$I_{bin} = I_1 - 0.752 \quad (1.23)$$

Thus their color is:

$$V_{bin} - I_{bin} = (V_1 - 0.752) - (I_1 - 0.752) \quad (1.24)$$

From this we understand that binary system composed of equal-mass stars has the same color as each single star.

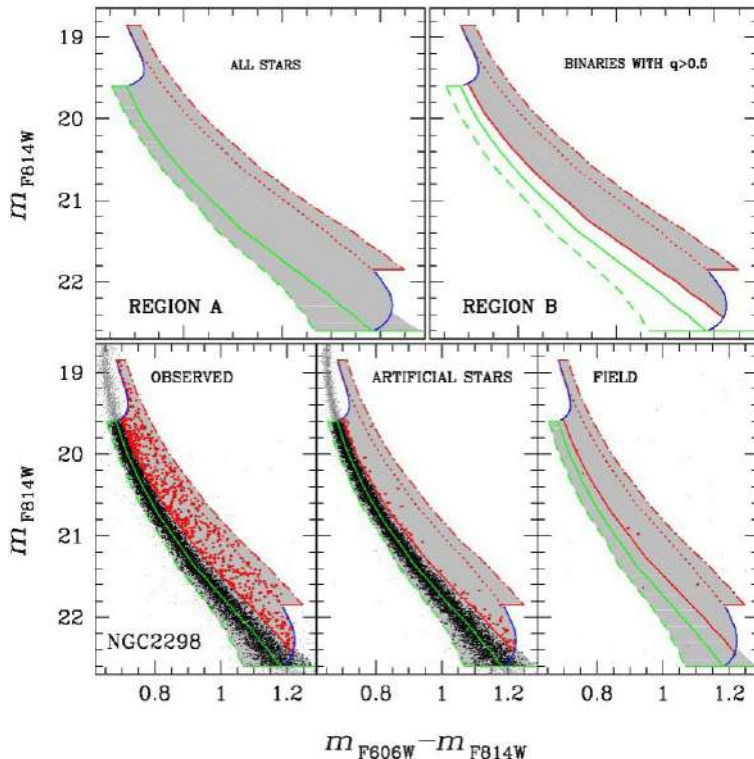


Figure 1.29: In this figure there is represented a method to estimate the binaries fraction. We can divided the region in two zone by a value of q , for example zone with $q < 0.5$ and zone with $q > 0.5$. We have to correct our data for star field and observational errors and then we can estimate the fraction.

1.13.3 Fraction of binaries

In figure 1.28 we found the way to distinguish binaries in the main sequence but this is not possible for all regions in the CMD. For example, going to faint magnitude, observational errors dominates so here is not possible to derive the fraction of binaries in a simple way. For those reasons, we are able to derive the fraction of binaries only for a small mass range.

Method to estimate the fraction of binaries of a stellar population is shown in figure 1.29.

1.14 Imaging with Hubble

To obtain useful data for observational CMD is necessary to use the best modern telescopes. One of the best and most used is the Hubble Space Telescope HST. Here there are some information about.

- Mirror diameter: 2.4 meters.
- Wavelength range: $\sim 0.1 - 1.7\mu m$ (WFC3).
- It was launched in 1990.
- It orbits in low Earth orbit, at altitude ~ 540 km with period ~ 55 min.
- Five Shuttle servicing missions from 1990.
- Cost > 10 billion \$

The most-used instruments on HST are:

1.14.1 The Wide Field Planetary Camera 2 (1993-2009)

It includes four cameras composed of 800x800 pixels each.

- WF2, WF3, WF4: Plate scale 0.10×0.10 arcsec/pixel

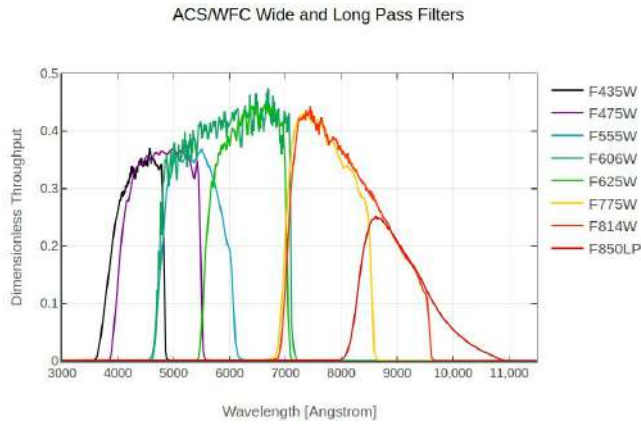


Figure 1.30: The range of ACS/WFC filters

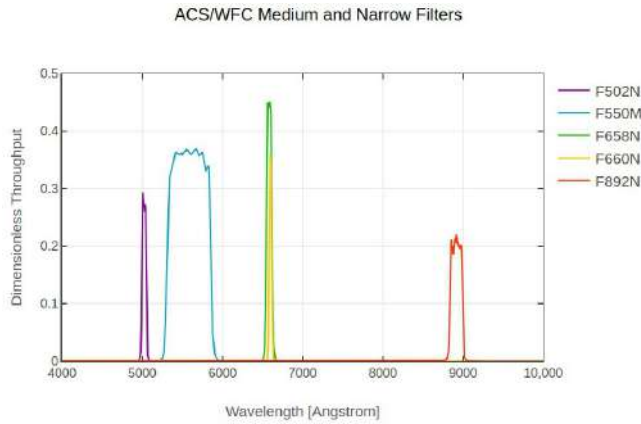


Figure 1.31: The range of ACS/WFC filters

- Planetary Camera Plate scale 0.05×0.05 arcsec/pixel

Wavelength range: $\sim 1200 - 10000 \text{\AA}$

1.14.2 The Advanced Camera for Surveys (ACS)

It includes three channels:

- High Resolution Channel (HRC): Field of view of 29×26 square arcsec; Wavelength range $1700 - 11000 \text{\AA}$; Plate-scale: 0.027 arcsec/pixel.
- Solar Blind Channel (SBC): Field of view: of 34.6×30.5 arcsec; Wavelength range: $1150 - 1700 \text{\AA}$; Plate-scale: 0.032 arcsec/pixel.

1.14.3 Wide Field Channel (WFC) of ACS

- Field of view: 202×202 square arcsec
- Plate-scale: 0.05 arcsec/pixel.
- Wavelength range: $3500 - 11000 \text{\AA}$

1.14.4 Charge Transfer Efficiency loss

The fraction of electrons that are successfully moved from one pixel to another during read-out is described by the charge transfer efficiency (CTE). Normal charge transfer efficiencies are 0.99999 - 0.999999, (one photoelectron is lost for every 100000 to 1000000 shifts!) If the CTE is only 0.999, you

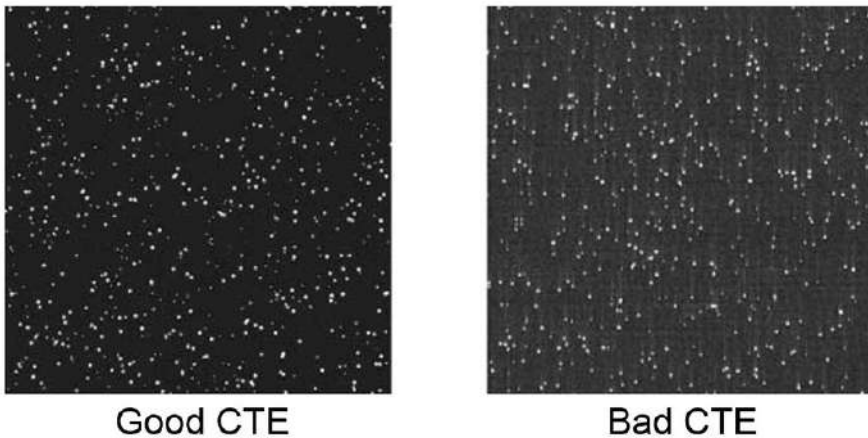


Figure 1.32: On right the original image, on left the corrected one for CTE

couldn't read most of the CCD. CCDs that have a very low CTE will leave streaks which are caused by charge/electrons being left behind after a transfer.

1.14.5 Point-Spread Function Photometry

All the point-like sources imaged by the telescope system can be represented by a point-spread function (PSF). The PSF gives ‘the shape’ of a star on the detector. Its amplitude will scale linearly with the brightness of the star forming the image.

In principle the recipe to derive the PSF model is simple:

- we must identify stars in our image;
- determine the sky under the stars;
- use isolate stars to derive the PSF model.

To measure stellar fluxes and positions we must fit the PSF model to all the star observed in the image. (allowing for the fact that the stellar image sits on top of the sky).

Chapter 2

White Dwarf

White dwarfs are the evolutionary end stage of more than 95% of all stars. They are stellar core remnants composed mostly of electron-degenerate matter, highly dense state of fermionic matter where particles must occupy state of kinetic energy, satisfying the principle of exclusion by Pauli. It has a mass comparable to that of the Sun enclosed in a volume comparable with that of the Earth.

White dwarfs (WDs) are the final evolutionary state of stars with masses smaller than $\sim 8 - 10M_{\odot}$. In a core of $8 - 10M_{\odot}$ stars the carbon (C) can be fused but not Ne . Hence, a $O - Mg - Ne$ WD may form. Instead, stars of very low mass will not be able to fuse helium, hence, a He WD may form.

2.0.1 White Dwarf structure

The white dwarfs have a isothermal electron-degenerate core surrounded by a non-degenerate envelope. The energy is provided by the internal energy of ions. White dwarf have no nuclear fuel and therefore it cools predictably with time.

2.1 The age-luminosity relations

The methods seen in the previous chapter to establish the age of a stellar population (turn off point of the main sequence, vertical method and horizontal method) are based on the physics of stellar evolution which means they are based on models describing internal nuclear reactions of stars. However it is very important to have a different and independent method to establish age of stellar population, not dependent on the physics of stellar evolution. A tool like this is, for example, the one based on analysis of white dwarfs during their cooling. Indeed the evolution of a white dwarf is a cooling process with a strong age-luminosity relations. The key point is that WD are driven by a temperature-color-age relation, NOT correlated with the physics of stellar evolution so they are the independent way to measure the age that we were searching.

To be more specific, white dwarfs have a very-small surface area to radiate their heat, so they cool gradually, remaining hot for a long time. As a white dwarf cools, its surface temperature decreases, the radiation which it emits reddens, and its luminosity decreases (Mastel 1952). We can define a white dwarfs cooling sequence (WDCS). The **Mastel law** relate the time t with the luminosity L , WD mass M , core atomic weight A , envelope molecular weight μ :

$$t \sim A^{-1} \mu^{-2/7} M M^{5/7} L^{-5/7} \quad (2.1)$$

In figure 2.3 we have a plot of simulated WD. We can see that as the time increases the bottom part becomes more populated.

To derive the ages is used the luminosity function: number of star per a given luminosity range. In figure 2.4 there are plotted four luminosity functions, two of a young populations and a seconds

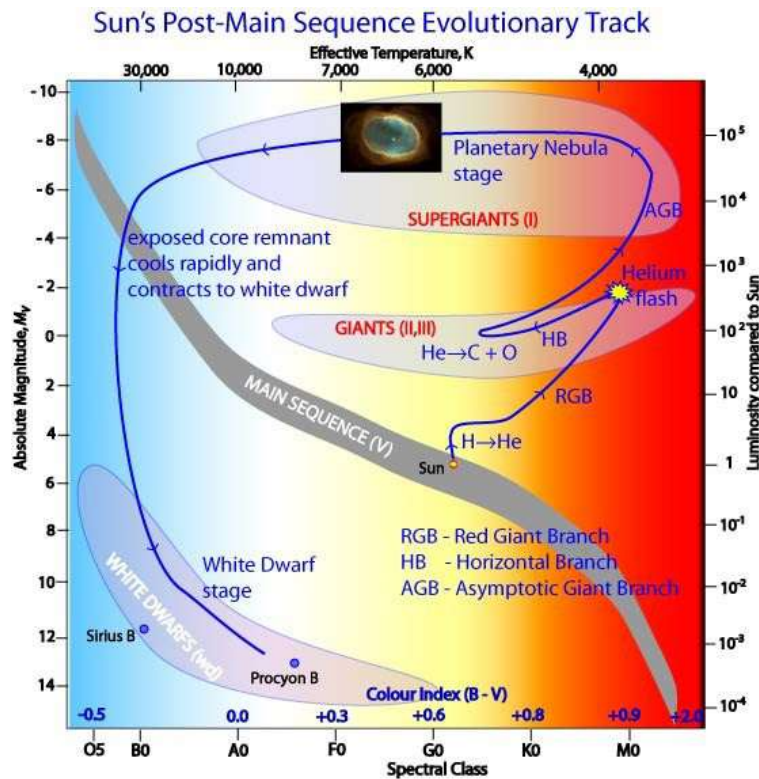


Figure 2.1: Evolutionary path of a solar-type star. It will expand and it will become a giant burning C and O in the core. Then it will spread out the external layers, forming a planetary nebula and finally it will follow the evolution of white dwarf.

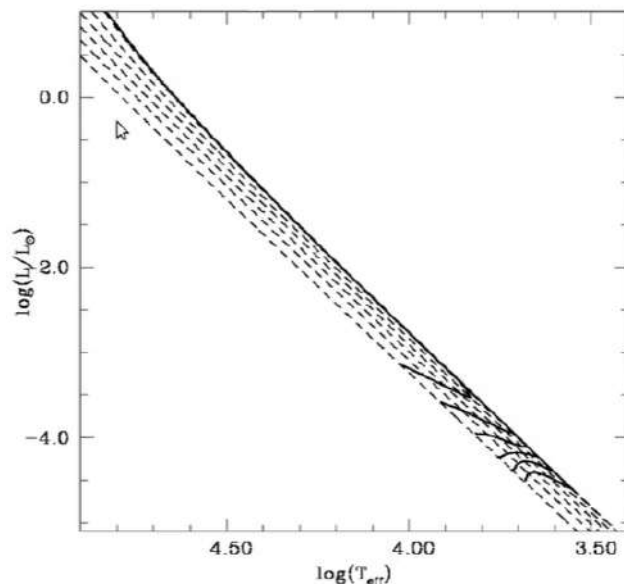


Figure 2.2: The Mastel law on theoretical plane.

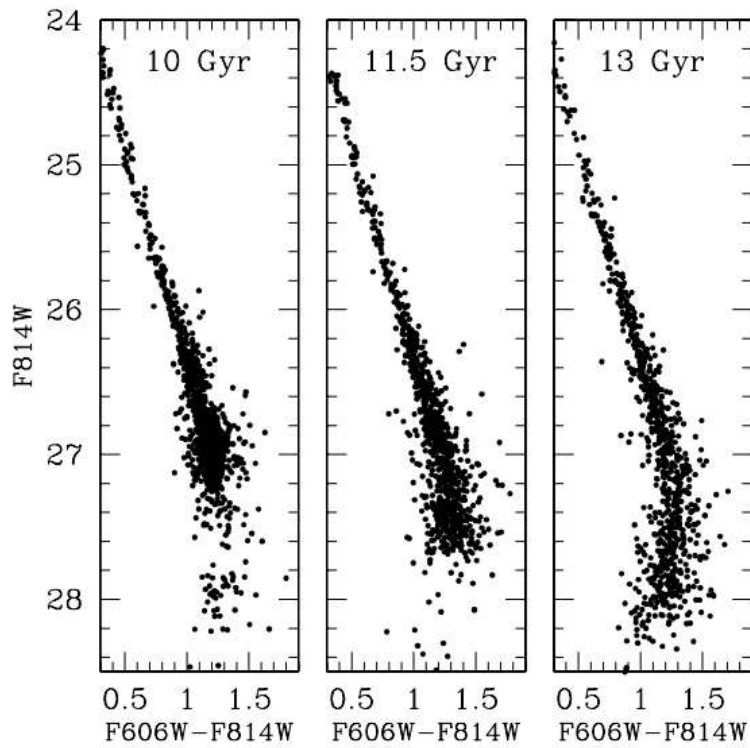


Figure 2.3: Simulated WD cooling sequences for simple stellar populations with different ages (Hansen et al. 2007). The distributions are more or less the same in the upper part, independently on the age, while in the bottom part seems depopulating increasing the age.

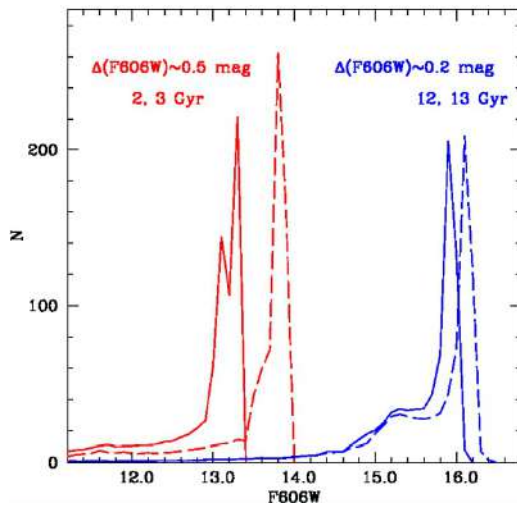


Figure 2.4: Luminosity function of WD cooling sequences for simple stellar populations with different ages.

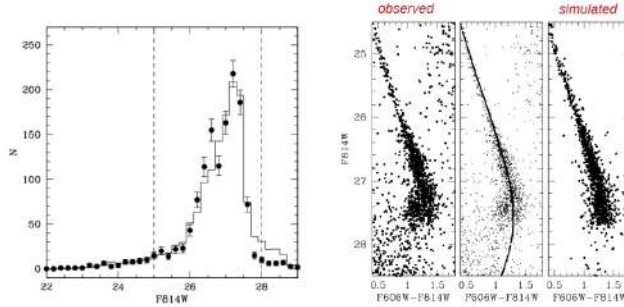


Figure 2.5: Comparison between the observed of WDCSs luminosity function of NGC6397 (dots) and the model corresponding to 11.5 Gyr (histogram). Hansen et al. (2007).

of old populations. Using this type of diagram we are able to derive the age studying the peak of the distribution. In particular the difference between two peaks of distribution corresponding to subsequent ages becomes smaller as the age increases; the difference between the peak of red solid distribution (corresponding to an age of 2 Gyr) and the peak of red dashed line (corresponding to an age of 3 Gyr) is bigger than the difference between two blue peaks (corresponding to ages of 12 and 13 Gyr). In general, for all stellar population, same age difference corresponds to small magnitude difference, which is quite challenging to observe.

Let us calculate the difference:

$$\begin{aligned} 2 \rightarrow 3 \quad \Delta_{F606W} &= 0.4 \text{mag} \\ 12 \rightarrow 13 \quad \Delta_{F606W} &= 0.1 \text{mag} \end{aligned}$$

This fact affects the sensitivity of the method. For comparison so we can assume that the sensitivity of the MSTO method is $\Delta_{F606W} = 0.1 \text{mag}$.

In the figure 2.5 on the left we see the luminosity function and the model which fit very well the data, on right the CMD observed compared with the simulated one. Let us compare the estimation of the ages with WDCS and with the MSTO:

$$\begin{aligned} t_{WDCS} &= 11.47 \pm 0.47 \text{ Gyr} \\ t_{MSTO} &= 11.6 \pm 1.0 \text{ Gyr} \end{aligned}$$

Observational Challenges: WDs exhibit faint luminosity: we need very deep and precise photometry of crowded region. As consequence ages from WDCSs can be inferred for nearby clusters only. As consequence, it is not possible compare two method for all clusters. In the other hand the MSTO method has a lot of challenges in the age derivation: one of the most difficult is the estimation of the metallicity (how content of metals change with the age). We've already seen how isochrone moves in the CMD due metallicity (isochrones with same age but different metallicity change the position of TO point) but they are given by models. With this dependence, however, we are able to define the age-metallicity relation.

Summary:

- The age-metallicity relation can be inferred with the MSTO method.
- The end of WDCS can be seen only for nearby GCs in the halo.

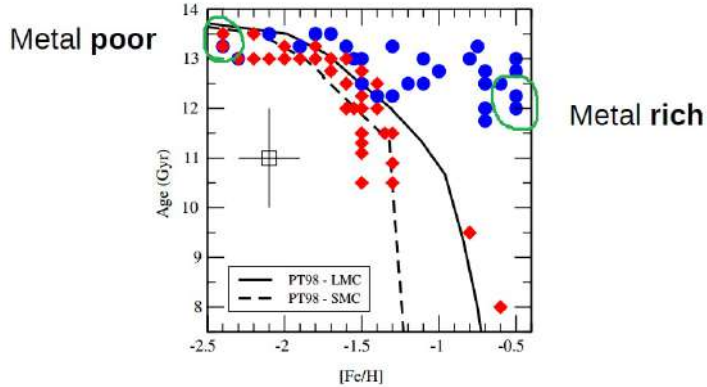


Figure 2.6: The age-metallicity relation that we've already seen in the previous chapter. In Green are shown a metal rich ad a metal poor GCs, that we use to test the model.

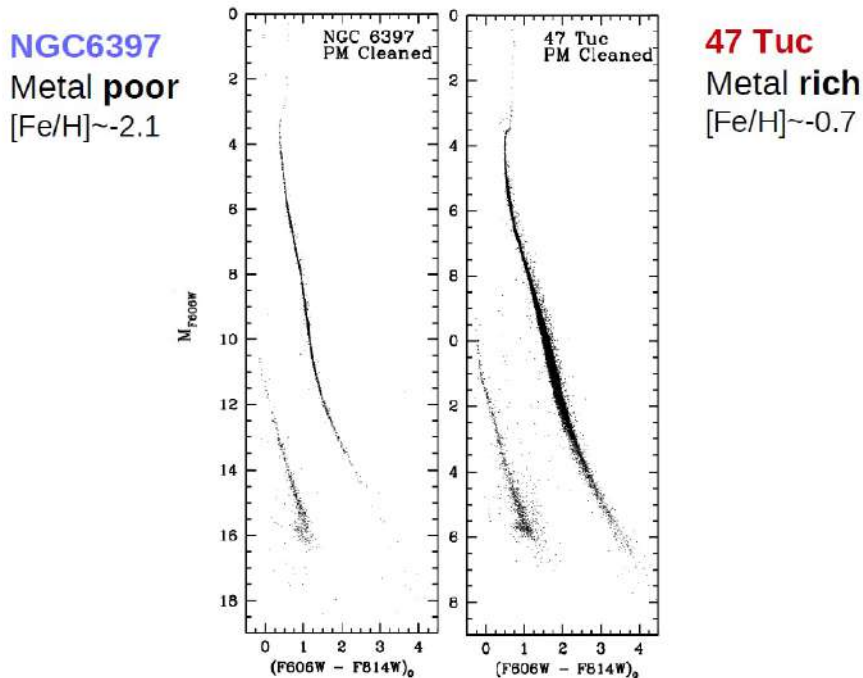


Figure 2.7: A CMDs comparison between a metal rich and a metal poor GC.

We want to test the age-metallicity relation and so the lambda model. A way could be using the WDCS to derive the age and compare to that of MSTO, if two method give the same results the relation and the lambda theory will be prove with two independent methods. This comparison is difficult due the bias of WDCS: we are able to use this way only with nearby GCs. A solution is the investigation of only a representative GCs and not all. In particular, we analyse one very metal rich and one very metal poor, as representative of the others. This is not the perfect way but it is the best we can do nowadays.

In figure 2.6 are shown in green a metal rich ad a metal poor GCs used to test the model.

In figure 2.7 there are the two CMDs of two cluster that are taken as representative. If the difference of the ages, derived by WDCS method, is around 2 Gyr the ages are agreed with the relation derived by MSTO and the lambda model.

Are two methods independent? If two method are dependent this test is useless. Look at figure 2.8, the WD sequences are overlapped very well. We deduced that: WDCS method does NOT depend on metallicity. Ages inferred from the WDCSs and on the MS turn off are based on different physics. WDCSs are crucial to validate MS turn off ages.

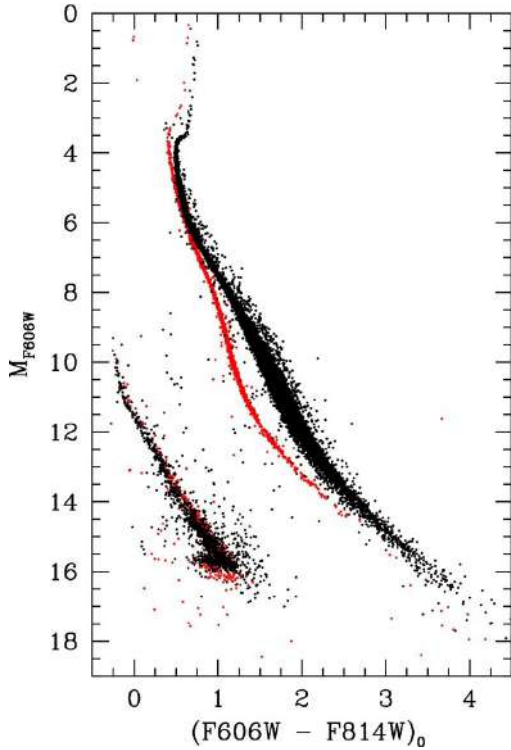


Figure 2.8: Comparison of two CMDs in the same diagram. Look at TO and the main sequence, TO and main sequence of 47Tuc is redder and fainter than NGC6397, in according to difference in metallicity. Look now at WDs zone: in contrast the position of the WDCS in the CMD does not depend on the metallicity. They match quite good. This is the observational proof that the position of WD in CMD do not depend on metallicity, making WD a powerful tool to estimate age independently. To be exactly red points in WD sequence are a bit fainter than black ones but this is a looking effect due to the age. In general, for stellar populations, the old one is the faint one.

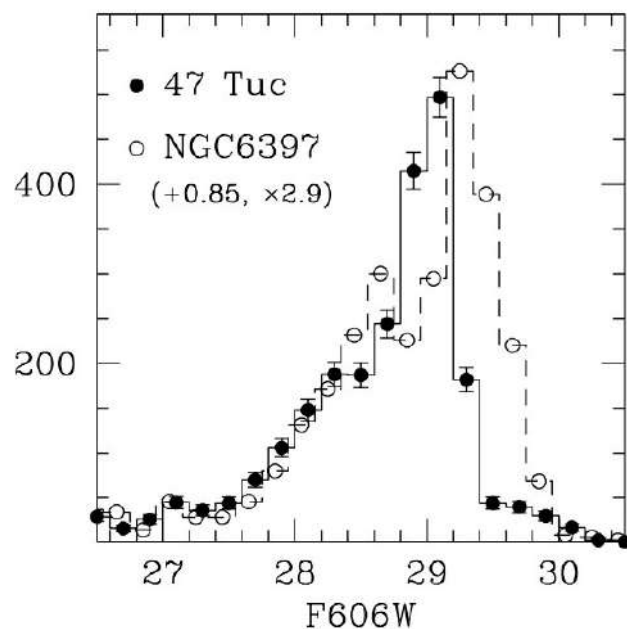


Figure 2.9: Comparison of luminosity functions of 47Tuc and NGC6397.

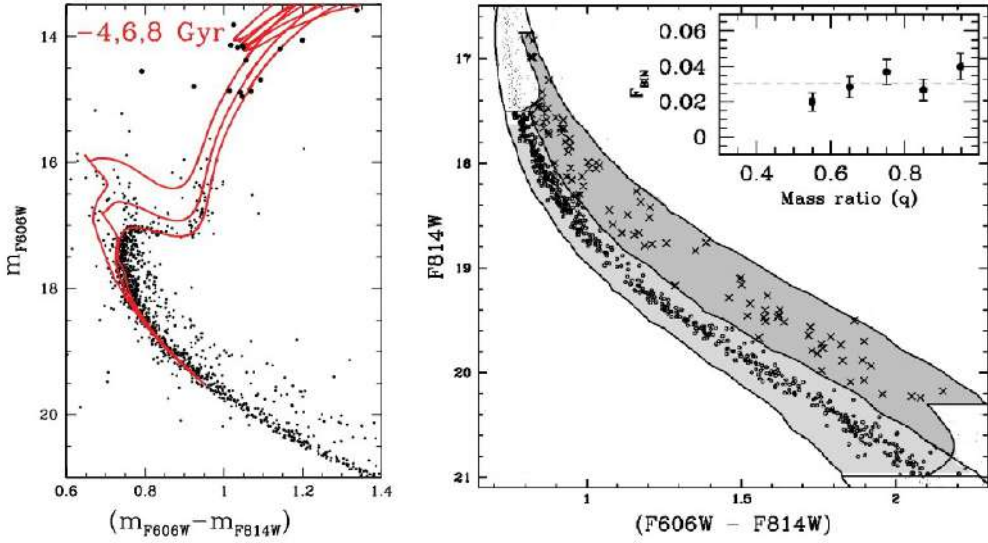


Figure 2.10: CMD of NGC6791

In figure 2.9 we can see the comparison between two luminosity functions: the solid line represents 47Tuc, the dashed line is NGC6397. With this diagram is clear that 47Tuc is ~ 2 Gyr younger than NGC6397. So, metal-rich clusters (like 47 Tucanae) formed later than metal-poor halo clusters (like NGC 6397).

Result: The physics behind two methods is different, so we can use the WDSCS method to test the MSTO method and the lambda model. Due the bias of WDSCS method we can analyze only a few GCs, so we chose two representative GCs: 47Tuc and NGC6397. Using the WDSCS method astronomers reveals that the ages are agreed with the estimations derived with MSTO method. So, the MSTO method is a liable method and the lambda model can fit the data.

2.1.1 The strange case of NGC6791

NGC6791 is a Galactic open cluster. It does not exhibit evidence of multiple stellar populations. Using the MSTO method the GC appears ~ 8 Gyr old. The first deep luminosity function of the WDSCS indicates that NGC6791 is ~ 2.5 Gyr old, in sharp contrast with results obtained from the main-sequence turn off. At the time of the discovery two explanations were presented. The age inferred from MS turn-off or from WDSCSs (or both) are wrong (a major challenge for stellar evolution?) or Exotic population of Pure-Helium White Dwarfs exists.

In 2009 Bedin et al. studied again the WDSCS of NGC6791, they discovered that the White Dwarfs Cooling Sequence of NGC6791 exhibits two (unexpected) distinct peaks.

There were two proposed solutions:

- There are two population of WDs with different composition: pure-He and normal WDs.
- There are an important fraction of binaries WDs.

The triggered point is that the separation in luminosity between the two peaks is about 0.75, which is the coefficient of two equal-mass binaries not interacting each other. We can distinguish single stars with mass ratio bigger than 0.75 so we can estimate the number of binaries. In particular Bedin et al. obtained that around 34% of stars are binaries. Using this value they simulated the cluster and reproduced the observations, confirming the second hypothesis. So adding those binaries present in the main sequence inside the simulations we found the double peak in WD. In the figure 2.11 we see the result of this work: the model fit very well the data and the double peaks.

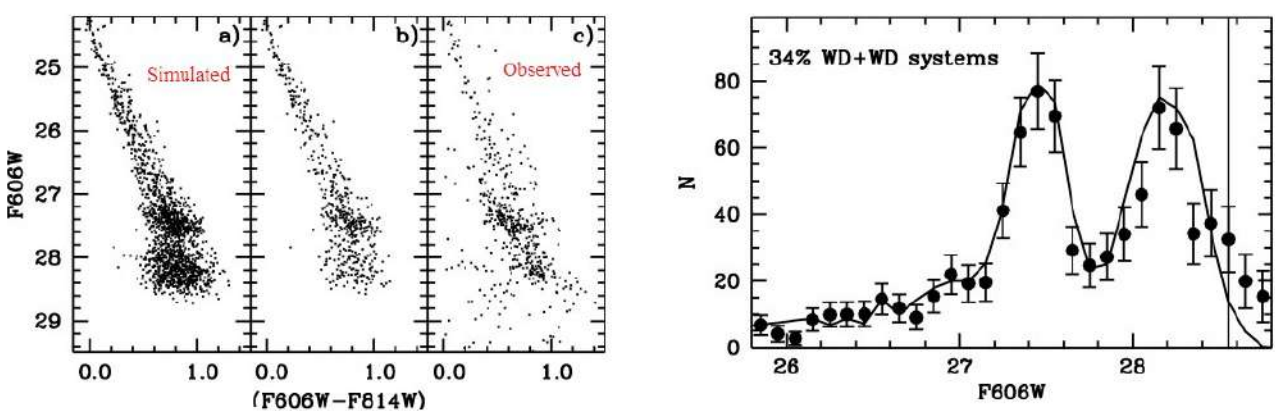


Figure 2.11: Comparison between model and observation

Chapter 3

Stellar spectroscopy

The stellar spectroscopy is a useful tool to study the stellar atmospheres. These are the region around stars that photons travel through. From spectra we get a huge amount of information. A limitation of spectroscopy is that we are able to get high resolution spectra only for brighter stars (while photometry is available for more stars but provides less information). There are many reasons to studying the stellar atmospheres:

- stellar atmospheres are the most important sources of radiation in the universe;
- stellar atmospheres are wonderful physics laboratories;
- stellar atmospheres are unique windows on stellar interiors.
- Moreover stellar spectra contain a fossil record of the history of the cosmos.

The evolution of a star is strongly connected to the formation of the elements. Using spectroscopy we can detect what elements are present in the outer layer of a star.

3.1 Stellar absorption: line formation

Let's think about an ideal case where we observe a source like a star emitting photons and those photons pass thought a prism. In this simple case a linear and continuum spectra is reproduced. However if a cool and thin gas screen is located in front of the source (like interstellar medium) or around the source (like the external part of a star, its atmosphere) inside the spectra there are some black lines. Assuming that the cloud is colder then the source (like in the case of a star) those lines are absorption lines. They provide us important information about the chemical composition of the source or of the interstellar cloud.

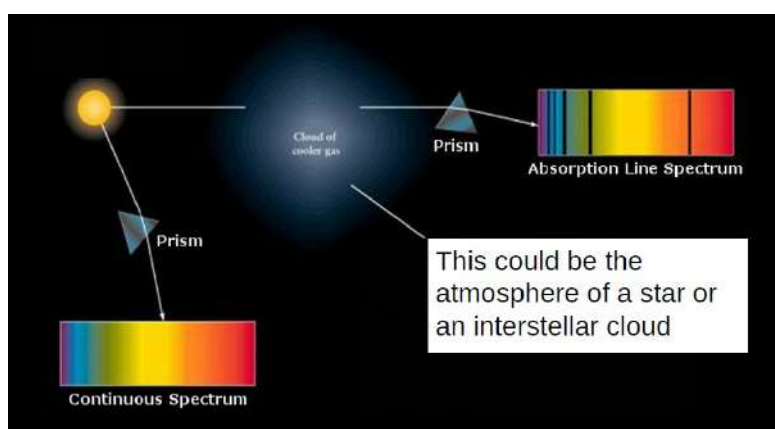


Figure 3.1: A cartoon that shows the process of stellar absorption.

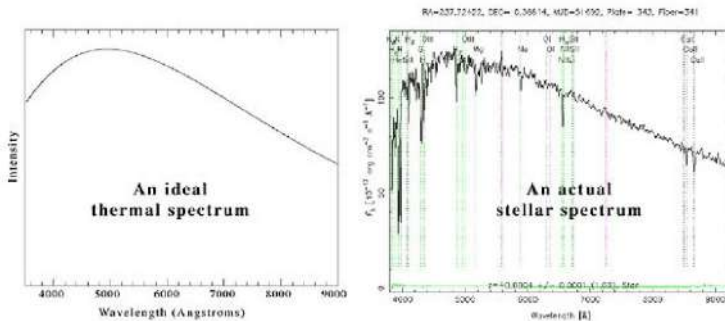


Figure 3.2: Comparison between an ideal spectrum (a black body spectrum) and a real spectrum.

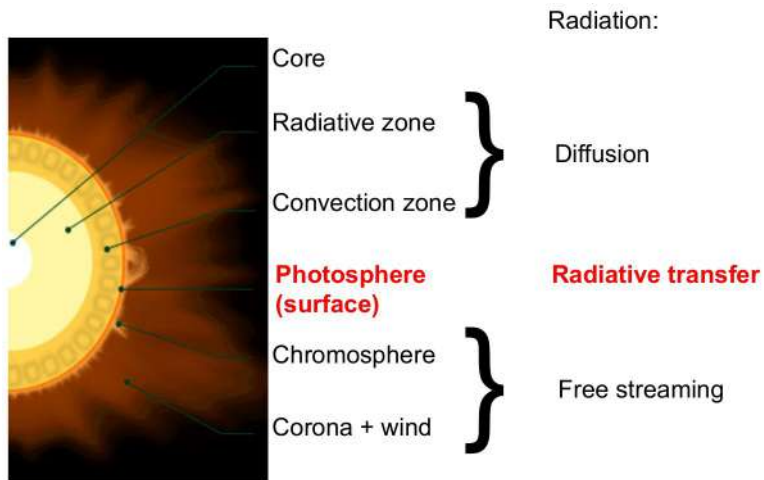


Figure 3.3: A cartoon that shows the stellar structure.

In figure 3.1 there is an scheme of absorption process. In figure 3.2 there is a comparison between a black body emission and a real star emission. A black body is shows a continuum emission while star spectrum shows a lot of lines. Finally in figure 3.3 there is a cartoon of general stellar structure. The most information we have from spectra come from the photosphere, as we said before.

To be more specific, in a spectrum we can find:

- The continuum region (region without lines), where τ is low and we see primarily the background.
- The region of spectral lines, where τ is large and we see the intensity characteristic of the temperature of the cool gas. Since the temperature is lower than central source, these appear as absorption features. Those lines are different also for their width: some lines are narrow and other are very large.

As we said in the previous chapter, the radiation from a star is similar to the Planck emission of a black body:

$$B_\lambda(T) = \frac{2hc^2}{\lambda^5} \frac{1}{e^{hc/\lambda kT} - 1} \quad (3.1)$$

The plot is shown in figure 3.4. From the plot we can see that the position of the peak depends on temperature. This feature is visible also from the observational point of view in figure 3.2. To be more specific, the Planck function is connected to the temperature of the source. Going from hot to cold stars, positions of peak moves to red wavelength, similar to what can be observed in the spectrum.

3.2 Information from the spectra

The main information that we can extrapolate from the spectra of stars are:

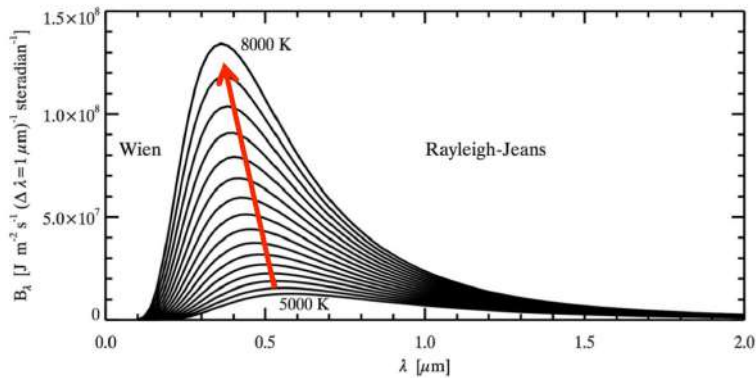


Figure 3.4: Planck function.

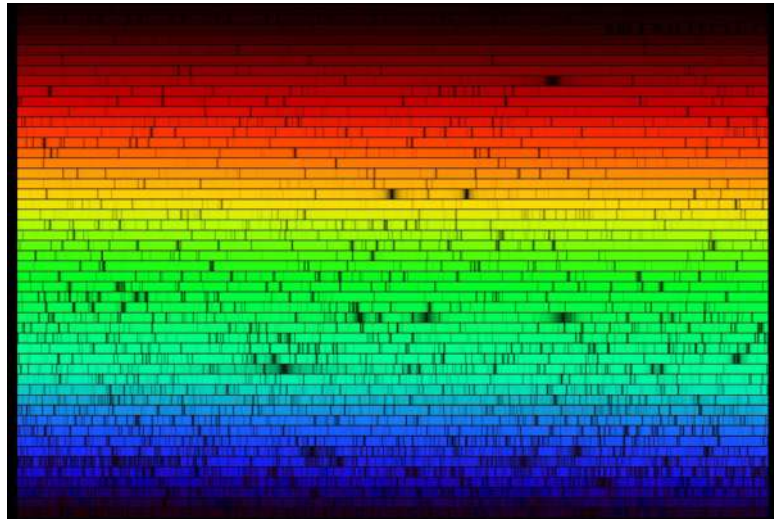


Figure 3.5: Sun's spectrum

- "Star ID": spectral type (O,B,A,F,G,K,M) and photometric classification.
- Atmospheric parameters: effective temperature, surface gravity and metallicity.

3.3 Abundance scales

There different ways to indicate chemical abundances inside a star. The most used and the most common are the **mass fractions**, indicated as following:

- X stands for Hydrogen;
- Y stands for Helium;
- Z stands for Metals which means all other heavier elements.

Another way is the so called '**12**' scales. In this case the abundance of a generic element X is compared with abundance of H in a logarithmic scale, as stated in the following relation:

$$\log \epsilon(X) = \log \frac{n_X}{n_H} + 12 \quad (3.2)$$

where $\log \epsilon(H) = 12$. For examples: $\log \epsilon(O)_\odot = 8.7$ dex means that O is 2000 times less than H in Sun.

The last method is the **[] scale**. It is represented by the following relation:

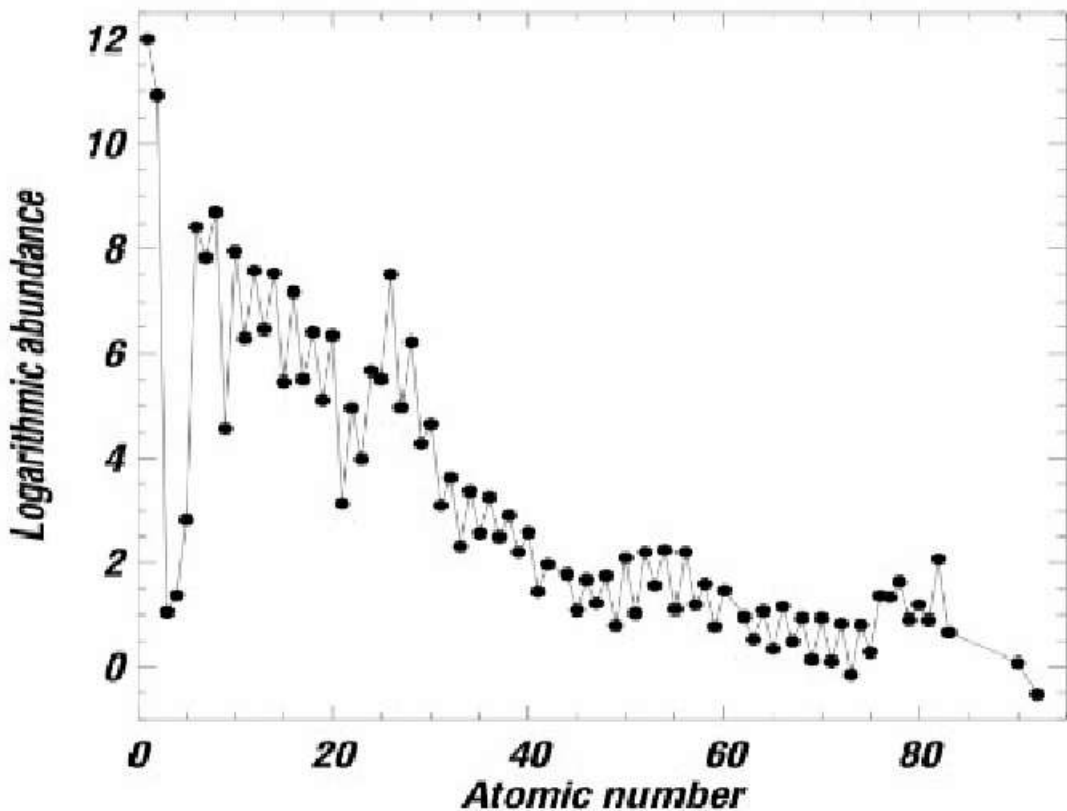


Figure 3.6: Element abundance in present-day solar photosphere: $X = 0.7381$, $Y = 0.2485$ and $Z = 0.0134$.

$$[X/H] = \log \frac{n_X}{n_H} - \log \frac{n_X}{n_{H\odot}} \quad (3.3)$$

for example: $[Fe/H] = -2$ means that star has 1/100 less iron than the Sun.

We can relate the abundances to the atomic number and build the diagram in figure 3.6 that refers to the solar photosphere. These abundances are derived from the spectroscopy and from the meteorites, that reflect the composition of the Sun.

3.4 Line broadening

When we see at a given spectrum we can see that each lines have a broadening, so, lines are not delta of Dirac but they have a certain broadening that depends on different processes. There are many components of broadening:

- 1. Instrumentation width** - This type of width is introduced by instrumentation used for observations. It can be limited but depends on the instrumentation. In general, having higher resolution on spectra (capability to separate lines with a given wavelength), we analyse very small part of the spectra but we collect few photons so we can observe only bright stars (not the faint ones). So it is necessary to find a compromise between the telescope capability and the target for observations.
- 2. Natural width** - It is due to the Heisenberg uncertainty principle (following relation) and it is described by a Lorentzian profile, very narrow.

$$\Delta E \cdot \Delta \tau = \frac{\hbar}{2\pi} \quad (3.4)$$

The transition between the same two different levels in different atoms can produce photons with slightly different energies due the uncertainty principle. As a consequence, spectral lines

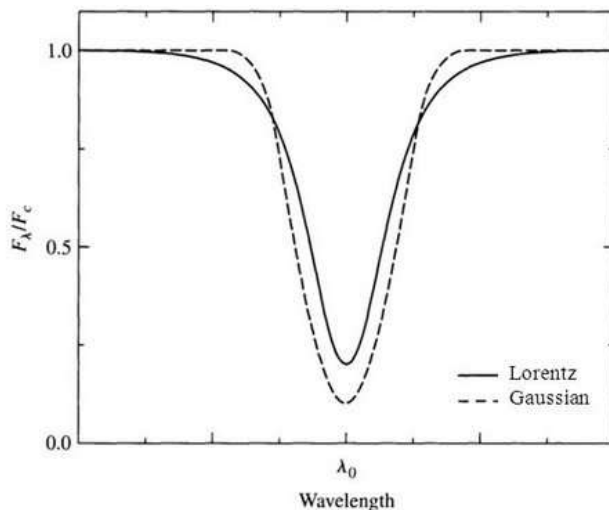


Figure 3.7: Comparison between Lorentzian and Gaussian functions.

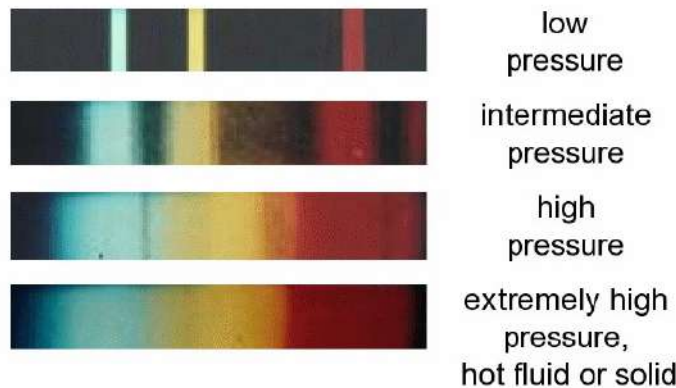


Figure 3.8: How broadening increases due to pressure.

are not infinitely sharp in wavelength (or frequency) but exhibit a spread in wavelength that is described by a Lorentz function.

3. **Pressure width** - It is due to collisions between particles and it mostly affects the wings of the spectral lines. It is described by a Lorentzian profile. We can see in figure 3.8 how the broadening increases due to pressure.
 4. **Thermal (Doppler) width** - It is described by Gaussian profile, very narrow. We know that particles follows the Maxwellian distribution of velocities, so due this distribution some particles have a bit difference velocity that corresponds to a little shift. Then taking into account the velocity distribution, the spectrum shows a broadening due the thermal motion (for which atoms randomly distributes the shift) and the Doppler effect.
 5. Other components are: Zeeman effect and the Stark effect.
- Zeeman effect:** Atoms in strong magnetic fields can align in quantum ways causing slight separations in the energies of atoms in the same excitation levels. This phenomenon splits the lines into multiple components. The splitting depends on the magnetic-field strength.
- Stark effect:** Perturbation by electric fields.
6. **Stellar rotation** - Also the rotation of the star could affect the broadening of line. The physics behind is the same of Doppler broadening. This process is shown in figure 3.10.

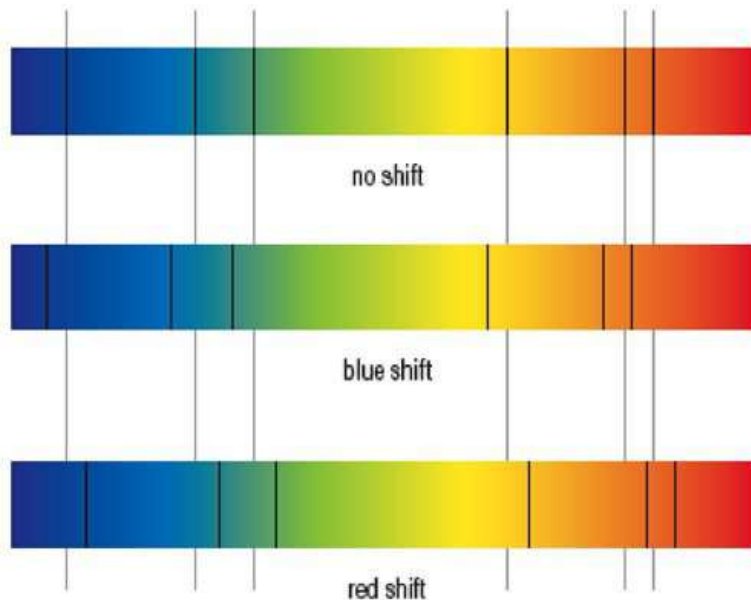


Figure 3.9: Doppler effect.

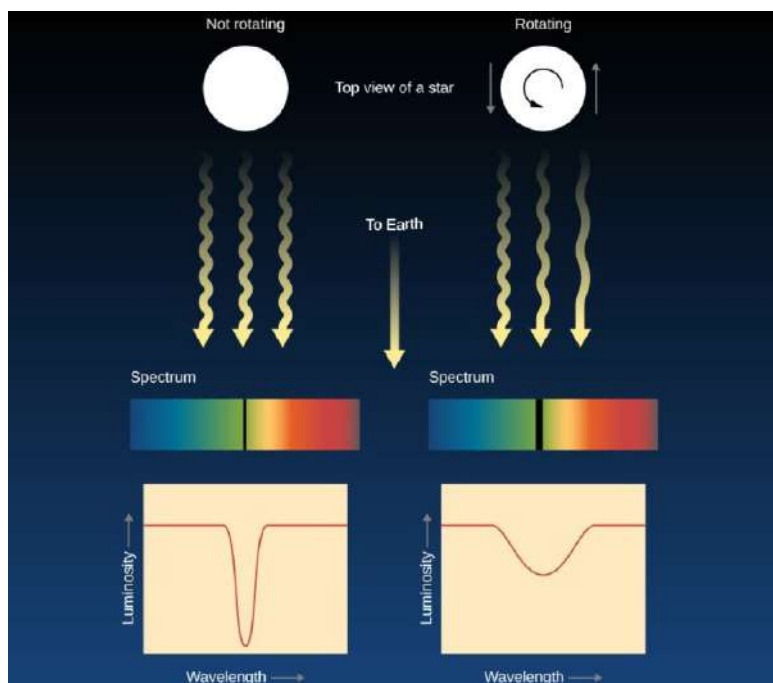


Figure 3.10: Rotation broadening.

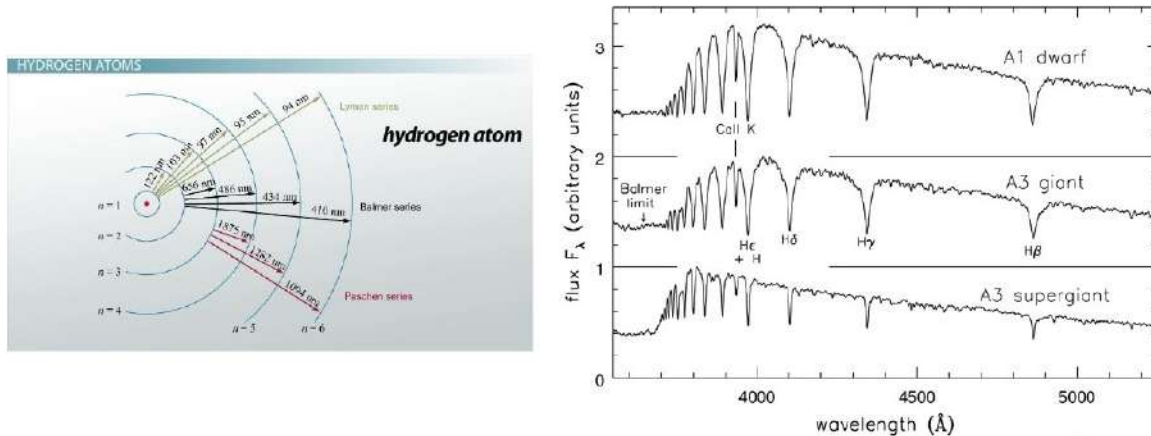


Figure 3.11: Hydrogen lines transition cartoon on left and hydrogen lines in stellar spectra on right.

3.4.1 Hydrogen lines

Inside stellar spectra there are some important lines such as Hydrogen ones. They are divided into three series.

- **Lyman series** (from $n=1$) appears in UV range.
- **Balmer transition** (from $n=2$) appears in optical range.
- **Paschen transition** (from $n=3$) appears in NIR range.

3.4.2 Helium lines

Helium is the second most-abundant element in stars. It is very important to recognize He to understand stellar evolution of globular cluster (where stars have also 40% of helium) however helium lines are detectable only in very hot stars (O-B). As consequence, we can analyse a small number of stars to show He content. Moreover those lines are not very deep so we need a very high signal/noise ratio to detect them and this means also a lot of time in observations.

3.4.3 Metal lines

Metal lines (all other lines different from H and He) become stronger as effective temperature decreases. They dominate the spectra of F, G and K stars.

In figure 3.13 we can see a diagram that shows the strength of the line as function of the spectral type. It is a useful tool to understand the main line for each spectral type star. So, according to the luminosity and to the temperature, the features inside the spectra are different. Hot stars are dominated by H and He while cold stars are characterized by huge presence of metals.

Note that spectroscopy is connected to photometry: stellar magnitudes are the convolution of the stellar spectrum with the transmission of the filter. Indeed light coming from each filter include integrate properties of a given region of the spectrum. Of course there is a huge variety of photometric systems with filter designed to cover some specific region of the spectra. Some filter are built to cover regions of the spectra significantly affected by abundance of specific elements. So using a combination of them, we can derive, for example, an estimation of metallicity.

3.5 Ages from the MS knee

Modern and future telescopes will provide images mainly in near-infrared so in the future we will become common study age of stellar population with the following method: the Main Sequence Knee. When we have a change of slope in the MS, the color is not increasing anymore so it is not proportional

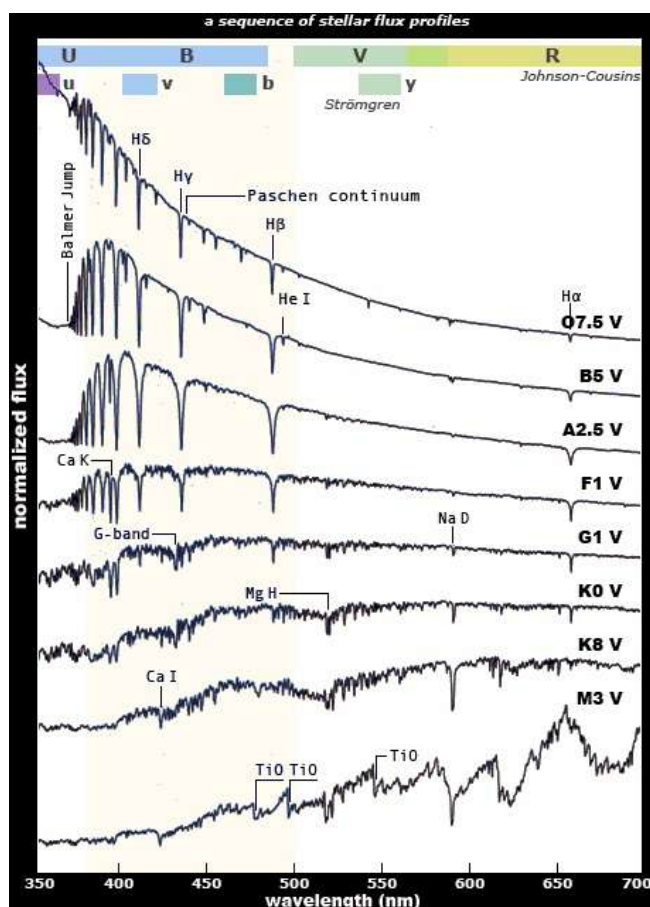


Figure 3.12: Comparison between spectra of different stellar types

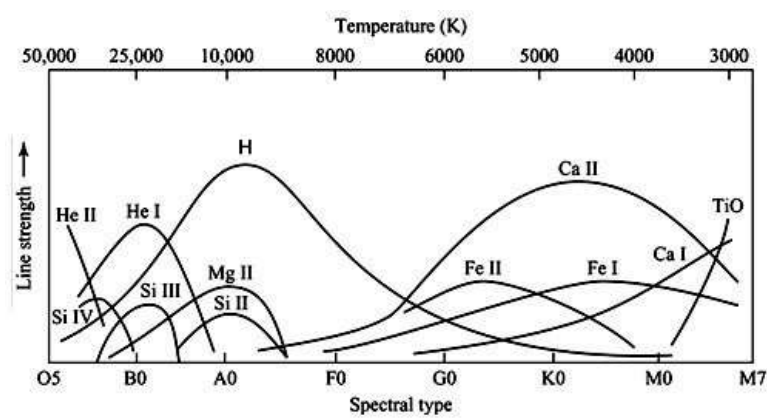


Figure 3.13: This diagram shows the main lines that appears in all spectral type stars.

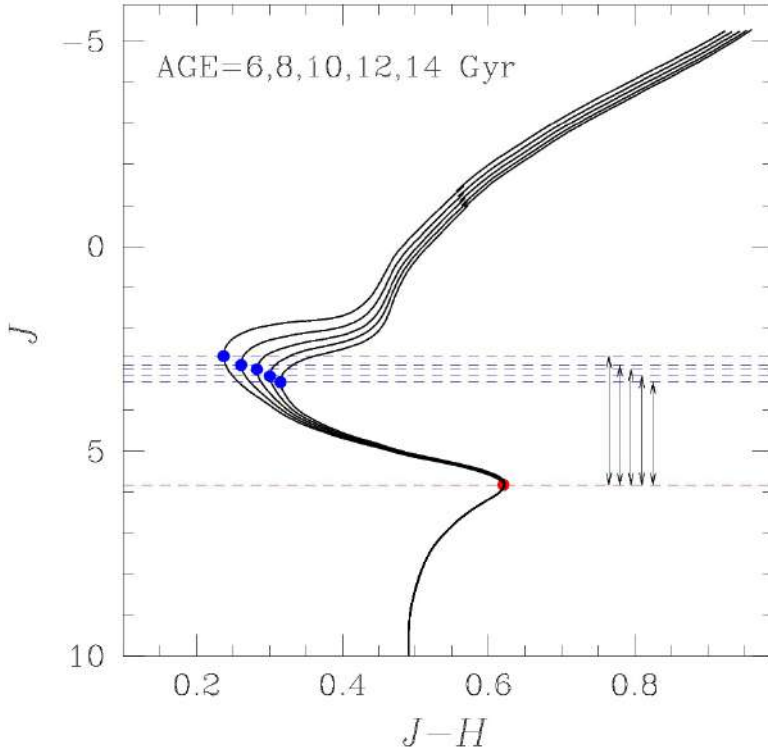


Figure 3.14: The MS Knee method in a schematic representation.

to the stellar temperature anymore due to a big bolometric correction that is associated to a physical phenomena: collision induced absorption of molecular hydrogen. This produces the point of Main Sequence knee. This point is well visible in CMDs made with near-infrared photometry. To infer the age of star cluster we measure the magnitude difference between the Main-Sequence turn-off and the Main-Sequence knee, indeed the position of TO point change dramatically with the age while the knee point remains in the same position, independently from age.

In figure 3.14 we can see how the difference in magnitude changes as the age increases. In particular increasing the age, the difference between two points became smaller (the TO point becomes a bit closer to the knee).

The **advantages** of this method are many:

- it does not dependent on cluster distance;
- it does not dependent on cluster extinction (TO point and knee are affected by same reddening);
- it does not dependent on photometric calibration;
- it involves large number of stars.

There are also some **disadvantages**:

- MS-knee stars have often faint so they are difficult to observe and their observations are associated to large instrumental errors;
- the luminosity of the MS knee is strongly affected by oxygen abundance.

In the bottom part of main sequence we are approaching the regime of M dwarfs. They are faint and cold stars, dominated by molecules such as oxygen and as consequence the MS knee is not a single one. Here there is a sort of splitting with stars following parallels main sequences. Therefore stellar populations with the same age but different oxygen abundances exhibit MS knees with different luminosities, as we can see in the figure 3.15. To derive the right position of knee is quite challenging.

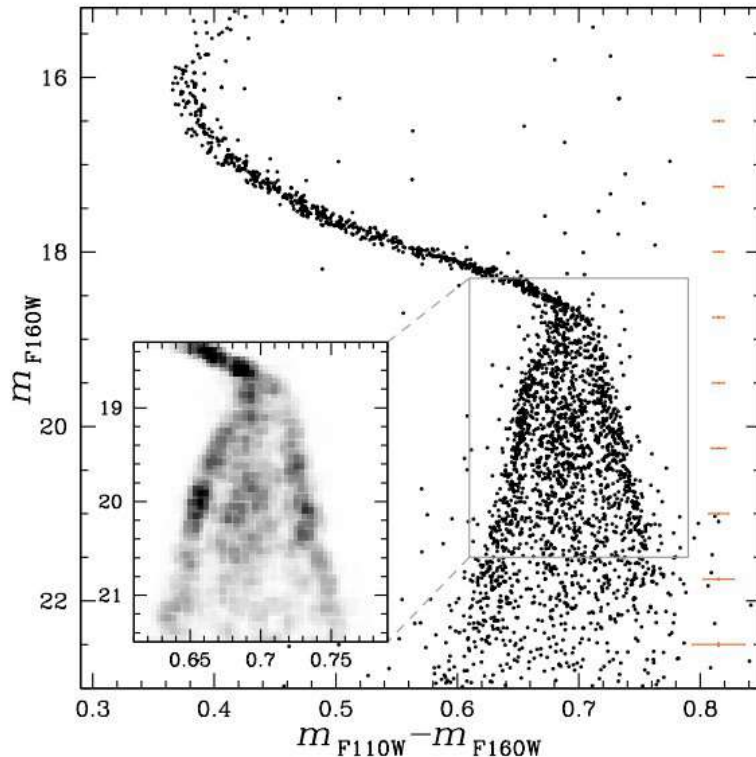


Figure 3.15: Distribution of stars in the bottom part of main sequence, according to their oxygen abundance.

3.6 Stellar parameters

From spectra we obtain many information about stellar parameters. Here there is a short summary of what we can estimate using spectroscopy.

3.6.1 Abundances

Effective temperature - T_{eff} is defined as the temperature of a black body with same luminosity and radius as the real star. The relation between dimensions and luminosity of a star and T_{eff} is:

$$L = 4\pi R^2 \sigma T_{eff}^4 \quad (3.5)$$

Surface gravity - $\log g$ is the logarithmic value of surface gravity of a star. Usually it is expressed in cgs units and as $\log_{10} g$ is given by:

$$g = MG/R^2 \quad (3.6)$$

Metallicity - As stated before, metals abundant is expressed by Z in terms of mass fraction or , in other words, by the ratio $[Fe/H]$. This is given by two different relations:

$$\begin{aligned} Z &= \frac{\text{Mass(elements heavier than He)}}{\text{Total mass}} \\ [Fe/H] &= \log \frac{(Fe/H)}{(Fe/H)_{\odot}} \\ [\alpha/Fe] &= \log[N(\alpha)/N(Fe)]_{\ast} - \log[N(\alpha)/N(Fe)]_{\odot} \end{aligned} \quad (3.7)$$

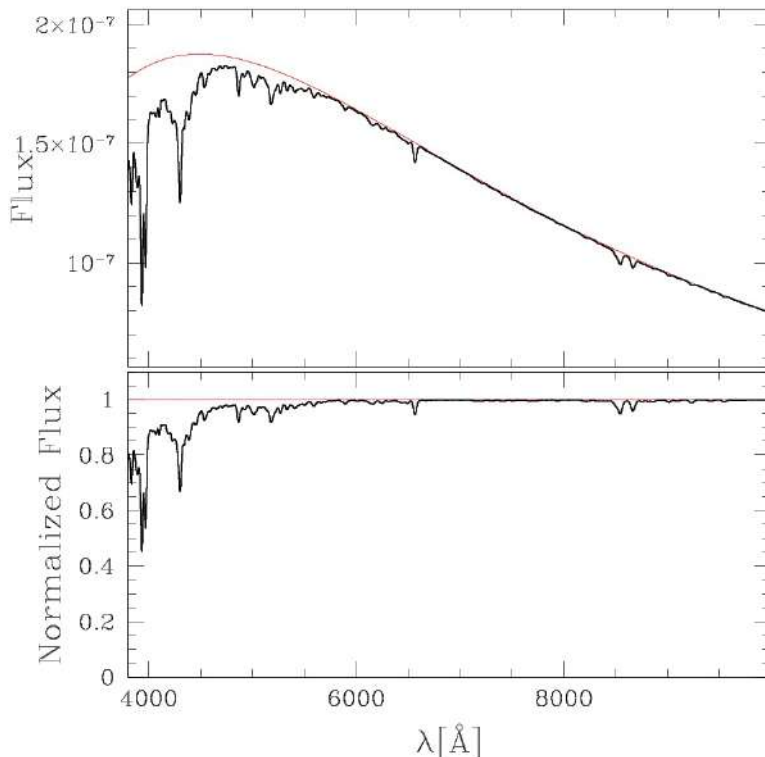


Figure 3.16: On top the Flux - wavelength, on bottom the Normalized Flux - wavelength

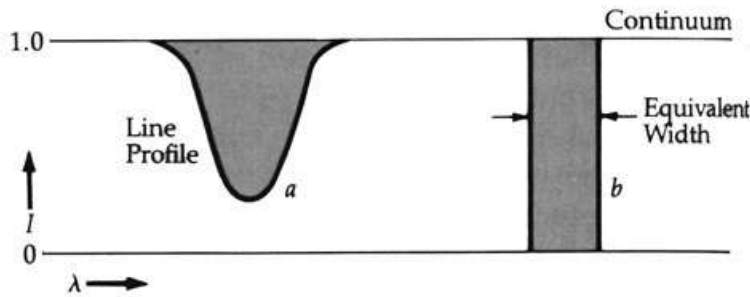


Figure 3.17: Cartoon to explain the equivalent width.

where α is an α -element, an element with an integer number of α particles in the nucleus. For example, stars having positive $[Fe/H]$ means that are super-solar in terms of iron while if it is negative, they have iron content smaller than the solar one.

3.6.2 How to measure the abundances?

We start from the spectrum, that can be represented in two ways: Flux - wavelength or Normalized Flux - wavelength.

The flux is a continuum but some flux is missing due to absorption effect. Normalizing the spectra (continuum=1) we can estimate how much flux is lost. In particular we start from measuring the **equivalent width**.

The equivalent width for an absorption/emission line is defined as the width of a rectangle whose height is equal to the height of the continuous and whose area is equal to the integrated area of the line.

This is a powerful tool indeed equivalent width is not dependent, by definition, on shape of the line (so it doesn't matter if the source is rotating) or on the instrumentation used for observations. The equivalent width indicates the strength of a line. An useful tool to get the abundances is the **curve**

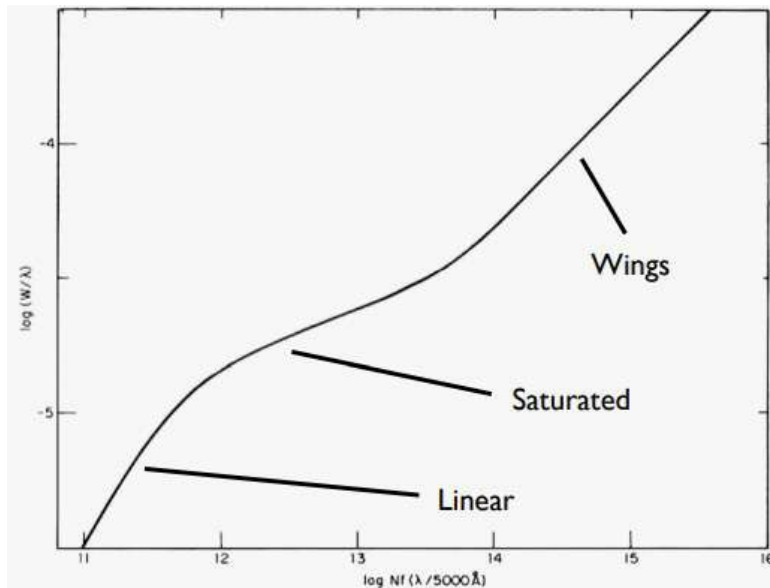


Figure 3.18: Curve of growth.

of growth, that describes the equivalent width of a spectral line as a function of the column density of the material from which the spectral line is observed.

In figure 3.18 we can see a model of curve of growth, used to infer the abundance of the gas making up the stellar atmosphere. It is easy to observe that the curve of grow has different slopes. Indeed we can distinguish three regimes:

- **Weak lines** where $W \propto A$ (equivalent width is proportional to the abundance): it is the linear part where the Doppler core dominates and the width is set by the thermal broadening $\Delta\lambda_D$. Depth of the line grows linearly with the abundance A .
- **Saturation** where $W \propto \sqrt{\log A}$: It is a plateau in which Doppler core approaches maximum value and line saturates towards a constant value. In case of saturation it is quite difficult to infer abundances due to a logarithmic proportion.
- **Strong lines** where $W \propto \sqrt{A}$: Here wings dominate and optical depth in wings becomes significant strength depends on g .

In figure 3.19 we can see the three regimes of the curve of growth and how lines becomes deeper due to absorption processes.

Obviously, one only gets the abundance of the particular ionization state and excitation level that produces the line. The Boltzmann and Saha equations need to be applied then and the pressure and the temperature of the gas known to derive an abundance of the element (i.e. of all ionization states and excitation levels).

3.6.3 Determining of the effective temperature

To determine the effective temperature, usually we start considering an element that is quite common. For example, if we study stars of red giant branch or old stellar populations, we use the iron, which is independent of the excitation potential (χ_{exc}) of the individual lines, in standard conditions.

We analyse many lines of a single element, sampling a range of χ_{exc} on x-axis and excitation potential on y-axis.

Final precision depends on spectral resolution, choice and number of lines and S/N ratios.

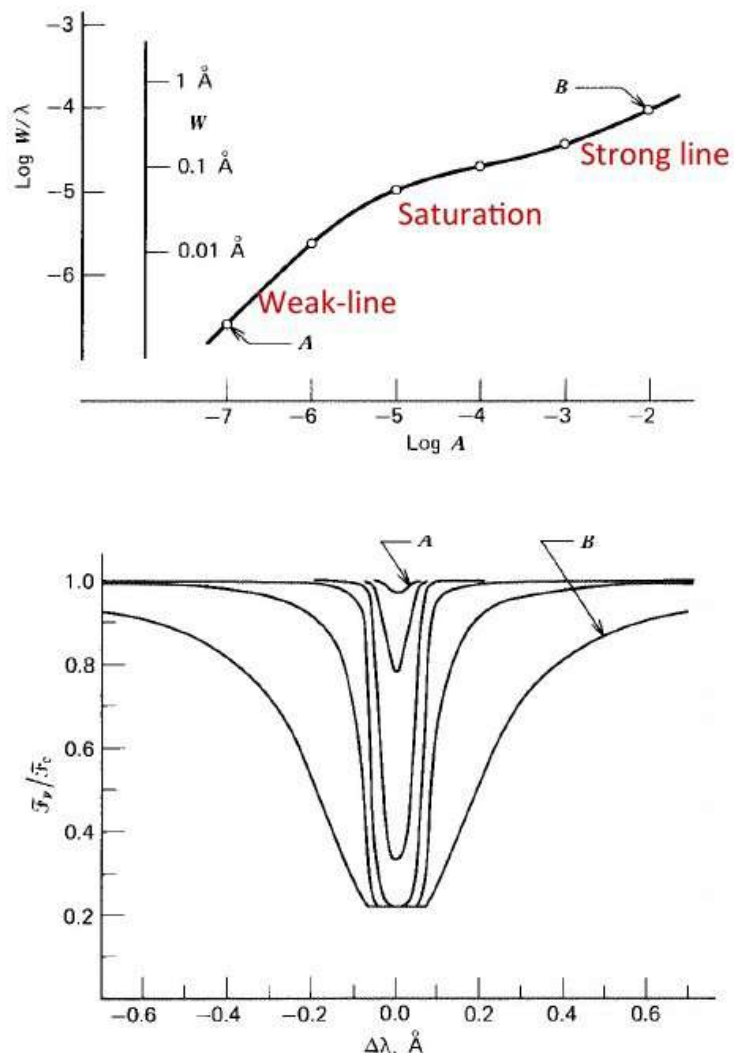


Figure 3.19: Curve of growth divided in the three regions.

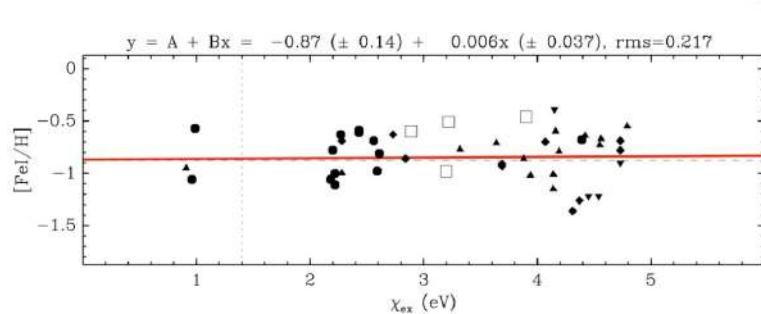


Figure 3.20: Plot of iron abundance as function of excitation potential.

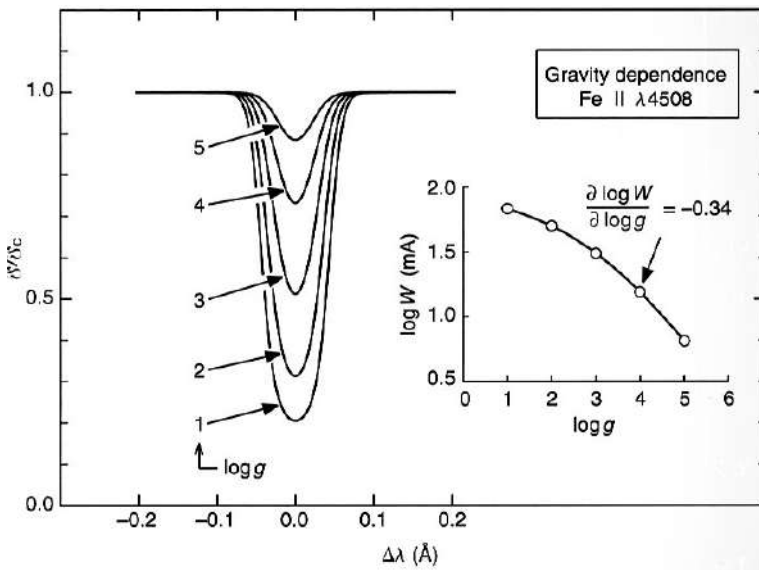


Figure 3.21: From the image it is clear that there is a dependence of lines on the gravity of star.

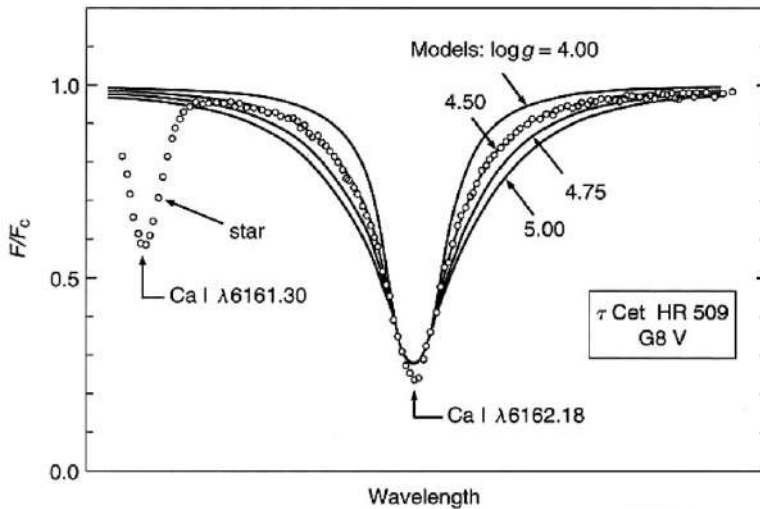


Figure 3.22: A strong line compared to many model for different value of $\log(g)$.

3.6.4 Determining of the surface gravity

Lines of different ionization stages (e.g. FeI, FeII) have different sensitivity to $\log(g)$. Indeed, by definition, gravity is related to $P_g \propto g^{2/3}$ and $P_e \propto g^{1/3}$.

For example in cool stars:

- FeI is the dominant species: as g increases the W_λ (equivalent width) remains constant.
- FeII is the minority species: g increases as W_λ decreases.

We can see this effect in the figure 3.21; as $\log(g)$ increases the line becomes fainter.

As a consequence, $\log(g)$ can be obtained by enforcing the same abundance obtained from different ionization stages.

Another method to derive $\log(g)$ is using the **Strong lines**, that are characterized by wings. The wings of strong lines can depend on the atmospheric pressure and thus on the surface gravity $\log(g)$.

Note that the strength of wings depends also on effective temperature and on the abundance.

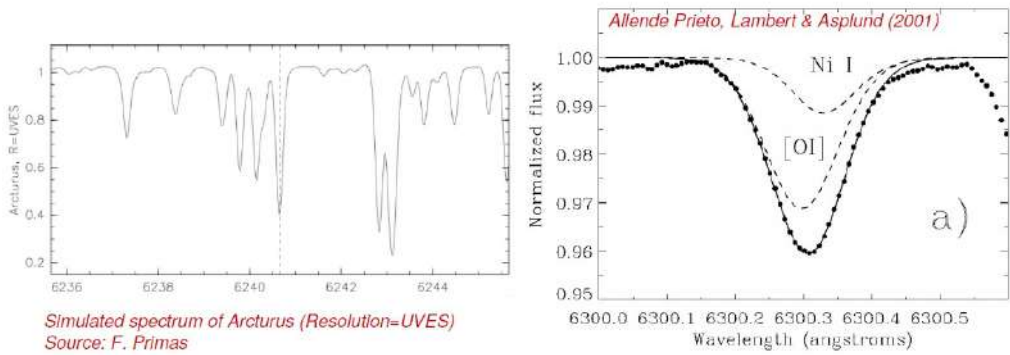


Figure 3.23: On left a synthetic spectrum, on right a fit of two crowded lines.

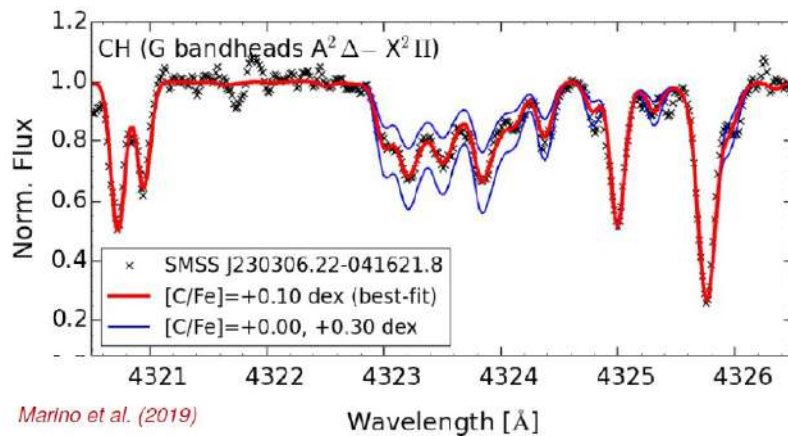


Figure 3.24: Comparison between the observed spectrum and many synthetic spectra. In particular we can see that the spectrum is not sensible to carbon abundance in all part of spectrum. In the first part of the spectrum, there are no features dependent on carbon abundance: the simulated spectra is the same regardless the abundance of carbon. Instead the second part is very sensitive to abundance of carbon.

3.7 Spectral synthesis

In real life, spectra are affected by crowding and blends. Most of the lines are not individual but there are inside forests of different lines. These represent major challenges for equivalent width determination.

To resolve this problem, an important step is to calculate the **synthetic spectra** to use in the fitting. Elemental abundances are often inferred by comparing the observed spectra with grids of simulated spectra with different chemical composition.

In figure 3.24 we can see the process of fitting to derive the elemental abundances. In this case a full spectral synthesis is required.

3.7.1 The Uncertainties in parameters

Uncertainties on parameters are given by the instrumentation, by signal/noise ratio of images, by the resolution and so on. The typical uncertainties in the estimated stellar parameters for late-type stars are:

- $T_{eff} \sim 100 - 300K$ (absolute error)
 $T_{eff} \sim 10 - 50K$ (relative error)
- $\log(g) \sim 0.1 - 0.3dex$ (strong lines)
 $\log(g) \sim 0.1 - 1.0dex$ (ionization balance)

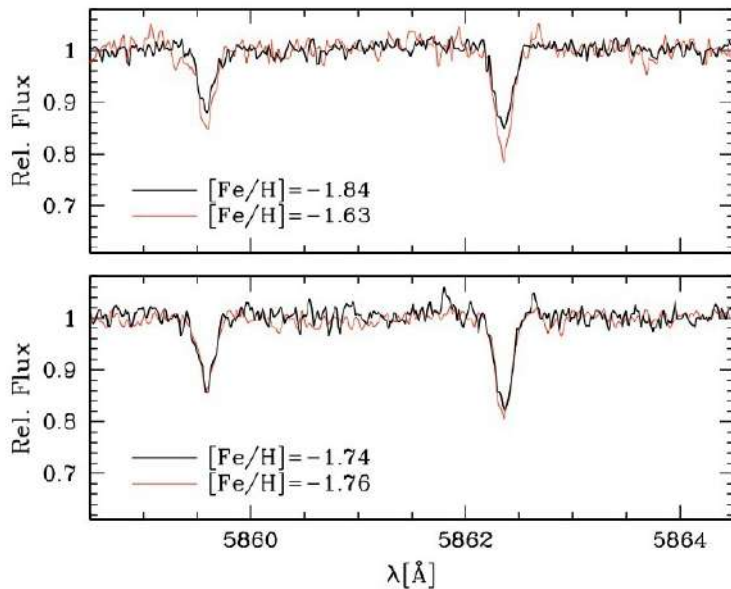


Figure 3.25: Spectra of two couple of stars in the Globular Cluster M22 with similar atmospheric parameters. Marino et al. (2009)

- $[Fe/H] \sim 0.1 - 0.5dex$

Uncertainties are larger for giant and metal-poor stars then for the Sun. In general, all methods have at least a minor dependence also on the other parameters. An iterative procedure to determine the stellar parameters is therefore necessary.

3.7.2 Relative abundances

The comparison between spectra of stars with the same atmospheric parameters allows us to detect very-small abundance differences that are not detectable in absolute terms.

In this way we clearly see these tiny differences, not observable in a classical spectra. This is a fundamental and powerful tool to study two important astrophysical open issues: the Lithium cosmology problem (discrepancy between content observed and the value predicted by the theory) and the research of extrasolar planets.

3.8 Relative abundances: An application on exoplanets

There are some techniques to detect an exoplanet:

- Direct imaging: the simplest method bot also one of the most difficult to use due the magnitude difference between star and exoplanet.
- Radial velocity: the most used method, it is an indirect method based on the measurements of the radial velocity. Indeed the star moves around the barycenter of the system exoplanet-star, so, from the radial velocity we are able to obtain mainly the mass of the planet.
- Transit: Another most used method based on the detection of the transit of the planet in front of the star. Measuring the depth due the transit we are able to obtain the radius of the planet.
- Microlensing.
- Pulsar timing.

All those technique are very powerful but they are very time consuming and we can apply them only for single stars. Maybe we can use the relative abundances to detect extrasolar planets around stars, analysing their spectra and comparing them with others similar ones. In particular it is known that

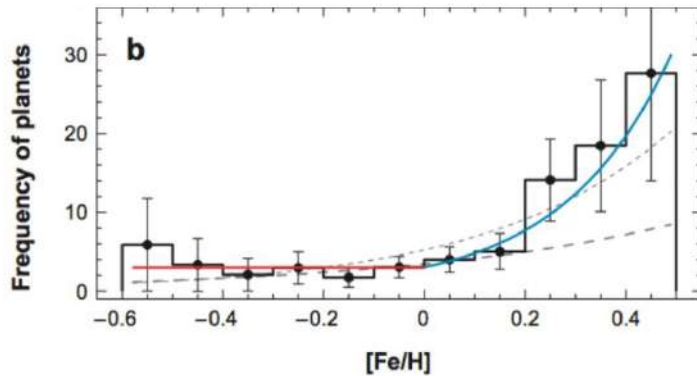


Figure 3.26: Gonzales et al. 1997

planets hosted are more metal-rich than average (e.g. Gonzales et al. 1997). To be more specific, as shown in figure 3.27, the frequency of stars hosting planets increases with the metallicity of the hosting star.

To be more specific, in figure 3.27 we can see that the peak is shifted to right, that correspond to a more rich population. There are three possible explanations for this:

- dependence on richer metallicity of the primordial cloud that formed the system. In this scenario, higher is the metallicity of primordial cloud, then higher is the dust/gas ratio in the protoplanetary disk. Higher is this ratio, higher is the condensation of solids that accelerates the formation of planets before the gas is lost;
- self-enrichment;
- a different galactic origin of stars hosting planets.

Melendez et al. in 2009 studied 11 solar twins using high resolution spectroscopy. Solar twins means stars very close to Sun in terms of parameters like effective temperature, surface gravity, evolutionary stage and abundances.

In figure 3.28 we can see these solar twins, whose parameters must satisfy this conditions, with respect to the Sun:

- $R = 65,000$
- $S/N \sim 450$
- $\Delta T_{eff} < 75K$
- $\Delta \log(g) < 0.1$
- $\Delta [Fe/H] < 0.1$

In figure 3.29 we can see the impressive result of the work of Melendez et al. Indeed the precision in stellar spectroscopy is better than 0.01 dex in $[X/Fe]$ and $[X/H]$. In this graph the relative abundances of the star is plotted against the atomic number. It is clear that the data does not follow a trend.

However, when we plot the relative abundances against the temperature of condensation we obtain the diagram in figure 3.30 that show a trend! This means that there is a highly-significant correlation with condensation temperature. From this figure it is clear that elements that easily form dust (with high condensation temperature, i.e., refractories) are under abundant in the Sun. So, the result is that the Sun is unusual!

The explanation: in the Sun planet formation locked up refractories but less of volatiles during the accretion phase. In the solar twins there was less planet formation and thus more refractories than Sun.

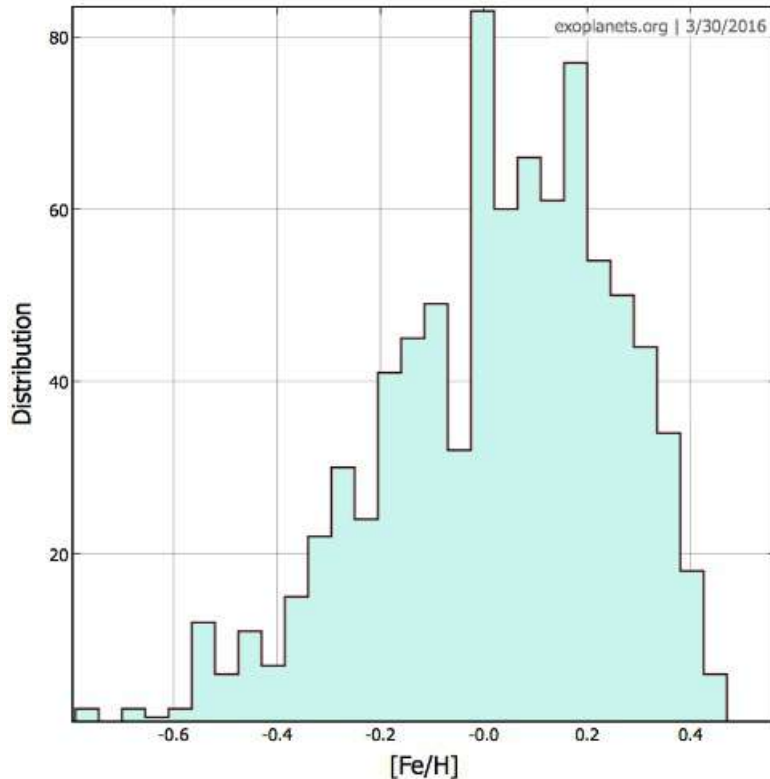


Figure 3.27: Relation between the frequency of discovered planet and the metallicity. The peak of the planets is a bit super solar.

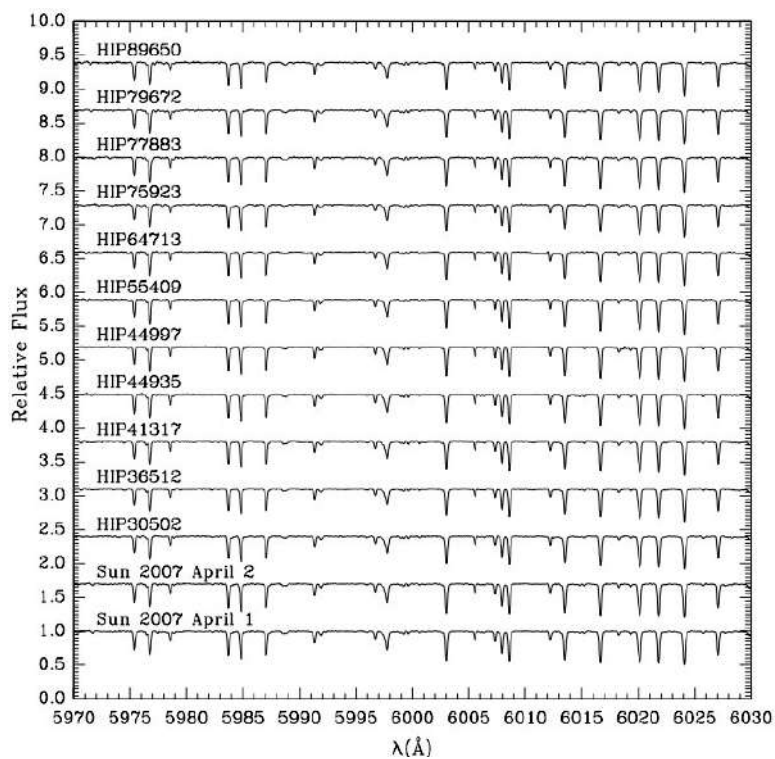


Figure 3.28: 11 twins solar from Melendez et al. (2009)

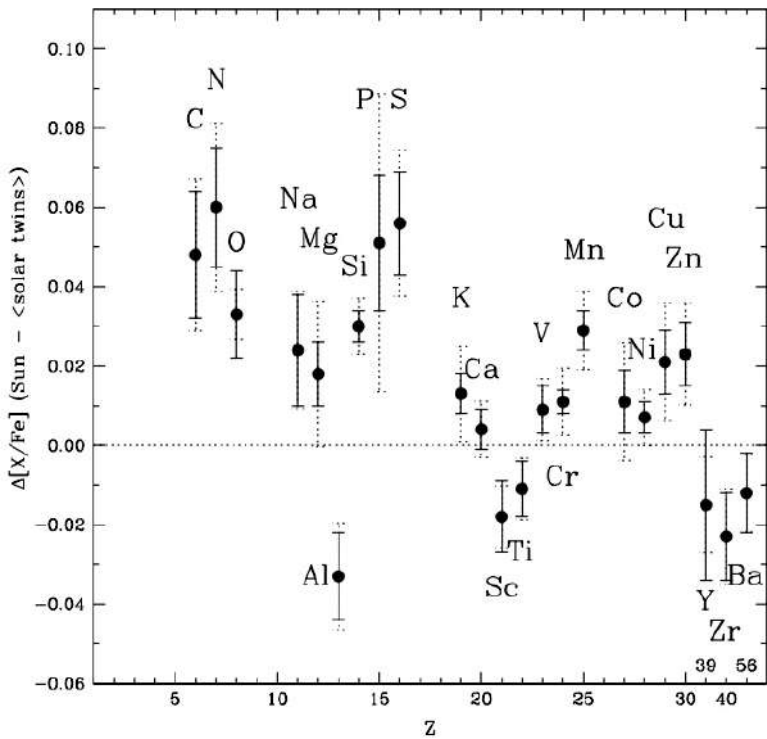


Figure 3.29: In this diagram are related the relative abundances with the atomic number. This graph shows the high resolution of the data in the work of Melendez et al. (2009).

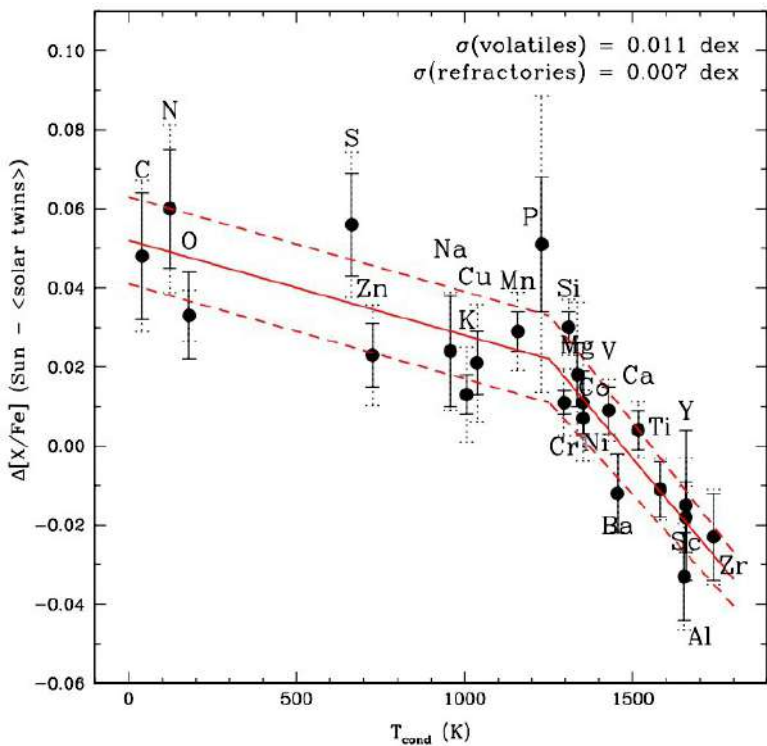
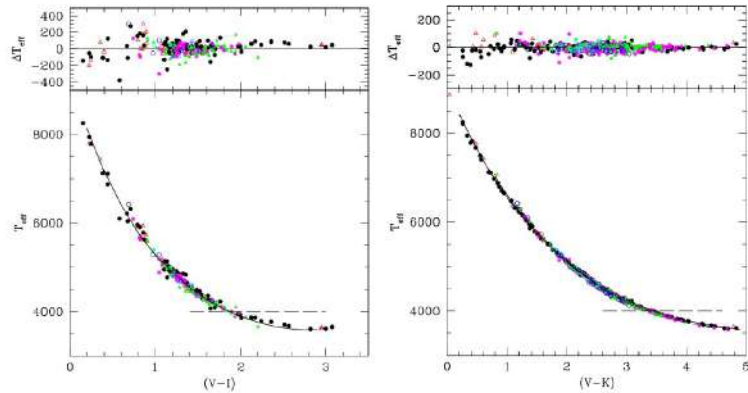


Figure 3.30: The Abundances against the temperature of condensation.

Figure 3.31: Empirical T_{eff} -color relations.

3.9 Stellar parameters: the photometry approach

In the previous sections we saw what and how stellar parameters can be provided by spectroscopy. Spectroscopy is a powerful tool but it is limited to bright stars and it is time consuming, observing each star one by one and this is not good if we are interested in a wide stellar populations. In addition it is necessary the presence of lines with different exitational potential. For example, if the star is very hot, there are few iron spectral lines visible. Eventually the spectrograph is limited in a short wavelength range in which there are no enough lines to properly constrain abundance and atmospheric parameters. However stellar parameters can be obtained also using photometry, applicable to a large number of sources, also the faint ones, even thought less precision, sometimes. For example, using the multi band photometry (combing images in different filter, so taken in different wavelength band) we can get also the atmospheric parameters. The most common multi band photometry is the RGB that stands for Red, Green and Blue images. They are images taken at red wavelength, at blue wavelength and at intermediate wavelength.

To be more specific, stellar parameters and in particular effective temperatures can be obtained by using stellar colours. To get the maximum leverage the two wavelength regions should be well separated in wavelength.

The first thing to do is to find calibration between colors and stellar parameters using samples of stars that are well investigated by other techniques, for example spectroscopy. Then, the same stars can be observed using photometry and we can get the color. After that, it is possible to plot the effective temperature as function of color. From those graphics, it is clear that there is an empirical relation between effective temperature and color.

In the figure 3.31 we can see the empirical relations, in particular in the plot the colors used are $V - I$ and $V - K$; the second is a wider baseline filter so the sensibility of relation is higher because two filter are more distance so we can a more sensitive slope. In this case the scatter of points is lower.

Actually there is a second order effect: the relation depends also on metallicity. This is particularly true for $B - V$ color while is less prominent in the other bands. This means that it is necessary also to know the metallicity and not only the color, to obtain the T_{eff} .

An advantage is that stellar colors are quantities independent from the distance but a disadvantage is that color is, of course, affected by reddening, the absorption effect due to interstellar medium. The reddening is different according to the wavelength (bigger in the blue side of the spectrum and smaller on the red side, according to the Withford law). Moreover, the reddening can be differential, which means that it is different according to the region of the sky we are observing. For all those reasons, correction of magnitudes by reddening is fundamental.

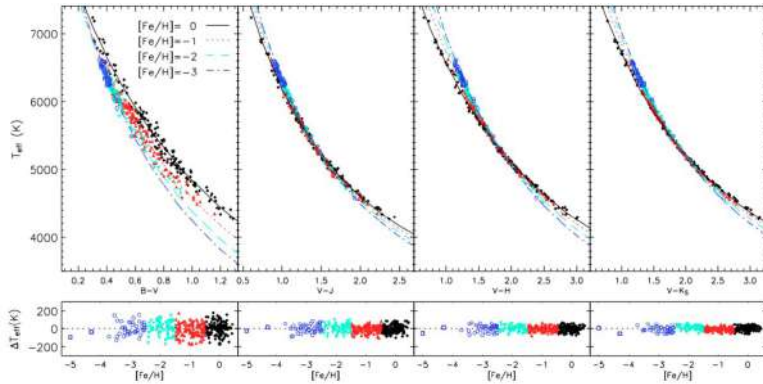


Figure 3.32: The relation change with the metallicity of the stars.

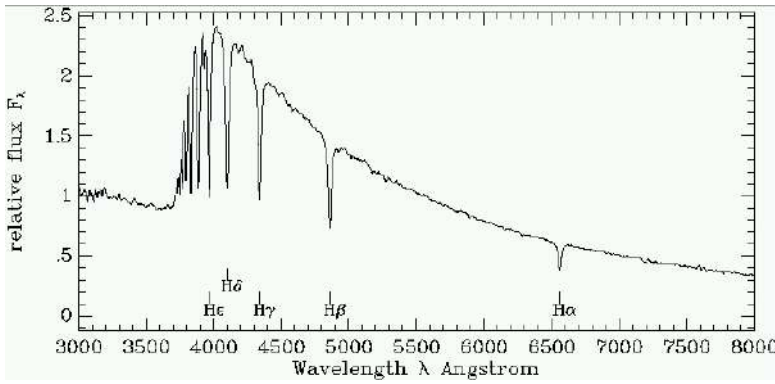


Figure 3.33: A spectrum of a star in which we can see the Balmer jump.

3.9.1 Opacity

Opacity, κ , indicates the ability of stellar matter to absorb radiation (energy transport equation). Of course, we need to consider all microscopic processes that can absorb photons at each frequency, ν : Bound-bound absorption (bb), Bound-free absorption (bf), Free-free absorption (ff), Electron scatter (es). All those processes can cause absorption.

In particular the opacity in stellar interiors depends on:

- **Level populations** of different ion species (dependence on T - Boltzmann equation- and on the degree of ionisation).
- **Ionization balance** (dependence on electron density and T , -Saha equation-)
- Electron density (dependence on density, ρ , on T and local composition, χ_i).

In summary:

$$\kappa_\nu = \kappa_\nu(\rho, T, \chi_i) \quad (3.8)$$

The opacity changes with wavelength, but in particular changes significantly when we approach to the Balmer jump.

3.9.2 Balmer jump

For wavelength $< 365 \text{ nm}$ photoionization from the level $n = 2$ of $H I$ can occur. The corresponding increase in opacity diminishes the emergent flux shortward of 365 nm : this is the Balmer jump.

In particular, in hot stars the Balmer jump depends only on the effective temperature while in solar type stars the Balmer jump also depends on gravity (the structure of bump and the flux are different).

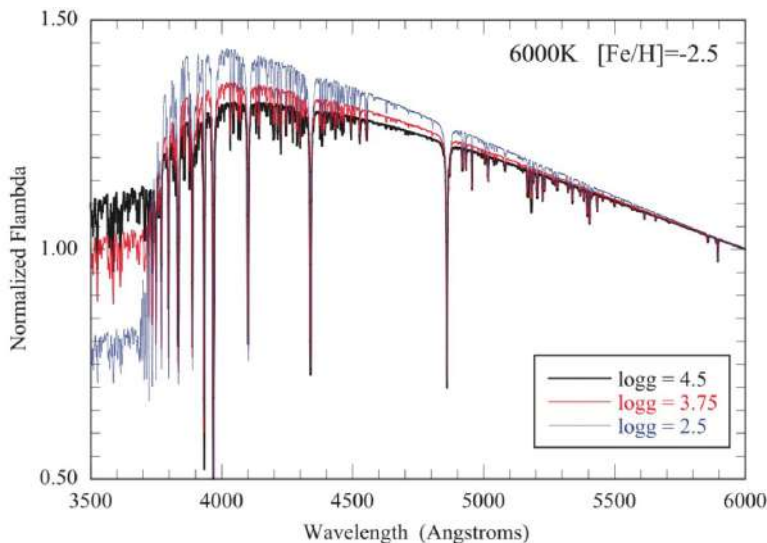


Figure 3.34: This diagram shows how change the Balmer jump as gravity increases.

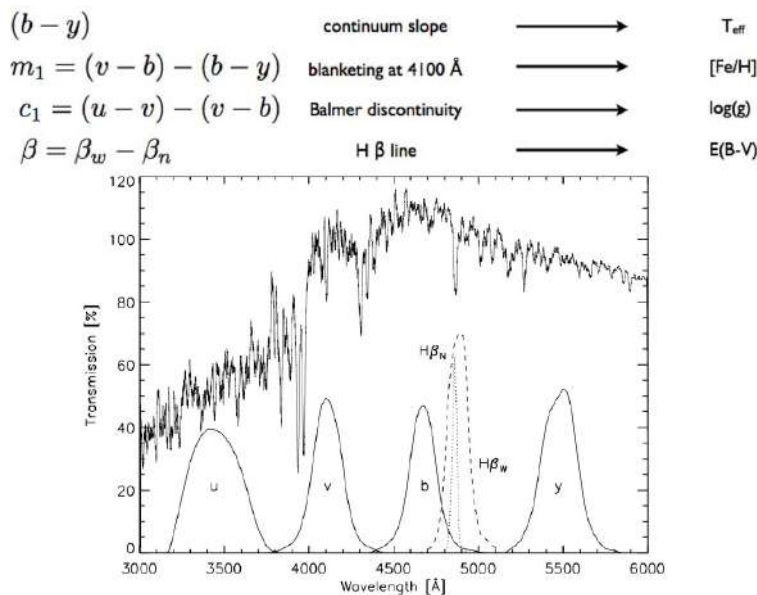


Figure 3.35: The Stroemgren photometric system.

3.9.3 Stroemgren photometry

What we can do is to built a system of filter not randomly distributes along the spectrum but organized in specific regions of the spectra to maximise the sensitivity to atmospheric parameters. This clever photometric system is the Stroemgren one.

In figure 3.35 is shown the system, that is composed by 6 filters: u , b , v , y , $H\beta_N$ and $H\beta_W$. The last two filters are either centered at the $H\beta$ line, but one is wide and the other is narrow. The wide get photons from line and from continuum, the narrow only by the line. Instead u and b and v do not correspond to the classic Johnson system (u is centered around 3500, v around 4000 and y around 4600).

Combinations of these filters could be used to get the atmospheric parameters.

- $(b - y)$ is sensitive to the slope of the continuum (slope of the black body) so can be used to derive the effective temperature.
- A combination of b , v and u filters can be used to fit the Balmer discontinuity and derive the surface gravity. In this case we refer to $c_1 = (u - v) - (v - b)$.

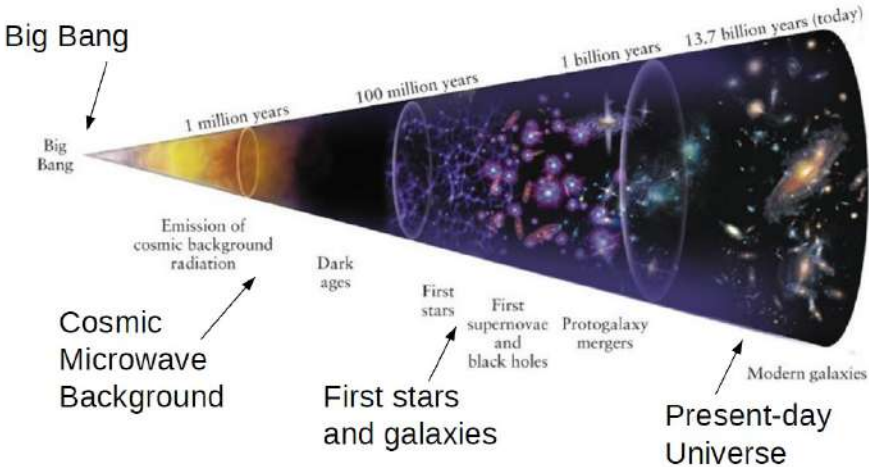


Figure 3.36: Cartoon that shows the evolution of the universe.

- A combinations between b , v and y , related to the blanketing effect at 4100 angstrom, can be used to infer the metallicity $[Fe/H]$. In this case we refer to $m_1 = (v - b) - (b - y)$.
- The difference between the $H\beta_N$ and $H\beta_W$ can be used to derive the relative magnitude between the line and the continuum, a quantity that is sensible to the reddening. In this case we refer to $\beta = \beta_w - \beta_n$ to derive $E(B - V)$.

3.9.4 Infrared flux method (IFRM)

Another and a bit sophisticated method is the Infrared Flux Method (IFRM). It is based on the comparison between the monochromatic flux in the IR with the bolometric flux. For this method it is valid the empirical equation:

$$\frac{F_{Bol}(Earth)}{F_{IR}(Earth)} = \frac{\sigma T_{eff}^4}{F_{IR}(Model)} \quad (3.9)$$

where bolometric flux is estimated. In general we compare observations and models looking for the best fit and from this method we are able to obtain a lot of information. For example, the IFRM allows to measure stellar angular diameters with accuracy better than 2% indeed:

$$\int_0^\infty F_\nu^{Earth} d\nu = \left(\frac{R_*}{r} \right)^2 \sigma T_{eff}^4 \quad (3.10)$$

for which:

$$\theta_D = \frac{R_*}{r} / 107.5 \quad (3.11)$$

where θ_D is measured from interferometry.

3.10 The Lithium cosmological problem

According to the big bang model, astronomers have predicted the amount of chemical abundances of elements that have been formed in the early universe. They inferred also the Lithium abundant, which formed in the primordial universe together with H and He .

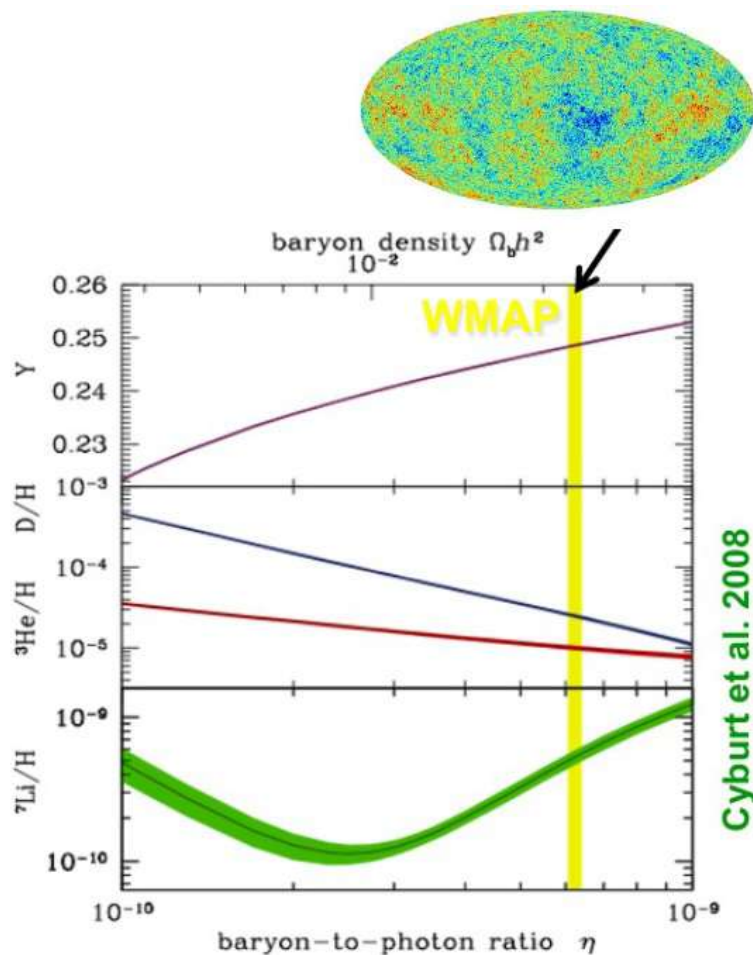


Figure 3.37: A model that predict the abundances of many elements as function of the value of barion-to-photon ratio.

Hydrogen, helium and lithium, were produced during the Big Bang nucleosynthesis (BBNS), when the universe was only a few minutes old.

Cosmic Microwave Background (CMB) anisotropies yield barion-to-photon ratio at decoupling. This map is fundamental to analyse structures and distribution of matter inside the universe. In particular, to prove the theory we want to derive the lithium abundance.

3.10.1 The value from the model

Using the anisotropies of CMB we can derive the barion-to-photon ratio and with the model in figure 3.37 we can derive the abundances of the pristine elements.

Results based on WMAP data conclude that the lithium abundance from Big-Bang nucleosynthesis is $[A(\text{Li})] = 2.7 \pm 0.06$ (Dunkley et al. 2009).

The point is that the production of Li depends on the temperatures and densities of the primordial Universe. From WMAP model basically we are able to infer mean density of baryon and temperature of the universe. So, if the big bang model is physically correct, we should be able to confirm the previous value of Li content.

3.10.2 The value observed

However derive Lithium in stars is quite challenging. Indeed Lithium in stars is readily consumed by fusion with protons at temperatures above $2 \times 10^6 \text{ K}$, such as is found in the cores of stars. For example, if the star is too massive, Li is destroyed in the core and if a star is metal rich they involve

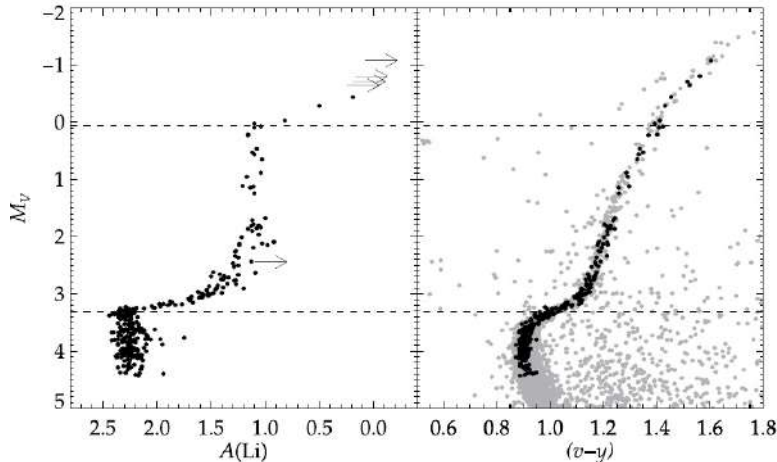


Figure 3.38: Results of NLTE analysis.

Li in many processes. On the other side, Lithium can be produced in interstellar matter by collisions with cosmic rays, or by the evolution of intermediate-mass Stars.

For those reasons, the ideal candidate to estimate abundance of primordial Lithium are old metal poor stars. The best approximation of stellar population that has pristine chemical composition are GC very metal poor with stars not evolved and not too distant in order to take spectra of single stars.

For example, the nearby and metal-poor globular cluster NGC6397 is an ideal object to investigate the cosmological lithium problem.

Homogeneous analysis of 349 MS, SGB, RGB stars from UVES/GIRAFFE VLT spectra are used in a huge work to derive the abundance. To do this research they used very high quality data and this is clear observing each spectra, able to detect the *Li* lines which are usually quite faint.

The result of this work is shown in figure 3.38. In the diagram are shown the stars used to derive the abundance. In the panel on right there is the CMD while in the panel on left it is shown the abundance of lithium as function of absolute magnitude. On this second graphic, we have un-evolved stars with *Li* abundance constant. Then there is a sort of drop in terms of *Li* content due to mixing processes from the interior. Indeed the material of interior has no *Li* so, as result of mixing phase, the abundance of *Li* drops from 2.3 to 1. A second similar phenomena is shown a second time, due to the evolutionary stage of the stars.

So what about the abundance of *Li* of un-evolved stars? There is a discrepancy with the model! In figure 3.39 is shown the discrepancy with BNN Discrepancy with BNN+WMAP predictions.

There can be many possibilities to explain this discrepancy between observational results and the theory. Maybe there is somethings wrong in our knowledge in stellar evolution. Someone built also diffusion and ad-hoc turbulence below the convective zone to reproduce the observations.

The baseline of the lithium abundance of old stars (or Spite Plateau) in the Galactic Halo is significantly lower than what is inferred from WMAP + Big-Bang Synthesis.

This fact is challenging our understanding both of stellar astrophysics and possibly even Big Bang nucleosynthesis itself.

Astronomers think that the solution can be find in the Stellar *Li* depletion while standard stellar evolution models for Sun and metal-poor turn-off stars do not predict appreciable Li depletion. Maybe there is an extra mixing due to rotation, diffusion or gravity waves. Another explanation, but quite speculative and not credible, can be something wrong in particle physics or nuclear physics in BBNS. Maybe stellar scale for T_{eff} is not correct or maybe there are some missing information about stellar structure and stellar evolution.

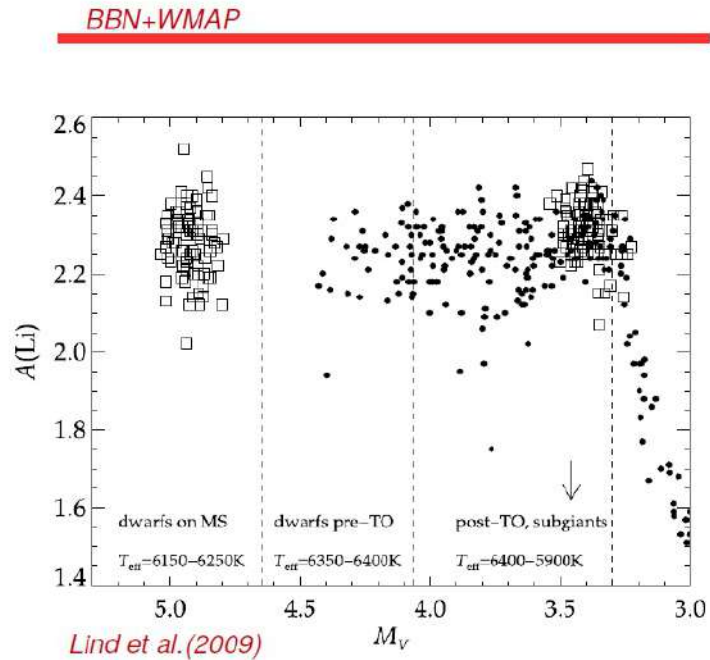


Figure 3.39: Discrepancy with BNN+WMAP predictions. It is quite clear the presence of a sort of plateau under the line suggested by model.

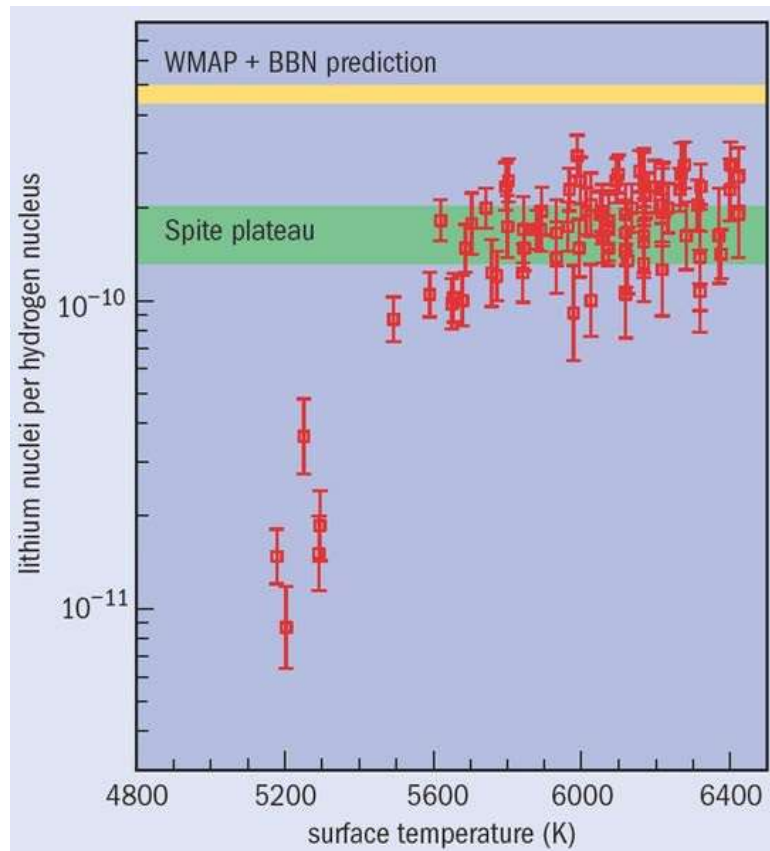


Figure 3.40: Discrepancy with BNN+WMAP predictions: in this plot the observation is based on stars in the galactic halo.

Chapter 4

Differential reddening

In the figure 4.1 on the left panel we observe a very complex stellar system indeed there are many samples of distinct stellar population. From this figure we can obtain a lot of information. Of course we need to be sure that features we observe are real.

On the other side, we can see that in the right panel there is a very strange CMD; there are some peculiar features. One possibility can be the presence of multi stellar population, another possibility can be that the cluster is affected by differential reddening. The first is a real and physical features that corresponds to presence of some crazy stellar population. The second possibility is an unreal features because is due to reddening process. The latter case needs the presence of some cloud in front of the cluster that absorb the radiation in different way across the field of view and different for each point of the sky.

4.1 Extinction

Interstellar space is permeated by interstellar medium (ISM). ISM is composed of gas and dust. The first tends to absorb and radiate at different directions, the second tends to scatter the radiation.

The main problem is that extinction is not uniform along the spectrum because varies as in the visible part of the spectrum. Recall the Whitford law: $A_\lambda = 1/\lambda$, so the extinction is more in the blue part than in the red part of the spectrum. In figure 4.3 we can see that an image in the visible shows a black region due the presence of gas, if we use the IR filters the black region is neglected. The stars behind the cloud are visible only in the red filters. As a consequence, the objects appear redder than they really are.

The change in apparent magnitude at wavelength λ due to extinction is:

$$\begin{aligned} m_\lambda - m_{0,\lambda} &= -2.5 \cdot \log(e^{-\tau}) \\ &= 2.5 \cdot \tau_\lambda \log(e) = 1.086 \cdot \tau_\lambda \end{aligned} \tag{4.1}$$

A spectrum affected by extinction shows that the red part is more or less the same, the blue part is drastically reduced, as consequence we see a shift of the emission peak. The absorption lines are not affected by extinction, their are always visible. In general a reddened spectrum appears like a spectrum of an advanced stellar type (for example a spectrum of F star becomes similar to the spectrum of G star).

The extinction law is derived empirically: A_λ/A_V is the absorption coefficient, normalised to the value in the visual band, and the wavelength. The difference $A_B - A_V$ is indicated as $E(B - V)$ and the ratio $A_V/E(B - V)$ is denoted as R_V . In figure 4.4 we can see the empirical plot and the different

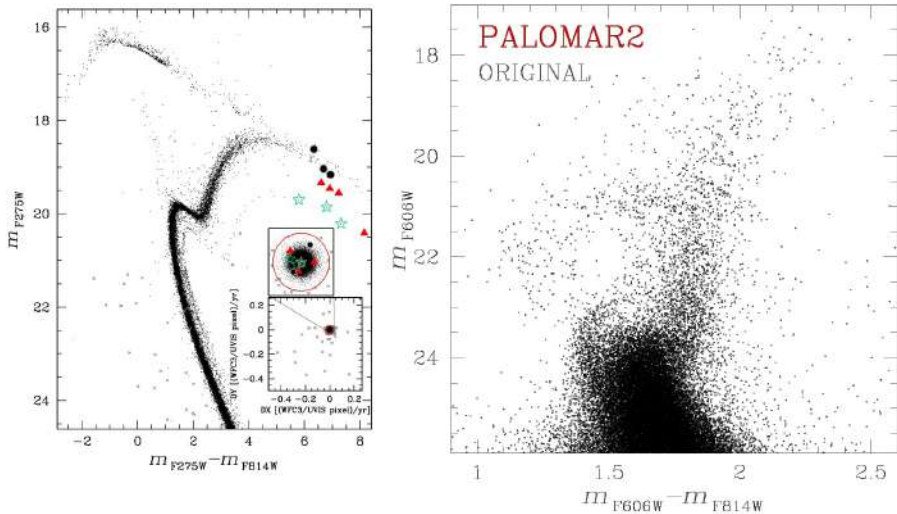


Figure 4.1: In the picture there are two different CMD. On right the CMD of a globular cluster that shows a probably second population, parallel to the main path. On left there is a very strange CMD.

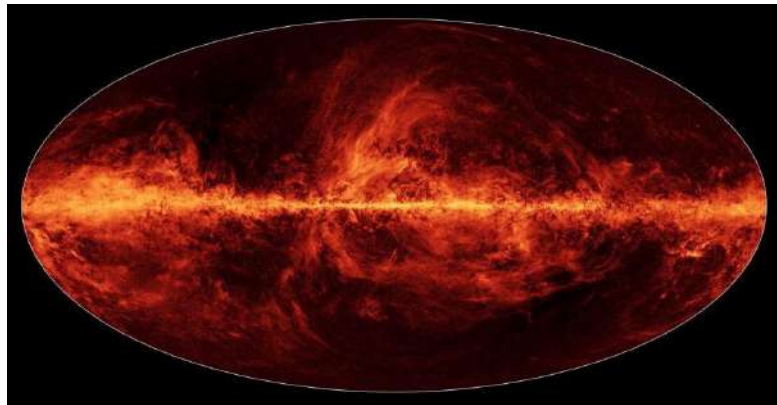


Figure 4.2: The reddening map of the Galaxy. The density of matter is different in each point of the map. In general absorption effect is bigger along the disk, where is concentrated the interstellar material, and lower perpendicularly to the disk.

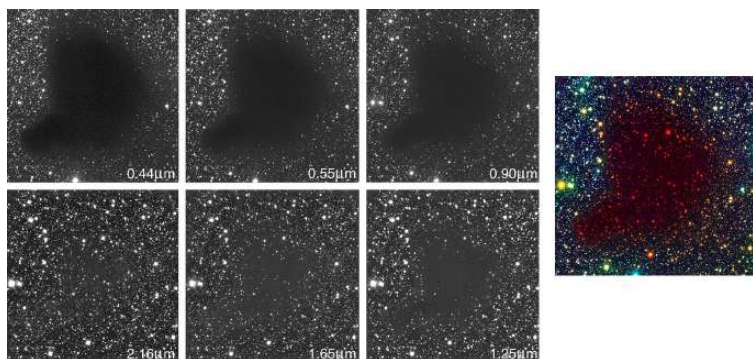
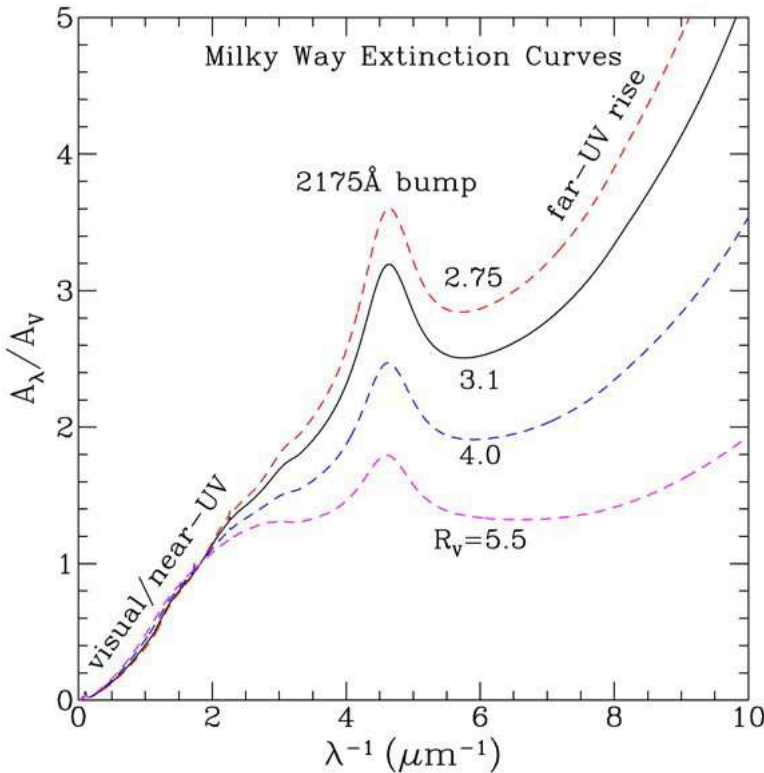


Figure 4.3: Same field of view in different filters.

Figure 4.4: The extinction law according to R_V ratio.

shapes that depends on the value of the R_V coefficient. Accepted values of R_V range from 3.1 to 3.3, although in peculiar directions it could be different. It changes dramatically in specific environment, along the galactic disk, or also observing other galaxies, also at high redshift. Determination of the reddening effect is therefore fundamental.

4.2 Schlegel reddening maps

Schlegel et al. (1998) combined the strengths of IRAS and COBE/DIRBE to create a relatively high resolution ($\sim 6 \times 6$ arc-minute, this means that the resolution is less than field of view of HST) 100-micron intensity map of the entire sky. These maps are one of the most-used tools by astronomers. We can use it to derive the average reddening value in a certain region of the sky to have less free parameters during the fitting of isochrones. In the fitting of isochrones the value of reddening that we can derive from the map is a first guess. Remember that the resolution of the Schlegel map is not high compared to the HST field of view so can get an average value for all stars in the field and we are not able to obtain different values for in the same field.

Astronomers used the far-infrared intensity ratio of $100 \mu\text{m}$ and $240 \mu\text{m}$ to measure the dust temperature and thereby trace the $100 \mu\text{m}$ dust column density (thanks to the model). The method is most accurate when a single dust temperature adequately describes the bulk of the dust that is absorbing/scattering background starlight. These conditions are not present for high reddening. Instead, when there is the presence of complex structures, this method can provide only an average, useful observing wide field but not in the case of very small field, like one of HST. Indeed this method is useful if there is only a one cloud. If we have many clouds the situation is more complex and this method is not very accurate.

4.3 The RGB bump

The density of stars is not constant everywhere along the path. The number of stars per equal magnitudes decreases from faint magnitudes to bright magnitudes. The time stranded by stars to

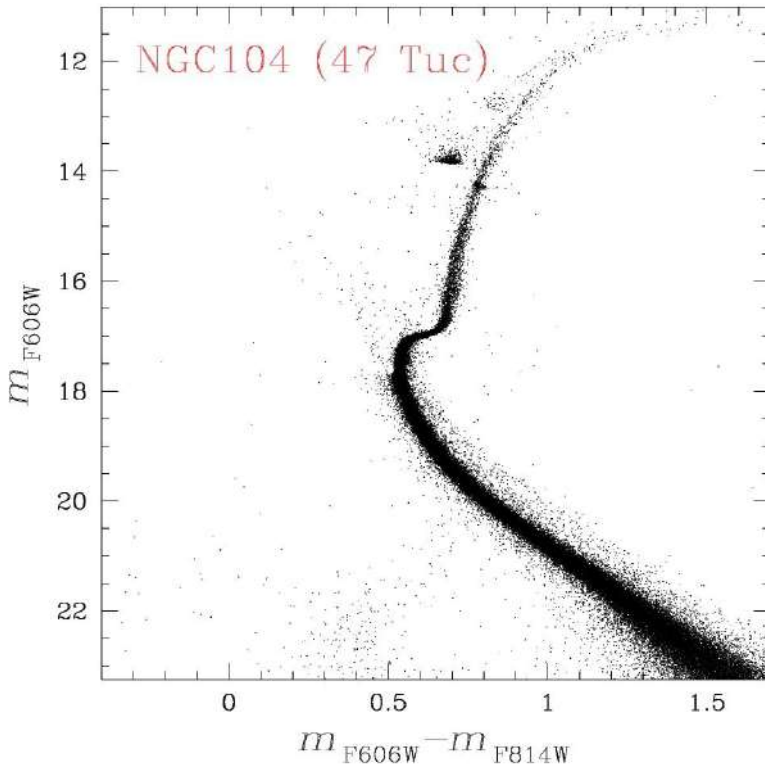


Figure 4.5: CMD of 47Tuc.

populate a given region of the diagram decreases with luminosity. As consequences, we have a lot of stars in the bottom of the RGB and less in the top region of the RGB. There is a point in the RGB where the density is higher than the near region, this is due the **RGB bump**.

In the figure 4.6 we can see that the density in that zone is higher. The RGB bump appears as a clump of stars along the RGB. It is well recognisable as an excess in the luminosity function of RGB stars.

The cause of this overpopulated zone can be explained if we consider the evolutionary path of a RGB star. What, that happens, is the following: during the ascent of the RGB the H-burning shell of a star steadily moves outward. Thereby the shell approaches the chemical discontinuity left behind by the first dredge up¹. The increase in opacity due to the larger hydrogen abundance just above the shell causes a temporary drop in the stellar luminosity. Once the shell has gone through the discontinuity, the luminosity starts again to grow monotonically. So, star passes through the same magnitude three times.

The RGB bump is produced by three-fold passage of the RGB stars through the same interval during their evolution. The position of the bump depends on the amount of helium, that is shown in the figure 4.7.

4.4 The red clump

One the other side, the **red clump** (RC) is a clustering of red giants in the CMD. RC stars are bluer (hotter) than RGB stars with the same luminosity ($T_{eff} \sim 5000K$). RC stars and horizontal branch stars are burning helium in their cores. In the dichotomy between the RC and the HB, RC stars are associated with younger and more metal-rich populations than those associated with the HB (See review by Girardi 2016).

¹When the dredge-up occurs the convective zone extend down to internal layers, dredge up the material produced by the thermonuclear reactions. A star after the first dredge-up shows in the spectrum the features of the helium burning: C/O low and low abundances of lithium and beryllium. The third dredge-up occurs when star is in the AGB phase.

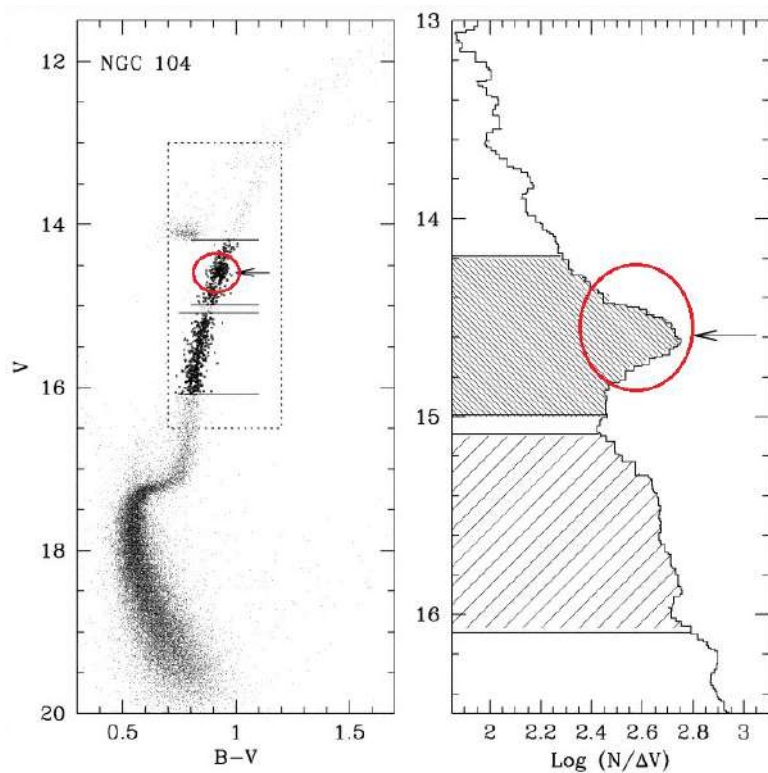


Figure 4.6: On right a zoom of the zone of RGB bump, on right the diagram that shows the magnitudes-density of stars relation.

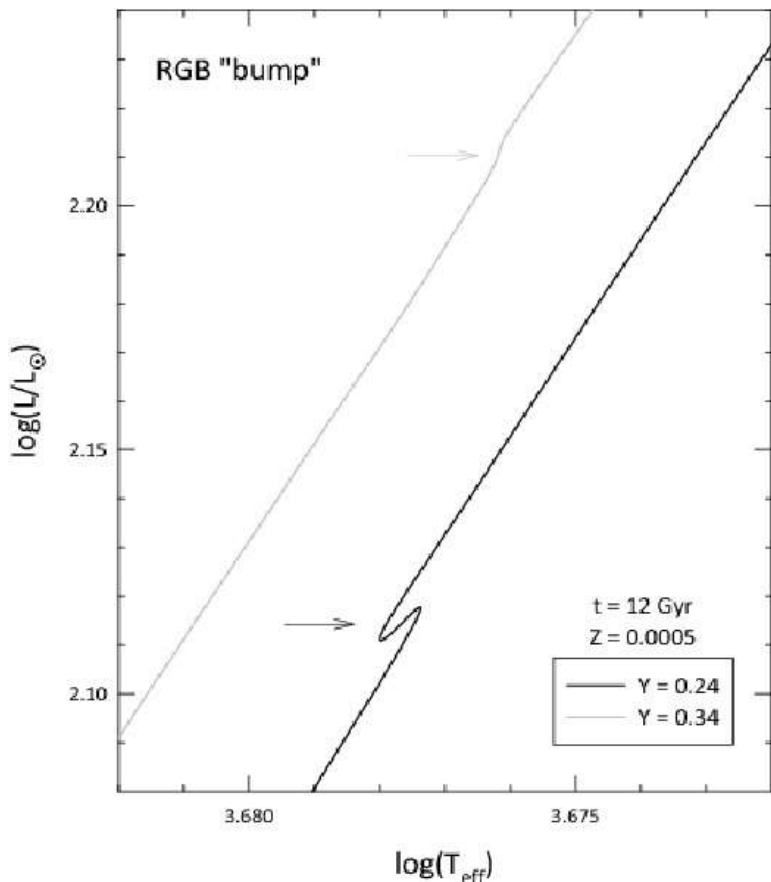


Figure 4.7: A CMD model where we can see the RGB bump.

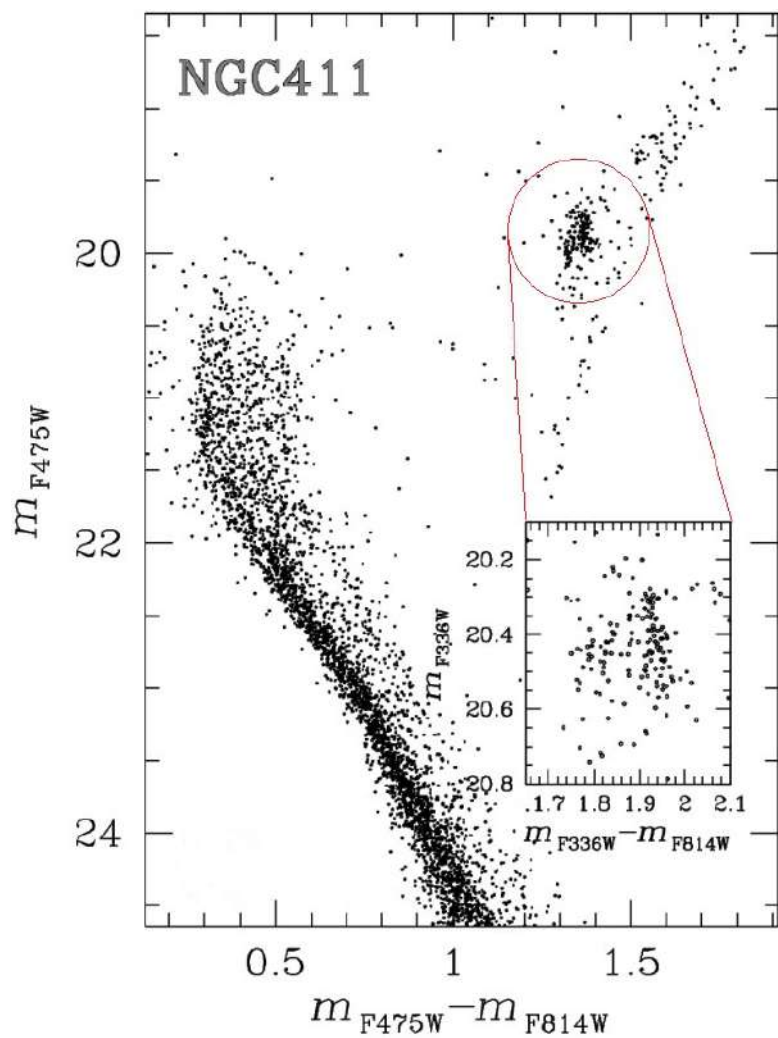


Figure 4.8: Zoom of the red clump in a CMD.

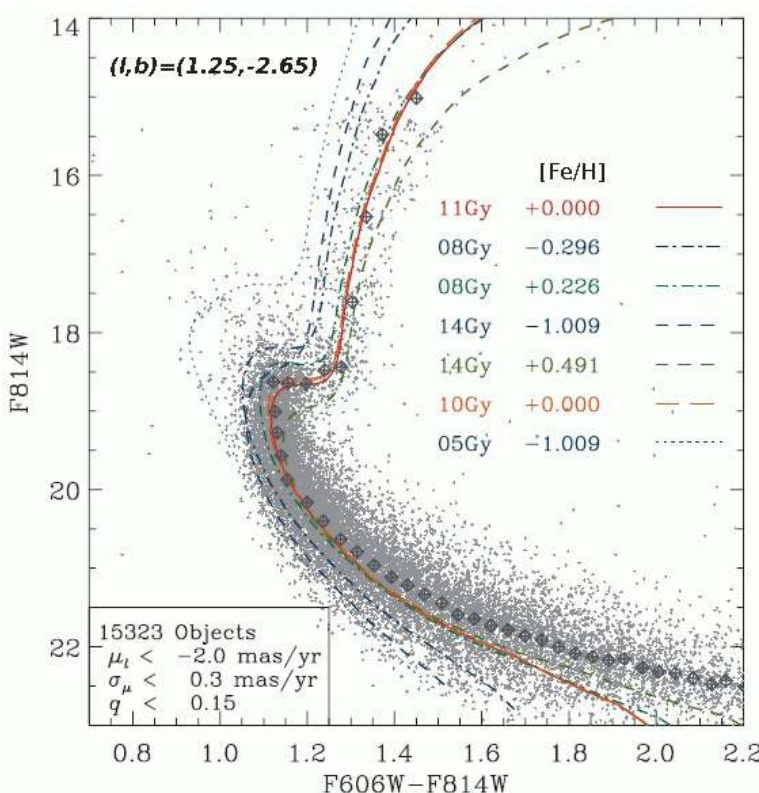


Figure 4.9: CMD of the bulge provided by HST in a very small field of view.

Some astronomers confused the red clump with the RGB bump, but they are very different features.

4.5 The Red Clump in the Galactic Bulge CMD

The Bulge is one of the main components of the Milky Way. It is massive ($\log(M/M_{\odot}) \sim 10$) and old (over 10 Gyr) and it is heavily obscured by interstellar clouds. The main issue of the bulge is that it is big, so, it is more difficult to study than a small object.

The Bulge is composed of complex of multiple populations of stars with different ages and metallicities (figure 4.9). Hubble Space Telescope provides high precision and deep photometry of the Bulge but in very small fields of view, we can see the result in the figure 4.9.

A telescope is using to obtain a survey of the stars in the bulge: The Visible and Infrared Survey Telescope for Astronomy (VISTA), that is a 4.1 m telescope located at Paranal. It works at near-infrared wavelengths. The telescope is equipped with the Vista infrared camera, ‘VIRCAM’, composed of 16 detectors (67,000,000 pixels). VISTA is the largest telescope dedicated to surveys in the near infrared. It can provide a useful and wide image of the entire bulge, combining many images taken with large field detectors.

The ESO near-infrared survey (VVV) exploits the Vista Telescope to cover ~ 520 square degrees. In the figure 4.10 we can see the Hess CMD provided by this huge survey. This diagram is a little different from the other CMD because each point is referred to a density of stars with given characteristics, so it shows the density of stars in the color-magnitude plane. In the diagram is drawn an arrow that shows the direction of the reddening: the plot is elongated in that direction. In this way we are not able to derive information of the bulge: a correction of the reddening is needed!

The idea to correct the differential reddening that affect the Hess CMD is to use the red clump stars.

First we observe a small field of view, where reddening is almost constant, and build a CMD, as that in figure 4.11, then we want to detect the red clump, but by eyes we are not able to distinguish

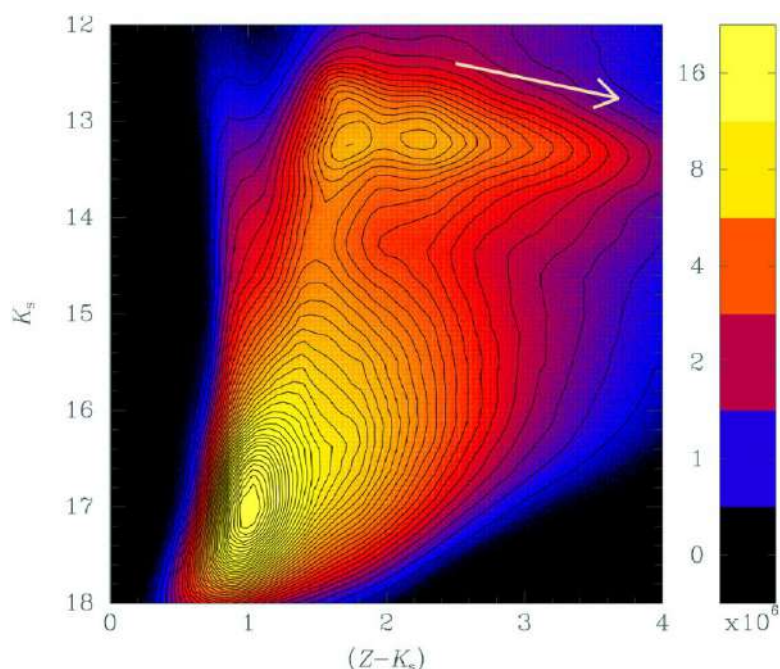


Figure 4.10: Hess CMD of 66 million stars from 300 square degree in the Bulge. Minniti et al.(2014).

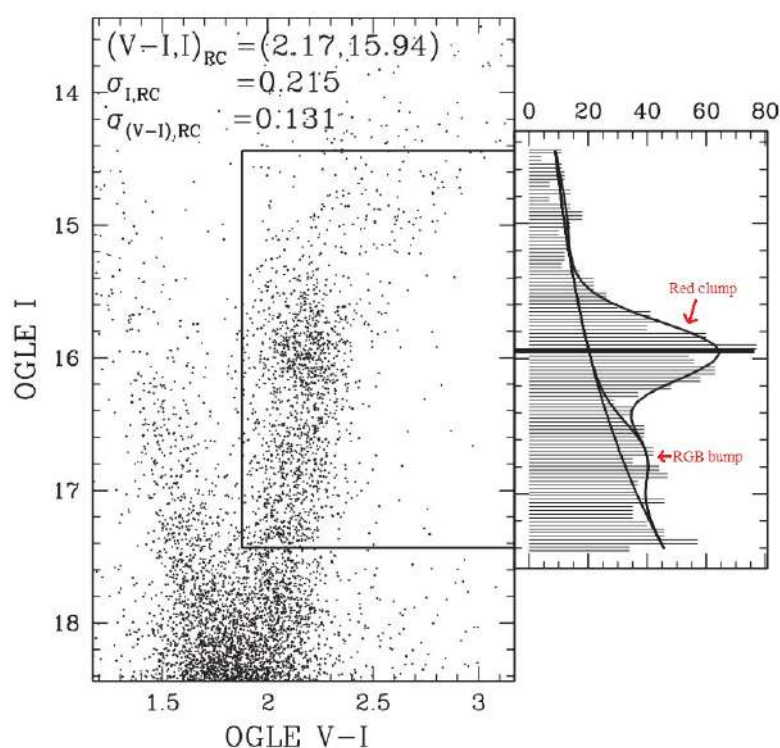


Figure 4.11: CMD of small region of the bulge.

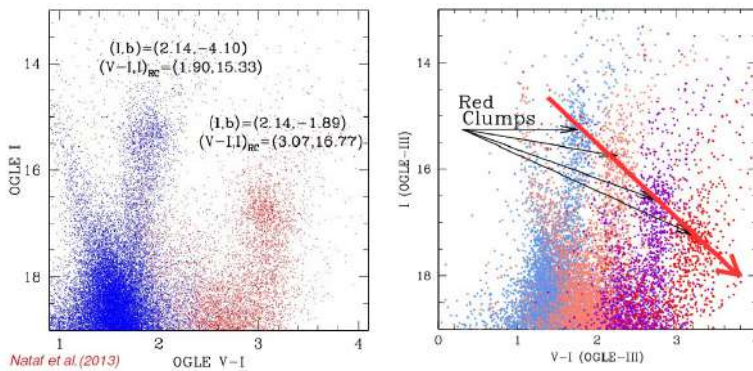


Figure 4.12: CMD of different stars from different part of bulge

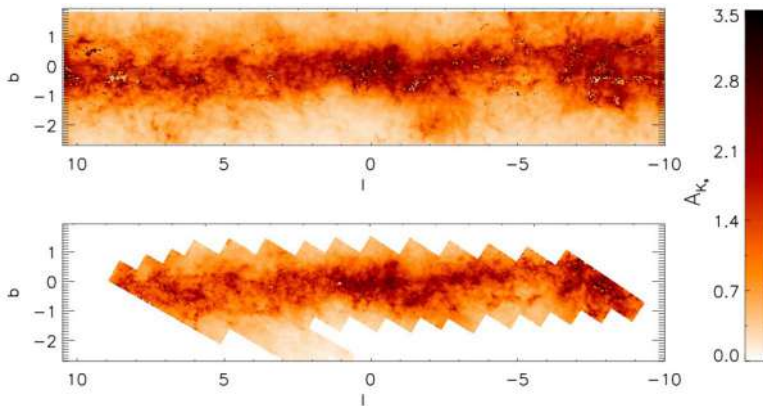


Figure 4.13: Reddening Map of the Bulge.

the overpopulated zone of the RGB bump from the red clump stars. This is possible studying the luminosity function on the right of the figure 4.11.

The color and magnitude of red-clump stars can change dramatically in CMDs of stars in different fields of view.

In the figure 4.12 we can see this effect: the position of the red clump stars change dramatically, according to their galactic coordinates. In general the relative color and magnitudes of the red clump are indicative of the amount of differential reddening in each region of the bulge. Moreover, they constrain the reddening direction in an empirically way, hence the reddening law. So we can derive the direction of reddening, that is shown in the figure 4.12 with the red arrow.

Two results: first the amount of the differential reddening, that means how much reddening is present in each region of the bulge, the second is the reddening law.

By comparing IR colors of the red clump of bulge stars in the VVV survey it has been possible to derive a reddening Map of the Bulge (resolution $2' \times 2'$ – $6' \times 6'$ better than that of the previous reddening map) that is shown in the figure 4.13.

Comparison

In the figure 4.14 we can see the difference between the absorption values derived from the latter method and from the Schlegel map. At large distance from galactic plane there is a nice agreement while approaching the plane ($b = 0$) there is a strong disagreement ($b < \sim 5$) between the reddening values obtained from the red clump and those inferred from the 100-micron intensity map of the sky. The discrepancy at the galactic equator is due to that the result from the Schlegel map is not reliable at such low galactic latitude.

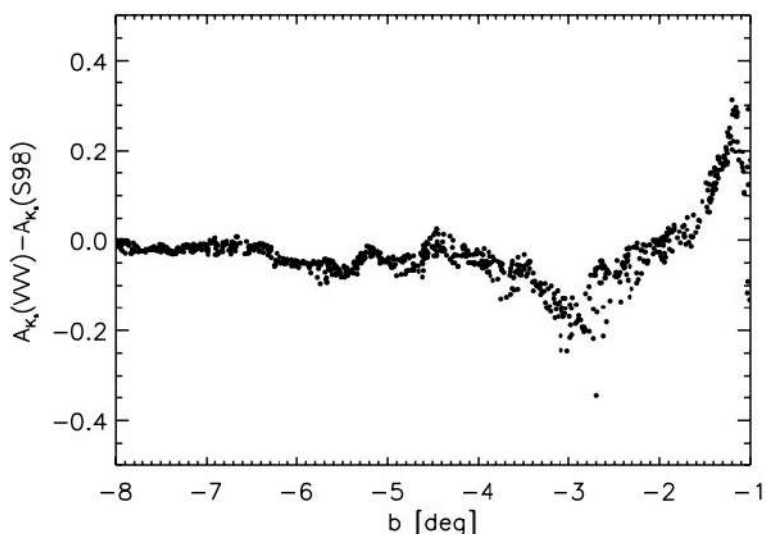


Figure 4.14: Difference between the absorption values by Gonzalez et al. (2012) and those of Schlegel et al. (1998) as a function of Galactic latitude.

Chapter 5

Binaries, Blue Stragglers, and other exotic objects in the CMD

5.1 Luminosity profiles of star clusters

Now we can investigate about binaries, blue stragglers, and other exotic objects in the CMD but first we have to introduce some properties of star cluster.

Star clusters can be described in terms of:

- **Core radius** (r_c): the distance at which the surface luminosity is dropped by a factor of 2.
- **Half-light (mass) radius** (r_h): the radius within which half of the luminosity (mass) is included.
- **Tidal radius** (r_t): the radius where the gravitational influence of the galaxy on cluster stars is larger than the influence of the cluster. Using other words, it is the radius at which cluster finishes.

5.1.1 King profile

From a mathematical point of view, there are different descriptions of luminosity profile of a star cluster. One famous but also the most used is the King luminosity profile by the name of the astronomer that found it in 1966. It is described by the following relation:

$$f = k \left(\frac{1}{[1 + (r/r_c)^2]^{1/2}} - \frac{1}{[1 + (r_t/r_c)^2]^{1/2}} \right)^2 \quad (5.1)$$

We can define the **concentration** of the model:

$$c = \log_{10}(r_t/r_c) \quad (5.2)$$

This model is a useful tool to fit the data in the surface brightness-radius plane and also in the velocity dispersion-radius plane.

In figure 5.2 we can see that the surface brightness profile and the velocity dispersion profile are well fitted. The King model works well for the vast majority of the GCs, about 85% of the objects observed.

Even if the King description for the 85% of GCs is very good, there is a small but reliable fraction of objects with a peculiar trend. In $\sim 15\%$ of GCs the luminosity continues to increase steadily all the way to the core region. So, in some GC, when we approaches in the center of the cluster, the

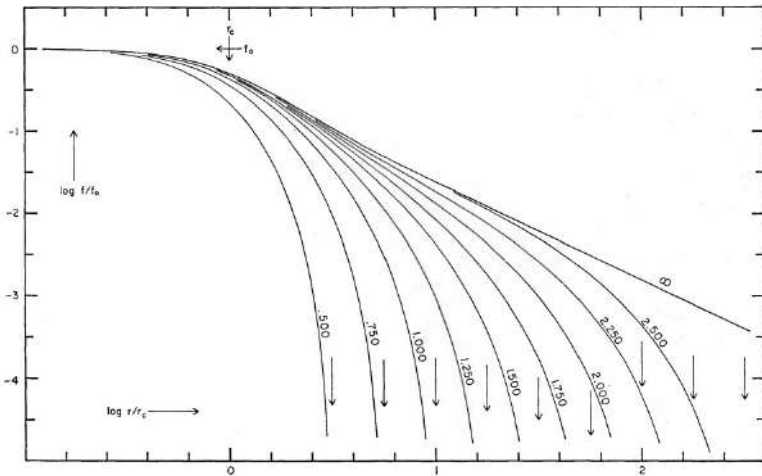


Figure 5.1: The King model for different values of concentrations. On y-axis there is the flux normalized to the cluster center and on x-axis is plotted the radius normalized to the core radius in logarithmic scale.

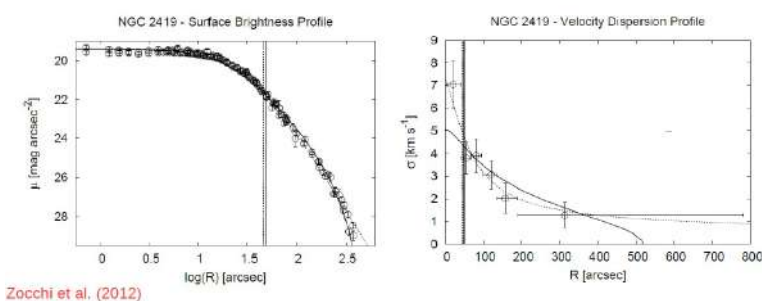


Figure 5.2: Two diagrams of NGC 2419: on left the surface brightness profile and on right the velocity dispersion profile as function of radial distance from the center of the cluster. The fit is very good in both cases.

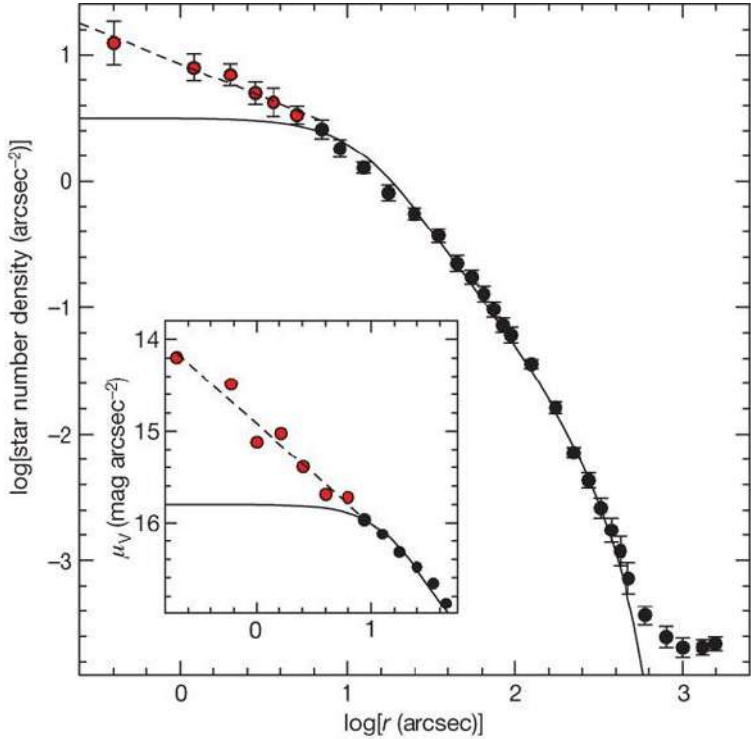


Figure 5.3: Projected luminosity profile of the core-collapsed globular cluster M30. Note the steep cusp in the inner region very far from the flat trend we expect from King description.

luminosity profile is not flat. There are different ways to interpret this trend. Two of them are the following:

- core collapse of the clusters;
- presence of intermediate-mass black holes.

5.1.2 Core collapse

The core collapse is a catastrophic dynamical process consisting in the runaway contraction of the core of a star cluster. However in a GC there are binary-binary and binary-single collisions, that are thought to prevent (or delay) the collapse of the core, thus avoiding infinite central densities.

5.1.3 Intermediate-mass black holes

Core collapse is not the only responsible for the luminosity increase. An intermediate-mass or massive black hole (BH) at core can also produce a cusp, due to an over-density of luminosity.

In the figure 5.4 we can see a model with a BH. It is clear that there is an increase of velocity dispersion approaching the core. However the presence of black holes in the centers of globular clusters is an open issue of present-day astrophysics.

5.2 Binaries in star clusters

To investigate the presence of exotic objects like exotic binaries or the content of dark matter is fundamental to derive the fraction of binaries in a star cluster.

Of course we are not able to detect all binaries but only few in a certain range of luminosity. Moreover we are not able to distinguish them from single stars due to observational errors that increase at faint magnitudes or if they are too bright so they merge with the TO point.

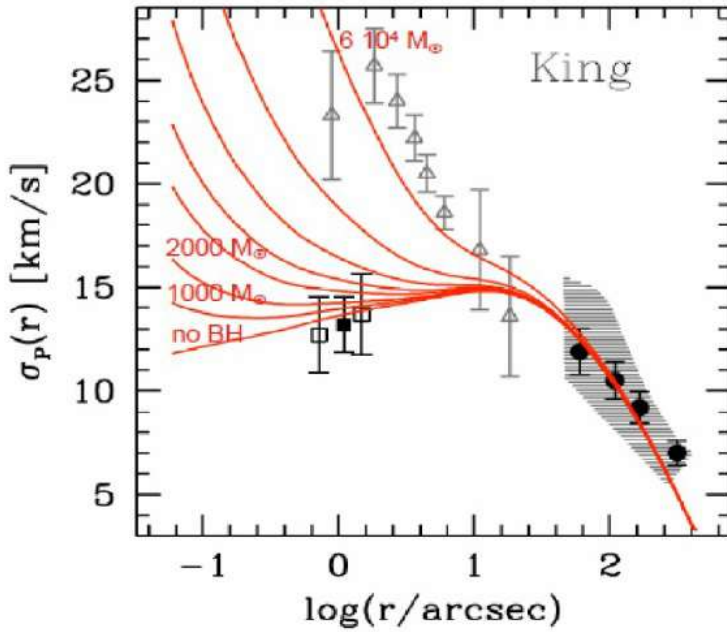


Figure 5.4: Velocity-dispersion profile of the massive GC NGC6388. Gray triangles are from Lutzgendorf et al. (2011), Black squares and circles from Lanzoni et al. (2013). Red lines are Jeans models corresponding to different masses of the central BH.

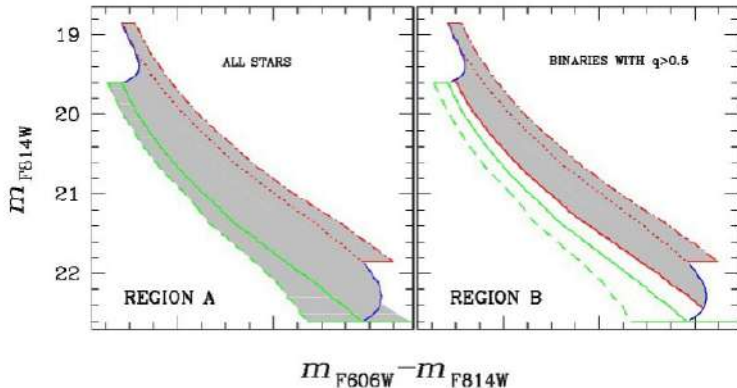


Figure 5.5: The fraction of binaries is provided from this diagram.

However previously we have seen how to measuring the fraction of binaries in a large number of clusters; the method is shown in figure 5.5. We can count the numbers of star in region A, populated by all stars (single and binaries) and in region B, populated only by binaries stars with $q > 0.5$ (otherwise stars are too close to the MS so it is not possible to distinguish them from observational errors), and estimate the fraction of binaries making a ratio between the two populations.

Pay attention to field stars that can be projected on the sky in the region we are observing and also to observational errors associated to photometry that can push stars in the region of binaries even if they are single. For those reasons:

- artificial stars are used to estimate the numbers of apparent binaries in the regions A and B;
- proper motions and/or models of the Galactic field are used to estimate the numbers of field stars in the regions A and B.

This is a powerful method to derive fraction of binaries, that can be used for all CMDs. This is what astronomers have done for many samples of GCs. In figure 5.6 it is shown a diagram plotting the

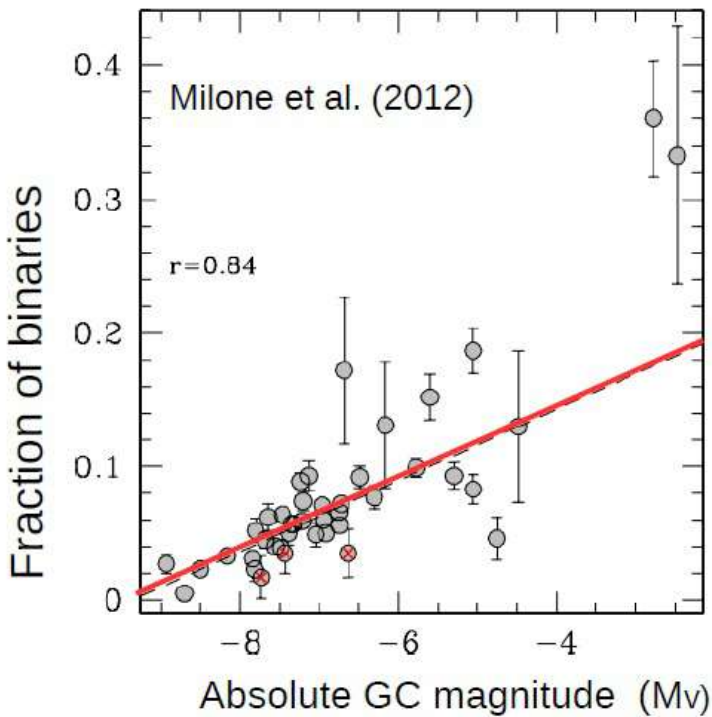


Figure 5.6: Relation between the fraction of binaries and the absolute magnitude of the GCs

fraction of binaries against the absolute magnitude M_V .

Fraction of binaries is different for every cluster, from few percent in massive cluster to more than 30% in less massive cluster. But what is clear from diagram in figure 5.6 is that the fraction of binaries anti-correlates with the mass of the host cluster: this means that there is a specific relation between fraction of binaries and absolute magnitude (proxy for the total visible mass).

The key point is the following: fraction of binaries does not depend neither on age nor on stellar collision rate but on absolute magnitude, which means depends on total visible mass.

There are some possible conclusions:

- massive clusters are more efficient in destroying binaries;
- collision is not an efficient channel in producing binaries.

One another important property of binaries is that the fraction is not constant in all star system but changes depending on the position in the system itself. Indeed the fraction of binaries, when properly normalized, follows a trend that is common to most clusters: it is maximum in the center of the cluster and then decreases, being quite constant in external region.

It is maximum in the innermost cluster regions, drops by a factor of ~ 2 , at a distance of two core radii and approach its minimum of ~ 20 per cent at about five core radii.

However in the figure 5.8 we can see that the fraction of binaries does not depend on the mass ratio.

Finally the fraction of binaries does not depend on the mass of the primary stars.

The final result is that the fraction of binaries depends from the mass of the host cluster and the normalized fraction of binaries depends on the radius (normalized to the core radius). In figure 5.10 we can see these relations.

Thanks to the relation between the mass and the fraction of binaries as seen before (binary fraction anti-correlates with mass of the host cluster), then we can derive the fraction with a measure of the absolute magnitude.

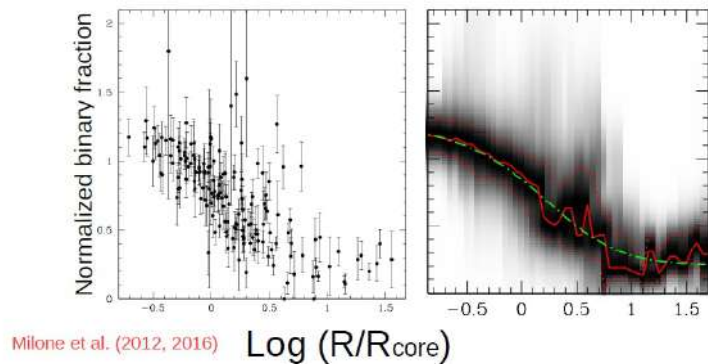


Figure 5.7: The normalised fraction of binaries.

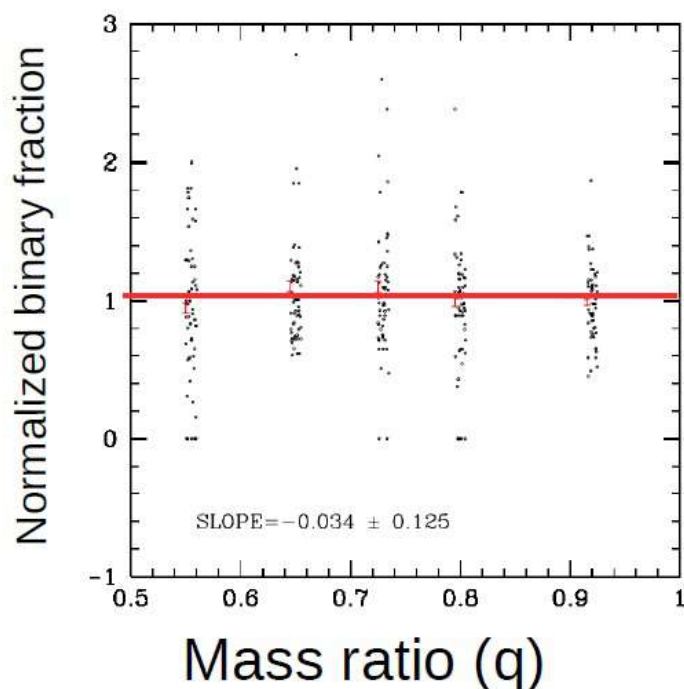


Figure 5.8: Relation between the fraction of binaries and the mass ratio.

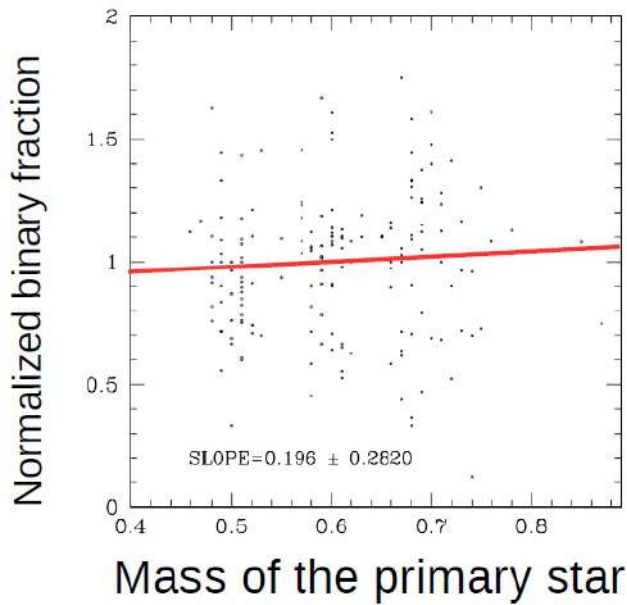


Figure 5.9: Relation between the fraction of binaries and the mass of the primary stars.

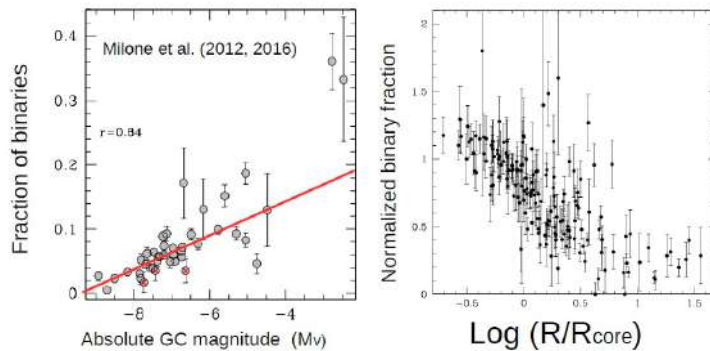


Figure 5.10: On left the relation between the fraction of binaries and the mass of the host cluster. On right the relation between the normalised fraction of binaries and the radius.

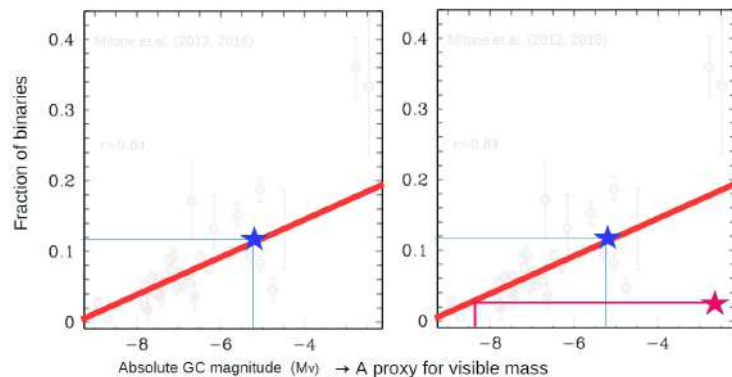


Figure 5.11: How to use the relation.

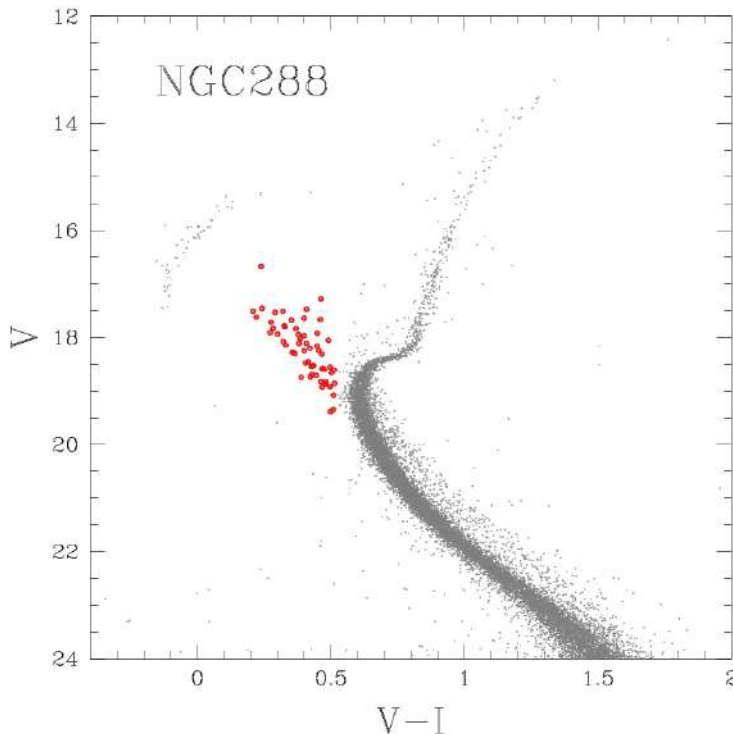


Figure 5.12: CMD of NGC288, in red are shown the blue stragglers.

This method is shown in figure 5.11 on the left panel. On the contrary, on the right panel we see a red star that is not located on the relation. This could be a feature due to presence of dark matter in the cluster, in fact, if the relation is correct, the cluster appears less luminous. Therefore we can calculate the difference on the x axis between the relation and the red star, hence the difference in absolute magnitude. With this we can infer the amount of dark matter in the cluster. This is one method to estimate presence of dark matter, independent on cinematic of stars so very powerful.

5.3 Blue Stragglers

Globular clusters are prototypes of old simple stellar populations. Their stars share all the same age. However observing some CMD it is possible to see clearly the presence of some stars, above the MS turn-off; they are blue stragglers. Blue stragglers (BSS) are main sequence stars in a stellar populations that are brighter and bluer than stars at the main sequence turn off. BSSs have been discovered by Allan Sandage in 1953, while he was working on the CMD of M3 but they are present in all GCs.

This peculiar type of stars seems consistent with stars younger than the bulk of stars. In figure 5.13 it is visible an isochrone of 12 Gyr plotting very well the CMD while BSSs are located between this isochrone and one of only 2 Gyr. This explain from an empirical point of view that they are very young stars.

Where are they come from? Field stars trapped by the cluster? Recent star formation within the cluster? We can immediately exclude differential reddening! Indeed differential reddening affects all sequences of the cluster. If they are associated to differential reddening, then we would expect that all other sequences are broad but this is not the case. All sequences are narrow and well defined so we can exclude differential reddening. What about other possibilities?

The other possibility is that they have been trapped by the cluster while it was orbiting around the Milky Way due to gravitational interaction but analysing spectra of stars, we found they have same metallicity of the cluster. Therefore it is quite improbable that the cluster trapped only young stars with same metallicity of itself and same age between them. For these reasons we can exclude this

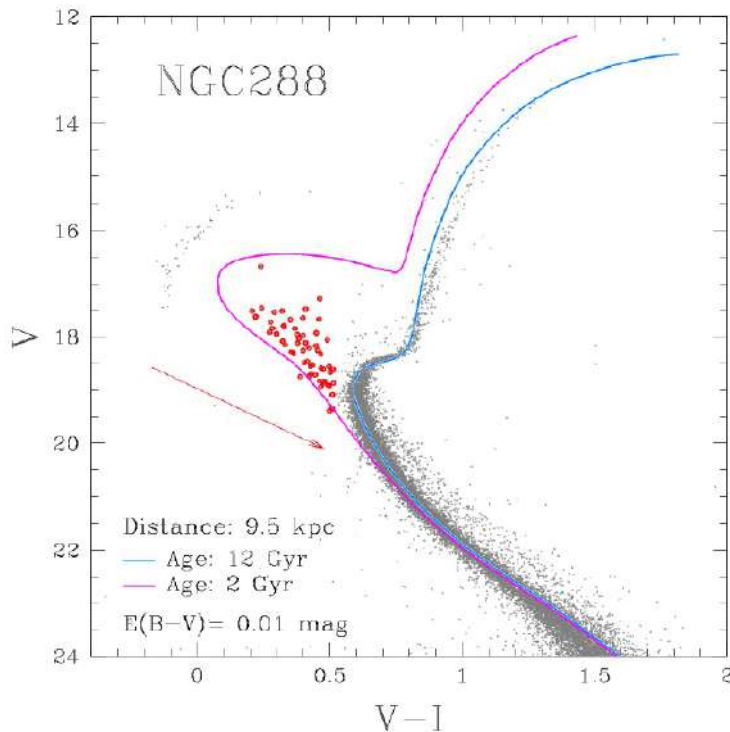


Figure 5.13: Fit of isochrones in order to estimate the age of these stars.

explanation.

On the other side, in the case of recent star formation, we can reject totally this explanation but in this case it is necessary change fundamental knowledge on star formation.

What is clear is that blue stragglers are among the brightest stars in ultraviolet bands and this can provide, for example, an explanation of UV excess in light coming from elliptic galaxies but this is another issue.

Coming back to BSS, two formation channels have been proposed for them.

- **Collision** of two stars, maybe in the same cluster, colliding in a process that bring the system in a kind of fusion.
- **Mass transfer or coalescence.** In this case we consider two stars orbiting around the same center of gravity, very close one to each other inside a binary system, for example. The primary transfers material to the secondary through the inner Lagrangian point after becoming a red giant and filling up its Roche lobe. The material is stripped off of the envelope of the primary. As the secondary is gaining material gradually, it becomes a more-massive main-sequence star with a hydrogen-rich envelope. This modified star can stay on the upper extension of the MS until finishing hydrogen burning in the core. The life time of this star is longer than a normal star with the same mass.

5.3.1 Testing the theories

A way to test the two channels theory is using the spectroscopy and analysing the surface composition of these stars. We know they have same metallicity of the cluster but what about lighter elements? If BSS are the product of mass transfer, then we expect that all blue stragglers, or at least some of them, have a strange chemical composition on surface, due to pollution given by the companion.

To understand better their composition, astronomers took many spectra using modern telescope with very high resolution spectra and multi objects spectrograph, able to analyse at the same time many stars.

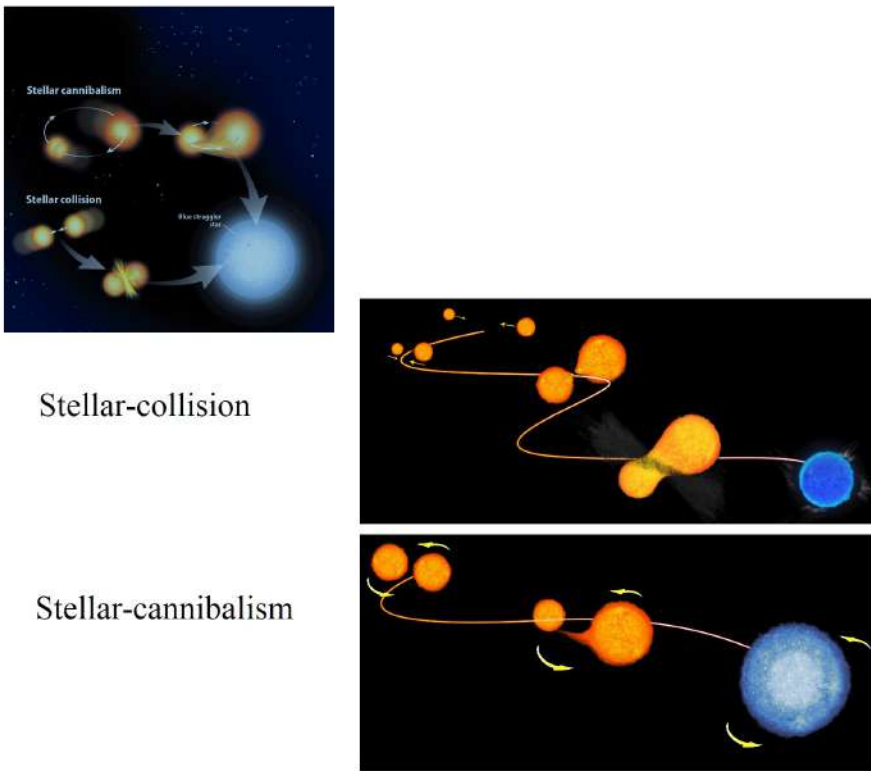


Figure 5.14: Two way of blue stragglers' formation

From that analysis we get that in general blue stragglers do not locate in the expected region of the diagram and, in particular, is clear the presence of a population of blue stragglers significantly depleted in Carbon and Oxygen with respect to the dominant population. This evidence would suggest the presence of CNO burning products on the BSS surface coming from a deeply-peeled parent star. It is considered as the signature of the mass-transfer formation process. This is shown in figure 5.15.

Another way to test the theories is studying the correlations between blue stragglers and the parameters of the host clusters. For example, analysing many GCs and plotting the frequency of BSSs against absolute magnitude (proxy of total visible mass) it is clear that there is a relation between them. In particular frequency of BSSs anti-correlates with cluster mass (hence it correlates with the absolute magnitude, M_v). This is shown in figure 5.16.

On the other side, a research form Moretti et. al (2008) base on a large number of star clusters,

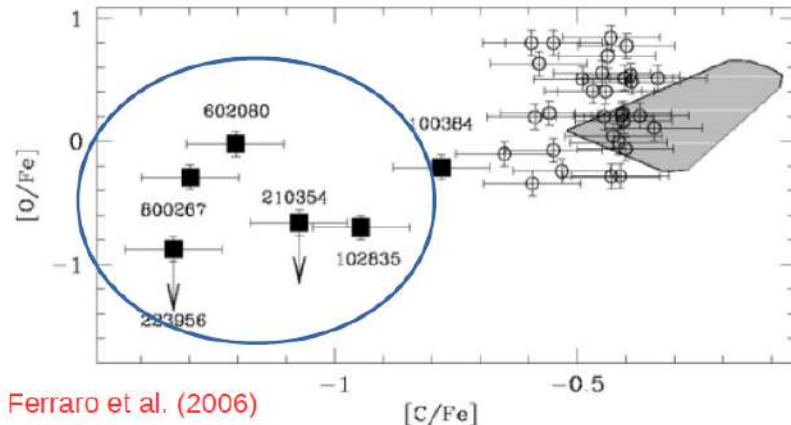


Figure 5.15: Diagram with Oxygen abundance against Carbon abundance. It is clear from this diagram that the vast majority of BSSs are located nearby the gray region (region of expected values). However there is distinct group of stars that present a important depletion in Carbon and Oxygen.

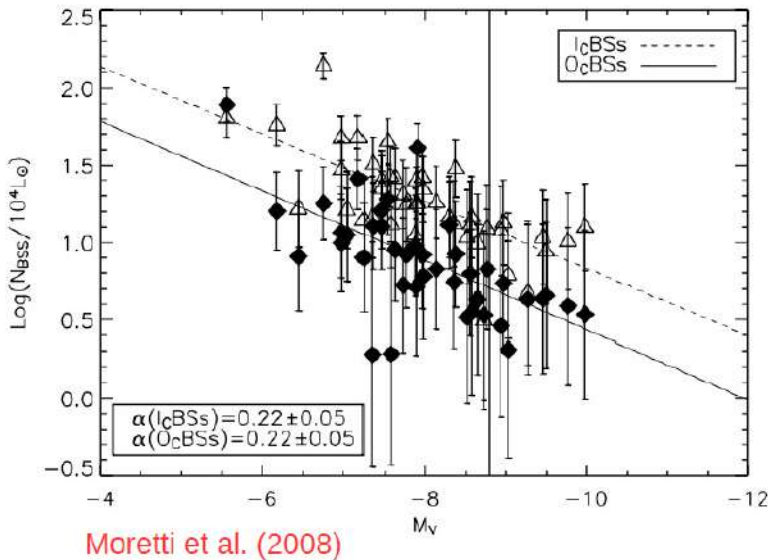


Figure 5.16: Diagram representing fraction of BSSs with respect to the total number of stars in a cluster against absolute magnitude. It is clear the presence of a relation.

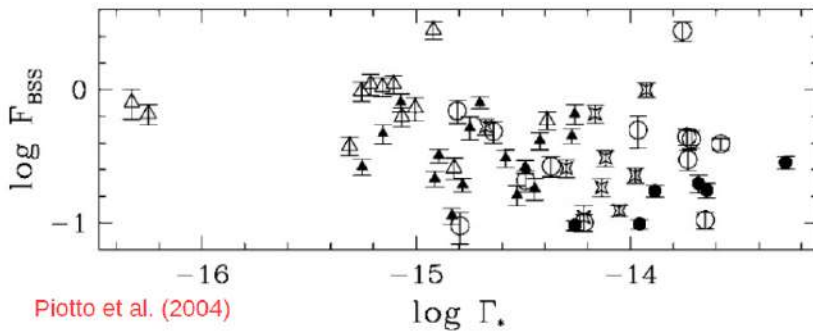


Figure 5.17: Diagram representing fraction of BSSs with respect to the total number of stars in a cluster against stellar collision rate. It is clear that there is no correlation between them.

derived an interesting graphic shown in figure 5.17. From this graphic, representing fraction of BSSs with respect to the total number of stars in the cluster against stellar collision rate, it is clear that there is no relation between them. This can prove that collision is not the exact formation channel for blue stragglers.

Summarizing:

- The frequency of BSSs anti-correlates with cluster mass (hence it correlates with the absolute magnitude, M_v).
- The frequency of BSSs does not correlate with the stellar collision rate.

This evidence suggests that the collisional channel for the BSS formation does not play a dominant role in clusters while mass transfer process is maybe the right one.

A third test is studying directly the CMDs obtained with high resolution on photometry. There is an example of CMD with high resolution in figure 5.18.

The globular cluster M30 (figure 5.18) exhibits two distinct sequences of blue stragglers. We can see that there are two types of points: the blue and the red. The blue population arises from direct stellar collisions. The red one arises from the evolution of close binaries that are probably still experiencing an active phase of mass transfer. This finding suggests that both collisions and mass transfer are

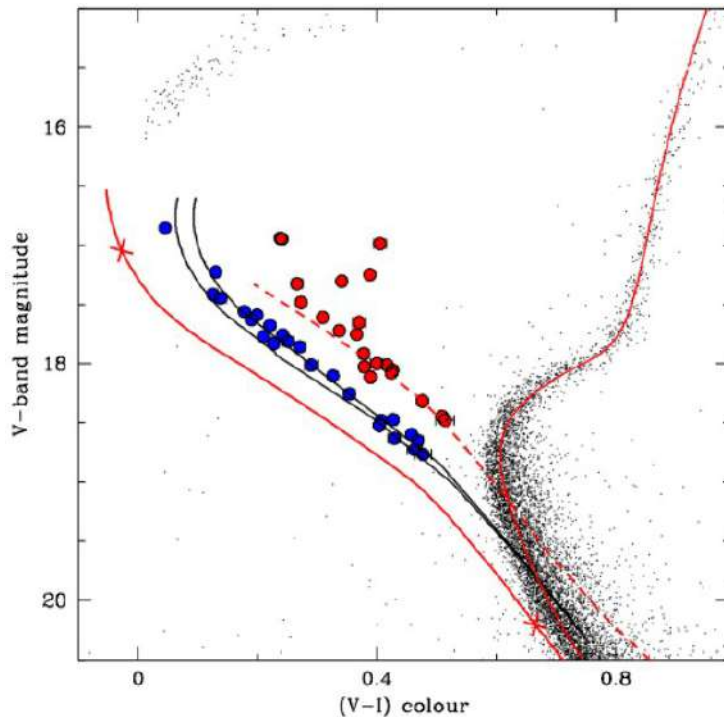


Figure 5.18: CMD of M30. In red and in blue two types of BSSs, the blues come from the collision, the reds from the mass transfer. The red solid line is the best fit isochrone, the orange line is the zero age MS, the black line is the isochrone that takes account to the collision formation and the red dashed line is the isochrone that takes account to the mass transfer.

efficient channels for BSS formation inside this GC. This is quite strange to observe and this means that we have to investigate more about blue stragglers.

5.3.2 Blue Stragglers & dynamical evolution

BSSs are the most-massive and luminous stars in stellar systems, regardless formation channels, so they can be used as test particles to probe dynamical evolution. The point is that there is a difference between real age and dynamic age. Using BSSs we can determine this difference and study the GC from a dynamical point of view.

We know GCs are old stellar systems with an age about $\sim 12 - 13.5$ Gyr and the average mass of a GC star is ~ 0.3 solar masses. Assuming this, we can distinguish GCs in different groups according to a physical principle: from dynamic evolution it is expected that massive objects, like BSSs, move to the center of stellar system while low mass objects are located in the external regions. In particular globular clusters have been grouped into a few distinct families on the basis of the radial distribution of BSSs and from this distinction it is possible to derive the **dynamical age**.

1. **Family 1: dynamically young GCs** - As visible in figure 5.19 in the first panel, BSS frequency is the more or less the same (constant) regardless radial distance from the center. The graphic appears flat showing that there is no peculiar relation between frequency and radial radius. From a physical point of view this means that the cluster is young in terms of dynamics.
2. **Family 2: intermediate dynamical ages** - As visible in figure 5.19 in the second panel, BSS frequency is maximum in the center of cluster and minimum at a characteristic radius, after which there is another increase of BSS frequency. Pay attention: they have same age as the previous family but from a dynamical point of view they are older.
3. **Family 3: dynamically old GCs** - As visible in figure 5.19 in the third panel, BSS frequency is maximum in the center of the cluster and then it decreases in the external region, without climb back up. This corresponds to dynamically old GCs.

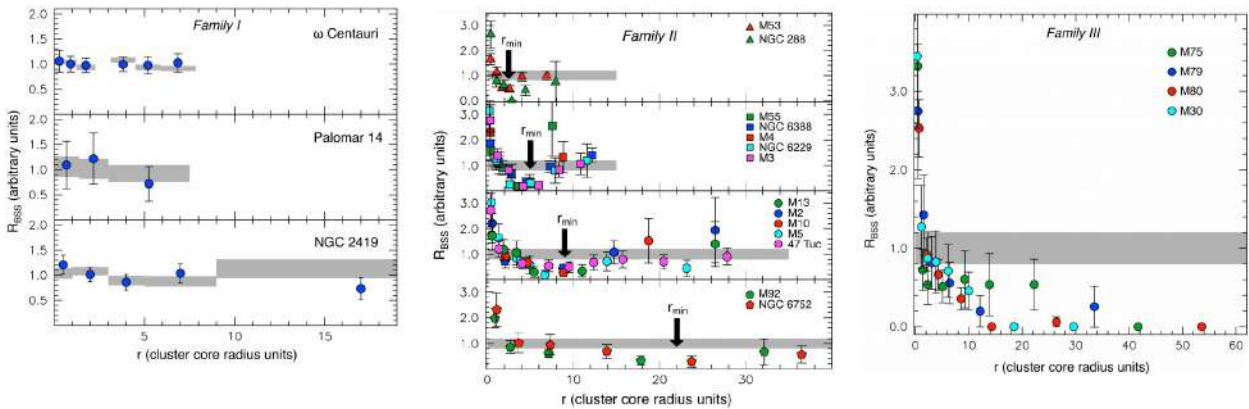


Figure 5.19: Three families of GCs depending in BSSs frequency against the radial distance form the center of the cluster.

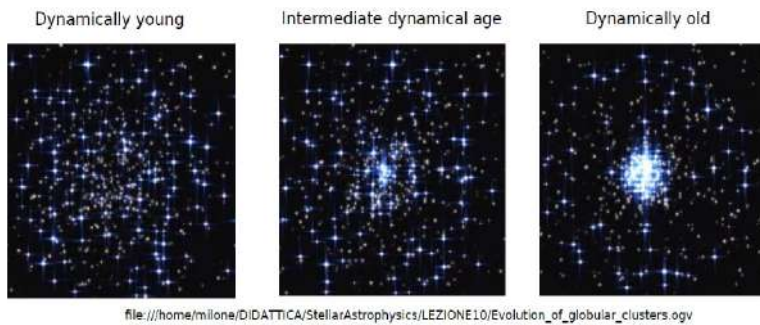


Figure 5.20: Cartoon of the three types of dynamical ages.

Basically what happens is due to gravitational interactions with surrounding objects for which cluster stars lose kinetic energy and momentum. Dynamical friction drives the objects more massive than the average toward the center, with an efficiency that decreases with increasing radial distance. See figure 5.20 where is shown the difference of dynamical age.

As said before, the mass transfer is the most reasonable formation channel. Assuming that BSSs form in this way, we can expect that some BSS come from the evolution of peculiar binaries for which there is a process of interaction and then mass transfer.

Previously we studied binaries systems of MS stars not interacting. Now we see some exotic binaries that we can detect inside CMD.

5.4 Types of binaries

5.4.1 WD-MS binary system

In figure 5.21 are shown two main types of binaries: on top these formed by two MS stars, on bottom these composed by a MS star and a white dwarfs (WD). Due their components, these type of binaries systems are located in the region between main sequence and WD sequence.

5.4.2 Cataclysmic variables

There are also other exotic objects like a particular type of binary called **Cataclysmic variables** CVs. CV stars are close binary systems and consist of a white dwarf and a cool (low-mass) secondary star, like one from MS.

- How CVs affect the evolution of dense stellar systems?
- How the environment affects the evolution of CVs?

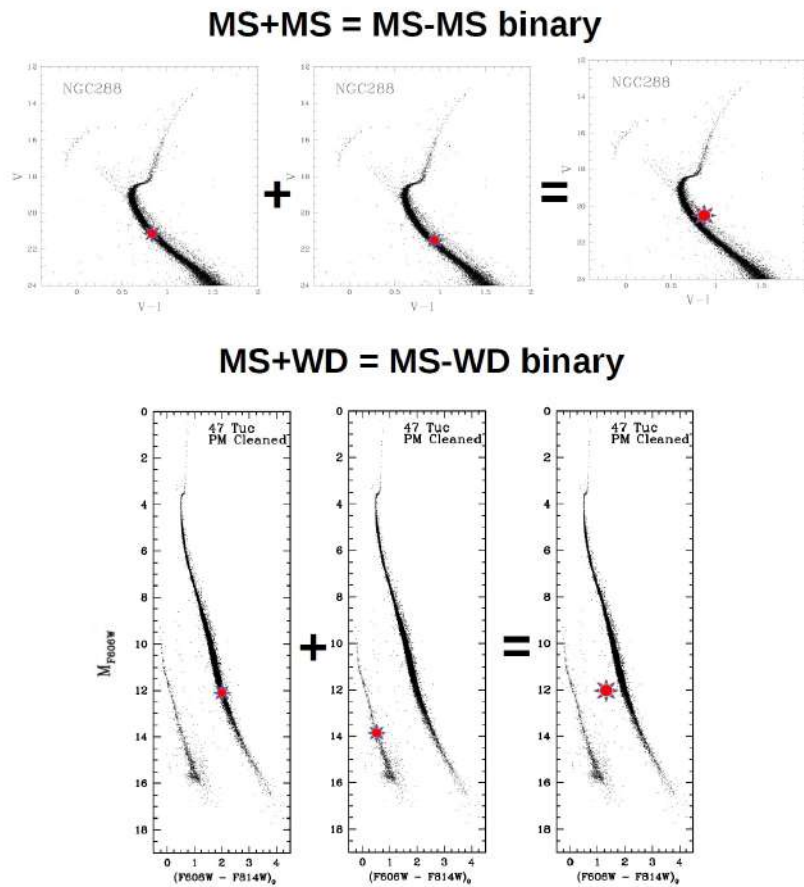
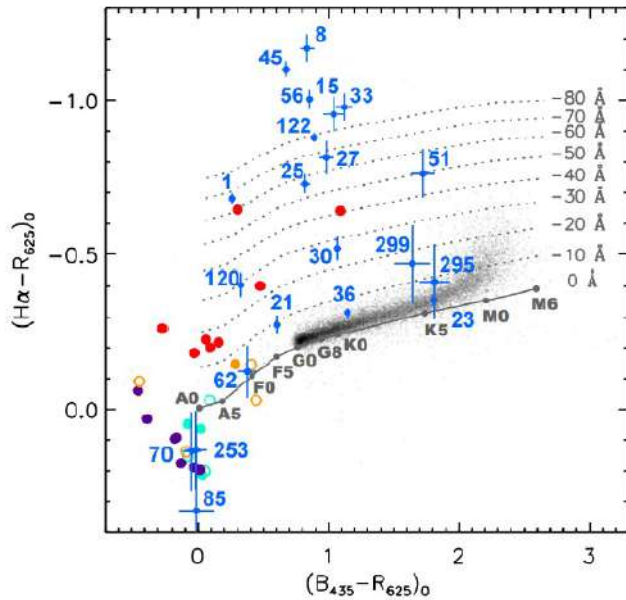


Figure 5.21: Types of binaries: in the upper panel there are simple binaries system of MS stars not interacting each other. In the lower panel there is an example of binary system composed by a white dwarfs and a main sequence star that, for this reason, is located between main sequence and WD sequence.



Rivera Sandoval et al. (2018)

Figure 5.22: Two color diagram from CVs to infer equivalent width of H-alpha emission.

- What are the physical properties of CVs?

These are some of the big questions we have about CV binaries. Nowadays what we know is the following.

- The total mass of CV systems is higher than the average stellar mass. Indeed it is composed by a WD and a MS star so total mass is bigger than 0.3 solar masses (average stellar mass inside a GC).
- CV spectra exhibit strong emission lines, with a strong H-alpha emission. So we can detect them from spectroscopy. Once we have detected these stars, we can spot them in the CMD: we see that in a optical CMD these systems are more concentrated near MS (due the fact that in optical the light is dominated by the MS star). On the other side in a UV CMD these are concentrated near the WD cooling sequence indeed the UV light is dominated by the WD emission. To study these stars usually is needed a two color diagram like $H\alpha$ -red filter vs. blue-red filters (one narrow filter like blue and one another but wider like red to analyse the flux). In figure 5.22 position of stars depends on presence of H-alpha emission so using this tool we are able to infer the equivalent width of H-alpha emission.
- We can distinguish two main groups, the bright and faint CV and we can compare their redder distribution with distribution of single stars. Usually the degree of concentration is indicative of the mass of each component so what we can do a comparison between cumulative distribution of three families: bright CV, faint CV and MS turn off stars. This work has been done plotting the fraction of stars for each group against radial distance from the center. The result is shown in figure 5.23.

From this we infer that CVs are more centrally concentrated than MS turn-off stars (proving that they are more massive than MS stars) while faint and bright CVs are equally segregated. Results on radial distribution indicate that CVs of 47 Tuc (subject of the study) have masses of $1.4 M_\odot$.

- CVs consist of a white dwarf and a cool (low-mass) secondary star that is transferring mass. Knowing that CVs have usually a mass about $1.4 M_\odot$ and knowing the mass of the secondary star (usually a MS star) then we can infer the mass of the companion.

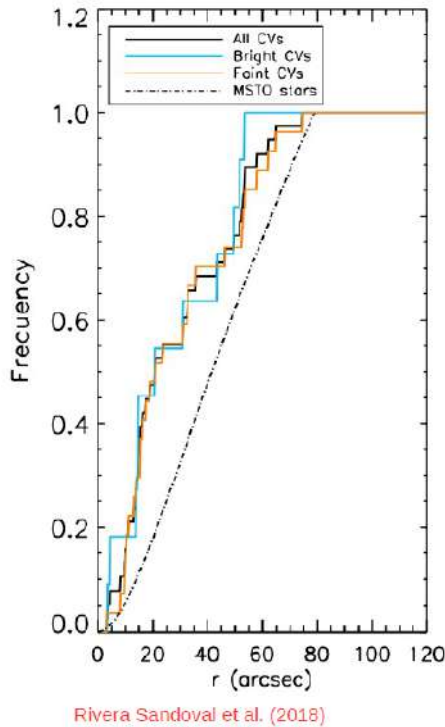


Figure 5.23: Frequency of all CV, of bright CV, of faint CV and of MS star against the radial distance form the center.

- In the bright WDs the secondary star has mass around $0.9 M_{\odot}$, so the WD mass is around $0.5 M_{\odot}$.
- In the faint WDs the secondary star has mass less than $0.2 M_{\odot}$, so the WD mass is around $1.2 M_{\odot}$.

Hence, there is a net increase in WD mass in CVs over the combined action of accretion and nova outbursts.

- The infalling matter forms an accretion disk around the WD. Moreover the material in the accretion disk loses gravitational energy and is responsible for *UV* and *X-ray* emission.

5.4.3 X-ray variables

High-resolution images taken from Chandra Telescope reveal at least 108 *X-ray* sources in 47 Tuc: 50% of millisecond pulsars (MSPs), 30% of accreting white dwarfs, 15% of main-sequence binaries in flare outbursts and 2 or 3 low-mass *X-ray* binaries containing neutron stars.

Between them there is another particular type of binaries called ***X-ray variables***. *X-ray variables* are close binary systems, which are sources of *X-ray* emission. An expanding star, for example a star moving from MS to RGB stage, (donor) is filling its Roche Lobe and transferring material that eventually spins up the compact companion (neutron star or black hole). The outbursts in the X-ray indicate that heavy mass accretion on the neutron star is taking place.

Concerning *X-ray* variables there are three classes of objects:

1. **Canonical binary MSPs** likely hosting He-WD companion with mass between 1 and $0.5 M_{\odot}$.
2. **Red back** systems in which the companion is likely a MS star with mass between 1 and $0.5 M_{\odot}$.
3. **Black widow** systems in which the companion is an almost exhausted MS star or a brown dwarf with mass smaller than $0.1 M_{\odot}$.

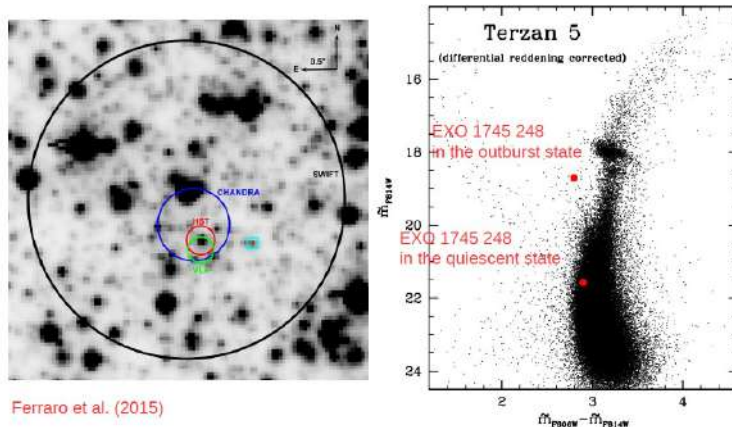


Figure 5.24: On left the precision on the position of the X-ray emission using different telescope, on right the CMD of Terzan 5, the red spot is the target that changed position due the outburst.

5.4.4 How to detect low mass X-ray binaries?

We can detect them using telescope in the X ray band, as Chandra or Swift/BAT from space (on Earth it is not possible to observe in this range). A rate increase from the direction of Terzan 5 was detected in the Swift/BAT hard X-ray transient monitor starting on 2015 March 13. Then Astronomers wanted to detect the optical counterpart: it was the neutron star EXO 1745-2348 located 6.8 arc seconds from the X ray source in a very compact region in the galactic bulge. HST immediately points the target. In particular that region was studied by HST previously, hence astronomers had an image before the X ray emission and after. Thanks to the comparison we obtained the position of the source.

In figure 5.24 on left we can see that the precision on the source's position was improved thanks to the optical counterpart revealed by HST. On the right panel there is a comparison between the position of the source during the outburst and before. EXO 1745-248 provides a link to the evolutionary chain connecting Low-mass X-ray binaries (LMXBs) to milliseconds pulsar (MSPs).

So, when an SGB star is expanding, it is transferring material to the neutron star companion that eventually spins up. The X-ray emission unambiguously indicates heavy mass accretion on the neutron star. This process is responsible for the acceleration of the MSP.

5.5 The initial Mass function

The initial mass function IMF is an empirical function that describes the distribution of mass in a stellar population. It counts the number of stars per unit mass. Astronomers try to discover if the IMF is equal for all the universe, like a universal trend, or if it depends on the environment like gas and dust.

One of the most famous IMF was proposed by Salpeter in 1955. He proposed a single power-low IMF:

$$\frac{dn}{dM} = kM^{-2.35} \quad (5.3)$$

where M is the stellar mass, n is the number density of stars and k is a constant. Hence dn/dM is the density of stars with masses between M and $M + dM$ so this type of formulation consider very small mass interval.

Therefore, from an observational point of view, we observe stars, we count number of stars per unit mass but plotting them, we obtain different results depending on the mass interval considered. A work by Kroupa (2001) suggested a 'segmented' IMF like the following:

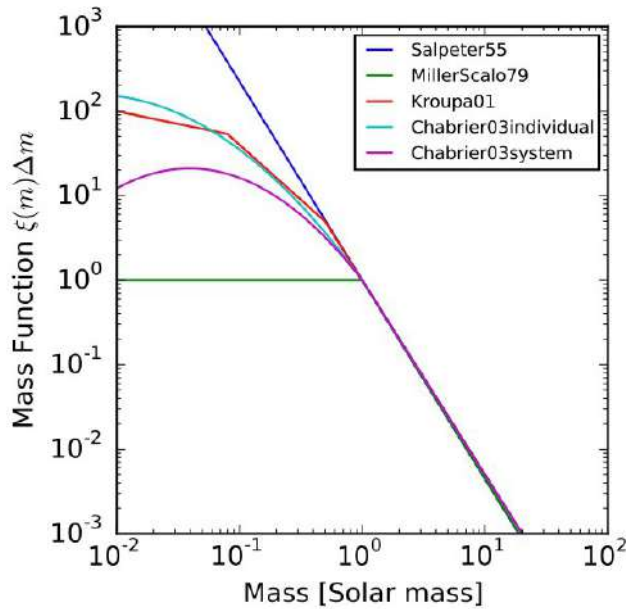


Figure 5.25: A plot with all proposed IMF by Kroupa.

$$\begin{aligned}
 dN &\propto m^{-2.3} dm \quad (m > 0.5M_{\odot}) \\
 dN &\propto m^{-1.3} dm \quad (0.08 < m < 0.5M_{\odot}) \\
 dN &\propto m^{-0.3} dm \quad (m < 0.08M_{\odot})
 \end{aligned} \tag{5.4}$$

An open question regard the presence of brown dwarfs or very low mass objects that someone suggest constitute a significant part of dark matter in galaxies having a very low mass function due to the fact they are not easy observable. However this is an idea discussed by scientists.

From an historical point of view, Salpeter mass function and Kroupa relations are ones of the most famous, but there are many other mass function proposed. In figure 5.26 they are represented in a graphic.

One of the main issue is the differences between the present-day mass function (PDMF) and IMF. The challenges for this problem are: firstly, the clusters' IMF is changed by dynamic and evolution of stars, and in the other hand, the IMF is sensitive to the binary fraction and the mass-ratio distribution of binaries.

For example in a stellar cluster there is a dynamic phenomena called 'redistribution of energy' that depends on the position of the star inside the cluster and on stellar mass: high mass stars go to the center of the cluster while low mass stars go outside, in the external region. Moreover some stars can be loss orbiting around big galaxies and there is also a problem of observing relatively nearby objects with small number of stars so with low statistics. For all these reasons we have to take into account that the region we are observing is not representative of all objects.

As consequence observing different objects (open clusters, GCs and so on) ISM is different one from another in terms of shape and slope.

Therefore to derive IMF is not easy and we have many questions: is IMF Universal? Does it depend on the environment? Is it constant in time? What is the relation with gas density or redshift?

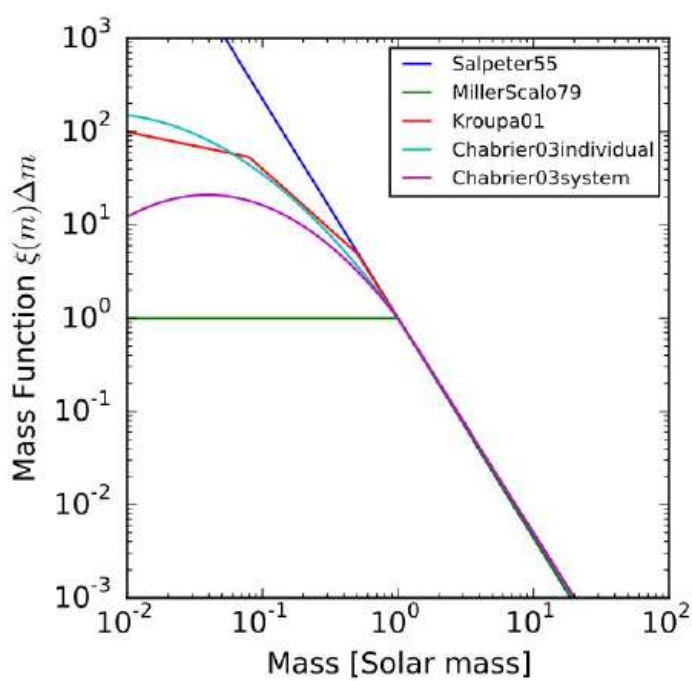


Figure 5.26: All mass functions proposed.

Chapter 6

Hunting Black Holes

6.1 Some important reminders

First of all we have to resume here reminders necessary to understand better the best way to search for a Black Hole.

As said in the previous chapter, it is important to remember that from a CMD is possible to infer a lot of information. First of all the turn-off point at the end of main sequence is a useful tool to establish the age of a stellar population. However the distribution of points inside CMD depends also on metallicity. Metallicity is a ratio from -2.5 for metal poor population to 0.5 for metal rich stars causing a shift of MS turn-off point and RGB branch to red and faint part of the diagram. Moreover it causes a different slope of RGB branch: more vertical for metal poor population and more horizontal for metal rich one.

Content of Helium is another important parameter to take into account observing a CMD: Helium-rich MS and RGB stars are bluer than helium-poor stars with the same luminosity (same magnitude in observational plane), same age and same metallicity. This means that the MS turn-off point is the same but RGB branch and main sequence split in a kind of parallel path.

Finally, wide color baselines are more-sensitive to helium variations than narrow color baselines.

On the other side changes in $[\alpha/Fe]$ ratio are a second order effect, not clearly visible by eye.

All those effect are resumed in figure 6.1.

6.2 Techniques to find Black Holes

There are many tools to investigate the presence on a black hole (BH) in a galaxy, in particular these items are used to detect a massive BH. We want to extend these techniques to a less massive BH.

Techniques:

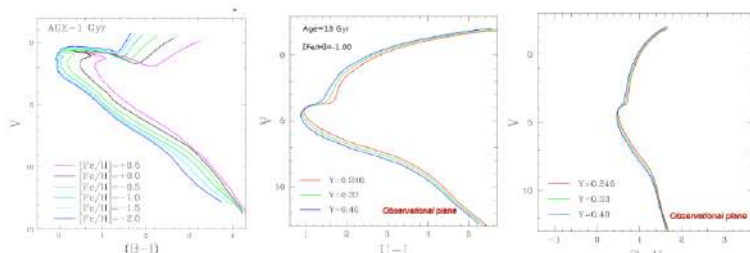


Figure 6.1: In first graphic, there is a dependence on metallicity, on the second one, dependence on helium content and on third one, dependence on color baselines.

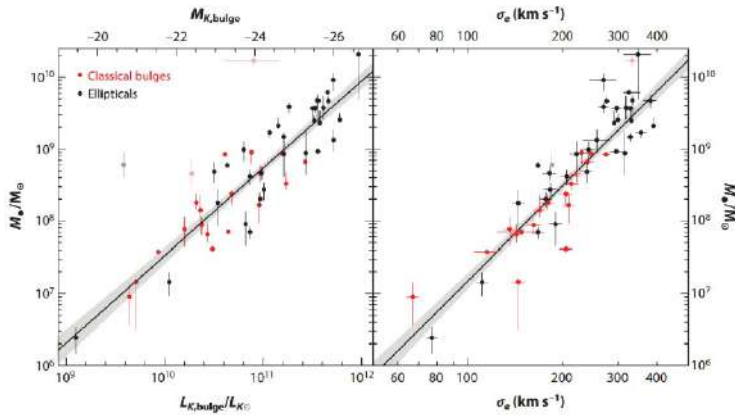


Figure 6.2: M-sigma relation.

1. **Spectroscopy:** is a way to obtain the radial velocity (comparing positions of lines in the spectra with expected position on laboratory) of ionized gas distributed in the central part of galaxy. This shows strong evidence of Keplerian rotation around a supermassive black hole mapping velocities of different regions. However this method is useful to derive presence of supermassive BH but not useful for every type of BH. Pay attention: this type of study is along the line of sight.
2. **M-sigma relation:** is a relation between the velocity dispersion a galactic bulge measured from velocities and the mass of the supermassive black hole.
3. **Proper motions:** can be used to derive the orbits of some stars near the hypothetical supermassive BH, then if the stars orbit around a 'black' point, there is a BH in the center of gravity. To get the proper motion on the sky plane we need a lot of images in different years. In this way we are able to infer the mass of dark object and its position. For example Sagittarius A is a compact radio source at the center of the Milky Way. The central light year of the Galaxy contains a dense star cluster. Sagittarius A appears to be slinging many of the cluster's constituent members at incredible speed, so fast that the presence of a Black Hole is now a 'paradigm'. Motion of central elements is shown in figure 6.3. From this analysis BH mass is about $4.10 \pm 0.60 \times 10^6 M_\odot$. Pay attention: this type of study is on sky plane.

The challenge is understanding if there is a BH less massive in the center of the more massive GCs. So, we are searching for an intermediate massive BH with a mass about $10^4 M_\odot$. There is the M-sigma relation so we can use it. If we just extrapolate this line to $10^4 M_\odot$ then we have a luminosity that is the same as faint dwarfs.

So from an observational point of view, we observe the core of the cluster looking for compact dense star cluster so GC are the best candidate. Distribution of light can be reproduced well by profiles like the King one. The King profile is also able to predict distribution of velocities.

The GC Ω Centauri is the more massive cluster that we know. It was studied in 2008 by Noyola et al. In the figure 6.4 we can clearly see that there is a large difference between the point and the red dashed line (King's profile).

In figure 6.5 we can see that the observations are consistent with a profile composed by a luminous component (continuous line) plus a dark component (dashed line): it does not fit the central part of the cluster where there is an over-density of stars and of luminosity, exact what we expect from a BH.

From figure 6.6 we can obtain that observations are consistent with a black hole of $\sim 40,000$ solar masses.

In figure 6.7 there is a comparison between the M-sigma relation derived for intermediate-mass black holes in globular clusters and that derived for supermassive black holes in some galaxies. These relation are not the same.

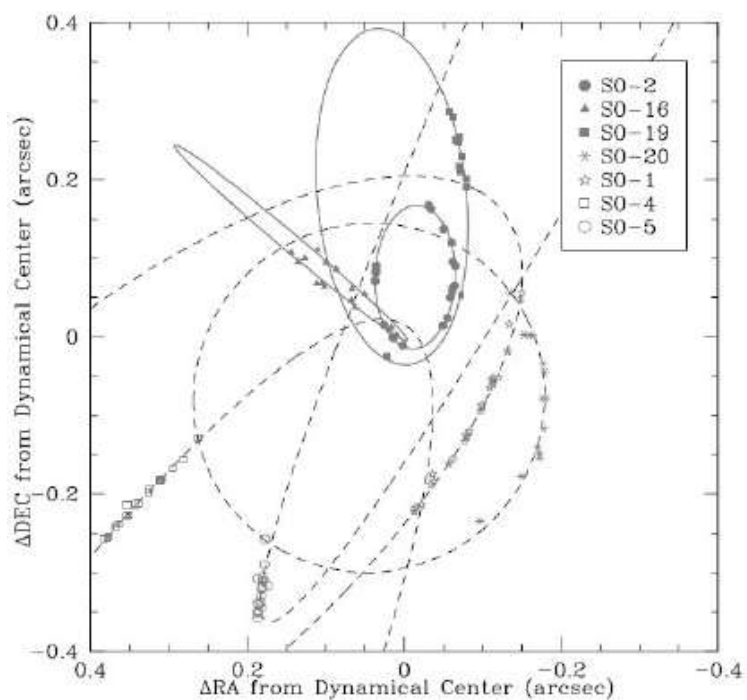
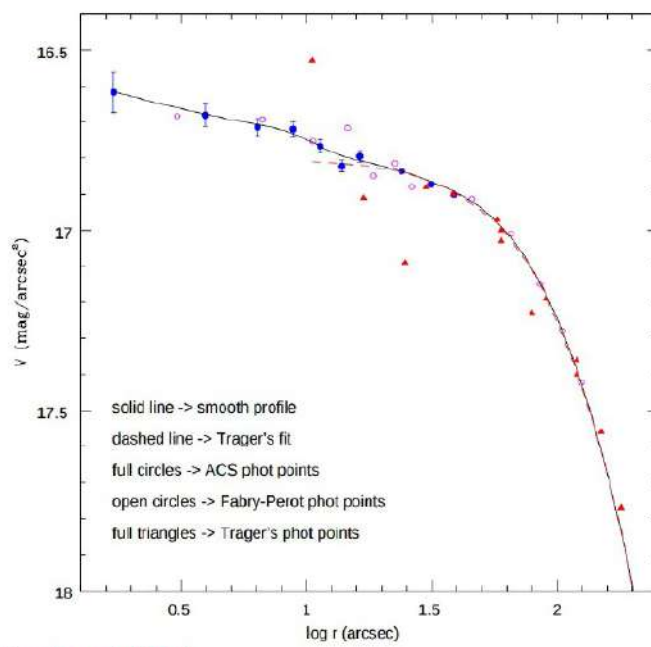
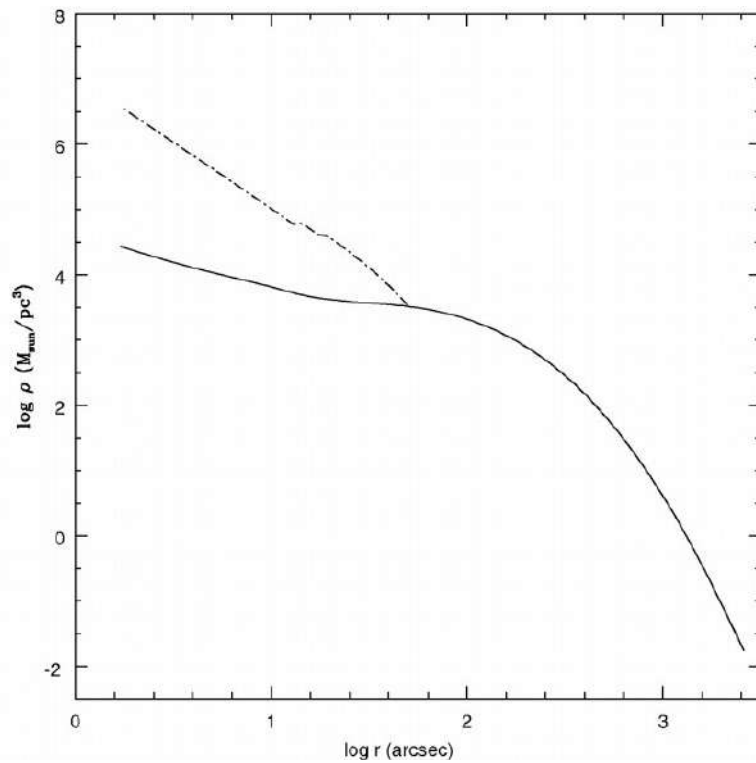
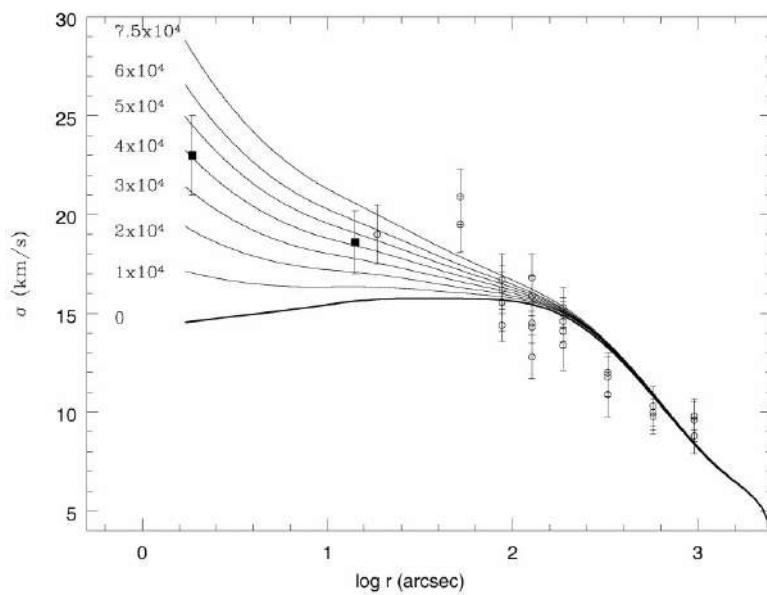


Figure 6.3: Motion of stars in Sagittarius A.



Noyola et al. (2008)

Figure 6.4: Surface-brightness profile of ΩCen.

Figure 6.5: Surface-brightness profile model for Ω Cen.Figure 6.6: Surface-brightness profile fit and observation for Ω Cen. The black solid line is representative for a model with no BH, the other grey lines are representative for models with different massive BHs.

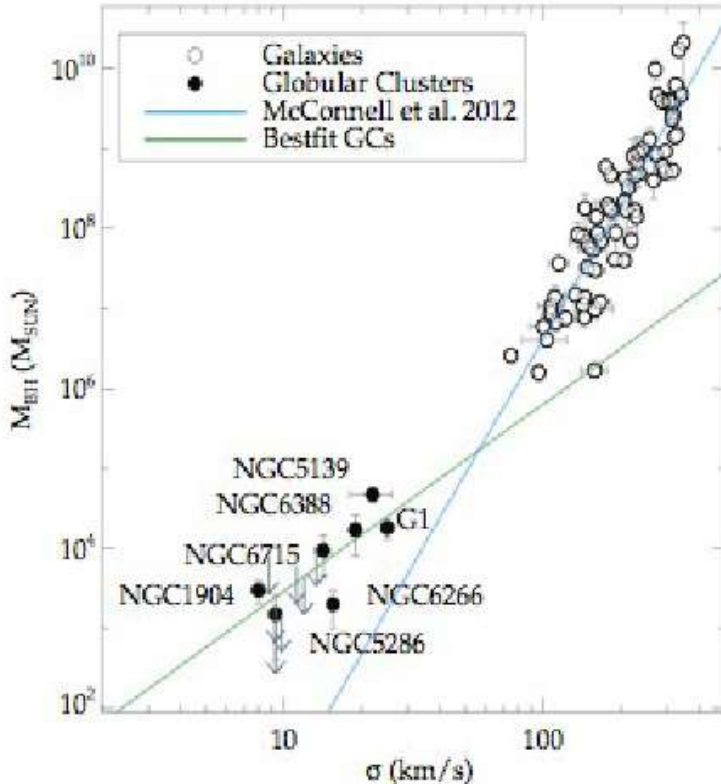


Figure 6.7: M-sigma relation for intermediate-mass black holes in globular clusters and in some galaxies.

More recent studies, done with HST (high-precision proper motions for $\sim 53,000$ stars in the central ~ 2 arcmin region from multi-epoch HST data), revealed a different scenario, indeed the mass of the possible black hole in Omega Centauri, if present, must be smaller than $\sim 12,000 M_\odot$.

We are researching these compact objects in a very dense and massive stellar group as the massive GCs. If the intermediate BHs are forming by collision of two stars in these very dense GCs we are more lucky to detect them.

Some couple of years ago we detect the first gravitational wave, now day, many of these events are detected. In particular the detected gravitational waves are produced by the merging of two stellar BHs. The GCs' environments is the best place in which these events can occur.

MUSE is an instrument of VLT, that couples the potential of an imaging device and of a spectrograph. Observations of NGC3201 as part of the MUSE spectroscopic survey of 25 Galactic globular clusters reveal a curious star with radial velocity variations of the order of $> 100 \text{ km/s}$.

The ‘curious’ star is a main sequence turn-off star with mass of $\sim 0.8 M_\odot$. It is stopped burning H and he is moving toward the RGB branch so it is expanding. What is peculiar is that neither radio nor X-ray source is known at the target’s star position (star is not a member of a binary as these we studied). Radial velocity measurements exhibit a period of ~ 167 days and Radial velocity variations of $\sim 150 \text{ km/s}$. The companion is consistent with a stellar-mass black hole with a minimum mass of $4.36 \pm 0.41 M_\odot$.

Chapter 7

The first stars

Astronomers use the name first stars to refer to the stars which were born firstly. Some refer to these stars with classification 'population III'. We suppose that these are composed of a pristine elements, hence a pristine chemical composition.

We said that an important issue of the IFM is understanding if the this distribution is universal or not. The answer is really connected to the studies of population III stars.

If the IFM is the same nowadays and at the early stage of universe, the population III stars has the same mass function of the population I (metal rich, mainly in the disk and younger) and II (metal poor, mainly in the halo and older). Then we could observe a lot of small population II stars.

If the IFM at early universe was different and with a positive slope for high masses (top heavy), there was a predominance of high mass stars. Massive stars evolve rapidly, hence now day we are not able to observe them.

Hydrogen, helium and lithium, were produced during the Big Bang nucleosynthesis (BBNS), when the universe was only a few minutes old. The population III stars are composted by this pristine matter, with no metal enrichment.

There are a few way to study these stars, one is based on the cosmology the other on the astrophysics. Two way are complementary.

7.1 The cosmology approach

We can use the 21 cm line, created by a change in the energy state of neutral hydrogen atoms, that provides information on the matter at very high redshift.

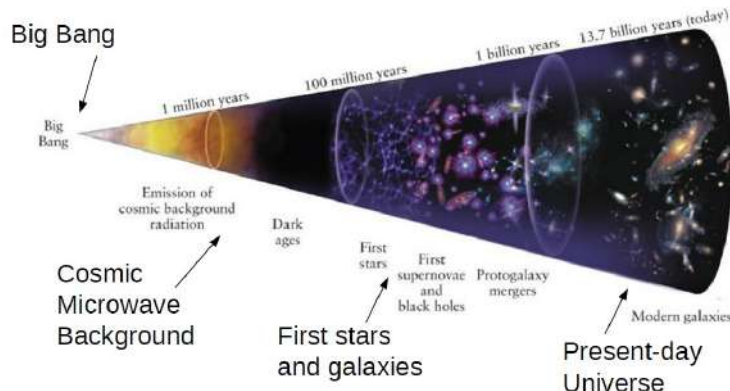


Figure 7.1: A cartoon that shows the evolution of the universe.

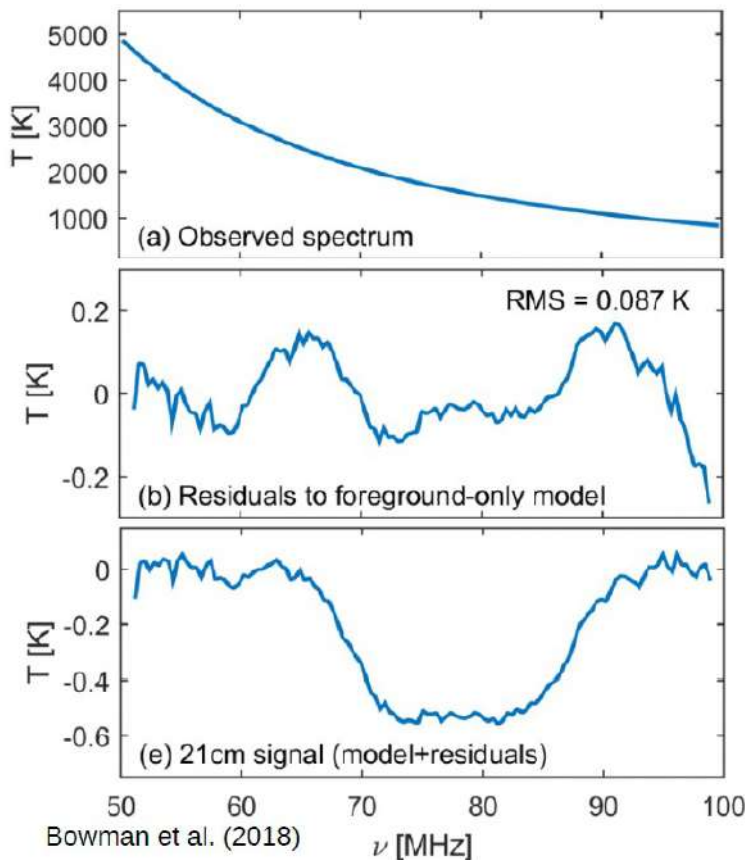


Figure 7.2: On top the spectrum revealed by Bowman, in the middle a diagram with residuals, on bottom the combination of the model and the residuals.

In the early Universe the electron spin temperature was coupled with the CMB radiation. But, when the first stars formed, the electron spin temperature was connected with the temperature of the gas. The gas was absorbing more 21 cm photons than emitting.

After a while, the first black holes formed and started heating the gas by emitting high-energy radiation so the gas became too hot to emit or absorb 21 cm photons.

If we build a diagram with 21 cm brightness against time we should observe a constant distribution before formation of stars, then a drop in the brightness when the first stars were formed (a plateau given by absorption) and then an increase of brightness when the massive population III stars evolved into BHs.

Bowman's work

Bowman and collaborators added together the CMB light from the entire sky. They integrate the emission from the entire sky at different frequencies. In this case the purpose is not to obtain high resolution images but we are interested in collecting all photons coming from the sky.

In figure 7.2 we can see the result from the Bowman's research. On top there is the spectrum the the radio telescope reveled. The observed spectrum is dominated by Galactic synchrotron emission, which is expected to smooth down with frequency (first graphic in figure 7.2) Then it is necessary to put on evidence the residuals given by foreground model (second graphic in figure 7.2). Finally they combined 21 cm models with residuals (third graphic in figure 7.2): each point is the integrated emission from entire sky.

Diagram in figure 7.3 shows the final result of their research. They plot the result against the redshift and the age of the Universe. The key point is that the Universe is expanding and as consequence the

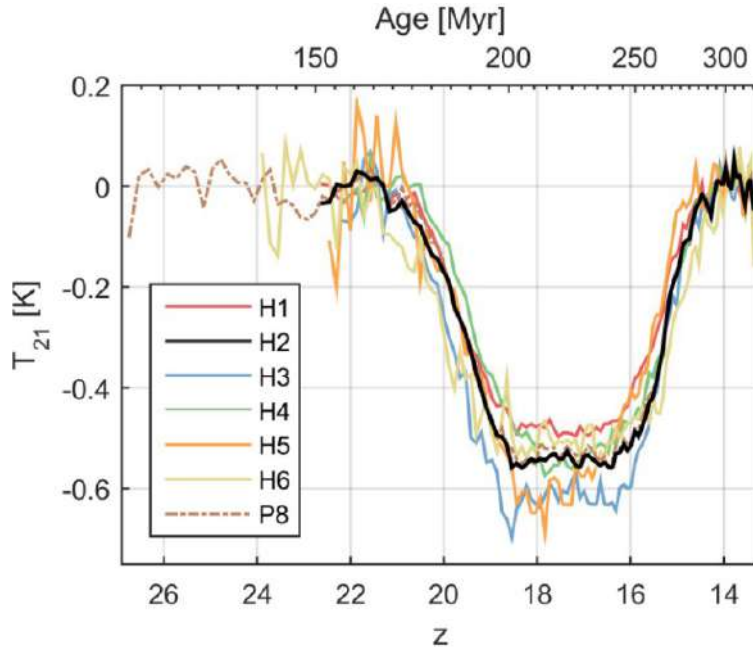


Figure 7.3: The 21cm temperature as function of redshift and the age of the Universe.

21 *cm* line emission changes in terms of frequency in time. This frequency can be converted in redshift and then the redshift can be converted in age.

To be more specific, the depth indicates the drop due to 21 *cm* absorption: the difference from zero temperature level up to the continuum level is supposed to be proportional to amount of gas. The width indicates the period between the onset of the very first stars to the onset of very active black hole growth.

However the depth is about twice as deep as expected: much more CMB is absorbed than predicted by models! As a possibility the gas was colder but we already know the temperature of the CMB, also taking into account the expansion of universe! Hence the hypothesis of a cooler gas is not the solution.

A speculation: The only thing colder than the CMB was dark matter. Maybe the Hydrogen lost some of its heat to dark matter? But dark matter never interact with regular matter except through gravity!

To conclude the cosmological approach, this is very useful to understand when these first stars formed but we are not able to infer more information about their physics and properties. To have a better knowledge of these stars is necessary an astrophysical approach. But first let's make a summary to recap what we know about population III.

7.1.1 Summary

Population III is a metal-free first population that lit up the Universe 100 – 200 *Myr* after the Big Bang. The suggested top-heavy mass function for pop III stars would render them unobservable today, given their corresponding short lifetimes.

As an alternative, Population III may have contained stars of significantly lower mass. If such Pop III stars formed, they would be still observable today. In that case, we would expect them to be eventually found in the Galaxy's halo and/or bulge. To detect them Kashlinsky et al. (2005) take an image of the bulge, subtract the sources that we observe and derive a map of the background brightness of the region. The background brightness is not uniform. The brighter zone are connected with a denser zone of first galaxies, whose we are not able to distinguish the single sources like population III. Again we can infer the time when first galaxies formed and again it is consistent with previous determination

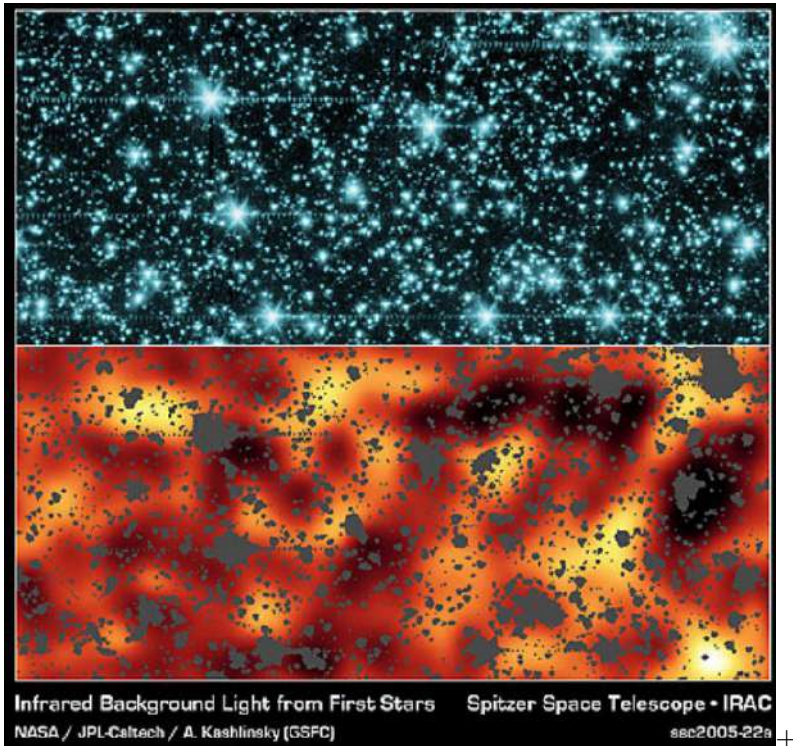


Figure 7.4: The background light from the population III stars.

($100 - 200 \text{ Myr}$ after the Big Bang) but we are not able to infer properties on first stars. In figure 7.4 Kashlinsky's result is shown.

Big questions - From what said before we will try to answer to some big questions:

- Where are Pop III stars? Are they still alive? (Do they really exist?)
- What are the properties of Pop III stars?
- To what extent Pop III stars contributed to the re-ionization of the Universe?

7.2 The astrophysics approach

With the cosmological approach we can derive the epoch in which first stars are formed while with the astrophysics approach we can derive the properties of these stars. In particular galactic archaeology observe huge details of stars in nearby universe to reconstruct events occurred before.

But what is the most appropriate place of Milky Way where to find population III stars? Let's think about our galaxy.

7.2.1 The Milky Way

The **disk** is described in terms of an horizontal thin disk plus a vertically-extended thick disk and even a more extended metal-weak thick disk. The thin disk is composed of young, metal-rich population I star ($[Fe/H] \sim -0.2$), thick disk stars have average $[Fe/H] \sim -0.6$ while the metal-weak thick disk is even more metal-poor $-1.0 < [Fe/H] < -2.5$.

The **stellar halo** has a spheroidal distribution that envelops the disk and bulge; it reaches out to $\sim 150 \text{ kpc}$ and contains old population II stars. Historically, the halo includes an inner halo that may have formed in situ during the evolution of the Milky Way ($[Fe/H] \sim -1.6$). Then there is a more-diffuse outer halo that originated from past accretion and tidal disruption of dwarf galaxies ($[Fe/H] \sim -2.2$).

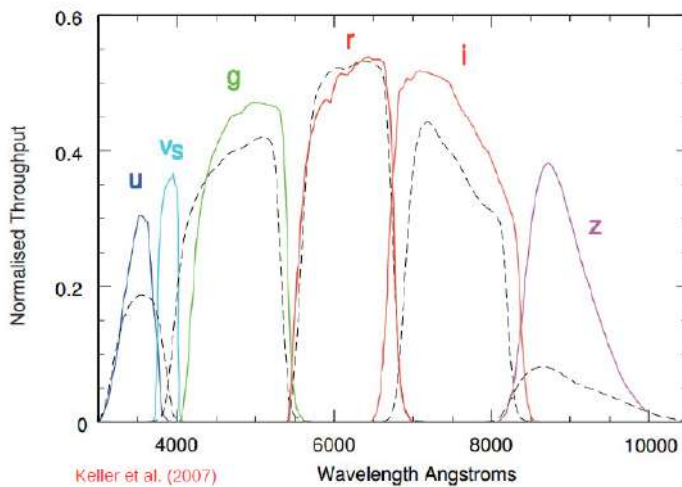


Figure 7.5: The Sky Mapper filter set.

7.2.2 Hunting the first stars

The halo is the best place in the Galaxy to research the population III stars for two reasons:

1. in the halo there are the most metal poor stars;
2. in the halo there are a few gas and dust, hence the reddening and the extinction is low.

According to some scenario of evolution of galaxy, the best place could be the bulge, but in this region there are an huge amount of gas and dust so it is not easy observe this region. In this case spectroscopy of very high resolution spectra and very high signal/noise of images.

Now days there is no evidence of population III stars, then to studying them we must look at the population II stars and derive properties of the progenitors.

We can learn about population III stars though the study of element abundance in the second and subsequent generations, composed by pristine elements and small amount of metals produced while population III were going out. The second-generation contains low-mass metal-poor stars that are observable at present day.

However it is not possible to observe single stars one by one having high resolution spectra for each of them. It is very time consuming and is almost impossible to find in this way very metal poor stars. For this reason the basic approach to select the candidates is the following.

1. A first selection of candidates from photometry indeed from stellar colors we can have approximate value of metallicity.
2. Observe candidates with low-resolution spectroscopy and obtain a second selection for spectra with low metallicity.
3. Follow up best candidates at high-resolution at large telescopes (Magellan, VLT, Keck);

One of the most important survey in the researching of population III stars is the Sky Mapper survey, that is producing multiband photometry of the entire southern sky. Observation are taken with an Australian 1.30 meters telescope with a wide field of view.

The Sky Mapper filter set is the following:

- *griz* that are similar to SDSS bands;
- *u* similar to the Stroemgren *u* band;
- *vs* centered on the *CaII* lines to generate a photometric index that is sensitive to metallicity.

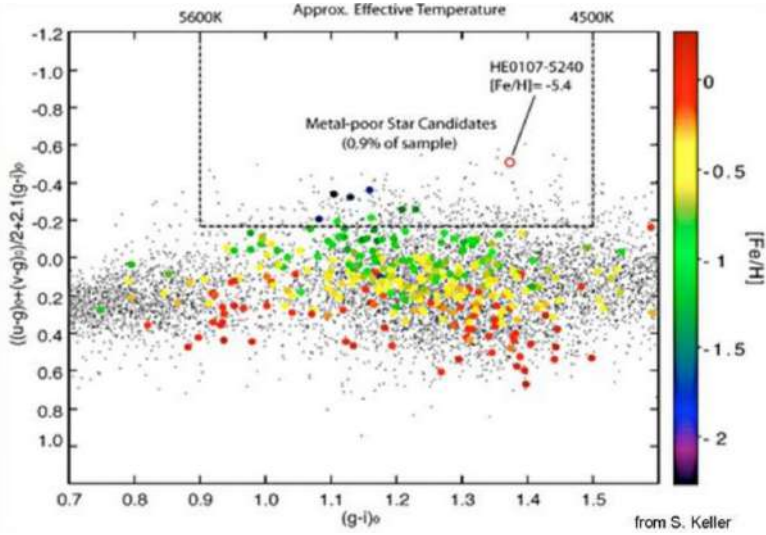


Figure 7.6: Pseudo-colors diagram. In the box we expect to find the population III stars.

In the figure 7.5 there is the filters set. The key of the survey is the v_s filter that is very sensitive to metallicity.

Thanks to these filters is possible build the pseudo-colors made with appropriate combinations of photometry. These colors are efficient tools to identify stars with different metallicities and to infer stellar properties like atmospheric parameters. In figure 7.6 there is a pseudo-colors diagram, which is used to obtain immediately metal poor stars. In the box shown inside the diagram we expect to find the population III stars characterized by the absence of metal lines inside spectrum.

In general presence of lines inside spectrum is a proxy of the presence of specific elements while the depth of lines is proxy of abundance of specific elements. To be more specific we expect that first stars are formed only of pristine elements (mainly H , He and Li) without lines associated to iron, calcium, magnesium or other metals so we expect also a different shape of the spectra.

A first discover was the Keller star: SMSS 0313-6708 that is visible in the right panel of figure 7.7. Look at the spectra of this star (7.7 on left), apparently there are no iron lines (a), using a more resolution spectrum (b) in that region we can see that iron is present but it is very less abundance and the line is dominated by the noise. The Keller star is the most iron-poor star with a value $[Fe/H] < -7.5$ with very low amount of iron, calcium, magnesium and carbon. Is the Keller star a Population III star? Or is it a second-generation star?

We know that a population II star must be composted only of hydrogen and helium. The Keller star has very low Fe but some Ca and Mg and high C . Hence it is not a population III star!

Three progenitors have been proposed for Keller star:

- **Low mass SNe ($< 10 M_\odot$)?** However Supernovae less massive than $< 10 M_\odot$ release large amounts of iron so we exclude low-mass pop III stars.
- **High mass SNe ($> 70 M_\odot$)?** SNe more massive than $\sim 70 M_\odot$ do not produce the observed C enhancement and lead to excessive N . So we exclude high-mass pop III stars
- **Intermediate mass SNe?** The progenitor is consistent with a low energy $\sim 50 M_\odot$ population III star!

According to the evolutionary model of a SNe of $40 M_\odot$, a central black hole is formed. The extensive fallback of material into the black hole traps the centrally-located iron and other heavy elements synthesised during the star's lifetime. Lighter elements (for example carbon and magnesium), residing at larger radii within the supernova progenitor, are dispersed in the explosion. The Keller star was formed from these dispersed material.

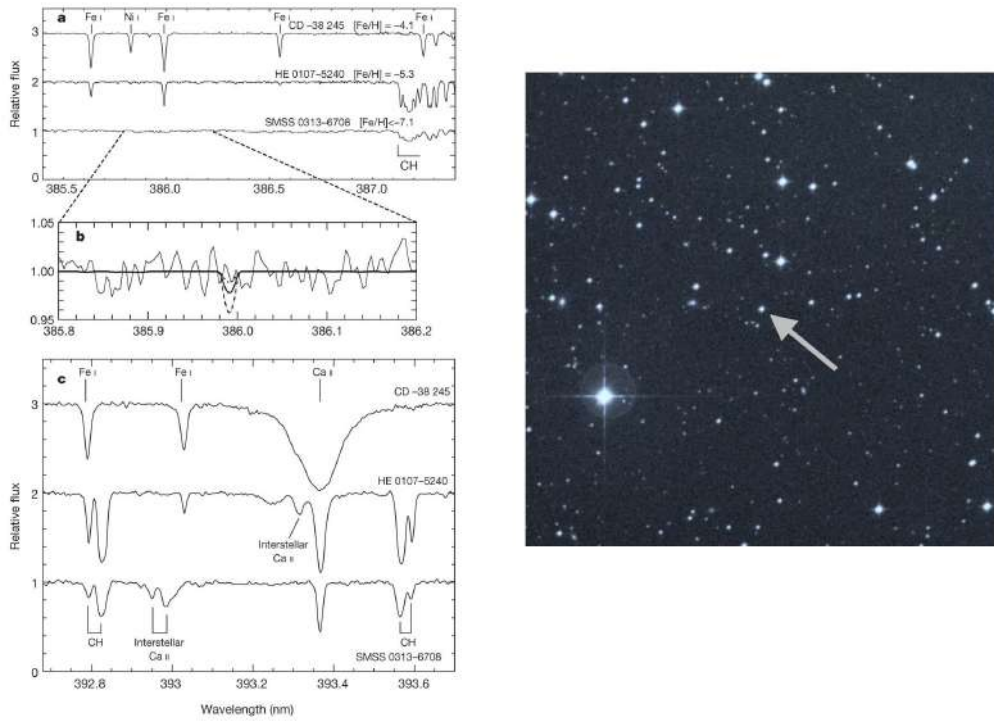


Figure 7.7: On the right the Keller star in the sky, on the left three diagrams: in the a) panel the spectrum in the region of iron lines, in the b) panel a zoom of the iron lines zone, in the panel c) the spectrum in the region of calcium lines.

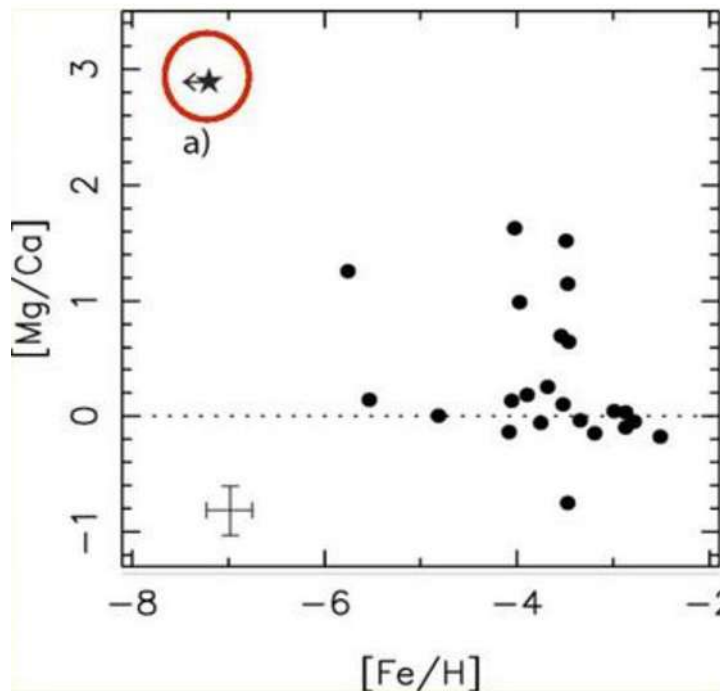


Figure 7.8: A diagram that relates the $[Ca/Mg]$ as function of $[Fe/H]$.

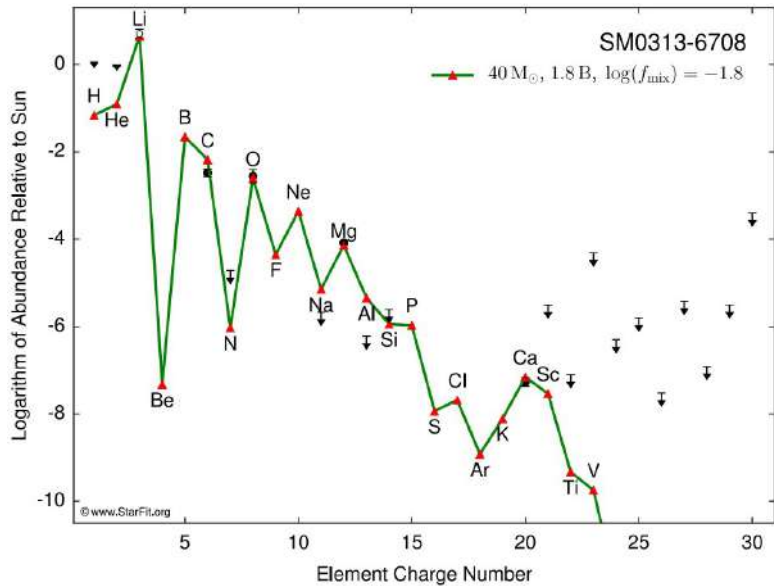


Figure 7.9: The element abundance of the Keller star (black dots) with respect to a model of SNe of $40 M_{\odot}$ (green line).

Another interesting and recent discovery is the Nordlander star found by an Australian astronomer with a metallicity $[Fe/H] = -6.2$. It is consistent with a second generation star formed from the ejecta of a low kinetic energy $\sim 10 M_{\odot}$ Pop III SN.

Chapter 8

Photometry of multiple populations

To search for multiple stellar population inside GCs is fundamental to understand how stellar systems evolved and to reconstruct events occurred during or after the re-ionization of the universe.

In the previous century, astronomers thought that globular cluster (GC) were composed by a simple stellar population, hence stars with same chemical composition and age. This thesis was supported by diagrams as those shown in figure 8.1, that shows the color magnitude diagram (CMD) of NGC 6397. This diagram is overlapped with a model of a simple stellar population that fit very well points distributed along a narrow and well defined curve. Similar studies have led to believe that in all GCs there is a simple population (SP).

However, in the last 10 years using 'super' telescopes, the research has shown that GCs are more complex systems. The CMD of GCs are not similar to a SP, but they are composed of multiple sequences, that correspond to different stellar population with different abundance of helium (He), carbon (C), nitrogen (N), oxygen (O), sodium (Na) and other elements.

An example is shown in the figure 8.2 on right, in which we can see clearly different paths so parallel isochrones to fit the data. In figure 8.2 are shown two different diagrams that reveal different population with different content of nitrogen and helium respectively. Then, to reveal the multi population (MPs) astronomers build a diagram to maximise the different contents of these elements: The chromosome map.

8.1 The chromosome map

To infer more information about multiple populations is necessary to introduce chromosome map of GCs.

How to build the chromosome map:

The building of the ChM is shown in figures 8.3 and 8.4. The process to built ChM has some steps:

1. find the limit models in the RGB zone (8.3 first panel);
2. verticalized the stars (8.3 others panels);
3. once the two diagram are verticalised, we obtain two quantities: ΔX and ΔY (8.4 Bottom panels);
4. plotting ΔY against ΔX we build the ChM (8.4 top panel).

The chromosome map (ChM) is a diagram that relates two pseudo colors of stars in different evolutionary phase (MS, RGB, SBG, AGB). The photometry used are made with a particular filters sensitive to specific chemical features. This diagram is different from the simple two colors diagram because the sequences of stars are verticalized in each direction. In this way the position of a star on the

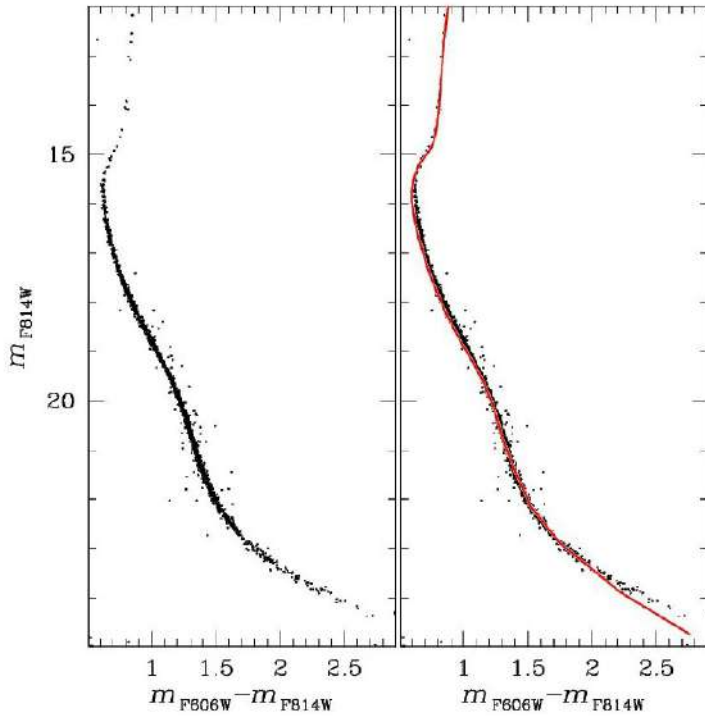


Figure 8.1: CMD of NGC 6397

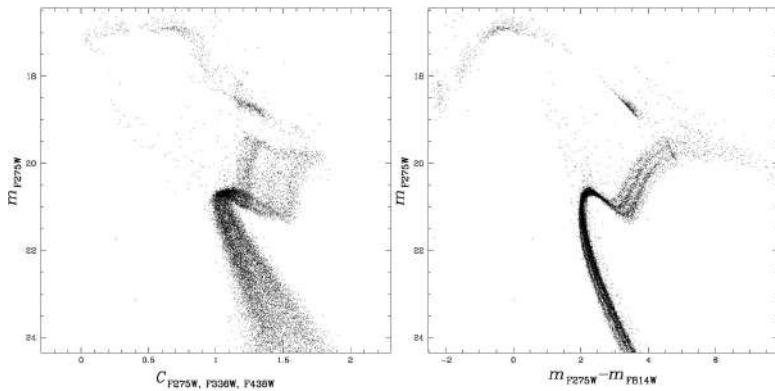


Figure 8.2: CMD of NGC 2808 and a pseudo-color diagram of NGC 2808. These diagram are sensitive to different content of nitrogen and helium respectively

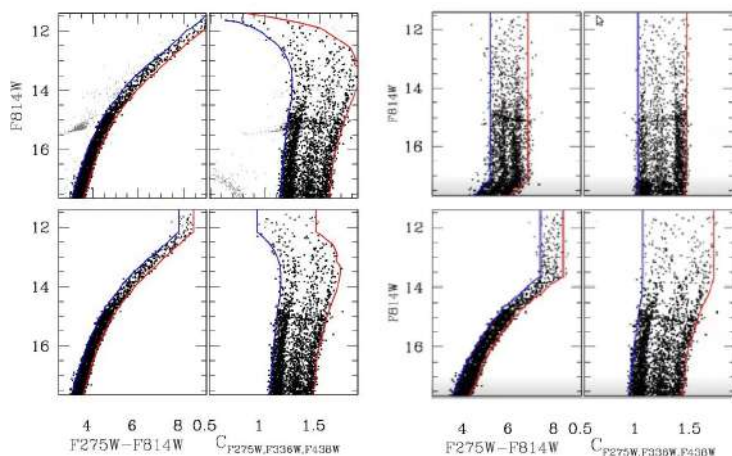


Figure 8.3: The verticalization process.

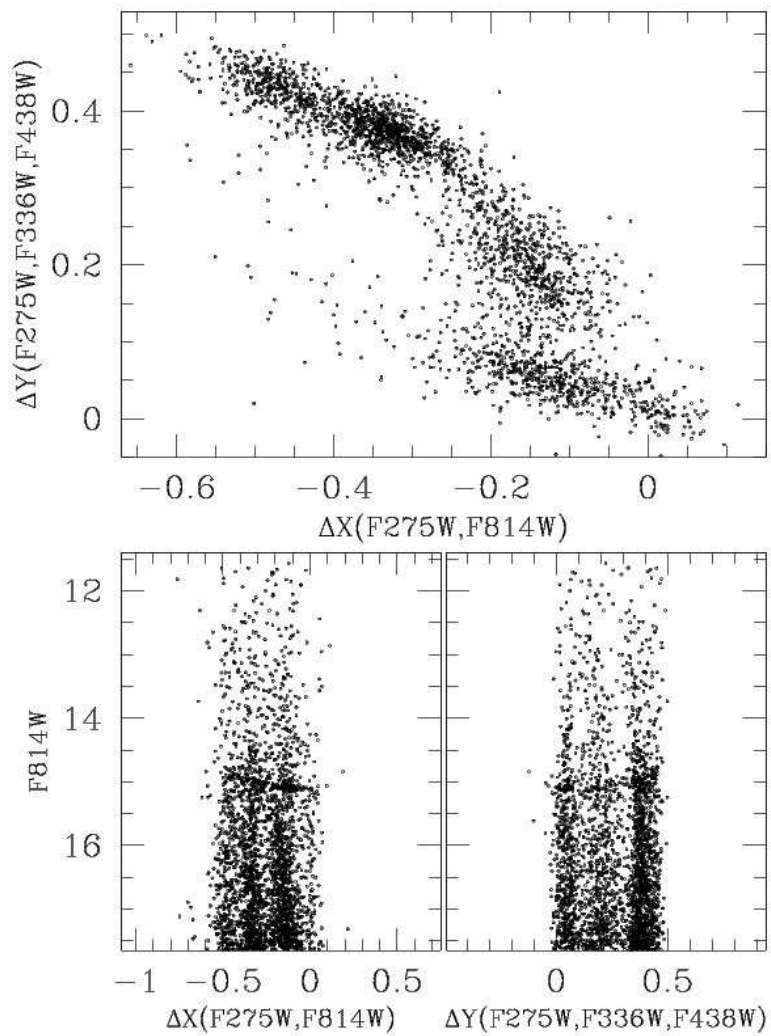


Figure 8.4: In the bottom panels the two verticalised diagrams, on top the chromosome map.

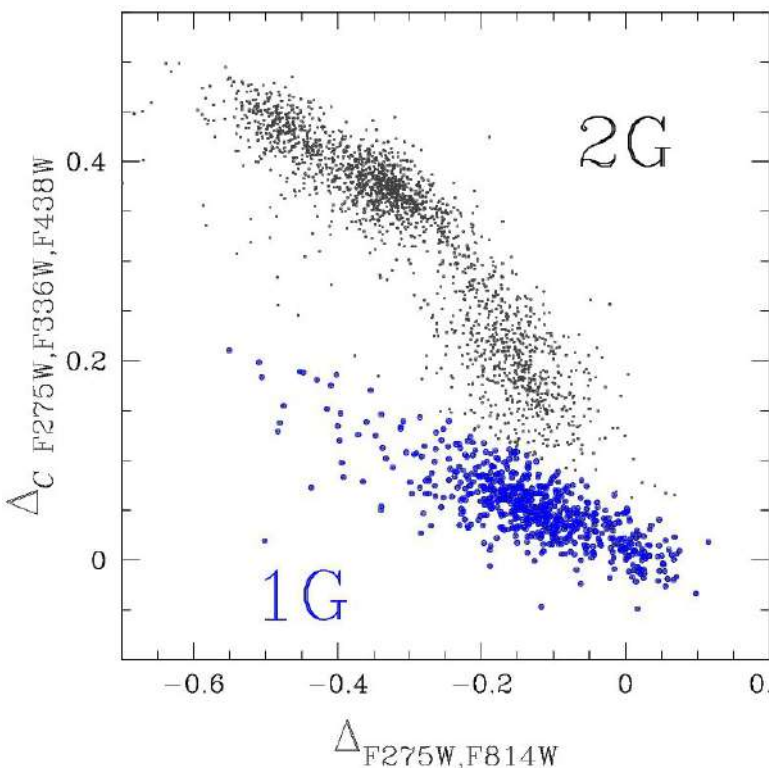


Figure 8.5: ChM from Milone et al. 2015, ApJ, 808, 51. In blue are shown the 1G stars in black 2G stars.

ChM depends only on its chemical composition. The quantity on x-axis is sensitive to the nitrogen abundance, instead the quantity on y-axis to the helium content. We can built ChM also for other elements to analyse others chemical abundances. According to this diagram, simple stellar population should be located at the origin of the two axis while we observe a large number of point distributed in the graphic.

In general chromosome map is a powerful tool: each point provide chemical composition of many stars at the same time, also abundance of Helium which is usually quite difficult to estimate.

Chromosome maps are very different according to each GC but in general it is possible to infer the presence of two groups of stars: stars of **generation 1** (1G) and stars of **generation 2** (2G). First generation has same chemical composition of pristine material from which Proto-GC formed at high redshift. They are located in the bottom part of the diagram. While generation 2 is characterized by a crazy chemical composition with huge amount of helium (about 40%) but depleted in metals.

These two groups are clearly shown in figure 8.5: in blue are shown the 1G stars in black 2G stars.

8.2 How did multiple populations form?

How did GCs and multiple populations formed in the early Universe? What is their contribution to the re-ionization of the Universe? Which is their contribution to the assembly of the Galaxy? These are few but very important questions, partially discussed in two different scenarios.

8.2.1 SCENARIO I: Multiple Generations

Look at a each MhC we can see that the first generation is a minority inside the GC, in particular 1G stars represent around 20% of the total mass of the GC. In the first scenario we assume multiple star burst occurred, then 1G is the first generation and 2G is the second generation formed from the polluted material expelled from the 1G. In this way the 1G must be dominant in the GC but we do not observe this evidence, rather we observe the opposite! This scenario assume that GCs were much more massive at formation (about 10 – 100 time than today) and they lost most of their 1G stars in the

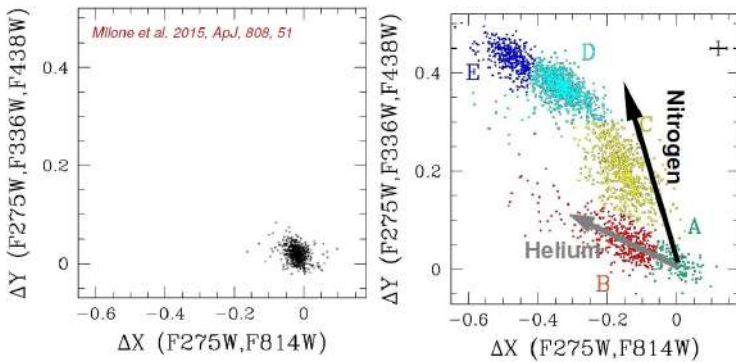


Figure 8.6: Comparison between two ChM: on left the ChM of a simple population, on right the ChM of a multi stellar population.

galactic halo. Actually observing halo stars and 1G stars they have similar metallicity and chemical composition. The greater implication of this scenario is that GCs have had a major contribution to the assembly of the Galaxy and the re-ionization of the universe.

8.2.2 SCENARIO II: Single Generation

In the second scenario we assume that the multiple sequences are the product of accretion of polluted material from stars of the same generation (no presence of multiple generations). Hence, there have been only one greater star burst and at formation GCs are more or less massive as today. As consequence, there have not been a major contribution to the assembly of the Galaxy and the re-ionization of the universe. The implication is the presence in the cluster of a peculiar stars very massive that now could be evolved in a black holes.

8.3 Ten properties of multi stellar populations

8.3.1 1G-2G discreteness

As stated before, all globular clusters host two distinct groups of first (1G) and second generation/population (2G) stars.

ATTENTION: Sometimes we say first and second generation, sometimes I and II population. In this last case we do not talk about the stellar population of the galaxy!!! 1G (or I population) stars are those stars that were formed firstly, 2G stars (or second population) are those stars that were formed secondly!!

The chemical composition of 1G stars is the same of the pristine material of cloud from which the stars are formed. The 2G stars were formed from the remaining material polluted with the expelled material of the 1G stars.

In figure 8.6 we can see a comparison between two ChM: on left the ChM of a simple population, on right the ChM of a multi stellar population. In particular in the right panel are shown the abundance vectors (the arrows) that indicate the direction towards which the abundance increases. The 1G extension is consistent with either helium variations or metallicity variation (the metallicity variation has the same vector of the *He* variation but with opposite direction). Variations of Helium in pristine material is really unexpected, maybe connected to Big Bang Nuclei-synthesis and formation of primordial BHs.

In figure 8.7 there is a ChM with the abundance vectors for many elements.

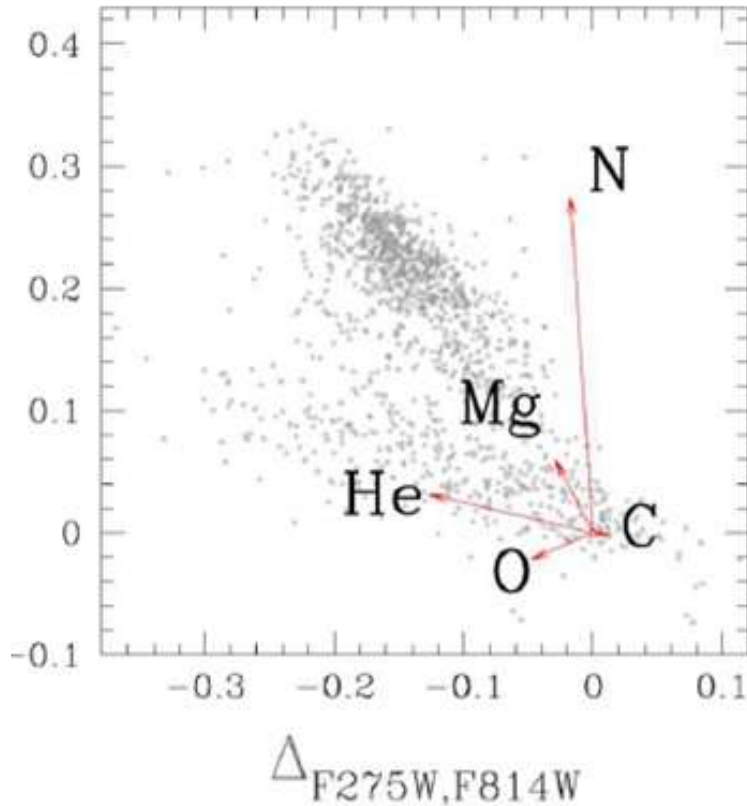


Figure 8.7: A ChM with the abundance vectors for many elements.

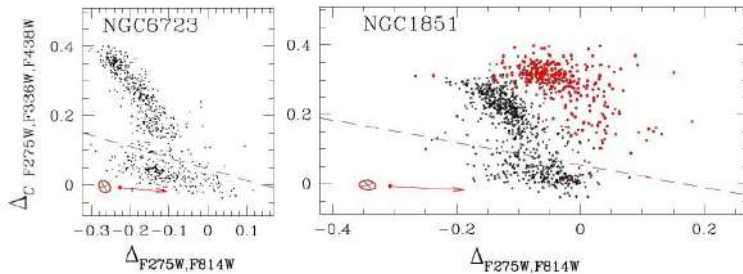


Figure 8.8: A ChMs of two types of GCs.

8.3.2 Ubiquity

Multiple populations are revealed and observed in all closest GCs: it is clear that this is a common phenomenon of observed GCs.

8.3.3 Variety

Properties of GCs are different from cluster to other cluster, as the amount of 2G stars, that range from 35% in M71 to value of 90% in ω Centauri. For example studying close galaxies, like Magellanic Cloud, with multi bands observations there is a large variety of properties. Many GCs in this galaxy have similar mass and morphology of GCs belonging to the Milky Way but with a large range of ages. So observing Magellanic Cloud it is possible to study multiple populations as function of redshift of cluster formation. Moreover, in this case some chromosome maps indicate the presence of multiple populations while other are consistent with simple stellar population (with no evidence of 2G), giving important samples to understand if multiple population is a universal law for GCs or not.

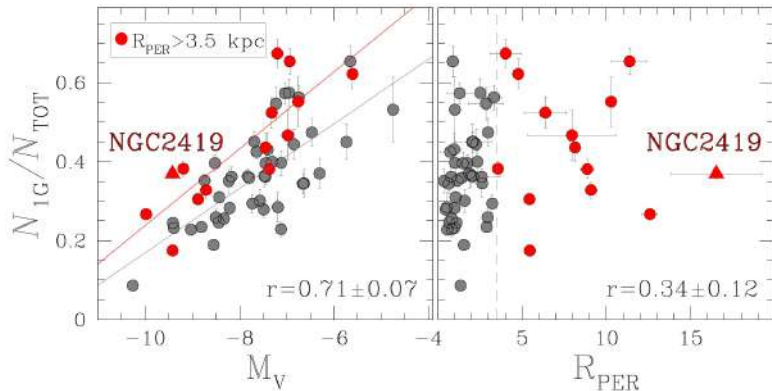


Figure 8.9: Relation between the fraction of 1G stars and the M_V (left) and with perigalactic radius (right).

8.3.4 Two classes of Type I and Type II

The most of GCs shows a single sequence of 1G and 2G stars, but around 17% shows multi sequences. For this reasons we talk about respectively GCs type I and type II. GCs of type I are normal GCs without peculiar features in ChM while GCs of type II are connected with the ChM of a nucleus of a dwarf galaxy that was cannibalized by the Milky Way or can be anomalous. In figure 8.8 there are some examples. Omega Centauri and M54, which is located in the nucleus of the Sagittarius dSph, are both Type II GCs.

8.3.5 Dependence on cluster mass

The maximum nitrogen and helium variation correlate with the cluster mass. Another dependence on cluster mass is the fraction of 2G stars that increases with GC mass. Studying a lot of clusters astronomers discover that only GCs with initial masses bigger than 100,000 – 200,000 solar masses may host multiple populations. Hence there is a possible mass threshold to have multiple populations.

8.3.6 Maximum Helium enhancement

From the diagram ($\delta Y - Mass$ or $\delta Y - M_v$) astronomers derive the maximum Helium enhancement that is $Y \sim 0.43$ (very crazy). This is an upper limit. Moreover maximum Helium enrichment provides constrains on polluters responsible for the strange chemical abundance of 2G.

8.3.7 Dependence on GC orbit and on the host galaxy

The fraction of 1G stars does not correlate with the perigalactic radius but clusters with large perigalactic radius host larger fractions of 1G stars than small-perigalactic radius clusters. In figure 8.9 on left there is the relation between the fraction of 1G stars and the M_V : we can see that the red line is up to the blue line, this means that the fraction of 1G star is greater in far GCs than the close GCs at parity of absolute magnitude.

In figure 8.10 we see two similar diagrams: on left the fraction of 1G stars as a function of present day mass, instead on right as initial mass. Look at the left panel: what has been identified is that Magellanic-Cloud clusters host larger fractions of 1G stars than Milky Way globular clusters. However the difference disappears when we consider initial mass function of the GC (left panel of figure 8.10). An hypothesis is that GCs lose most of their first generation due the interaction with the host galaxy,in particular Milky Way interact more than the Magellanic Cloud.

In figure 8.11 we plot the 1G fraction as function of 1G and 2G mass. The first plot shows a mild anti-correlation, the second plot, with 2G mass, shows a strong anti-correlation. This could be explain with a 1G star loss in the history of GCs. Astronomers build a simulation to derive the loss rate and the simulation can reproduce the observation. This fact has an important implication: fractions

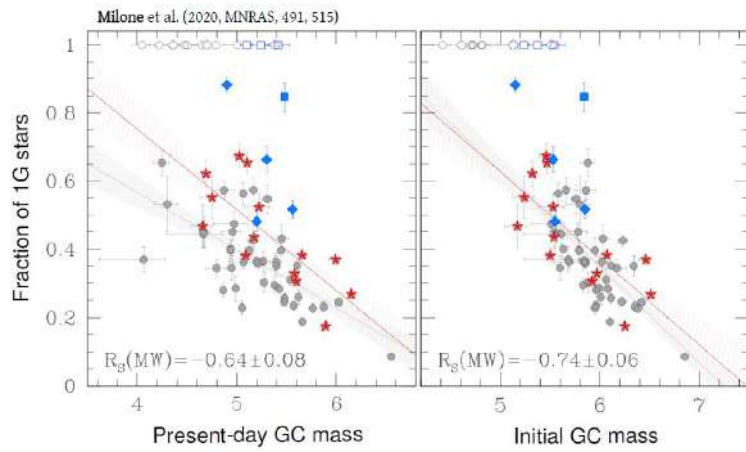


Figure 8.10: Relation between the fraction of 1G stars and mass of the GC, in particular on left the fraction is a function of present day mass, instead on right of initial mass.

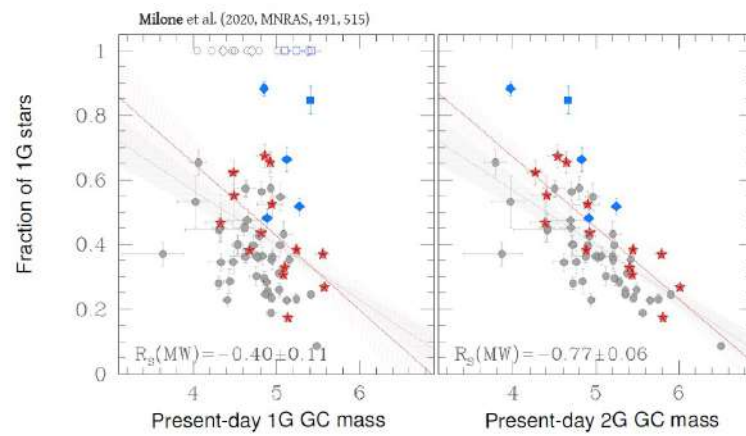


Figure 8.11: Relation between the fraction of 1G stars and the present day mass of 1G (on left) and of 2G (on right).

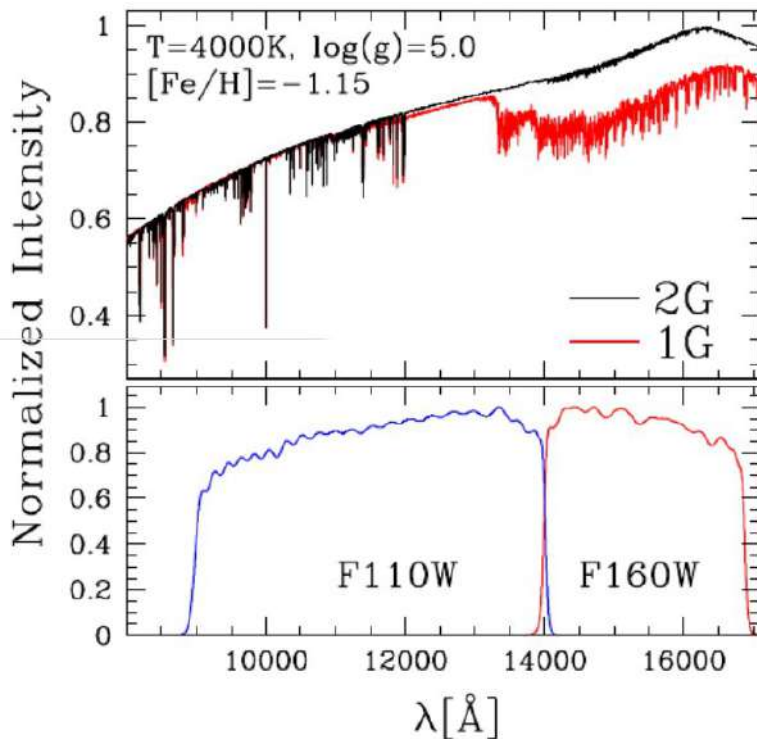


Figure 8.12: On top the spectrum of a 1G and 2G star, in the bottom panel the transmission of two filters of HST.

of 1G and 2G stars in Milky-Way and Magellanic Cloud GCs are consistent with the scenario where Globular clusters were significantly more massive at formation and preferentially lost 1G stars.

8.3.8 No dependence on stellar mass

Most of the information on multiple populations is provided by massive stars ($\sim 0.6 - 0.8 M_{\odot}$), indeed multiple-populations of low-mass stars are almost unexplored.

From a spectroscopy point of view, it is necessary to collect a large amount of photons so only bright stars (which means the most massive in RGB and sub-giant branch) are observable. On the other side, from a photometric point of view, present-day detectors are not sensitive in UV band in which we detect multiple populations. This means that it is not easy to infer precise measurements of faint stars in UV like low-mass stars. As consequence investigation on multiple populations is limited in a small range of masses, missing the vast majority of stars.

Observations in visible band are not a good solution because in this band separations between sequences are quite small.

A right solution for this problem comes from the water molecule. The 1G stars present in the atmosphere a lot of compound of oxygen as water, that causes an absorption in the spectrum. The 2G stars present a few compounds so a less absorption.

In figure 8.12 we can see the difference between the absorption in a 1G star and in a 2G star. Using $F110W$ (J filter) the difference in flux must be zero, instead in $F160W$ (H filter) there is a larger difference. The difference is visible as a difference in color in CMD for low mass stars. Using this filters we are able to separate two generations stars in low mass part of the CMD, the unexplored one, providing information about stars not studied before.

Why is so important studying the MP at low mass regime? The answer is connected to scenario of formation. In the second scenario the multiple sequences are the product of accretion of polluted material from stars of the same generation. The phenomenon of accretion was studied by Bondi. In

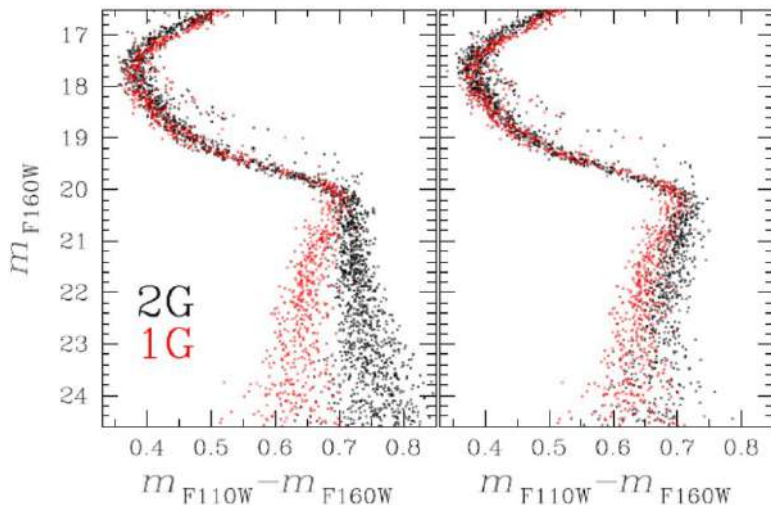


Figure 8.13: Simulation of two scenarios: CMD using the filters $F110W$ and $F160W$.

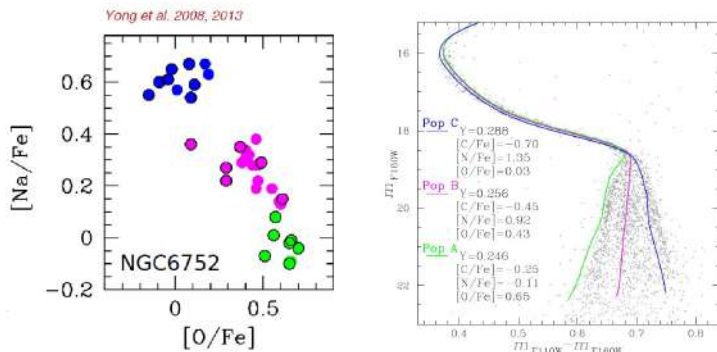


Figure 8.14: On left the ChM and on right the CMD of NGC 6752. On left panel, green points are 1G stars with normal contents of O and Na , pink and blue points are instead sub-groups of 2G stars depleted in O . If scenario 1 is correct we expect a large color variations corresponding to oxygen depletion. But if scenario 2 is correct we expect only a small variation in oxygen and small variation in color on CMD.

case of Bondi accretion, the amount of polluted material is proportional to the square of stellar mass. Then, giant stars accrete more polluted material than low mass stars.

In figure 8.13 we can see the simulation of what we should observe in case of 2 populations with different abundance of oxygen. In case of multi generation the chemical abundance is the same for massive and low mass stars indeed we observe a separation between two generation. On the other side, in case of single generation plus Bondi accretion massive stars accrete more material and we do not observe the separation because low mass stars do not accrete enough material.

So the point is to derive the chemical composition for low and massive mass stars: if we obtain the same chemical composition we are in first case, else in the second case.

Thanks to the ChM astronomers discover that the RGB of NGC 6752 hosts three stellar populations with different oxygen abundances (figure 8.14 on left). Using the infrared eye of the Hubble Space Telescope, the photometry unveils three stellar populations of very-low-mass stars. To reproduce the path of the three population, isochrones, with different oxygen abundance, are used in the fitting (figure 8.14 on right).

In general multiple stellar populations of GCs have distinct abundances of some light elements, including C , N , O , Na .

Multiple populations among low-mass and massive stars share the same chemical composition and the water molecule unveils three distinct populations of very-low mass stars.

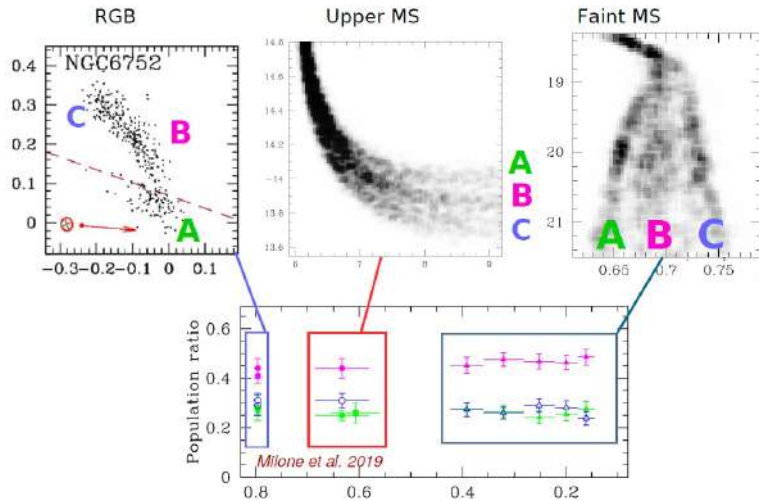


Figure 8.15: On top from left to right we see: the ChM, the CMD of the upper MS and the CMD of the fainter MS. In the bottom panel we compare the population ratio derived from the three diagrams as function of mass.

The result of the investigation is that multiple populations of low mass stars share similar oxygen contents as 0.8 solar-mass stars. Then, we exclude any scenario where 2G stars formed via Bondi-like accretion of material polluted by more-massive stars.

Another parameter to invalidate the second scenario is the mass function.

In figure 8.15 we can see the ChM and the CMD for three zone of the MS. For each diagrams we derived the population ratio (number of 1G stars over the total number of stars) for different mass range. In the bottom panel we compare the population ratio derived from the three diagrams and discover that the three population have similar mass functions (in this case the mass function is not number of stars for mass range but mass ratio for mass range). In the case of Bondi-like accretion we expect different mass function but we observe the contrary.

8.3.9 More centrally-concentrated 2G

If scenario 1 is true, 2G stars are expected to be concentrated in the center of the cluster: 1G stars ejects material that falls int the gravity center of the cluster and then, when conditions of gravity and pressure are the right ones, 2G stars form in the cluster center at high redshift. Then cluster evolves and these initial conditions are partially deleted by dynamic evolution. However observing some GCs, in particular in the external part, some signatures of initial distribution of 1G stars are still visible. Analysing radial distribution of 1G and 2G stars, it is clear that often (but not always) 2G stars are more centrally-concentrated than the 1G.

8.3.10 2G stars exhibit anisotropic motions

Using GAIA telescope, for example, it is possible to measure with high resolution the motions of stars inside GCs. It has been found that 2G stars show stronger anisotropies and smaller tangential-velocity dispersion than the 1G. On the other side, talking about rotations, 47 Tucanae presents 1G and 2G stars with same rotation while other GCs, like M5, have 1G and 2G stars that exhibit different rotations, indicating a strange distribution of stars.

8.4 Globular cluster and the missing satellite problem

we have seen that simulations based on the lambda CDM model predict that dark matter clusters hierarchically. We expect ever increasing number counts for smaller-and-smaller sized halos. In contrast to what is predicted by the Lambda-CDM model, the number of dwarf galaxies (that we observe)

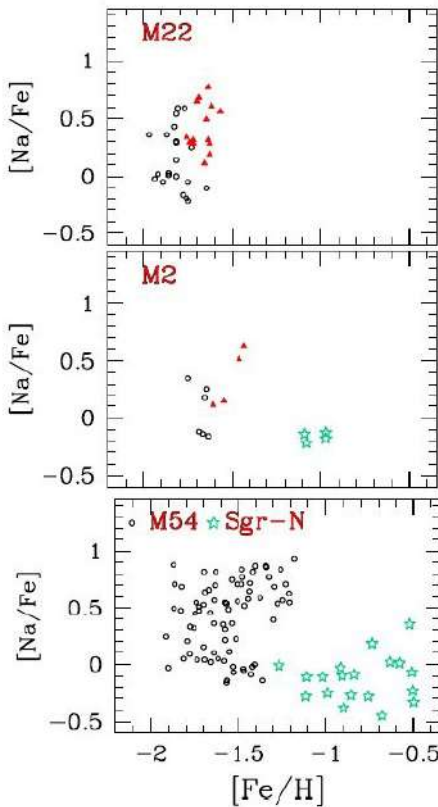


Figure 8.16: In these three panels there are $[Na/Fe]$ vs $[Fe/H]$ diagram. In the bottom panel: in black the stars of M54 and in green the stars of the Sagittarius dwarf galaxy. In the first and second panels: in black the stars with same iron abundance (similar to type I GCs), in red stars with a different pattern and in green other stars with different composition, these could be the remnants of the surrounded dwarf galaxy stars.

is orders of magnitude lower than expected from simulation. In the previous chapter we talk about the possibility of an interruption of star formation in the smaller halos due the reionization. There is something wrong with with the model? Another possibility is actually we are observing some of this satellites but we do not recognize the extra-galactic nature of them.

8.4.1 The case of M54

M54 (NGC6715) is a massive globular cluster quite close to the galactic bulge. After many years from the discovery, the observations have reveled that the GC is the nucleus of the Sagittarius dwarf galaxy. The question now is: are anomalous GCs the remnants of dwarf galaxies destroyed by tidal interaction with the Milky Way? What is their contribution to the missing-satellite problem of the lambda-CMD scenario? This GC is actually the nucleus of the dwarfs galaxy while other authors support that if formed outside the galaxy but around it. Then for dynamic fraction it ends up in the center of the galaxy. In both cases it is the nucleus of the galaxy, which is now involved in a process of destruction due to tidal forced by Milky Way. We expect that in some Gyrs it is impossible to disentangle between MW's stars and dwarf galaxy's stars.

So M54 is not a normal GC but is an **anomalous object**, a new class of stellar systems.

We have already seen that $\sim 18\%$ of the studied clusters are 'anomalous' (Type II) GCs. We know that GCs present a similar light element composition, so in the diagram $[Na/Fe]$ vs $[Fe/H]$ we should not see a spread distribution. This is true for type I GCs but false for type II GCs. Anomalous GCs include the nucleus of the Sagittarius dwarf galaxy, M54. Are all GCs of type II remnants of dwarfs galaxies destroyed by tidal force of the Milky way?

In figure 8.16 we can see three chemical abundances diagram that compare the composition between

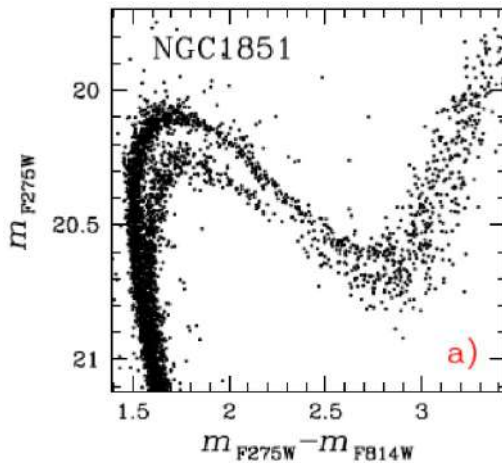


Figure 8.17: The splitting of the SGB of NGC 1851

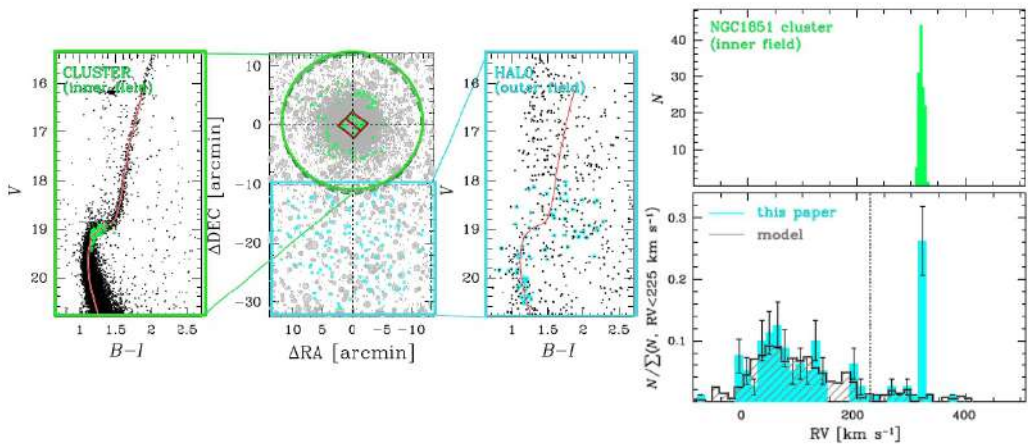


Figure 8.18: Spectroscopic analysis of M54.

M54 and other two anomalous GCs. For this diagram it is clear that anomalous GCs are characterized by large spread in iron abundance and some clusters, like M2, are depleted in lighter elements. This means that in these stellar systems there was an on-going star formation and sub-sequences stellar generations have been polluted by the ejects of supernovas. To have supernovas, however, is necessary a very big stellar system like dwarfs galaxies to form additional stellar generations. So it is tempting to speculate that anomalous GCs, similarly to M54 are the remnants of dwarfs cannibalized by the Milky Way.

Maybe M54, M2 and M22 in figure 8.16 are examples of their groups and we are seeing the same phenomenon at different evolution.

For example M54 is at the beginning of its interaction with Milky Way so there are visible also a lot of stars of the dwarfs galaxy. M2 is instead a much evolved system indeed we can observe a (smaller) number of stars: in this case maybe the galaxy has already been destroyed by tidal interaction with the Milky Way. Finally, in the case of M22, all stars of the dwarfs galaxy have been lost in the Milky Way while the nucleus (the GC itself) is still alive.

One property of type II GCs is the split of the SGB, as shown in figure 8.17. Look in more details NGC 1851. It is surrounded by a halo that is visible from the tidal radius of 700 arcsec (41 pc) to more than 4500 arcsec ($> 250 \text{ pc}$). It is a very huge distribution of stars but this halo contains only approximately 0.1% of the dynamical mass of NGC 1851. How formed this stellar distribution at high radius, where gravitational field of the galaxy is stronger? How can it resists?

In figure 8.18 we can see the CMD of the cluster and of the halo. Deriving the radial velocities we are

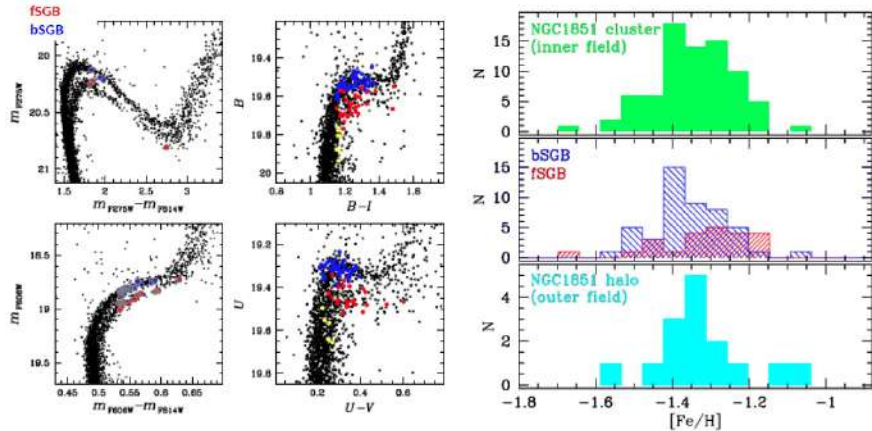


Figure 8.19: Chemical analysis of NGC 1851.

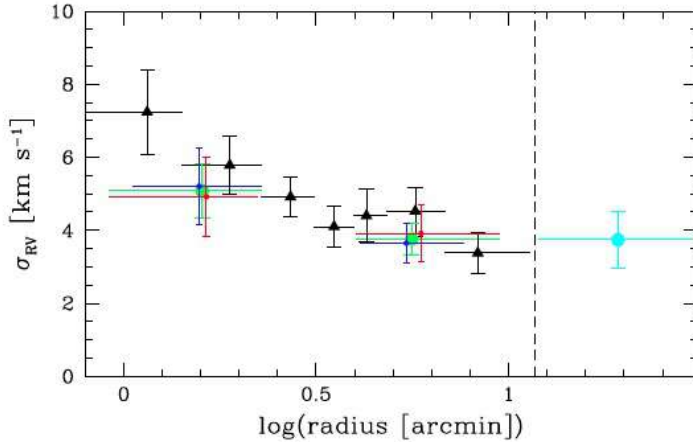


Figure 8.20: The velocity dispersion of NGC 1851.

able to detect the stars which are dynamically linked to the cluster. The distribution in RVs confirms the presence of a halo of stars dynamically linked to NGC 1851. How is it possible to generate a structure which is stable from a dynamical point of view that contains just 0.1% of visible mass? Is the cluster surrounded by an halo of dark matter?

Analysing the abundance, in particular the distribution in $[Fe/H]$, the halo stars present composition similar to that observed in the cluster (figure 8.19).

Astronomers studied the chemical abundance of element that are formed by s-process. The stars cluster show two different group of stars, one poor and one rich, respectively bSGB and fSGB. Instead the halo stars around NGC 1851 populated mostly by s-poor stars. This fact is simulated by a scenario in which NGC 1851 is the remnants of a galaxy.

The s-rich and the s-poor groups appear dynamically similar. The velocity dispersion does not drop to zero outside the tidal radius (dashed line in the graphic) of NGC 1851: the blue point is about 4 km/s . Therefore the diagram in figure 8.20 is not similar to that of a GC but similar to that of a galaxy.

These peculiar features are explained by two different scenarios.

Two scenarios

1. **Evaporation of stars:** NGC 1851 is loosing into the field preferentially s-poor stars.
2. **Dwarf galaxy relict:** NGC 1851 is the nucleus of a dwarf galaxy disrupted by tidal interactions with the MW, and the halo represents the relic of the dwarf where the cluster was embedded

(Bekki & Yong 2012).

8.5 Analysis of some Chromosome Map

The pictures that we have seen are all based on photometry, which is a powerful tool because we are able to study a large number of star in a small amount of time. Spectroscopy is more challenging because we can observe a few stars for a lot of time and only the brightest star can be investigated in details. The ChM is a photometric diagram that shows information about the chemical composition for a few elements (for example helium or nitrogen), but we are not able to investigate other elements like sodium (Na) with photometry. In same case a spectroscopy analysis was made to investigate the nature of the multiple sequences, in particular some stars are selected and astronomers derived the spectra of them. By using spectroscopy the conclusions are the same:

- the multiple sequences on CMD correspond to stellar populations with different chemical abundances;
- elements showing variations are associated with the H-burning. We see increase in the H-burning products, like Na , N and decrease in elements destroyed in these processes like O and C . Not all elements present a variation, some are constant for all sequences;
- multiple sequences are populated by stars with different chemical composition.

M4

By using the spectroscopy astronomers build $[Na/Fe]$ vs $[O/Fe]$ diagram. The result is comparable to the ChM for M4, a GC that shows a simple chromosome map. In particular the 1G stars show the same chemical composition and metallicity of the halo stars of Milky Way while 2G stars composition is not comparable to halo stars composition. Actually this is one of the reason that supports the idea that GCs have lost preferentially 1G stars in the halo interacting with the Milky Way.

8.5.1 Horizontal Branch

One of the most complicate issue of the stellar evolution is the the horizontal branch phase. The so called **second parameter problem** concerns the morphological path of the HB. One of the parameters that affect the path is the metallicity (metal rich GCs have short and red HB while metal poor GCs have on average blue and extended HB) but not in some case GCs with same metallicity show different HB. However there are other parameters that affect morphology of HB. Many second parameters have been proposed like H variations, He variations or exotic parameters like presence of exo-planets orbiting some stars and responsible for extra-mass loss which GC blue. Maybe multiple populations can provide the key to understand this second parameters.

We have seen that in M4 there are two population detected thanks to $[Na/Fe]$ vs $[O/Fe]$ diagram, these stars correspond to two different paths on the RGB. Also in terms of HB, it shows two groups: one blue and one red. Astronomers studied these stars and discovered that these stars correspond to two generation stars of M4. The blue HB stars are 2G stars (rich in sodium and depleted in oxygen) instead the red HB stars are 1G stars.

There is a clearly connection between the chemical composition of the generation and the HB morphology.

Multi sequence on CMD, second parameter problem HB and chemical anomalies in stars are different faces of the same problem.

NGC 2808

This is a more complex stellar system. The ChM shows 2 generation and each of them different populations. This characteristic is the same that is detected with spectroscopy. In particular there

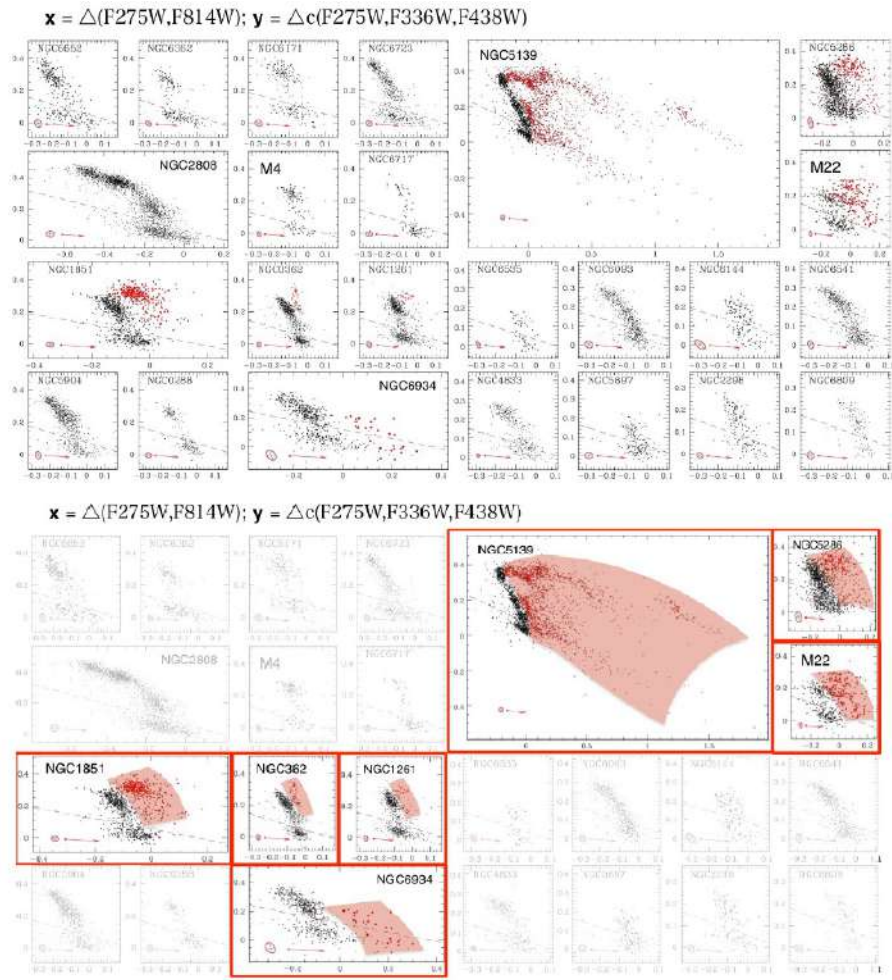


Figure 8.21: Caption

are variations in magnesium and silicon for the most massive and metal poor stars. This provides unique information about stellar evolution: this indicate that polluter stars (the ones responsible for 2G stars) reach in the interior certain temperatures to produce specific elements.

Anomalous GCs

We have seen that about 18% of GCs present a different ChM, these are called type II. The others ($\sim 82\%$) are *normal* GCs, also called type I.

Anomalous GCs have some peculiar features:

1. a distinctive chromosome map (figure 8.21);
2. split in RGB in visual filters. The fainter sequence correspond to the peculiar type II group of stars on ChM (shown in red in figure 8.21). This features is visible not only in UV filter that is sensitive to the atmosphere of star, this split is also visible in visual filters, which are not sensitive to the atmosphere but to the interior of stars. Then this feature in connected with the composition of stars and not with the atmosphere;
3. variation in heavy elements and C+N+O (variation in metallicity and s-process), even larger than variations in dwarfs galaxy.

In figure 8.21 there are some ChM of GCs, in the bottom panels are shown the GCs that are type II and in red are shown the second group of stars that are peculiar. Some GCs present a minority of these 'red stars', some instead are dominated.

8.6 Formation scenarios of multiple stellar populations

8.6.1 Scenarios with multiple generations

We consider here the case of multiple stellar generations which means multiple bursts: each block in chromosome map with different chemical composition corresponds to a different stellar population formed in a different epoch and possible in a different region of the cluster.

Asymptotic Giant Branch scenario

The first generation (1G) forms with a full Initial Mass Function which means that there were low mass stars as well as high massive stars. Then, massive 1G stars explode as SNe. The expelled material has high velocity and the explosion sweep off the material left from 1G (the pristine). After > 30 Myr AGB stars start ejecting material that collects in the cluster center. The cluster accretes pristine gas from the surroundings. Then in the center there is a mix between the pristine material and a polluted material ejected from AGB. The 2G forms in the cluster center. The Globular cluster loses a large fraction of 1G stars into the Galactic field.

Fast-Rotating Massive Stars

The polluters are fast-rotators massive stars (masses $\sim 25 - 150 M_{\odot}$). Fast-Rotating Massive Stars (FRMSs) lose mass through a slow mechanical equatorial winds and produce material rich in H-burning products. Second-generation stars may then form due to gravitational instability in these discs, which are fed by both the FRMS ejecta and pristine gas.

The mass-budget problem

Regardless the nature of polluters, second-generation stars born out from the material polluted by first-generation massive stars. However the present-day second generation comprises the majority of cluster stars while 1G stars are usually a smaller fraction.

Making some simple calculations:

$$M_{\text{progenitor}} \sim M_{SG(\text{today})} \cdot 20 \cdot \varepsilon^{-2} \quad (8.1)$$

where M_{SG} is the present-day mass of the second generation; ε is the canonical star-formation efficiency; the factor 20 accounts for the fact that only ~ 5 of the mass of 1G come out with the right composition to make the 2G.

For a typical mass of 2G stars: $M_{SG(\text{today})} \sim 10^5 M_{\odot}$. This implies a progenitor mass of $\sim 2 \cdot 10^8 M_{\odot}$.

Multiplying this estimate by ~ 200 (the number of GCs in the Galaxy) we find that the total amount of gas needed to form all Galactic GCs is $\sim 4 \cdot 10^{10} M_{\odot}$ with $\sim 4 \cdot 10^9 M_{\odot}$ dissolved 1G stars (GCs were 10 time greater, this means that the vast majority of 1G was lost around the MW). Such mass is comparable with the mass of the Galactic halo!

Consequences of this are:

- the progenitor of Globular clusters were as massive as dwarf galaxies and lost most of their first-generation stars;
- they could provide a significant contribution to the mass of the Galactic Halo;
- they could provide a significant contribution to the reionization of the Universe.

8.6.2 Scenarios with a single generation

In this case Globular clusters host a single stellar generation, but with different populations.

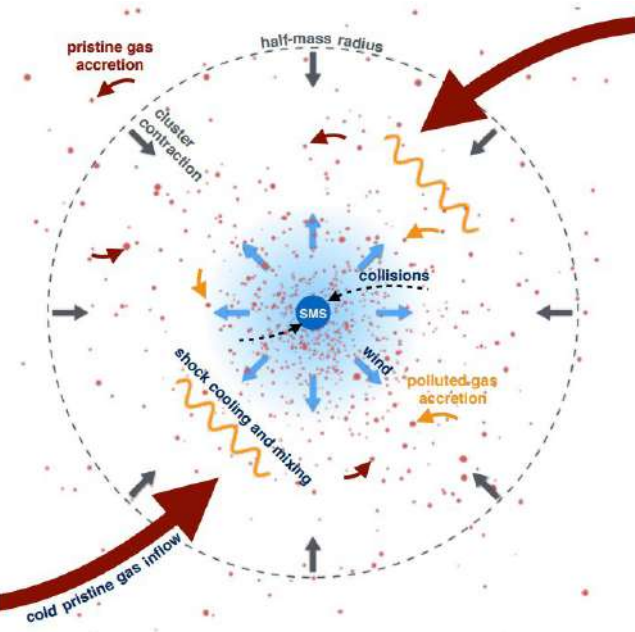


Figure 8.22: Super massive star model (Gieles et al, 2018).

8.6.3 Supermassive Stars

GCs form in converging gas flows and accumulate low-angular momentum gas, which accretes onto protostars. This leads to an adiabatic contraction of the cluster and an increase of the stellar collision rate.

A super-massive star (SMS) can form via runaway collisions if the cluster reaches sufficiently high density before two-body relaxation halts the contraction. This condition is met if the number of stars is $> 10^6 M_{\odot}$ and the gas accretion rate is $> 10^5 M_{\odot}/Myr$, reminiscent of GC formation in high gas-density environments, such as – but not restricted to – the early Universe.

SMS are characterized by strong stellar winds, that mixes the outflowing material with inflowing pristine gas. The protostars accretes this polluted material processed by the SMS. In SMS a rejuvenation phenomenon occurs due the inflowing material that reaches the star. Because of the continuous rejuvenation, the amount of material ejected by the SMS can be 10 times higher than its mass. This would provide a solution to the mass budget problem!

The material ejected by the SMS is enriched in Helium and in C,N,O. We expect a super-linear scaling between the amount of processed material and cluster mass (figure 8.23). In agreement with the observations! Note that in the SMS scenario (by Gieles et al.) all stars have the same age. There are NO multiple generations of stars!

Is there any observational evidence for super-massive stars? The 136a star cluster in 30 Doradus hosts at least seven stars with masses larger than $100 M_{\odot}$.

Nowadays we are waiting for future observations of James Webb Telescope to obtain data in order to verify scenarios shown previously. In particular we will be able to analyse low mass stars and compare their properties with high mass properties.

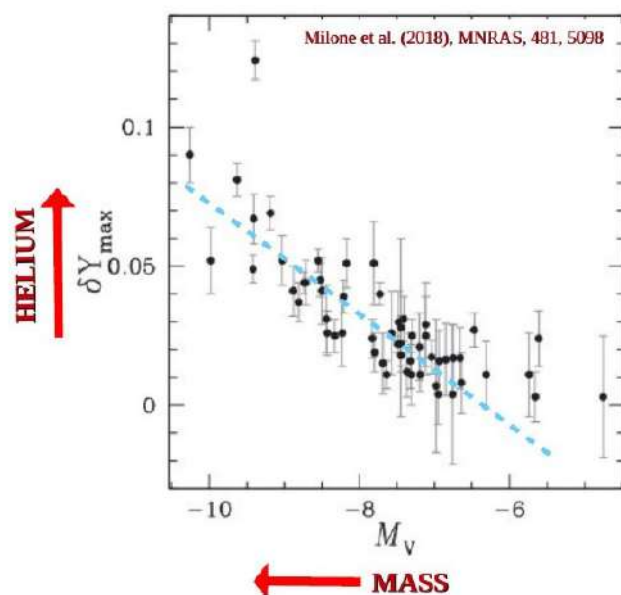


Figure 8.23: Super-linear scaling between Helium and mass.

Chapter 9

The extended Main Sequence Turn off phenomenon

Galactic Globular Clusters are among the most ancient objects of the Universe. We study the present-day old clusters to understand how they formed in the early Universe, nearby us. Indeed observing GCs quite close we can obtain huge amount of information while it is quite difficult study very distant objects from which we have few information.

In general in MW we have only old GCs, in the LMC and SMC there are GCs with a wide range of ages, so there we can study the young and intermediate GCs and derive some general information.

A few years ago astronomers thought that old CGs are characterized by multiple stellar population, instead the young star clusters were considered prototypes of single isochrones: stars of same age, same distance and same chemical composition.

Then, by using a new camera of HST with appropriate filters, the situation for young stellar cluster changed; using appropriate combinations of filters an high degree of complexity is visible. In figure 9.1 we can see the difference between and old CMD and a new one. On the right panel are shown the main characteristics of young cluster:

- a **split Main Sequence**, merging in the bottom part of the diagram;
- **extended MSTO (eMSTO)**. This is not due to differential reddening because the spread at the MSTO should be also in all other sequences but it is visible only in the upper part of MS. This suggest we are observing multiple populations few Myr just after the formation.

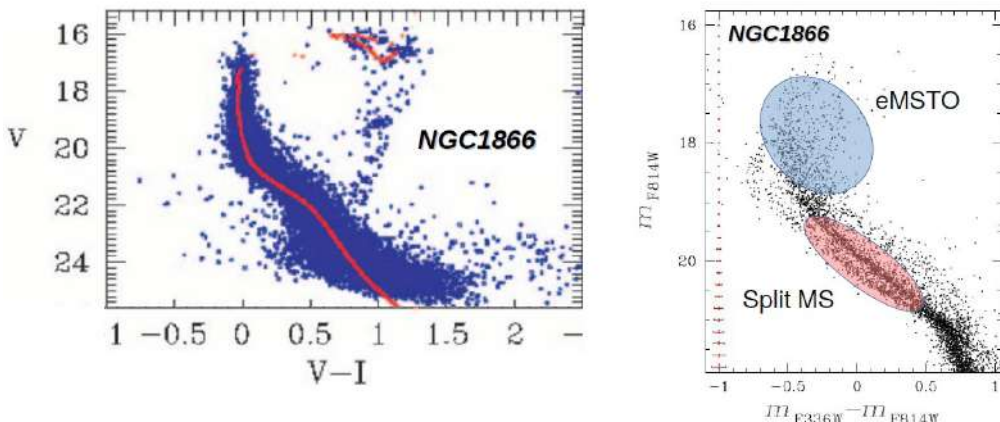


Figure 9.1: Comparison between CMD of a young cluster (NGC1866) a few years ago and now days.

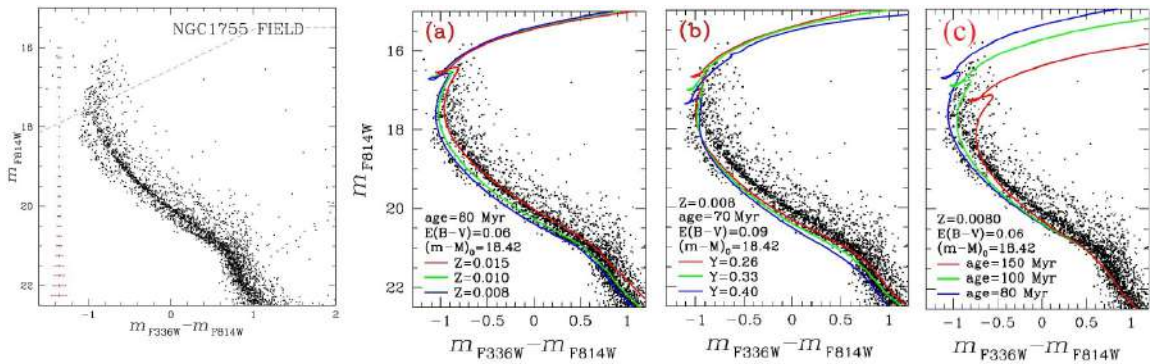


Figure 9.2: CMD of NGC 1755: in panels a,b,c are shown different models to reproduce the morphology.

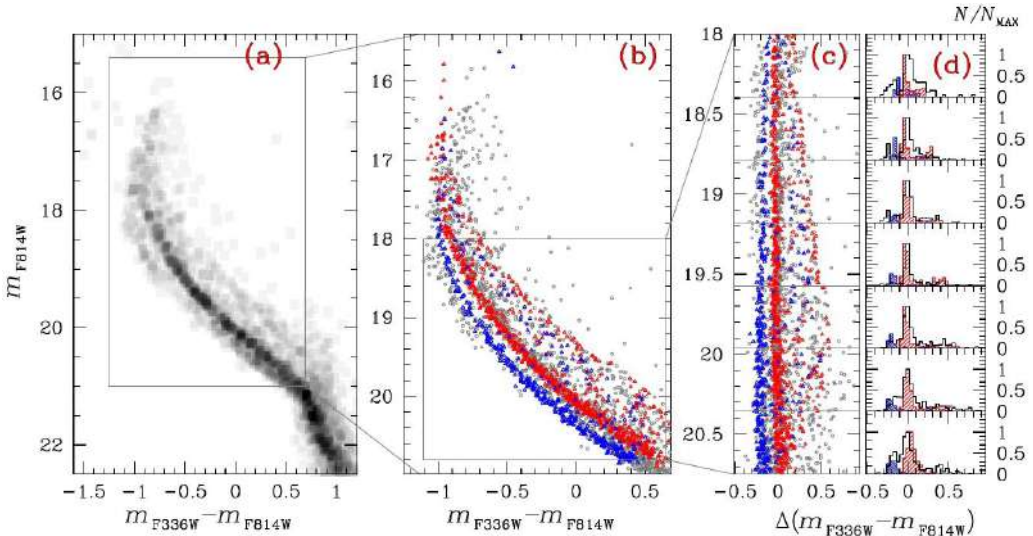


Figure 9.3: CMD of NGC 1755: in panels there is the model for stellar population with different rotation rates.

These feature are detected also in other clusters, hence these are not a peculiar features of one cluster but a common features for young clusters.

The extended MSTO and split MS is a common feature of $\sim 1 - 2$ Gyr star clusters in both Magellanic Clouds. On the other side, in clusters older then 2 *Gyr*, split in MS disappears and extended MSTO remains.

So if we interpret extended MSTO as prolonged star formation history, the age spread should be included between 50 and 200 – 300 *Myr*: the same time for AGB stars to evolve and to eject in intracluster medium the material from which 2G formed.

Do the young counterparts of the old Galactic clusters host multiple stellar generations? This is an open question because the evolution is not clear.

Let's now talk about double main sequence. Possible causes of the double main sequence are the following:

- **Different helium abundance:** the helium different can be detected in visible band as multiple sequences. Look at figure 9.2 panel b): the split is not reproduced using different helium populations (isochrones diverge in the bottom part of MS) so this is NOT the reason.
- **Metallicity variation:** in type II GCs we have population with different iron content; these clusters are connected with the nuclei of dwarf galaxy cannibalized by MW. If young cluster shows metallicity variation we can exclude that connection between the iron content variation and that scenario. Look at figure 9.2 panel a): metallicity variation reproduce sequences but

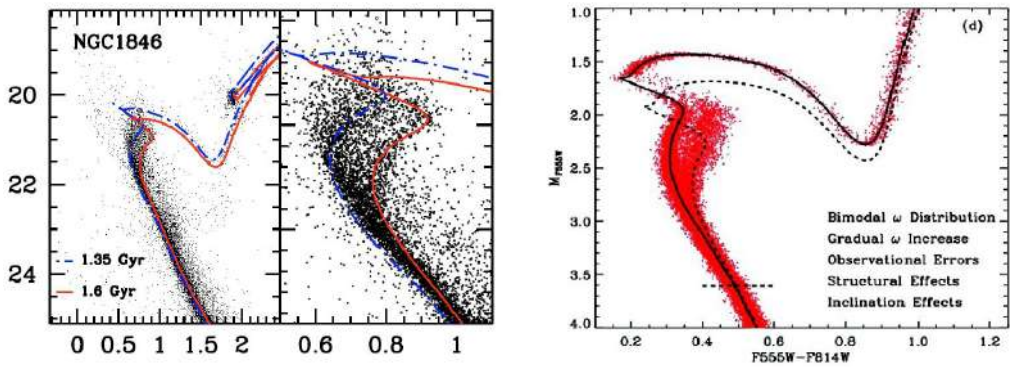


Figure 9.4: CMD of NGC 1846: in panels there are two models to reproduce the eMSTO.

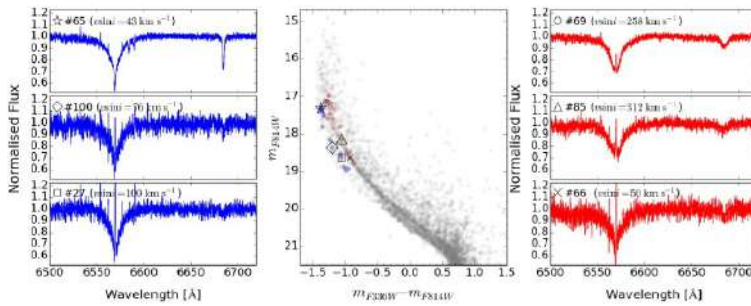


Figure 9.5: Spectroscopic analysis for some stars from two sequences of NCG 1818. Data are taken with GIRAFFE@VLT spectrograph.

the pattern is different with respect to the morphology of young cluster. So the explanation is not metallicity variations.

- **Age difference:** in some scenarios GCs correspond to multiple stellar generations or formation prolonged for a certain period. If these are the younger counterparts of GCs with MP and if scenarios are correct, we expect this range in terms of age. If we take isochrones of different ages, of same He contents and metallicity, in figure 9.2 panel c) isochrones are able to reproduce eMSTO but not the split of MS.
- **Different rotation rate:** look at figure 9.3; the double main sequence is consistent with two stellar populations with different rotation rates. In figure 9.3 are shown simulations of the most updated models of stellar rotations, reproducing stars with same age but different rotation rate: double MS seems to be fitted quite well.

Possible causes of the extended turn off:

As consequence, possible causes of the extended turn off can be:

- **age difference:** the extended main-sequence turn off is consistent with a prolonged star formation;
- **different rotation rates:** coeval stellar populations with different rotation rates can mimic an extended main-sequence turn off.

Look at figure 9.4, both model can reproduce the morphology of the young cluster. We cannot disentangle between two phenomena but we can analysis on stellar rotation. So a forward step is done by using the spectroscopy to derive the rotation for some stars from the two sequences. Indeed we know that for a fixed line in the spectra, rotating stars presents more broadened lines: the equivalent width is the same but in the case of rotating star we have broad profile.

In figure 9.5 we can see the result of spectroscopic analysis: the red stars shows broader lines than

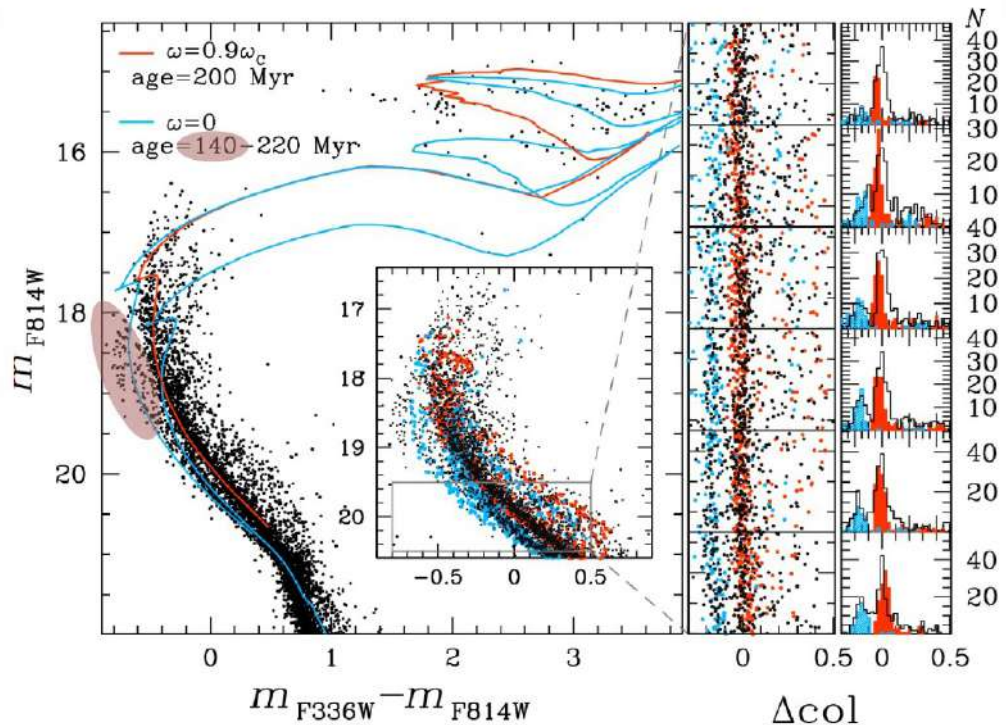


Figure 9.6: CMD of CG with isochrones; the red one is referred to a population with fast rotation instead the blue one to a slow rotation population.

blue stars. In conclusion red-MS star rotate faster than blue-MS stars. Of course it is important to take into account that we are observing the projected velocity so basically we need to account for projection angle but the result is the same: we are observing a complex system with stars rotating much faster then others.

In particular many fast rotating objects have been discovered, like Be stars characterized by emission in $H\alpha$ region of the spectrum. Sometimes inside this emission line, there is also an absorption line caused by the presence of a disk around the star.

In this cluster there are also many binaries not interacting each other and some objects located in the red side of binary region: some of them are field stars but other are triple systems or binaries with Black Holes.

From a physical point of view, high rotation rate change the stellar structure, making the star more similar to an elliptical shape. As consequence the surface is brighter but the luminosity is the same so effective temperature decreases and the star appears fainter and redder. Moreover there is an effect of gravitational darkening: the luminosity is different according to the observational angle between the star and the observer due to the fact that we observe stars with different inclination so we analyse different portion of the surface.

Is the rotation enough to reproduce the pattern? Let us look at figure 9.6. On the CMD there are two isochrones: the red one is a fast rotation population, the blue ones are slow rotation populations with two difference ages. Using only two isochrone with same age and different rotation we are not able to reproduce the stars highlighted in grey. These stars are reproduced with a blue isochrone with younger age.

In conclusion, the split MS and the eMSTO are consistent with multiple populations with different rotation and different age. Hence, age can not be completely ruled out. Indeed the presence of rotation do not exclude difference in age.

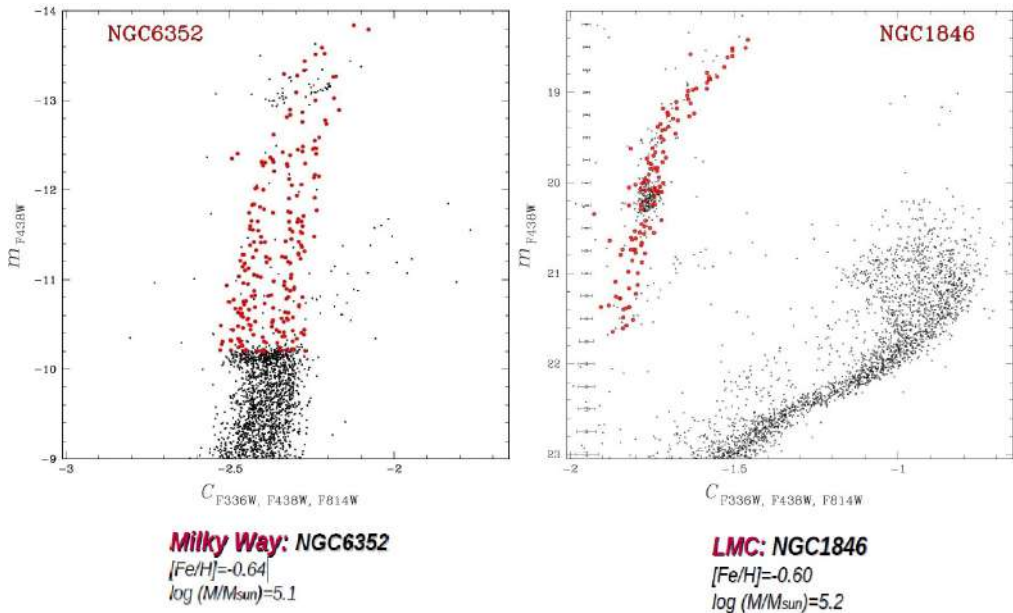


Figure 9.7: Comparison between two pseudo colors diagram that show the sequences on the RGB zone: on left NGC 6352, on right NGC 1846.

9.0.1 Comparison between some properties of Galactic and extra Galactic GCs

We have seen that CMD of Galactic GCs (of MW) show multiple RGBs paths that have different chemical composition. If we look at an intermediate-age star cluster from LMC, we do not see evidence of multiple RGBs. This difference is visible in figure 9.7.

In old Globular Clusters, the population ratios does not depend on stellar mass as we have already seen studying the diagrams in figure 9.8. Let us analyse the population ratio in young and intermediate age clusters from LMC and SMC. We observe a strong relation between the fraction of blue-MS stars and the stellar mass, as shown in figure 9.9: the fraction is about 30% at high masses, then there is a drop to 20% around $3 M/M_{\odot}$ and then there is an increase up to 40%. In average the fraction of blue-MS stars is about 30% in all the LMC clusters. It seems slightly smaller in the SMC clusters.

In general, what we can do is a comparison between MW and LMC-SMC GCs to understand the main differences.

Milky Way GCs

- They show chemical difference in $C/N/O/Na$.
- Most scenarios assume a difference in age between stars with different chemical abundances.

Young/Intermediate-age Magellanic Clouds clusters

- They show no chemical differences.
- The multiple stellar populations are linked to different rotation rates.

What is fundamental in both cases is to understand the role of the environment in formation processes and evolution of these objects. For example we can make a comparison with Open Clusters in the MW.

9.0.2 The comparison with respect to Open clusters

MW open clusters are similar to young and intermediate age Magellanic Clouds clusters, for example they both have a wide range of age and same metallicity.

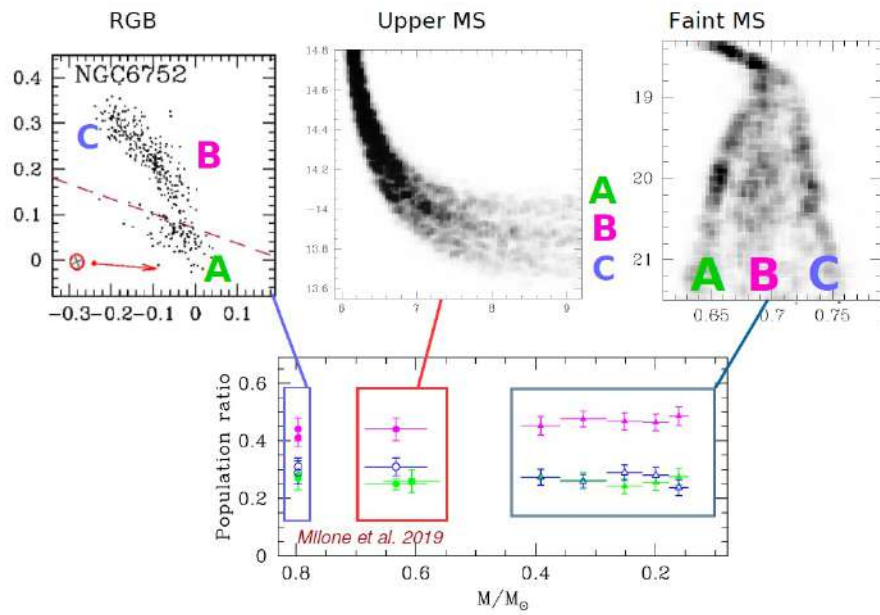


Figure 9.8: These diagrams show that the population ratios, derived from three different part of the CMD, are the same.

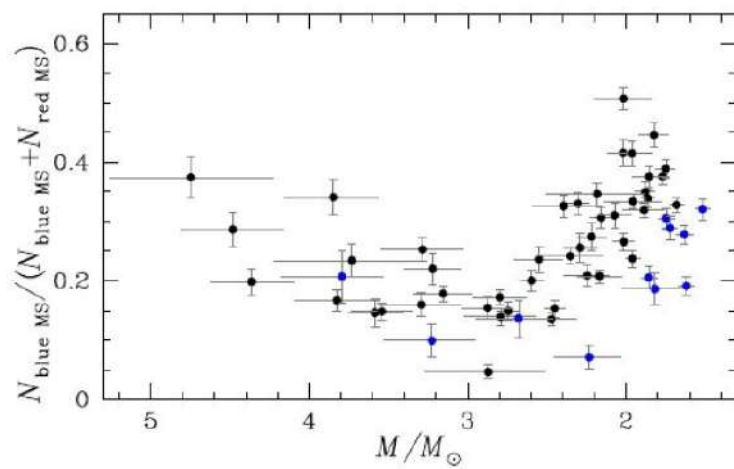


Figure 9.9: Diagram that shows the strong relation between fraction of blue-MS stars and stellar mass.

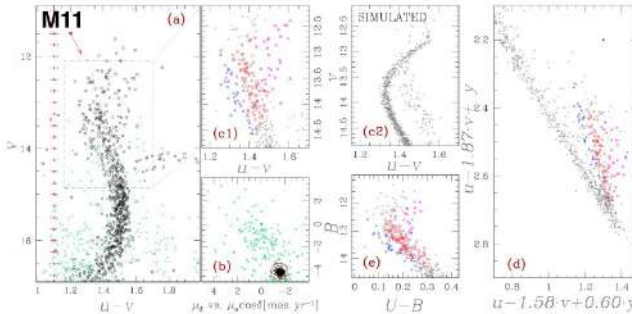


Figure 9.10: CMD of M11, a Galactic open cluster.

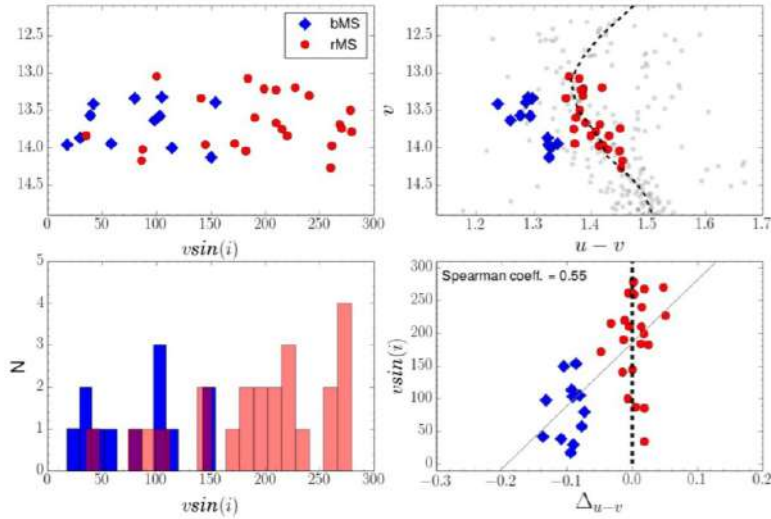


Figure 9.11: Spectroscopic and rotation rate analysis of M11

Galactic open clusters are not easy to investigate in the past due the contamination of field stars. Thanks to Gaia Space Telescope now we are able to disentangle between clusters' stars and those of the field of view.

Let us look at figure 9.10: open cluster M11 is similar to Magellanic Clouds clusters as they host similar extended Main Sequence Turn-Offs and split MS.

Let us analyse the rotation rate of blue and red stars of M11: the result is shown in figures 9.11 and 9.12, the red-MS stars rotate much faster than blue-MS ones.

In conclusion, MW open clusters and Magellanic Clouds GCs have same properties! Extended MSTO are a common feature of Milky Way GCs so this is not a peculiarity. A useful scheme to resume features and differences between MW GCs, young and intermediate age MCs clusters and MW open clusters is shown in figure 9.13.

Having all these information, we will try to answer to some big questions: are young LMC clusters the counterparts of the old Galactic clusters with multiple populations? Do they host multiple stellar generations?

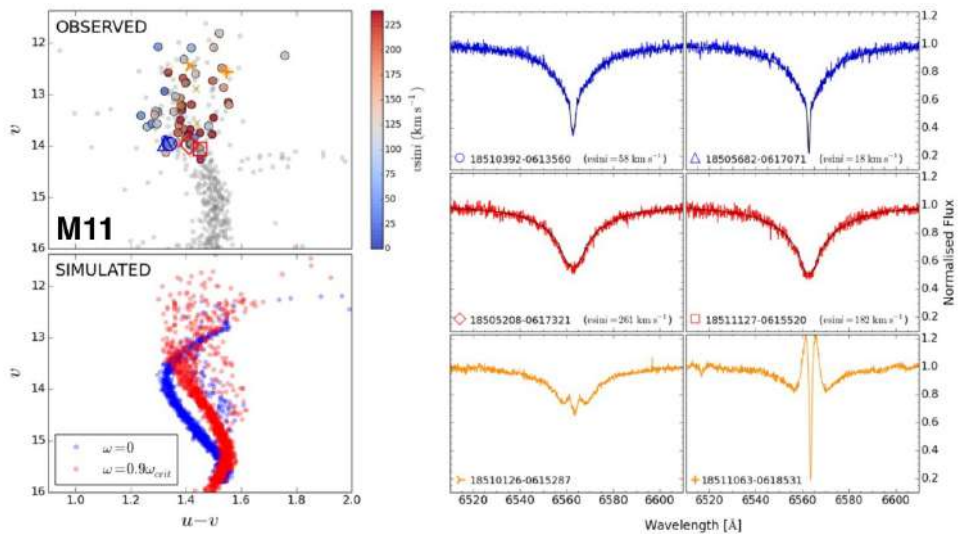


Figure 9.12: Spectroscopic and rotation rate analysis of M11

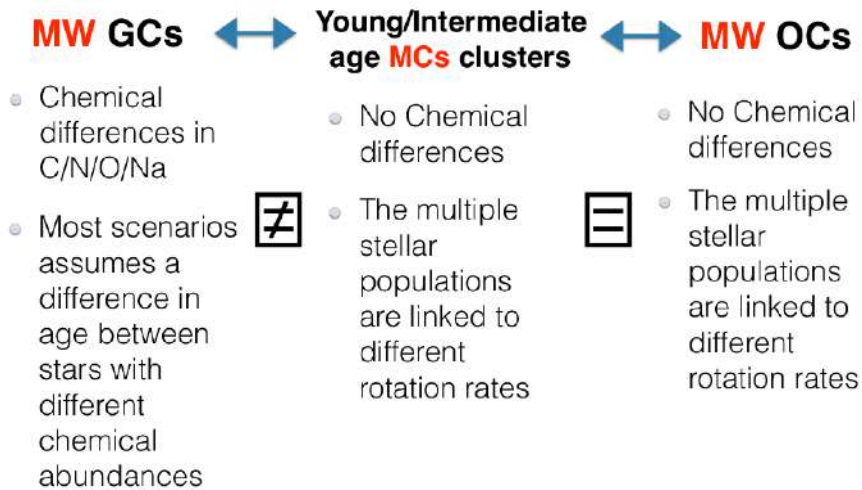


Figure 9.13: Summary for MW GCs, young and intermediate-age MCs clusters and MW open clusters.

Chapter 10

Galaxy: The bulge

If we look at a spiral galaxy, we can see an over density in the central region: this zone is called bulge. From observation this region is redder than the surrounding regions (arms).

Historically, bulges and elliptical galaxies are called **spheroids**. Some bulges (**classical bulges**) and elliptical galaxies share several properties: e.g. they lie on the same fundamental plane. Other bulges do not share the properties of ellipticals. These **pseudo-bulges** look like bars and derived from dynamical instability of the disk.

Studying the Galactic bulge of MW is very difficult due to the huge size in sky by our point of view and because we are not able to disentangle the bulge's stars from the other stars.

10.1 How did Bulge form at high z ?

Due to the challenge of observing bulge inside galaxies, there are two complementary approaches.

1. Observations at high-redshift to see bulges in formation. The advantages are that we can study more objects at same time and the entire galaxy is inside a single image but the disadvantage is that bulges are very small, a few pixels in images so we can infer a lot of details.
2. Galactic archaeology: investigation of the Galactic bulge (MW) to map its structure, dynamics and stellar populations in great detail. In this case advantages are many: the object is very close to us so we can infer a lot of details, especially in spectra of brighter stars. It is also possible to study kinematics, proper motions and radial velocity and investigate precise CMD taken with HST, observing also faint stars in the bottom part of the MS. Indeed the Bulge of the Milky Way is the only bulge that we can resolve down to low mass stars. But there also some disadvantages: the bulge is huge so not observable in one single image, properties of stars in one direction can be different in other directions and it is only one bulge, maybe not representative of all bulges of all galaxies. Finally it is subjected to very high level of differential reddening, quite challenging to resolve.

10.1.1 Observations of bulges at high-redshift

Observations at high-redshift have revealed central concentration (i.e. bulges) in massive galaxies at $z \sim 2$ (figure 10.1). In particular star formation has almost ceased in the center while continuing in the surrounding disks (figure 10.1).

In massive galaxies ($\log(M/M_\odot) > 11$), star formation is quenched from the inside out, on time-scales less than 1 billion years in the inner regions up to a few billion years in the outer disks. Then the star formation is stopped in the bulge and continues in the disk. These galaxies sustain high star-formation activity at large radii, while hosting fully grown and already quenched bulges in their cores.

The total stellar mass and bulge mass grow synchronously in $z \sim 2$ galaxies.

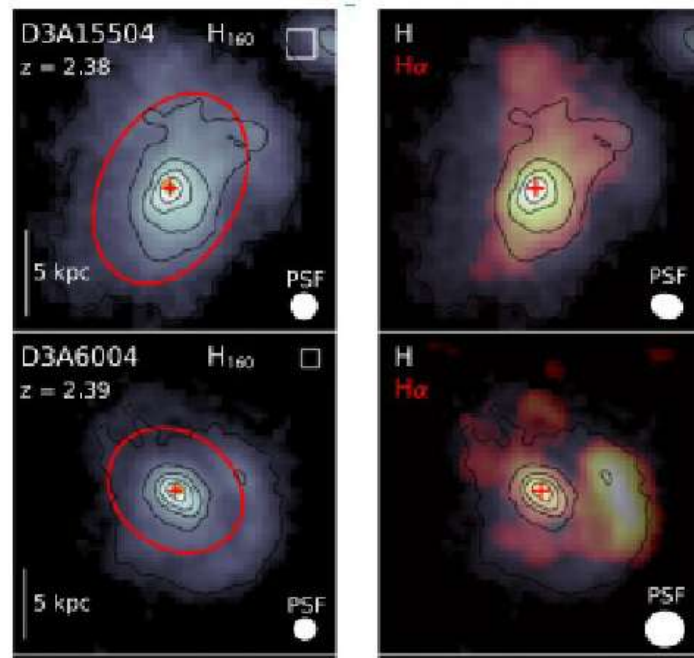


Figure 10.1: Two galaxies observed in two different filters. On left is shown the pick of light, corresponding to the bulge; on right the H α observation reveals the star formation region. Observations are made in near infrared to partially resolve the reddening problem.

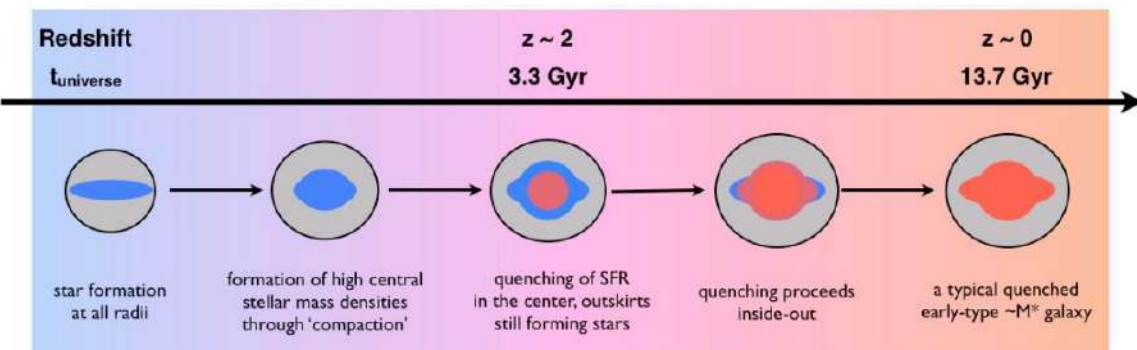


Figure 10.2: The quenching process.

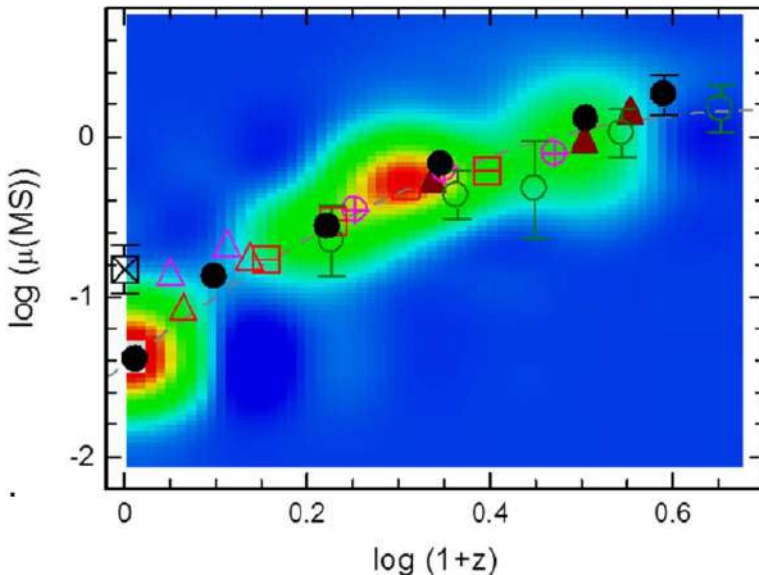


Figure 10.3: Graphic showing higher gas fraction for high redshift bulges.

Quenching process is concurrent with their total masses and central densities approaching the highest values observed in massive spheroids in today's universe.

In general the disks of high-redshift galaxies are in many aspects very different from those in the nearby universe:

- they have much higher gas fraction ($\sim 50\%$) than nearby disks, which scale like $\sim (1 + z)^{2.6}$;
- they are more compact for a given stellar mass, with their effective radius scaling as $\sim 1/(1 + z)$.

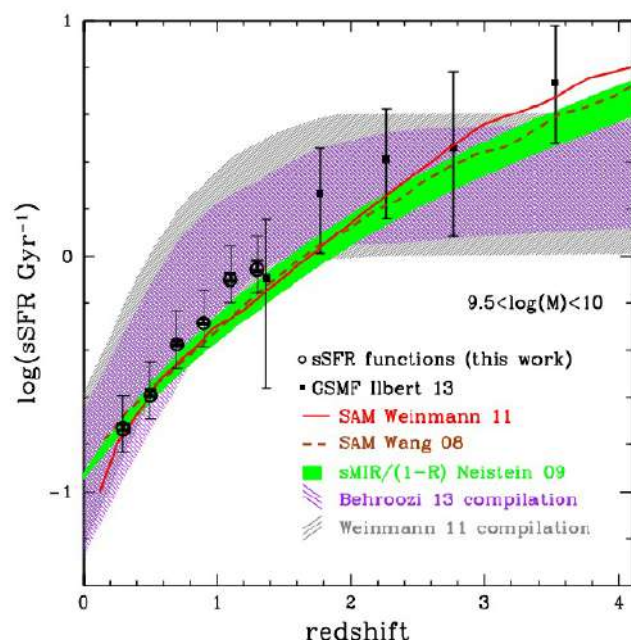
Features described before are physically shown in figure 10.3.

Likely as a result of higher gas content and gas density, the star formation rate at fixed stellar mass increases as $\sim (1 + z)^{2.6}(1 + z)^{2.8}$. This relation is very clear in figure 10.4

10.1.2 Bulge formation scenarios

There are many scenarios proposed to describe bulge formation.

1. Bulges are due to giant clump formation and their migration and coalescence to the center. In this case we expect massive building blocks merging together and forming the bulge. In figure 10.5 in first two panels there are a simulation in the upper part and observations in the lower part. If this scenario is correct we expect formation of the bulge in the galaxy and the presence of some clumps still alive nearby the bulge.
2. Bulges form from the overall violent disk instabilities that lead to the central pileup of a large amount of star-forming gas with a very short depletion time. In both scenario I and II, bulges form rapidly out of the disk, in a gas-rich, highly dissipative environment.
3. Bulges form as a result of dissipationless merging of sub-units (classical bulges). Gravitational forces and torques disrupt the orbital paths of stars, resulting in the randomised bulge orbits. Hence they have properties similar to elliptical galaxies: stars have random orbits, bulges exhibit spherical shape and the distribution of light is described by a Sersic profile.
4. Bulges form as a result of dissipationless bar formation in stellar disk, as result we obtain a pseudo-bulge. Starting from a pure exponential stellar disk (same size as the Milky Way), N-body simulations predict that:
 - the disk develops a bar-forming instability;



Ilbert et al. 2015

Figure 10.4: Relation between star formation rate and redshift.

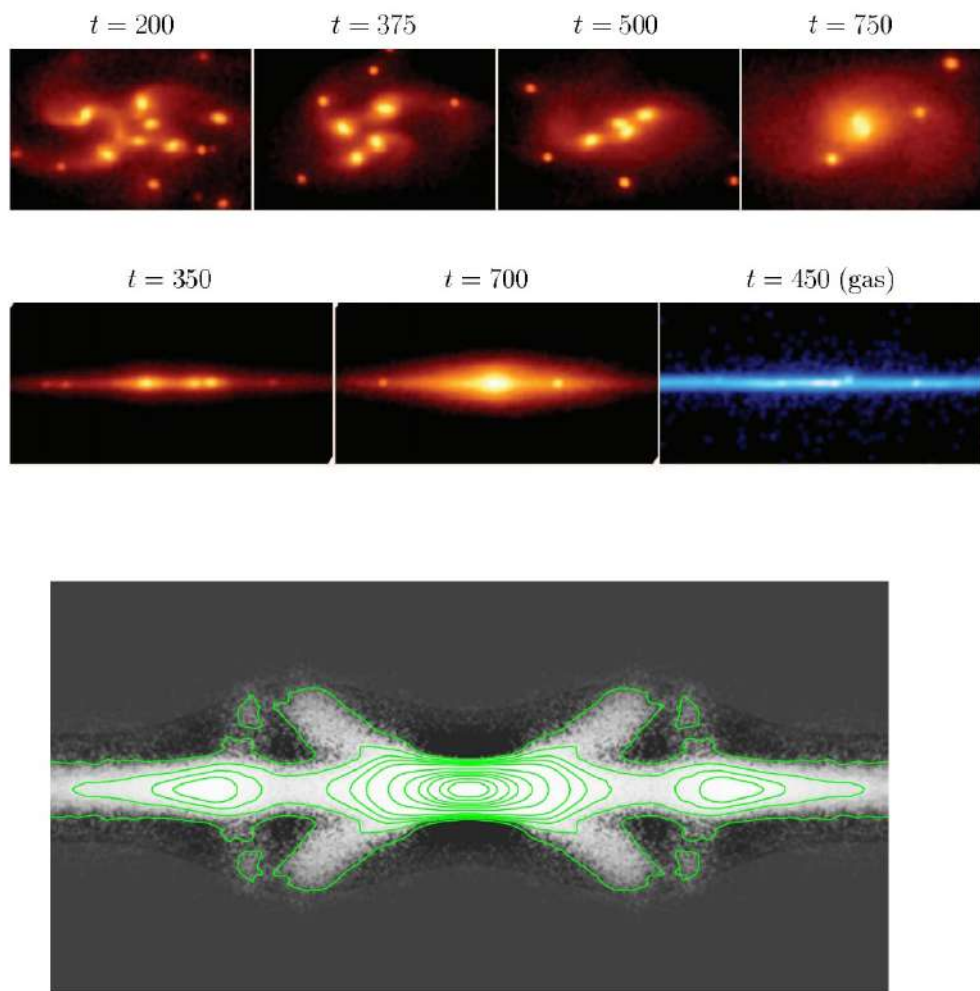


Figure 10.5: Simulation for scenario I and IV.

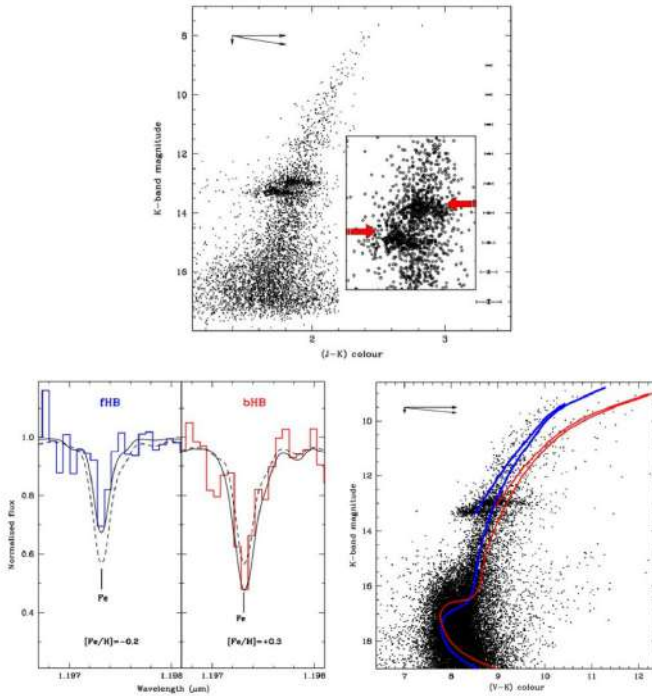


Figure 10.6: CMDs of Terzan 5 in the upper panel. On bottom panel on left a spectra of the two populations and on right plot with isochrones of the two populations.

- once formed, the bar is subject to buckling instability resulting a:
 - cylindrical rotation;
 - boxy peanut with X-shaped bulge (presence of a bar).

The four scenario is not necessarily in contradiction one with the other: we have to study more observed objects and infer more information to constrain a scenario.

Case of CMD of Terzan 5

Terzan 5 is a massive Globular Cluster in the bulge. About this object we have many questions: What is its age? What about metallicity? How many stellar populations does it host? Usually observing a CMD is quite easy to answer but in this case it is a difficult challenge. As shown in figure 10.6 upper panel, CMD of this bulge cluster is very complex due to presence of multiple stellar population distributed along spread sequences due to a high level of differential reddening. Indeed it is located in the Galactic bulge heavily obscured by clouds where stars are not visible in ultraviolet and investigated mainly in near infrared, significantly less affected by reddening.

However we can recognize the turn off point at the base of the graphic, then sub giant branch and, in the upper part, the RGB. It is clear that in general it is a metal poor cluster. Moreover in figure 10.6 in the upper panel, CMD shows error bars increasing from bright stars in the upper part of the diagram going down to fainter stars.

What is peculiar of this object is the presence of two over-densities of stars, in particular two red clumps. These are not caused by reddening effect because it is clear stars are not located along the direction of reddening. How to get information on them? Using two complementary tools! Using photometry and fitting the data with isochrones, it is clear that this cluster hosts two stellar populations with different metallicities ($[Fe/H] \sim -0.2$ and $+0.3$). Same result is obtained from spectra (bottom panel on left in figure 10.6): blue stars are metal poor (poorer than the Sun), while red stars are relatively metal rich. Metallicity variations inside clusters are not peculiar features but this cluster is characterized by a big variation.

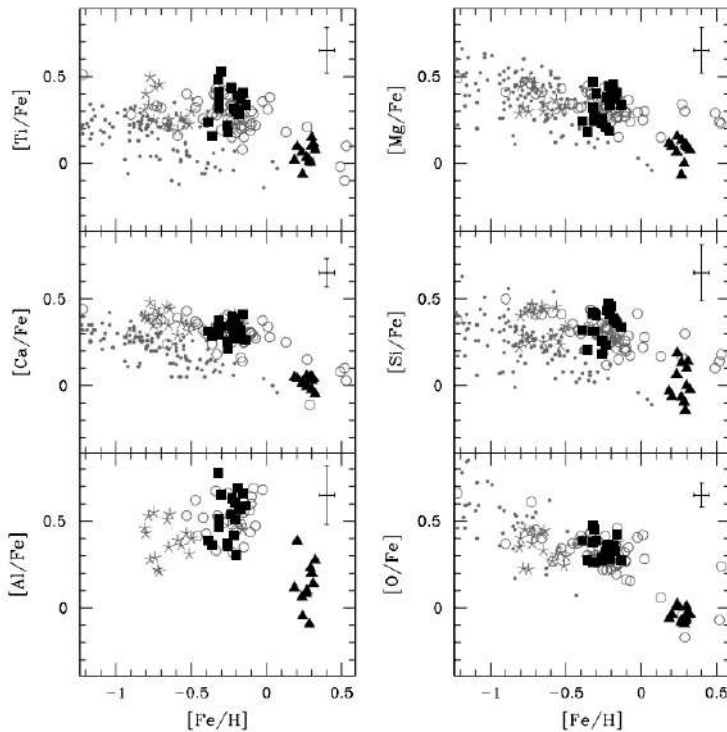


Figure 10.7: Abundances of some elements for Terzan 5 stars (black filled points) and bulge stars (grey points).

Another important features of Terzan 5 are the plots of the abundances of some elements as Ca , Ti , Al , O , Si and Mg as function of iron content (normalised to the H content). These plots are shown in figure 10.7: we can see in black the GC's stars while the other grey points are bulge's stars. All diagram shows a drop of abundances when stars approach the solar value of H content. This feature suggests that Terzan 5 is a remnant of the building blocks of the Bulge (scenario I of Bulge formation).

According to this work it seems we have found the solution of bulge formation process which should correspond with scenario I but in next sections we will some results showing discrepancy with this scenario.

10.1.3 The age of the Bulge

Let's now return to the bulge of Milky Way. There is no sharp distinction between bulge and disk! We refer to the inner ~ 3 Kpc of our galaxy as bulge but there is no clear limit between the bulge and the others parts. So, the first problem in the investigation is the huge size and the no clear limit. The second problem is the differential reddening that affects all small parts of bulge. Moreover it is very difficult to disentangle between bulge stars and stars of other components projected on the bulge or field stars. Finally, while GCs are characterized by discrete stellar populations and discrete chemical composition, the bulge has continuous variations of chemical abundances which correspond to broadening sequences.

For all these reasons the investigation of the CMD is very complex and quite difficult.

The CMDs of the bulge is shown in the figure 10.8. Here data come from near infrared observations, in order to minimize reddening effect. There is also contamination of field stars and of stars projected on the bulge but belonging to other components. For this reason in CMD on left panel in figure 10.8 are recognisable MS, MSTO, Red Clump and RGB of the bulge but also MS and Red Clump of the disk.

On the contrary in right panel in figure 10.8 there is one of the best CMD of the bulge, cleaned up from contamination of stars and corrected for reddening. Despite this high accuracy photometry, also here sequences are still broadened.

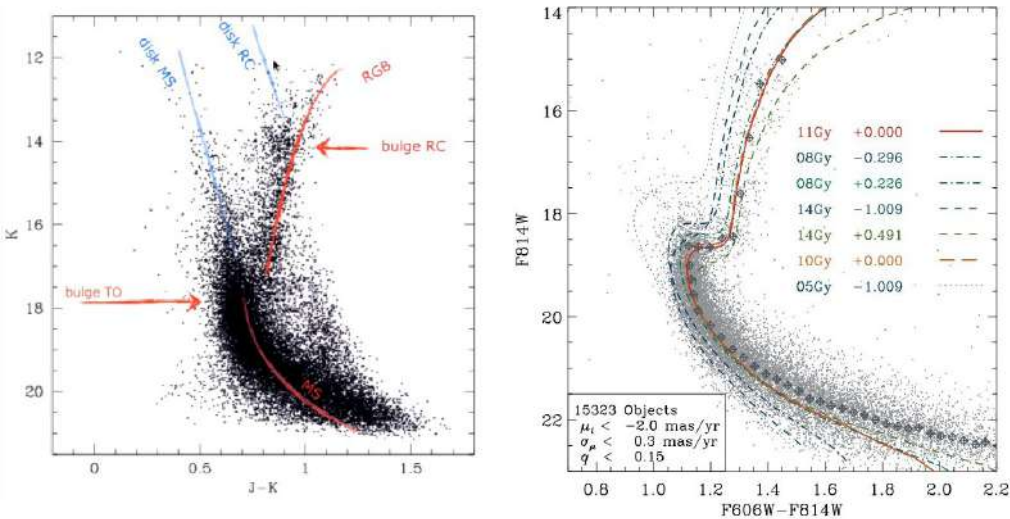


Figure 10.8: CMD of bulge in near infrared where reddening is lower.

The broadening is due different metallicity population that are no discrete. In particular, fitting the best CMD on right panel in figure 10.8, we found different sequences with also different ages. We expect old stars. Indeed from this work we found that stars younger than 5 *Gyr*, if present, comprise less than 5% of the total number of Bulge stars. So from this work there is no evidence for a younger bulge. The same conclusion comes from the chemical evolution models. To be more specific, this is an upper limit because above the MS is not possible to disentangle between blue straggles and young population. Moreover this 5% includes also fraction of binaries so the CMD is consistent with a value about 0% of young stars.

Summarizing:

- *Conclusion from chemical evolution models* - the Bulge formed at the same time and even faster than the Galactic halo;
- *Conclusion from the CMD* - the Bulge is as old as Globular clusters, ($\text{age} > 10 \text{ Gyr}$) with no trace for any young stellar population.

A new method to infer ages for Bulge stars is based of five-band HST photometry in five fields. Proper motions obtained for observations in different epoch are used to separate Bulge members from the bulk of disk stars. The key is not use the CMD but a two colors diagram created using appropriate filter in order to have reddening-free (not affected by differential reddening) diagrams from multi-band photometry. In this case the position is affected by the evolutionary stage and by the metallicity but not by reddening effect, which is very important in bulge region.

In figure 10.9 on top are plotted simple populations on reddening-free diagram, on bottom panel bulge stars.

Reddening-free diagrams from multi-band photometry are used to identify stellar populations with different metallicity. In the bottom panels Renzini et al. (2018) splitted the stars in four region according to metallicity identified by different colors (panel on left): it goes from red metal rich to blue metal poor stars. Once identified the stars with different metallicity they build the CMD on right panel.

In figure 10.10 we can see on left the CMD with only the metal richest and the most metal poor stars (red and blue points), on left the luminosity function (reminder in next subsection) of these two population (red and blue points) compared with respect to four models with different combination of metallicity and age.

The conclusion looking at the figure is: the bulk of Bulge stars are $\sim 10 \text{ Gyr}$ old and only $\sim 3\%$ of stars are younger than $\sim 5 \text{ Gyr}$.

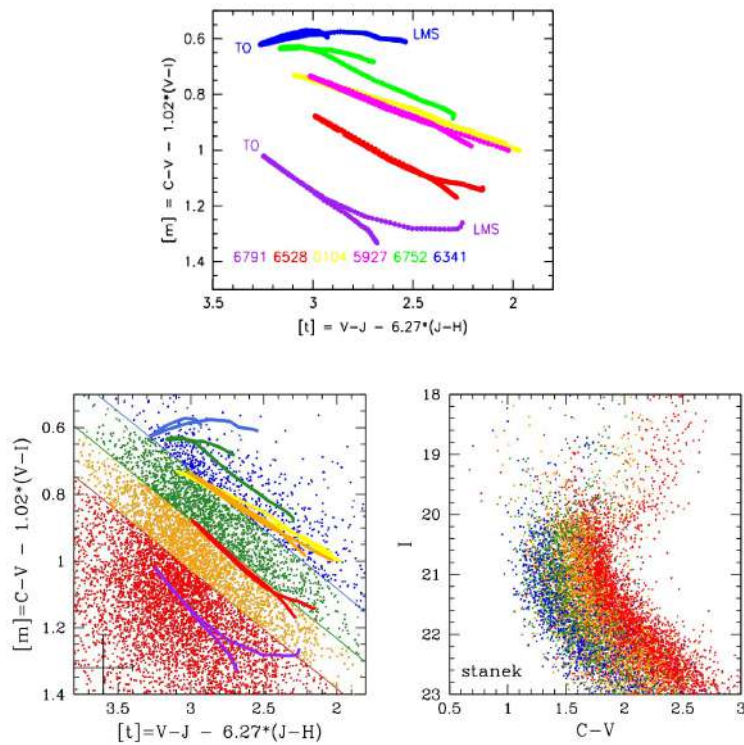


Figure 10.9: Reddening-free diagrams: On top panel for stellar population, on bottom panel for the bulge.

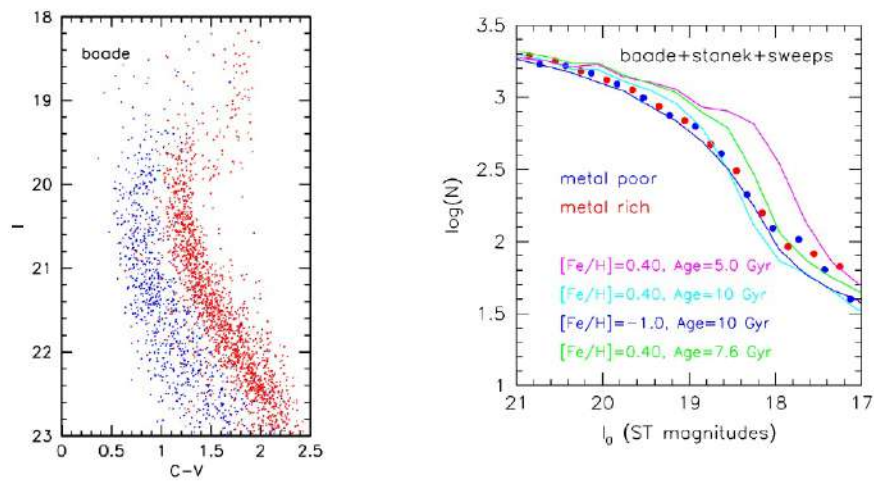


Figure 10.10: On left CMD of the most poor and the most rich stars, on right the luminosity function of these two population compared with models.

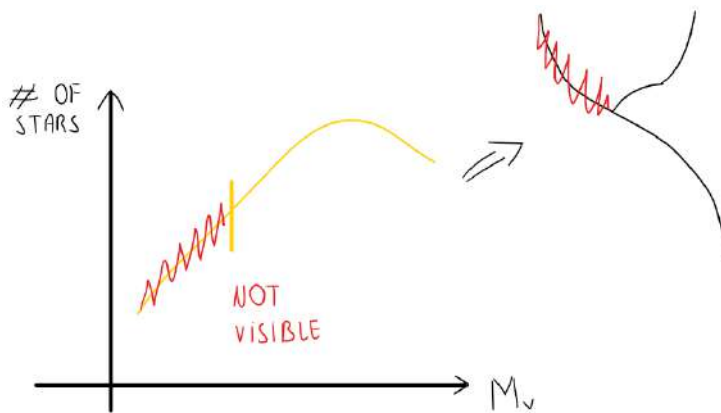


Figure 10.11: Luminosity function.

According to this work the bulge has old stellar populations, comparable to the bulge of external galaxies where all star formation history occurred very fast after the formation of galaxy.

Luminosity function: a reminder

The luminosity function is a distribution that relates the number of stars to the luminosity interval. The main difference between a young simple stellar population and an old one is the brighter part of the distribution. Indeed, the brighter stars evolved faster and we do not see their contribution in the luminosity function in an old stellar population (figure 10.11). Then, luminosity function changes in time due to evolution of stars and from dynamical point of view: so to infer the ages of a population we look at the luminosity function (LF).

10.1.4 Other approaches

The previous method are base on photometry and luminosity function. Now let us use the spectroscopy to infer age of stars in the bulge. In general spectroscopy is sensitive to atmospheric parameters, allowing us to create from observational point of view a gravity-temperature diagram indicative respectively of magnitude and color and sensitive to the age.

The brighter stars in optical and near infrared, the best target for spectroscopic analyses, are RGB stars. However these stars are not very sensitive to the age (they are most sensitive to metallicity and He contents) and this is true both for photometry and spectroscopy. So RGB stars are quite easy to investigate with spectroscopy but not very useful to derive the age.

On the other side, the most sensitive stars to the age are stars situated around the Turn-Off point. Unfortunately they usually very faint stars (magnitudes about 19 – 20), difficult to observe with present day tools and at which are associated larger error bars. In this case spectroscopy can not be done or eventually can not be done with high resolution.

So to observe TO stars we need some extraordinary events: to observe them and derive spectra we need a **microlensing event**. Indeed in these cases, during microlensing events, faint Bulge stars can brighten by several magnitudes. This phenomena is caused by the passage of the star in a strong gravitational field created by some dark objects. For some physical reasons, the star is much more brighter so the star became a good target for spectroscopic analyses.

There are many surveys created to search for microlensing events, mainly in crowded region where there is an over-density of stars so the probability to find this event is higher. Of course it is necessary that dark object and the star are located along the line of sight.

A example of gravitational microlensing is shown in figure 10.12: photometry realized by huge telescope found these events and then using spectroscopy we infer stellar properties. Bensby et al. get high-resolution spectra of dwarf stars in the Bulge when they are microlensed. In 2013 they found this

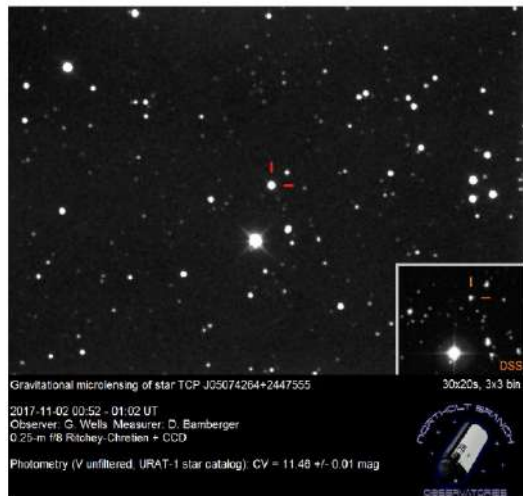


Figure 10.12: Gravitational microlensing of a star.

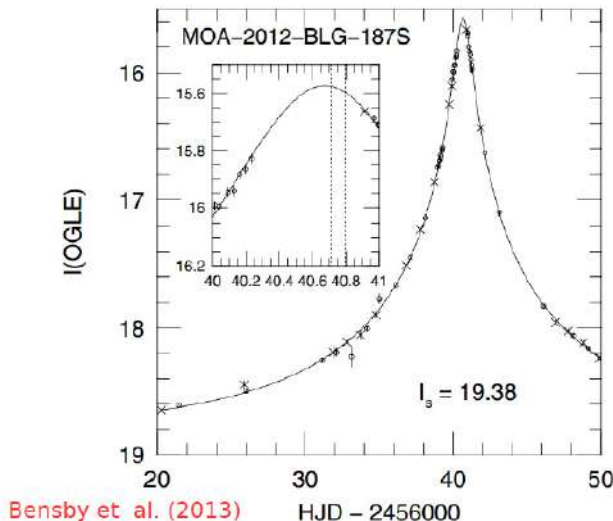


Figure 10.13: Change in luminosity during microlensing event.

microlensed star, that changed its magnitude from 19 up to 15.4, a huge difference in luminosity! In figure 10.13 it is shown the increase in luminosity during microlensing event.

These stars are close to the MS Turn-Off so they when they are microlensed they are useful to study part of CMD usually not very well studied. In particular from high resolution spectra they inferred gravity, temperature and metallicity. Using those elements they created the observational plane with gravity against temperature in logarithmic scale ($\log(g)$ vs $\log(T_{eff})$). This graphic is shown in figure 10.14. Here red points are observed microlensed stars while gray curves are isochrones with different ages. It is clear that these stars are located around MS TO so they are very useful to derive the age.

The next step is a metallicity-age diagram of these microlensed stars, as shown in figure 10.15.

Studying diagram in figure 10.15, they founded that $\sim 30\%$ of the microlensed dwarfs are younger than $\sim 7 \text{ Gyr}$, only few stars have ages of $\sim 1.5 \text{ Gyr}$. This is a discrepancy with the result obtained with photometry, for which bulge has almost totally old stars. So by spectroscopy we derive an important fraction of young stars, in contrast with photometric result.

In more details: stars with $[Fe/H] < \sim -0.4$ are old, with ages of $10 - 12 \text{ Gyr}$ while stars with $[Fe/H] > \sim 0.4$ span a wide range of ages. This is an evidence for a two-component Bulge?

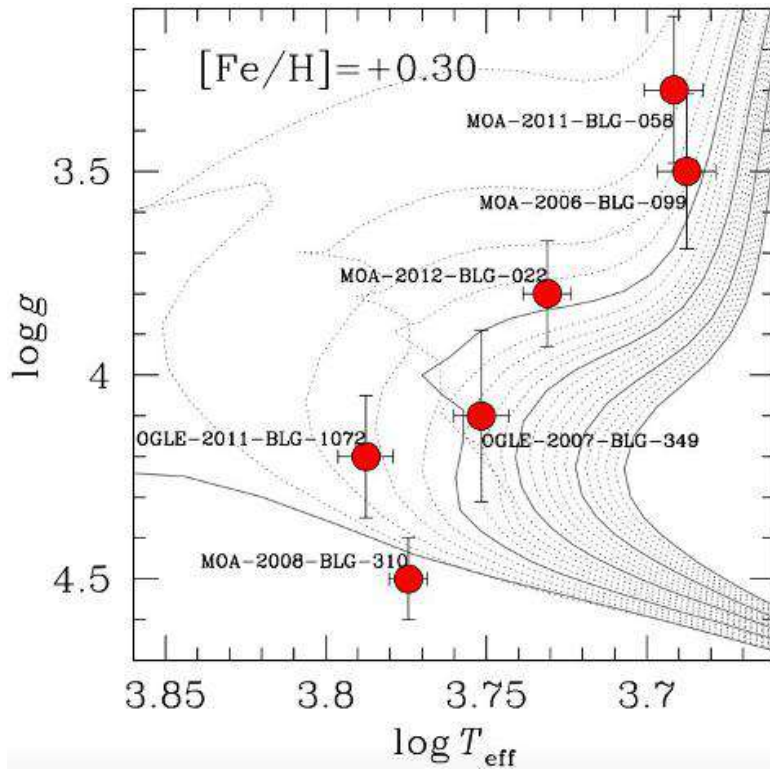


Figure 10.14: Observational plane with $\log(g)$ vs $\log(T_{\text{eff}})$ of microlensed stars in the Galactic bulge.

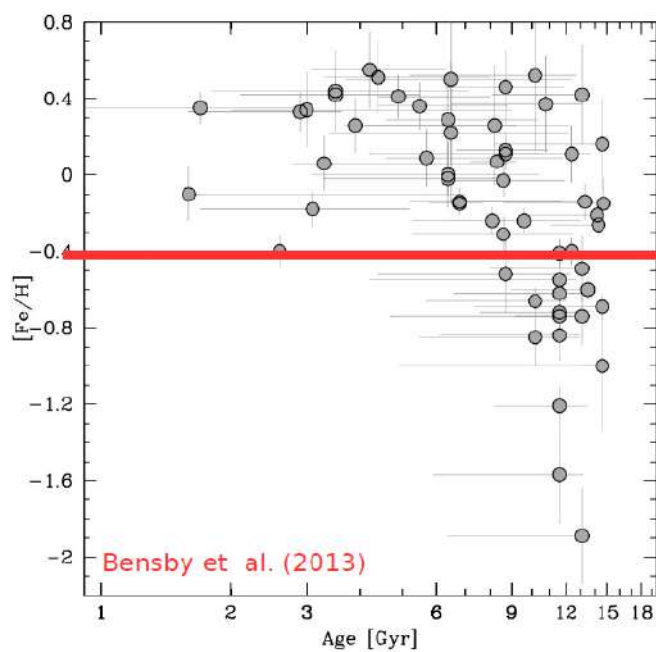


Figure 10.15: Diagram with metallicity against age.

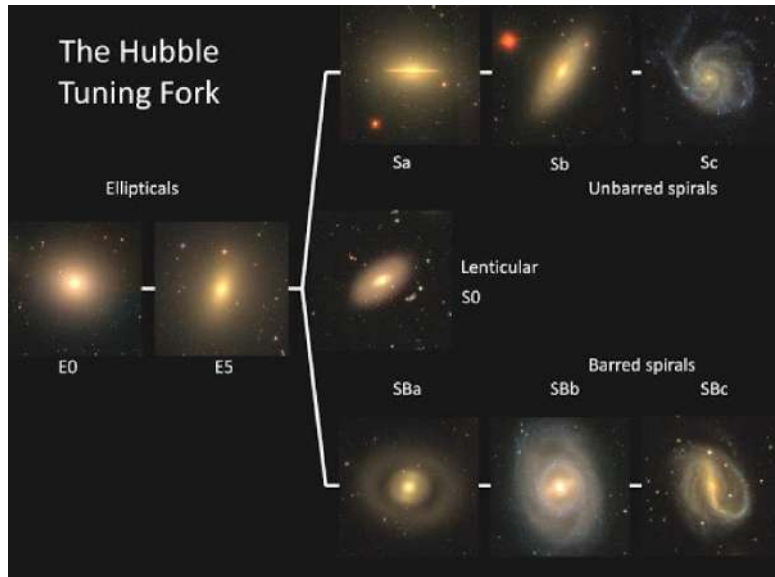


Figure 10.16: The Hubble classification of galaxy.

Results for 90 microlensed dwarfs confirm the discrepancy between ages inferred from spectroscopy and from HST photometry. Maybe the bulge is composed by more than one structure?

10.2 The structure of the Bulge

Galaxies exhibit wide variety of shapes shown in figure 10.16. Indeed observing external galaxies, there is a big variety of morphology: galaxies with a very small bulge, others composed mainly by bulge more similar to a spheroidal distribution, others with a bar structure crossing the bulge.

However, in general, the main components are:

- disk with a mass about $\sim 6 \times 10^{10} M_{\odot}$;
- bulge with a mass about $\sim 10^{10} M_{\odot}$;
- halo with a mass about $\sim 10^9 M_{\odot}$.

Pay attention: this is not the total mass! This is total visible mass, without taking into account dark matter. Considering visible mass halo is the less massive but considering also dark matter, it is the most massive (10-100 times the other components).

As seen previously, the Bulge is a massive and old component of the Milky Way for which there are four different scenarios to explain its formation. Moreover, as stated many times, it is quite difficult to study the Bulge due to its big extension, due to contamination of other components and presence of huge amount of gas and dust. For this reason we have to collect near infrared data and made some clever investigations.

For example, Stanek et al. in 1994 made a very simple but important work. Using Infrared data of COBE satellite, he observed three different part of the bulge as shown in figure 10.17 and counted the number of stars. In particular he counted stars in three different field of view characterized by same Galactic latitude (same distance from the plane of the galaxy) but with different longitude.

They found that counts of stars are very peculiar: for a fixed luminosity interval, stars at positive longitudes are more numerous than those at negative longitudes. So stars at positive longitudes are brighter (closer) than those at negative longitudes. This means that the Bulge is a bar!

The bar has axis ratios 1.00:0.35:0.26 (assuming equals to 1 the major axis, other axis are 35% and 26%), and an inclination angle of ~ 25 degrees with respect to the Sun.

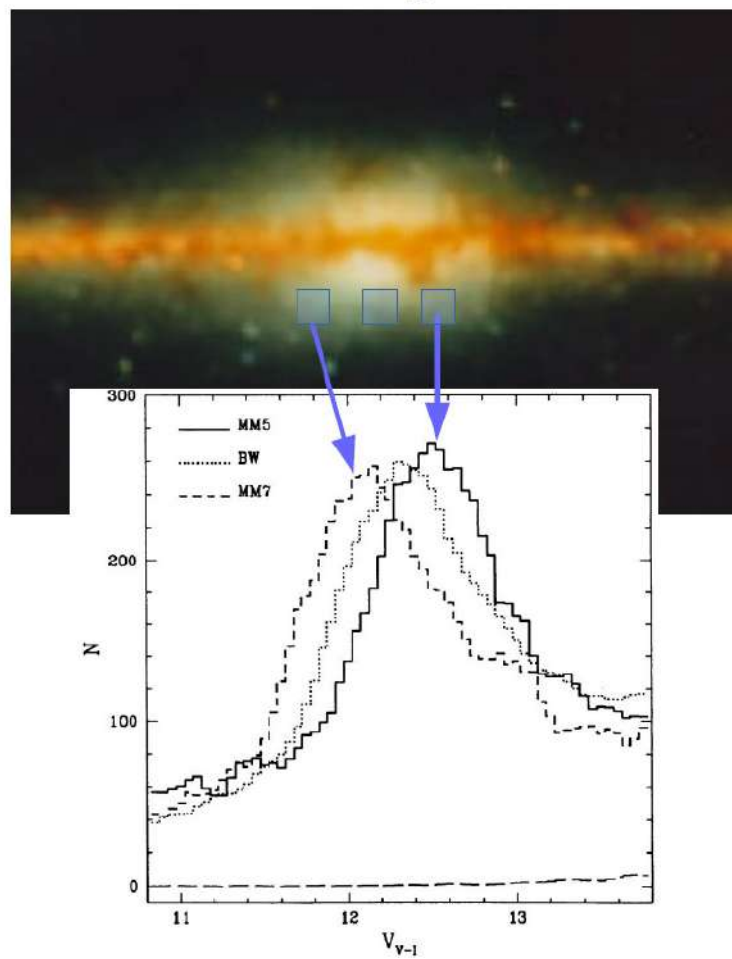


Figure 10.17: Luminosity function for three different part of the bulge with same latitude.

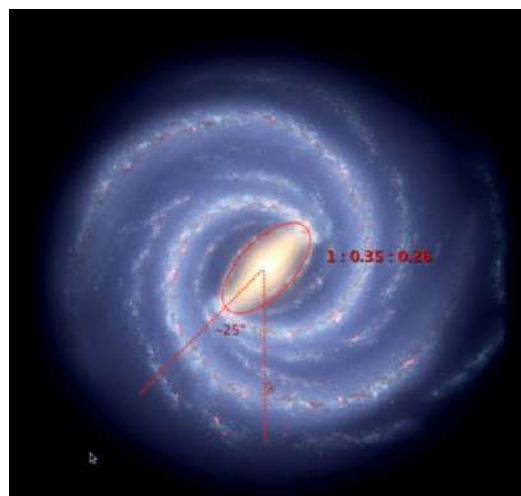


Figure 10.18: The cartoon that represent MW bar.

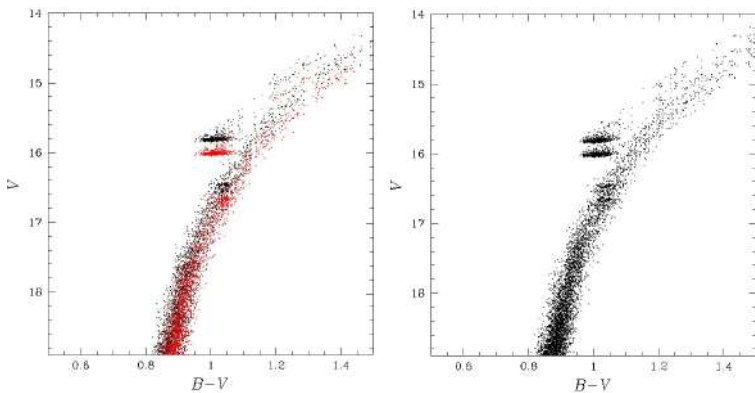


Figure 10.19: In figure models (simulations) of two equal population with different distance. On left two populations are colored with in black and red, on right they have same color. So from observational point of view stars at different distances are not usually distinguished inside sequences but we are able to disentangle these two over-densities of stars at different distance at level of Turn-Off point or at level of Red Clump.

An alternative way to investigate the structure of the bulge

To investigate the Galactic bulge we use a feature of the CMD which is a powerful tool to studying the stellar evolution but also to get the distance and the properties of the stellar population. This feature is the red clump (RC).

As seen in the previous chapters, the red clump is a feature of a metal rich old population. It is a clustering of red giants in the CMD: they are stars bluer (hotter) than RGB stars with the same luminosity ($T_{eff} \sim 5000 K$).

RC stars are associated with younger and more metal-rich populations than those associated with the HB even though both type of stars are burning Helium in their cores. On the contrary Horizontal Branch stars are associated with old stellar population.

We have seen that two equal population but with different distance appear shifted each other. The farthest looks like fainter with respect to the closest population. At level of MS and RGB is very difficult to disentangle two population, but it is possible at level of RC.

In particular, a characteristic of the bulge is the presence of this double distribution of stars, visible in CMD of all regions of the bulge. This feature is present almost everywhere regardless the position in the bulge but the relative number of stars in the two red clumps changes from one position to another.

So we can use Red Clump stars as tools to detect the relative distances of these over-densities of stars, based on their luminosity at different position with respect to the center of the bulge.

In figure 10.19 we can see a model for two population with different distance.

From observational point of view stars at different distances are not usually distinguished inside sequences but we are able to disentangle these two over-densities of stars at different distance at level of Turn-Off point or at level of Red Clump.

What we observe is similar to the panel on right: the double Red Clump is consistent with two stellar populations of same age, same metallicity but with different distance. In particular, the distance between the two RCs decreases toward the Galactic plane and it is proportional to the difference in magnitudes between the two Red Clumps peaks.

Therefore from theoretical point of view, stars belonging to two different Red Clumps are just shifted vertically along magnitude (the more distant is also fainter) but they have same color.

Features in the MS or in the SGB are not easy to use like the RC due the error that increases for fainter magnitudes. Sometimes the errors are high and the RCs are spread out (see figure 10.20), then it can be helpful derive the luminosity function and detect the two peaks of two RCs (see figure 10.21). The difference in magnitude between the RCs can be easily converted into distance and derive

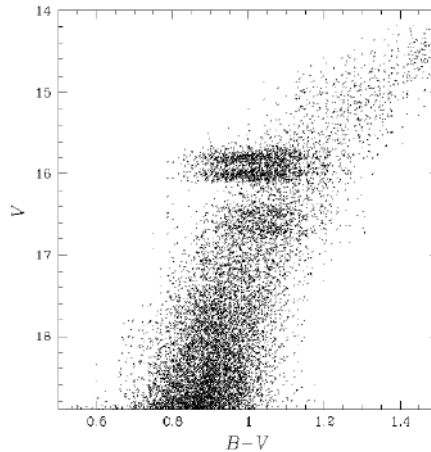


Figure 10.20: Observational errors that spread out the CMD.

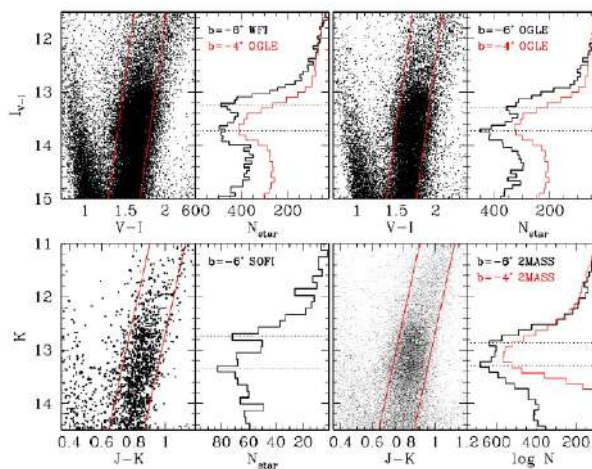


Figure 10.21: Luminosity function used to detect the two peaks of two Red Clumps. Those are real observations, not simulations.

the relative distance of these objects from the center of the bulge and, as consequence, the structure of the bulge.

Let's now look at figure 10.22: distances of the two Red Clumps as a function of latitude (i.e., in the X-Z plane where each point corresponds to the position of one Red Clump) reveal that the Bulge exhibits an X-shape component. This is what we expect from scenario 4 seen previously for bulge formation.

Summarizing we investigate population in different part of the bulge, derive the distance of RCs and build the diagram in figure 10.22. If we compare the CMDs of stars of different direction we also see the effect of differential reddening, then we observe a vertical shift due the distance difference but also a color shift due to reddening.

The color and magnitude of the red clump stars can change dramatically in CMDs of stars in different fields of view. At figure 10.23 we can see this effect. The relative color and magnitudes of the red clump are indicative of the amount of differential reddening. Moreover, they constrain the reddening direction, hence the reddening law. By comparing IR colors of the red clump of bulge stars in the VVV survey it has been possible to derive a reddening Map of the Bulge (resolution $2' \times 2' - 6' \times 6'$).

Once we have correct for reddening the CMD of the bulge, we can investigate the metallicity of stars. The best way will be the spectroscopy, but we are not able to obtain high resolution spectra of an

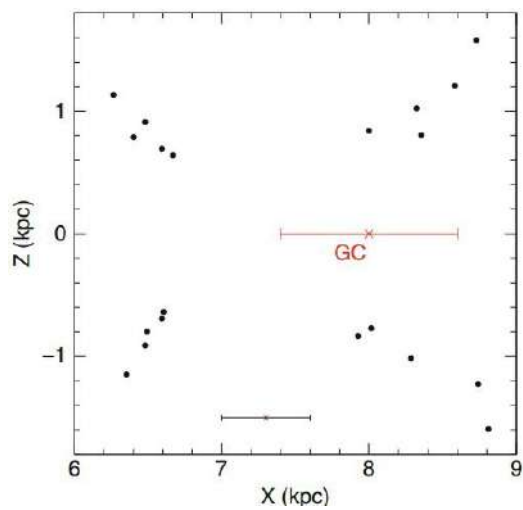


Figure 10.22: The result from the analysis of distance of RCs stars.

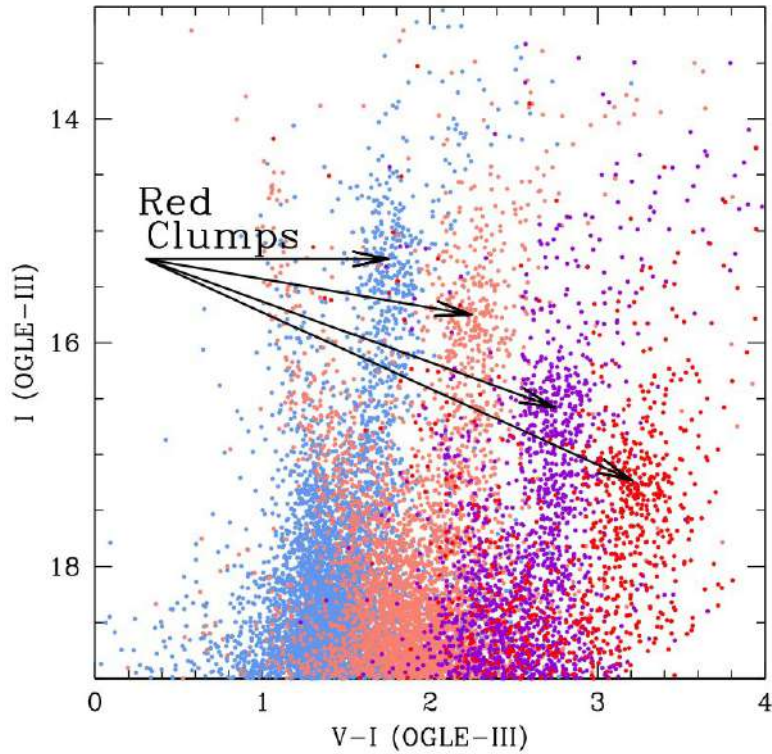


Figure 10.23: CMD of bulge stars, with different colors are marked stars from different part of the bulge. The arrows show the RCs.

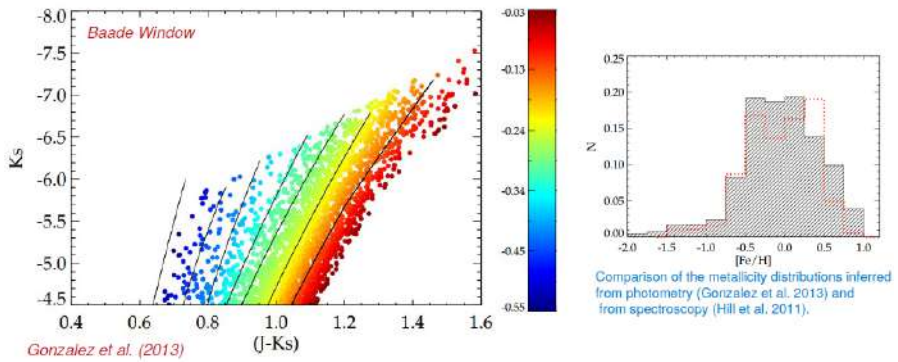


Figure 10.24: On left CMDs in Baade Window and on the right metallicity distribution: it is consistent with results from spectroscopy.

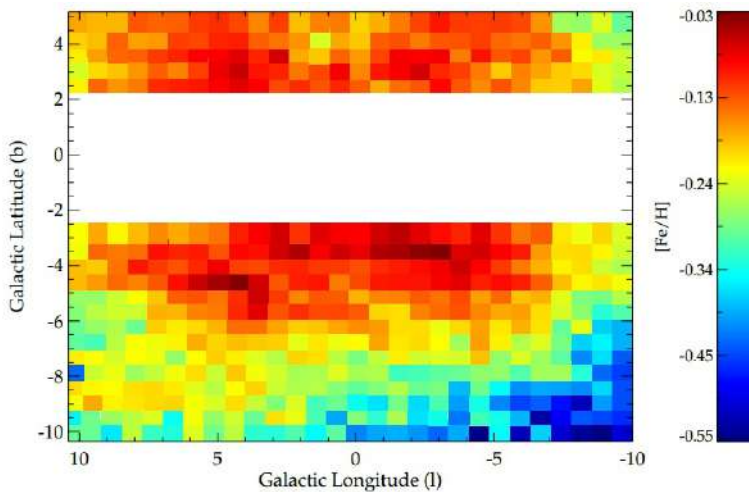


Figure 10.25: Result of the analysis of the metallicity distribution of many parts of the bulge. This is the photometric metallicity map

huge amount of stars. We use the photometry, of course it is less accurate but we can investigate million stars all together.

Reminder: the RGB slope is sensitive to metallicity: when RGB is almost vertical it indicate a metal poor regime, on the contrary a metal rich one. So the slope of the RGB in the differential-reddening corrected CMDs from VVV (ESO near-infrared survey) allow to derive a complete metallicity map of the Bulge.

Astronomers derive the metallicity distribution function for different part of the bulge and derive the average metallicity for each part. It is shown in figure 10.24 the CMDs obtained in Baade Window where reddening is lower and the metallicity distribution inferred by photometry which is consistent with that inferred from spectroscopy.

In particular metallicity goes from almost solar metallicity in the center region to more metal poor stars outside the center. However the most prominent feature of this map, shown in figure 10.25, is the presence of four lobs. This feature reveals the boxy-peanut shape of the bulge.

The body-peanut shape of the bulge is also confirmed by stellar density maps that show the structures traced by the Red Clump. In figure 10.26 are visible diagrams with galactic longitude against X position and galactic latitude against X position. In particular at latitude -5° we observe two blobs that merge when we move towards the plane. Their relative distance increases when we move towards lower latitudes.

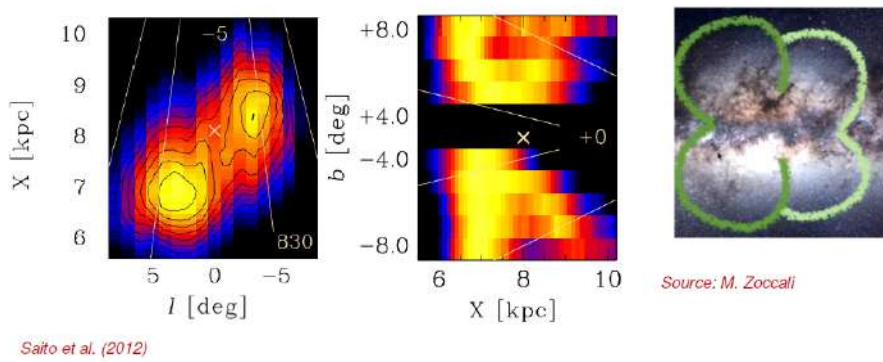


Figure 10.26: X+shape visible also from stellar density.

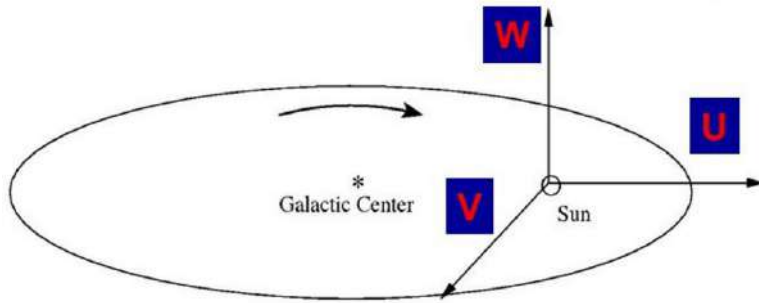


Figure 10.27: The system of reference for radial velocities.

10.2.1 Kinematics

Another feature that we expect according to scenarios discussed previously is particular motion of the stars. For classical spheroidal bulge we expect random orbits while for bulge coming from evolution of the disk, stars are expected to have big motion. Therefore study kinematics of stars can prove one scenario or another.

So firstly, we identify the RC stars, those of the brighter and those of the fainter Red Clumps. Then we get high resolution spectra of these stars to determinate the radial velocities.

We have to set a system of reference. The center is the Sun, the U direction points to the GC but the direction is outward, the W direction is perpendicular to the Galactic plane, the V direction is orthogonal to the U direction and lies on the Galactic plane, (figure 10.27).

Dynamical models of peanut-shaped bulges predict:

- different motions of bright and faint RC stars along the V direction. Due to stars on elongated orbits, which are streaming along the arms of the X-shaped bulge;
- same motions along the U and W directions.

Proper motions and radial velocities are used to derive stellar orbits for faint (blue line in figure 10.28) and bright red clump stars (red line in figure 10.28).

In figure 10.28 is shown the comparison between the model and the observations.

Bright RC, which traces the closer over-density of bulge stars, shows an excess of stars moving towards the Sun. An excess of stars receding from the Sun is seen in the far over-density, which is traced by faint red clump stars.

Stellar motions are consistent with predictions of dynamical models of peanut-shaped bulges: motions almost indistinguishable along U and W direction but different along V. In particular the different motions along V direction between bright and faint Red clump stars are explained by the presence of stars on elongated orbits, which are most likely streaming along the arms of the X-shaped bulge.

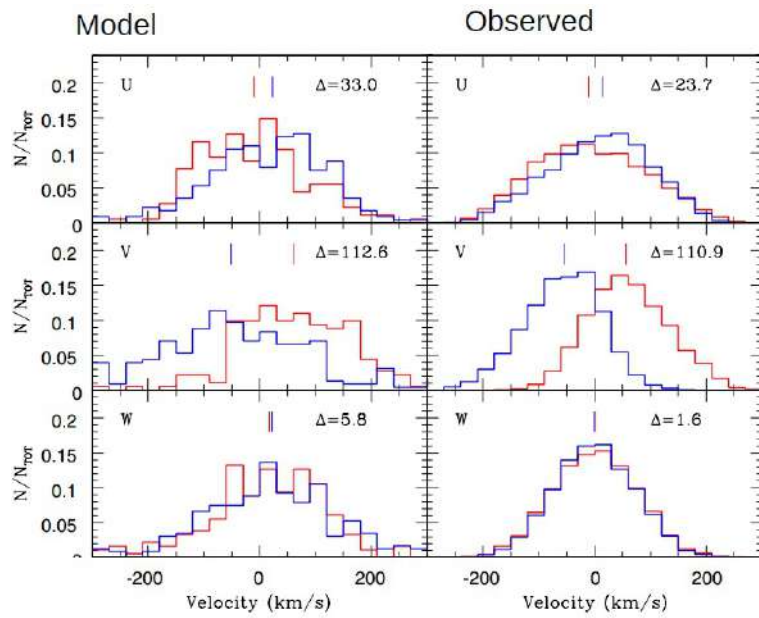


Figure 10.28: Result of the analysis of the velocities.

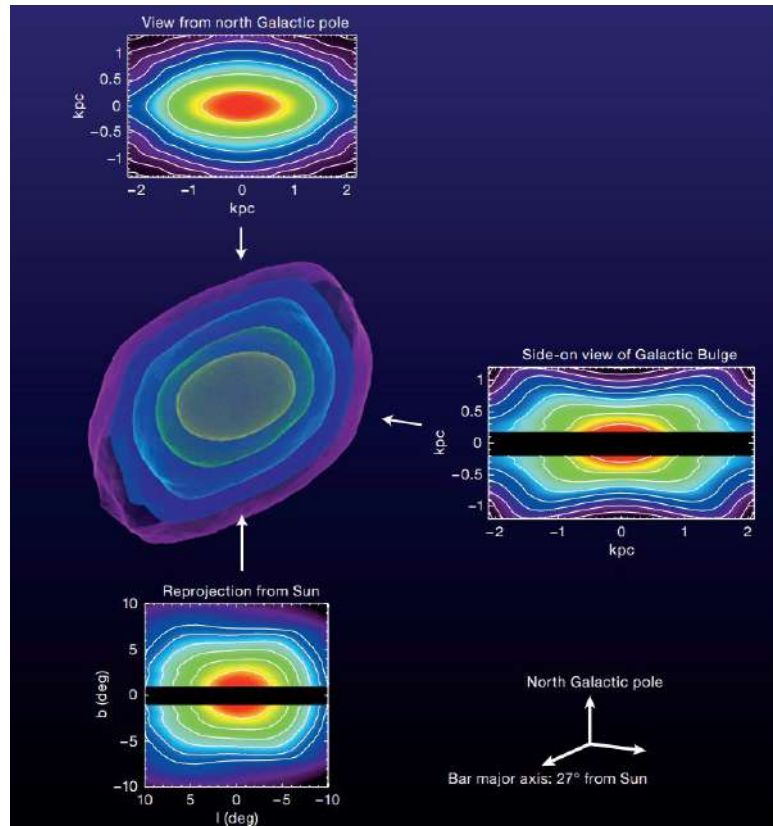


Figure 10.29: Model of MW bulge: the bulge is a bar with boxy-peanut X shape, according to scenario number 4 for bulge formation.

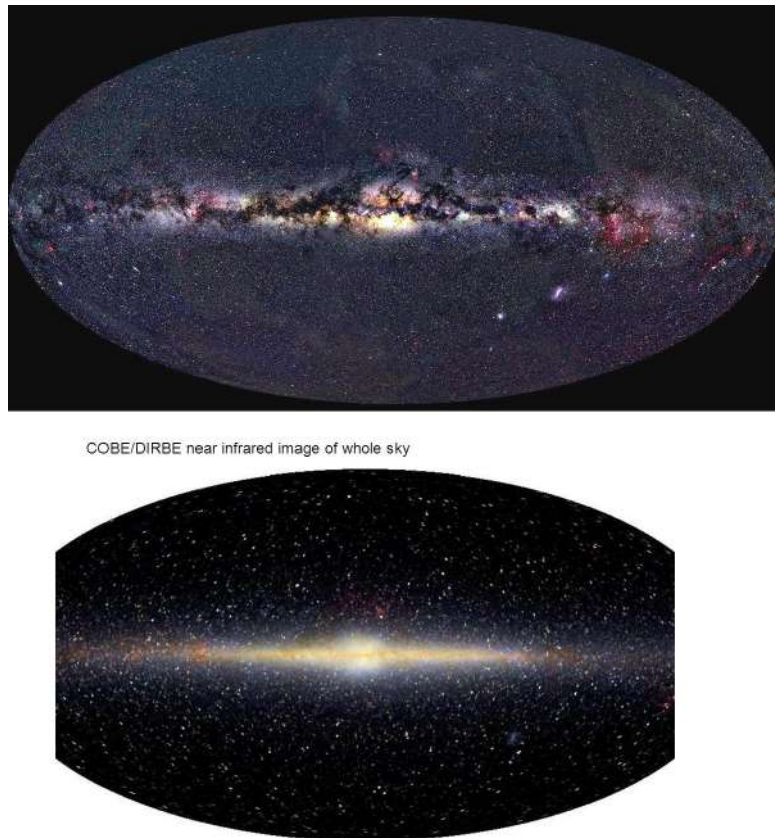


Figure 10.30: Observations in optical (top) and IR (bottom) of the bulge.

10.2.2 Optical vs. infrared observations

Now we try to spot this X-shape bulge from direct imaging, even if it is a complex process. Indeed, as said many times, the bulge is very extended and it is rich in gas and dust so there is a huge extinction. To partially resolve these problems we can observe many small regions in near infrared or infrared.

For example, in figure 10.30 we can see a comparison between IR and optical observations. In IR the dust are not a problem. Infrared light reveals the structures of galaxies in spite of dust, which blocks crucial details in visible light.

Solution - The subtraction of a model of how stars would be distributed in a symmetrical bulge from WISE observations highlight the X-shape of the Bulge. The result is shown in figure 10.31.

This X-shape, however, is not a peculiarity of our Galaxy. Indeed this structure is present also in external galaxy, like spiral galaxy NGC4710 considered a galaxy very similar to the Milky Way.

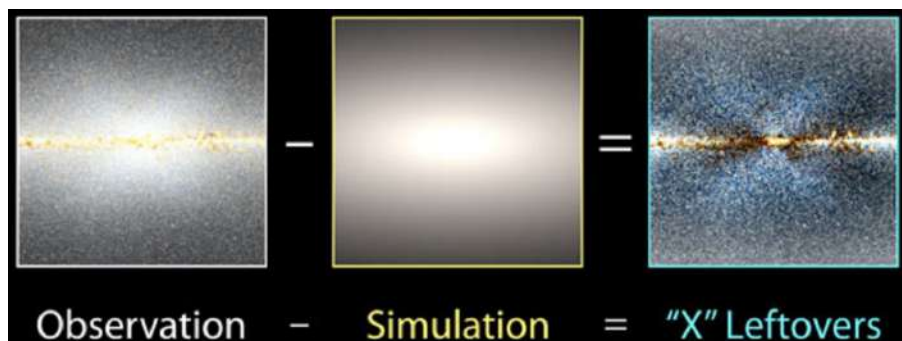


Figure 10.31: To see the X-shape of the bulge we can subtract a model of symmetrical bulge to the observed image.

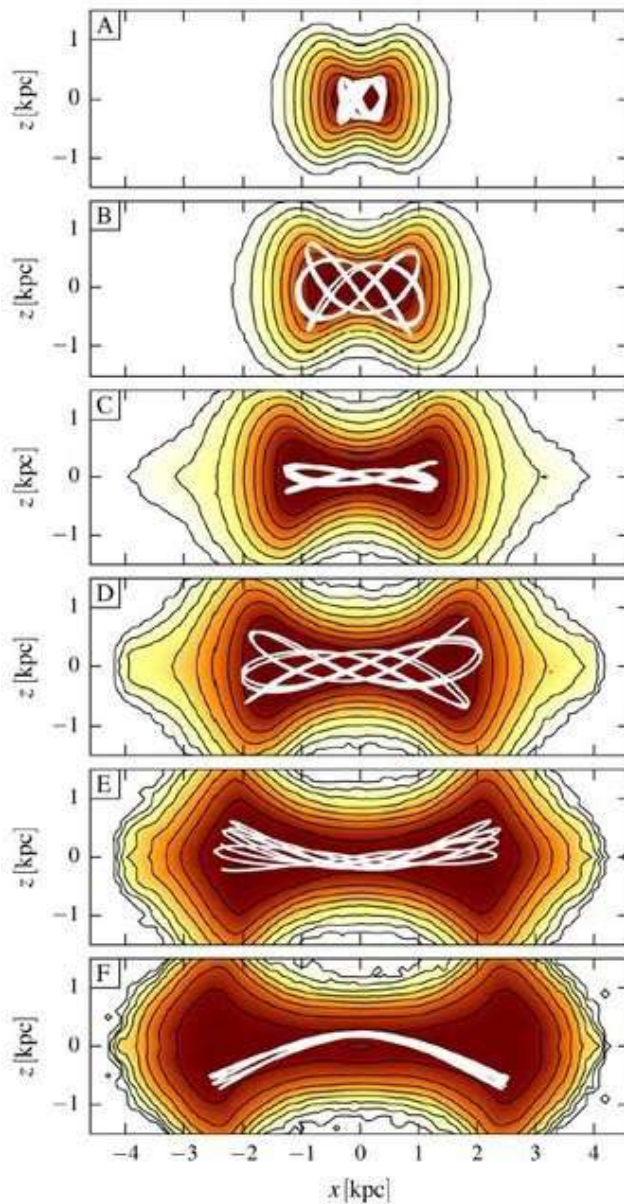


Figure 10.32: Model of the evolution of the X-shape of the bulge.

10.2.3 The X-shape component of the Galactic Bulge

The X-shape is a natural dynamical process that happens to bars. The disk instability (due e.g. by spiral arms) drives stars to the center in elongated orbits. This process forms a bar that is unstable: stars start buckling ending up in families of stable orbits in shape of eight, banana, or anti-banana (figure 10.32).

10.2.4 The rotation of the Bulge

However the bulge seems to more complex then what we believed. To understand better its structure we need more accurate data, like ones coming from BRAVA.

BRAVA (Bulge Radial Velocity Assay) is a large-scale radial velocity survey of the Galactic bulge. The aim is to advance the knowledge of how Galactic bulge and Milky Way formed. Radial velocities from the BRAVA stars are used to test and constrain dynamical models of the bulge, and to quantify the importance, if any, of cold stellar streams in the bulge and its vicinity.

In particular, they obtained radial velocities for $\sim 10,000$ M-giants stars inside the bulge. Analysing

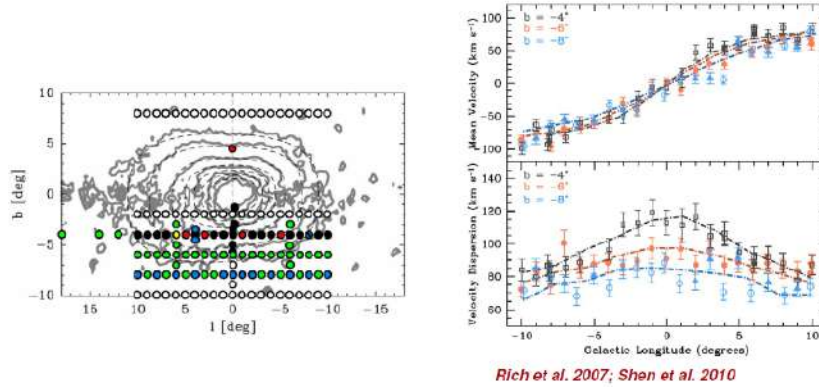


Figure 10.33: Radial velocities analysis from BRAVA project.

these stars, they found that bulge stars exhibit cylindrical rotation which means that the Bulge is rotating like a solid body. Results of this work are shown in figure 10.33. On right panel there are two graphics: one mean velocity against Galactic longitude and one velocity dispersion against Galactic longitude. In this second case at 0 longitude (corresponding to the center of the bulge) there is a peak of velocity dispersion. This is a feature of cylindrical rotation.

However cylindrical rotation is expected if there is only a bar. On the contrary a spheroid is expected to have a significant variation of rotation with latitude. Are we in a BULGE-LESS galaxy?

10.2.5 Study of Galactic bulge structure using RR-Lyrae

RR Lyrae are variable stars very bright and characterized by peculiar light curve. For this reason they are easy to identify.

They are also traces of the metal-poor population of the Bulge, while Red clump stars trace the metal-rich population.

The vast majority of RR stars have been found at 8.5 Kpc which means inside the bulge. For this reason we expect that also RR-Lyrae show the same properties derived from the Red Clump stars.

However, studying their distribution in the bulge, astronomers found that RR Lyrae stars are arranged in the shape of a spheroid and not in a X-shape structure like RC stars! They do not shape the bar traced by the Red Clump as shown in figure 10.34.

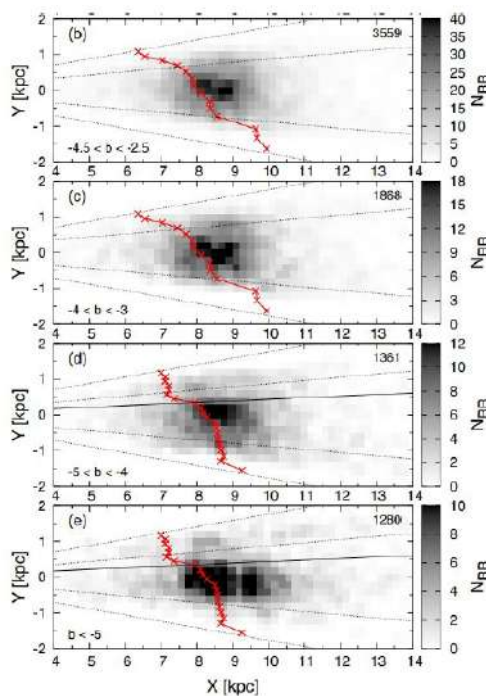
In particular RR Lyrae stars exhibit hot kinematics and null or negligible rotation. They are members of a separate population from the bar/pseudobulge!

10.2.6 Chemical abundances in the Galactic Bulge

High-resolution multi fiber spectrographs (like GIRAFFE at VLT) allow to observe large number of spectra simultaneously.

From these high resolution spectra, astronomers found evidences for **metallicity gradient** along the minor axis of the Bulge. The Baade window ($b \sim -4$ characterized by lower level of reddening) hosts the most metal-rich stars, whereas the average metallicity decreases towards lower galactic latitudes.

What is peculiar is that metallicities of ~ 400 bulge stars are consistent with a **bimodal distribution**, difficult to reproduce. This feature (shown in figure 10.35) means that there are two components: the metal-poor stars, which are consistent with a classical bulge, and the metal rich stars, which are consistent with a bar structure. Of course, to get this conclusion we need to take into account the



Dekany et al. (2013)

Figure 10.34: According to X-shape model, RR stars should follow the red line but, on the contrary, they are located at the center in a spheroidal distribution.

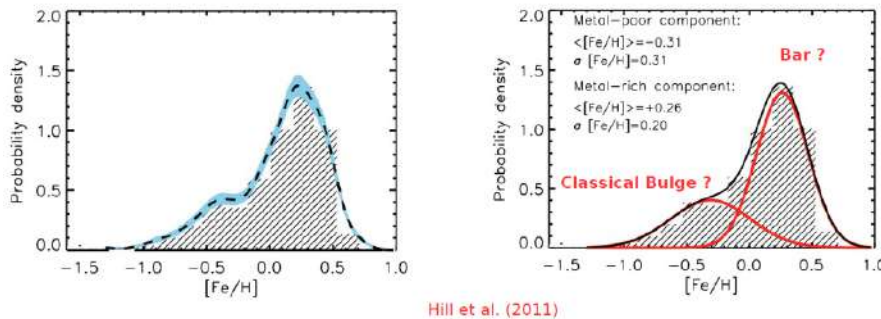


Figure 10.35: Bimodal distribution inside probability density against metallicity diagram.

observational errors, by smoothing the metallicity distribution and deconvolving for observational errors.

The vertex deviation, lv , is indicative of the elongation of the stellar velocity distribution. By analysis of lv , astronomers derive that: metal-poor stars have vertex deviation close to zero, hence, they have a spheroidal velocity distribution. On the contrary metal-rich stars have negative lv , indicating that they evolve in an elongated (ellipsoid) velocity distribution. These results are shown in graphic 10.36.

Thank to the GIRAFFE survey astronomers discover that the metal poor population is more centrally concentrated than the metal rich one! (in contrast with previous observations). This is a clearly confirmation that Galactic bulge is not only a pseudo-bulge, but it is a bimodal bulge.

The model expect a density distribution of 48% of metal poor stars and 52% of metal rich stars. In contrast to metal-poor stars, the metal-rich population is arranged in a boxy distribution, consistent with an edge-on bar. Metal poor and metal rich density distributions are shown in figure 10.37.

The bar/buckling instability may have developed at a relatively late time in the evolution of the Milky Way, while a bulge was already in place and formed at very early cosmic times.

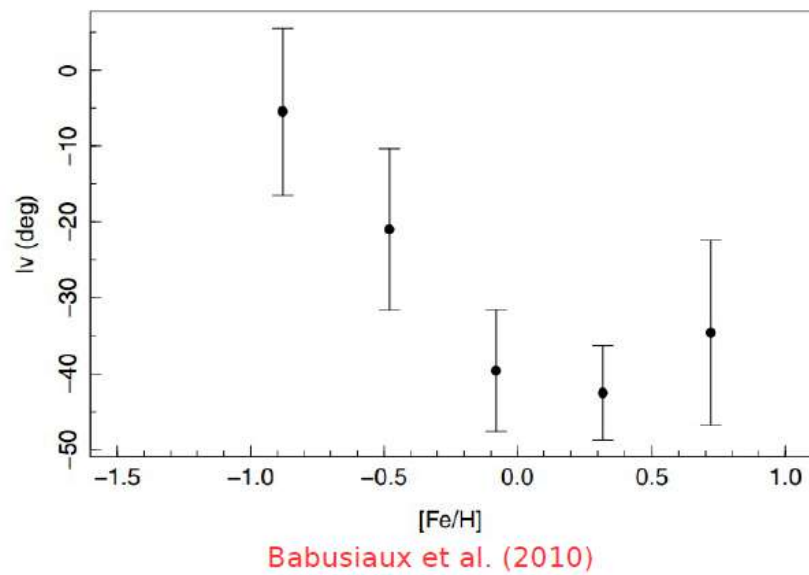


Figure 10.36: Vertex deviation for metal poor and metal rich stars.

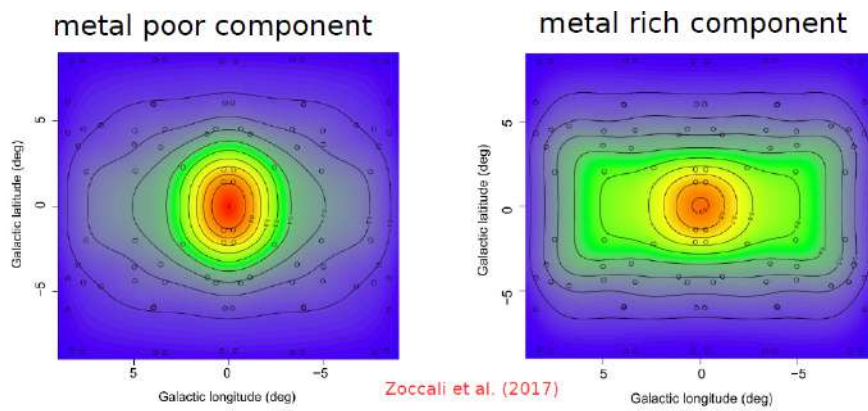


Figure 10.37: Density distribution of metal poor and metal rich component.

Chapter 11

Galactic archaeology with the Milky Way Disk

We have seen that a galaxy is mainly composed by a bulge, the oldest component, and by a disc, the most massive component, and an halo, spheroidal distribution of visible mass. There are no clear boundaries between different components but the key point is to understand how they are connected one to each other.

The stellar halo has a spheroidal distribution that envelops the disk and bulge. It reaches out to 150 kpc . It contains old Population II stars (remember that population I is young and metal rich while population II is old and metal poor). It is very centrally concentrated: half light radius of halo is around $0.4 - 0.5 \text{ kpc}$.

What is the origin of the halo of our galaxy? It is something connected to evolution of galaxy itself or it is built up from external objects that merged together and formed our galaxy? Like dwarfs galaxies or GC there were more massive in the past? What is sure is that in the halo there are signatures of past merging history of MW. According Big Bang scenario, we expect big galaxies formed from several small objects and we expect today to observe many satellites or remnants of satellites however we do not. This is the missing satellite problem seen previously.

In literature it is used to divide the halo in two parts:

- **inner halo:** may have formed in situ during the evolution of the Milky Way ($[Fe/H] \sim -1.6$);
- **outer halo:** originated from past accretion and tidal disruption of dwarf galaxies ($[Fe/H] \sim -2.2$).

On the other side, the disc contains a substantial fraction of the barionic mass of the Milky Way. Much of the evolutionary activity in the Galaxy takes place in the disk. The disc of various galaxies are best described by two populations, one with shorter and one with longer scale-heights, dubbed the *thin* and the *thick* discs.

In figure 11.1 we can see two images of the same galaxy with different exposure time. On left we can see the thin disk, on right the thick disc. This double-disc behaviour is also inferred from observations of edge-on galaxies. Moreover the disk is not regular going to the external part of the galaxy: there is some kind of irregularity like over-densities of stars that were confused with galaxies in the past. These are interesting structures connected with dynamical evolution of stars in the disc.

To investigate the population in the thick disc astronomers used the colors of the integrated fluxes of the stars, observing galaxies similar to the Milky Way. The red colors of thick discs have led to the tentative conclusion that they are made of uniformly old stellar populations. But the age-metallicity degeneracy of broad-band colors prevents from strong conclusion: indeed taking an old stellar population but very metal poor, it will be bluer than MS stars metal rich with same age.

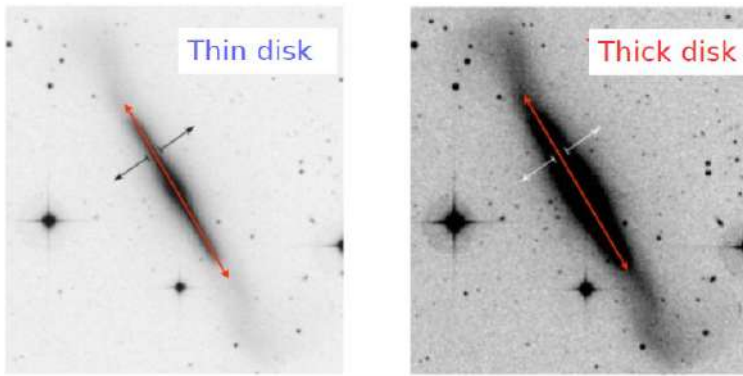


Figure 11.1: Two images of the same galaxy with different exposure time. On left we can see the thin disk with short exposure time, on right the thick disc with long exposure time.

Summarizing: in the internal part of the disk we are dominated by blue light emitted by young stellar population with ongoing formation while going in the external part of the disc the color became redder and redder: here there are old stellar populations not extremely metal poor.

11.1 The formation of the disc

It is difficult to define a net limit between thin and thick disc. Are the thin and thick disc in the Milky Way real separated structural entities? The two components could be the product of the evolution and have the same nature or could have different birth (like merging for the thick disc). The latter case expect that the thick disc is formed via an external mechanism (accretion and/or mergers). The first case, instead, is based on the internal dynamical evolution (primarily in form of radial mixing), which drives the evolution from a pure thin disk to a couple of thin and thick disks. We can try to discriminate among these scenarios using stellar kinematics. In terms of kinematics, thin disc stars are cooler which means that these stars have smaller vertical velocity (W direction, orthogonal with respect to the Galactic plane). Thin disc stars have higher Galactic rotational velocity compared to thick disc stars then we refer to them as kinematically hot (due to the high vertical velocity). Low rotational velocities imply higher velocity dispersion for thick disc stars, which then point to older ages, either born hot or heated up.

Let us investigate the velocity dispersion of stars population with different ages.

In figure 11.2 we can see the result of this investigation. It seems that by evolving stars gain vertical velocity. The age–velocity dispersion relation suggests a vertical age gradient. The result suggest star formation along the disk with small dispersion of velocity on W direction. Then, when stars evolved, they start increasing the velocity component along W , moving far away from Galactic plane. This age gradient is clearly visible in figure 11.3.

11.2 Asteroseismology

One alternative way to obtain independent determination of age (without using isochrones or models based on isochrones) is based on asteroseismology.

This new astrophysical field is based on very high precision photometry that detects very small variations in terms of flux. These type of measurement with this high accuracy are not able form ground but only form space.

For example, Kepler mission, launched in 2009 makes asteroseismology. It search for habitable planets and it provides high-precision photometry to detect planetary transits. But the secondary mission is to monitor variability of over 100,000 stars for asteroseismology.

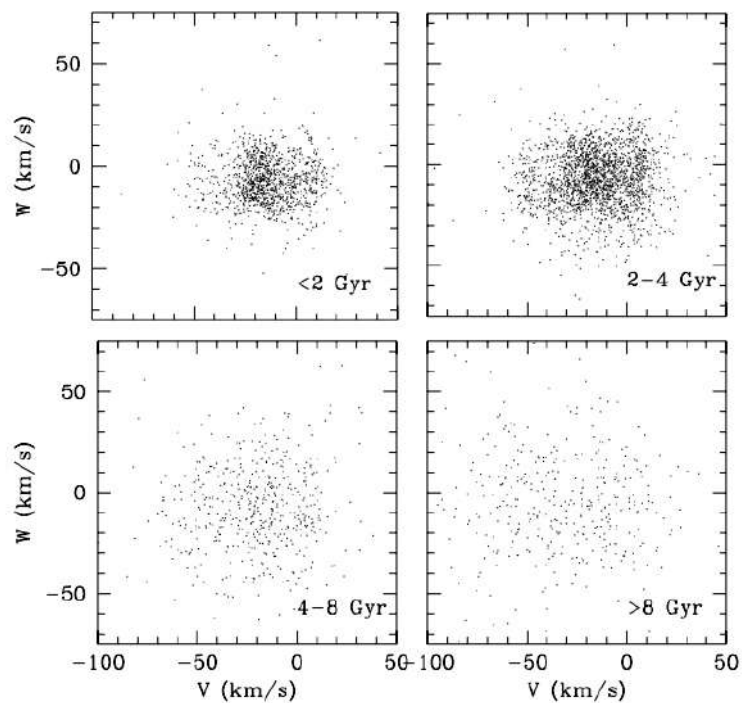


Figure 11.2: Velocity dispersion of population with different ages.

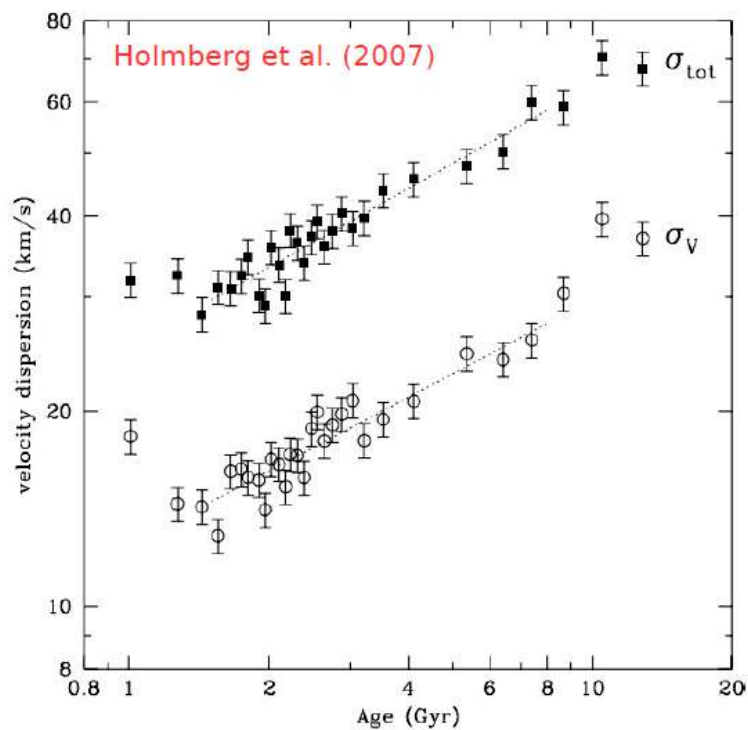


Figure 11.3: Velocity dispersion as function of age.

Indeed the space-borne mission Kepler/K2 allows us to robustly measure global oscillation frequencies in thousands of stars, in particular red giants, which in turn make it possible to determine fundamental physical quantities, including radii, distances and masses. In particular we observe the brightest and the most isolated stars (so the most appropriate) to get precise determination of flux oscillations. From complex observations and complex physics associated with oscillation, we infer many properties in an independent way, like the age.

For example, Miglio et al. (2016) made an interesting work deriving the mass for RGB stars and HB stars of K giants stars in M4. The result was very interesting! They obtained mass of RGB stars and HB stars (a bit less massive the RGB ones) in agreement with values obtained using isochrones and indicating a mass loss from HB stars. The offset with respect to independent masses is lower, or comparable with, the uncertainties on the average RGB mass (4 - 10%, depending on the combination of constraints used).

This was first determination of mass loss for old stellar population using asteroseismology.

We have said that the disk is a huge area in the sky with a lot of stars with different properties: here stars do not have same age or same distance. So we cannot use the isochrone to infer the age, another way is to use the asteroseismology.

Comparing the age derived by asteroseismology and by the isochrones in a cluster we can see that with two unconnected method we obtain the same result, so the measurements are fine.

To validate the other parameters that we can infer by using the asteroseismology we can use the Stroemgren photometry. It is a photometric system that is used to infer some stellar parameters like the surface gravity, the effective temperature, the iron content and the color excess (see previous chapter).

By combining the data from the asteroseismology and the Stroemgren photometry, astronomers derive the ages of a lot of stars. This is the main goal of SAGA (Stroemgren survey for Asteroseismology and Galactic Archaeology): this survey transform Kepler field into a new benchmark for Galactic studies, similarly to the solar neighborhood. This is possible thanks to the coupling of classical and seismic parameters that provide accurate effective temperatures, metallicities, distances, surface gravities, masses, and radii.

In figure 11.4 we can see the result: measure of vertical age structure of the Galactic disc. In particular low-mass, i.e. old red giants dominate at increasing Galactic heights, whereas closer to the Galactic plane they exhibit a wide range of ages and metallicities. This means that going at high altitude Z from Galactic plane we are dominated by low mass stars which are also the oldest.

Another important result is the following: age of the star, from Galactic plane toward higher altitude, is not constant but we have an age gradient. In particular, parametrizing the observations as a vertical gradient returns approximately $4 \text{ Gyr}/\text{kpc}$ for the disc. The ages of stars show a smooth distribution over the last 10 Gyr (first panel of figure 11.4). Summarizing, age increase moving to higher altitude.

There is also evidence for a flat age–metallicity relation for disc (last panel in figure 11.4). These results are consistent with a mostly quiescent evolution for the Milky Way disc since a redshift of about 2.

11.3 New modern studies: APOGEE and GAIA data

In the last few years we have the opportunity to use new modern and very accurate data for our studies. In particular APOGEE (the Apache Point Observatory Galactic Evolution Experiment) is a spectroscopic survey of high resolution observation in Near Infrared (in order to minimize the reddening effect) that provides spectra of almost ~ 500.000 luminous Milky Way red giant stars.

These data, used together with GAIA photometric measurements, provide age estimates for most stars.

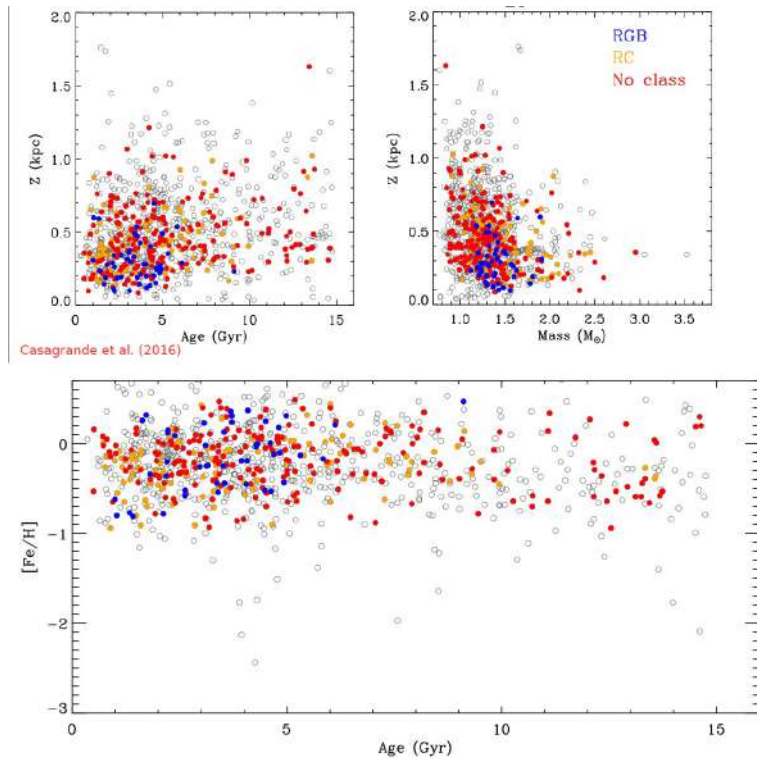


Figure 11.4: Result of the combined dataset of asteroseismology and Stroemgren photometry. Z is the altitude from Galactic plane: going at high Z we are dominated by low mass stars which are also the oldest.

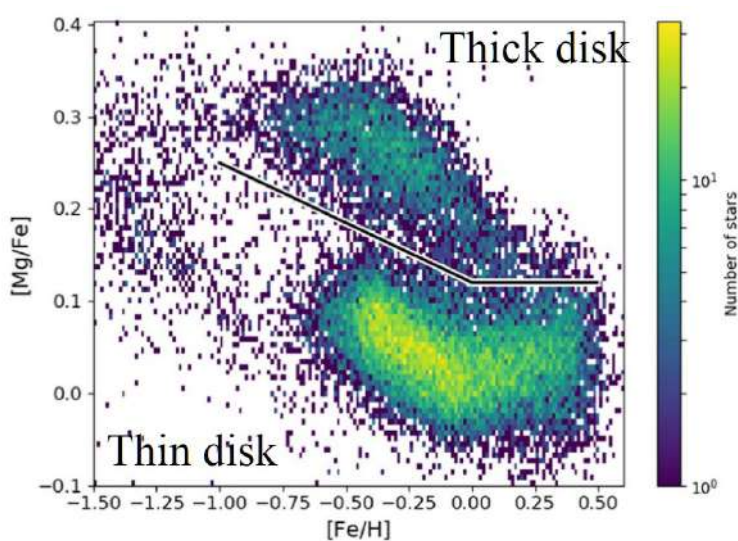


Figure 11.5: Map of $[Fe/H]$ against $[Mg/Fe]$ of disk's stars.

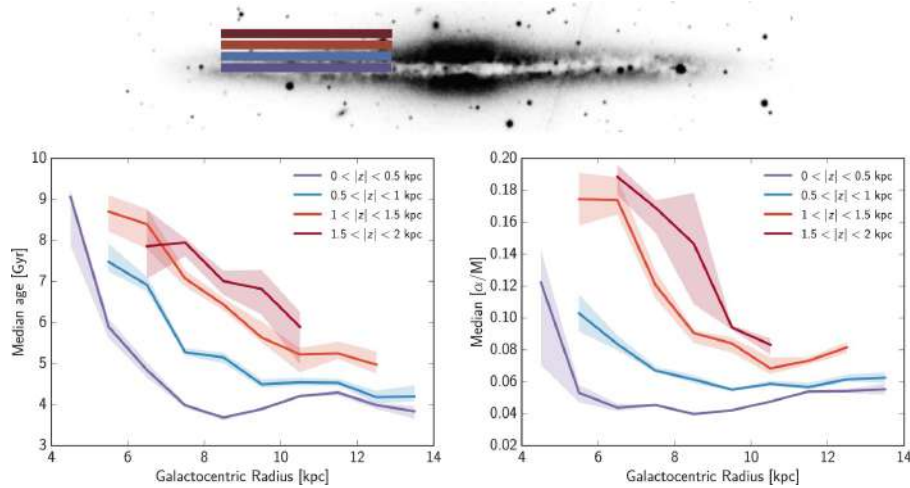


Figure 11.6: Martig et al. (2016) have used a different way to derive the age gradient in the thick disk.

From these data, we discovered that Milky Way is not characterized by a single disc but it is a complex structure with presence of two components clearly separated. In figure 11.5, the Milky Way has a ‘double’ disc, whose components have distinct chemical composition, ages and kinematics. Thin disc stars are observed to be on average more metal rich and less alpha-enhanced than thick disc stars: this is important because it tells us about chemical evolution of stars and the impact of Supernovae events. For example in case of SN1A there is production of iron and depletion in alpha-elements. So, looking at this diagram, it is clear that Supernovae events had a different rule in the evolution of these two components.

On the contrary Martig et al. (2016) have used a different way to derive the age gradient in the disk. In figure 11.6 we can see the result. They studied the age of stellar populations in different regions of the Galactic disc at different altitude from Galactic plane.

In first diagram we see that going to higher Galactic altitude, for a fixed radius, stars are older and older reaching maximum age in the center of the Galaxy. It decreases going in the external region. To be more specific, in galaxies where old stars are centrally concentrated, thick disks are radially extended. We can see that the trends are very similar to those with the alpha enrichment (on right). An explanation is the following: younger stellar populations flare in the disks’ outer regions, bringing those stars high above the midplane. The resulting geometrically thick disks therefore show a radial age gradient, from old in their central regions to younger in their outskirts.

11.4 GAIA and Enceladus

In the recent year the situation changed, in particular due to the DR2, the second survey of GAIA. By GAIA we derive proper motion and distances. WE can derive CMD and proper motion analysis of very high resolution, improving our knowledge.

In figure 11.7 we can see the CMD of halo stars derived by GAIA.

Panel on left is largely affected by reddening effect. There is also another component: the distance. We have seen many times CMD of clusters characterized by same distance for all stars while here there can be also a huge difference in terms of distance.

Panel on center is corrected for reddening: we can use some 3D maps but also a very simple and clever idea: plot stars with low reddening effect, with $E(B - V) < 0.15$.

On panel three are then plotted stars with velocities bigger then 200 km/s so belonging to the halo. The result is impressive: Gaia DR2 reveals two distinct sequences in the CMD of halo stars.

In figure 11.8 we can see the isochrones fitting of these two distinct path on CMD: the blue one has

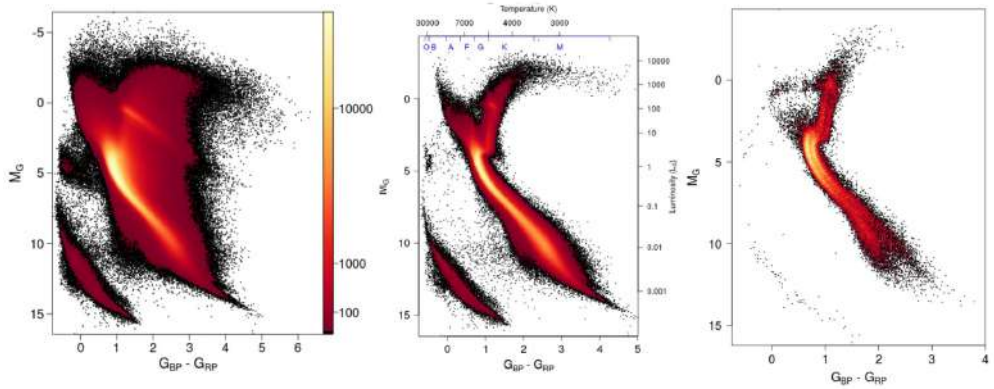


Figure 11.7: CMDs derived by GAIA photometry: on left CMD of $\sim 66,000,000$ stars, in the center CMD of stars with $E(B - V) < 0.015$, on right stars with $V_T > 200 \text{ km/s}$ (the halo stars).

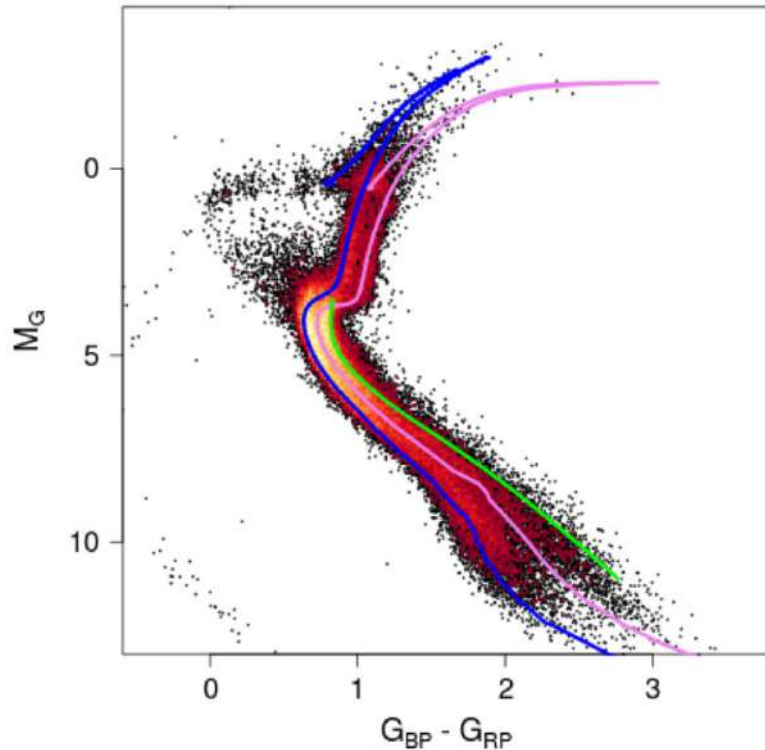


Figure 11.8: CMD of halo stars with isochrones fitting. The blue one has $[M/H] = -1.3$ and age of 13 Gyr ; the magenta one $[M/H] = -0.5$, age of 11 Gyr .

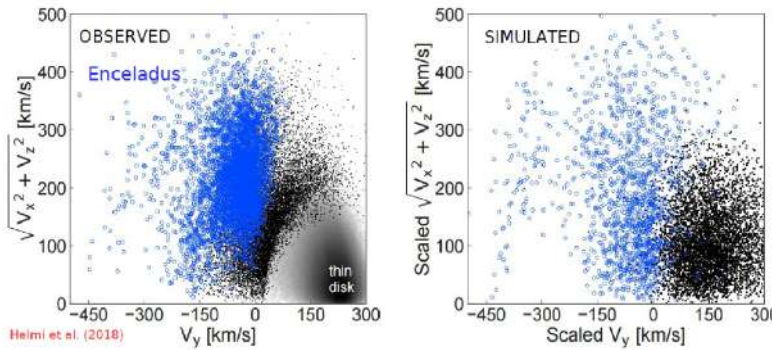


Figure 11.9: Map of proper motion of near Sun stars. On right the simulation, on left the observed.

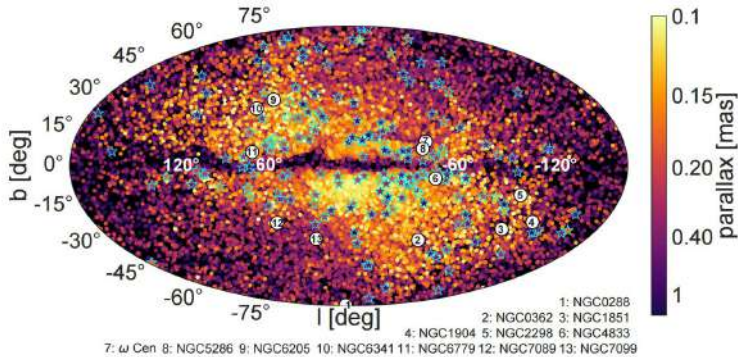


Figure 11.10: Map of the parallax in the Galaxy.

$[M/H] = -1.3$ and age of 13 *Gyr*, the magenta one $[M/H] = -0.5$, age of 11 *Gyr*. These are real and not a feature of differential reddening because we have selected only stars with a small color excess.

GAIA investigate also the proper motion for the near Sun stars.

In figure 11.9 on left we can see the result of the proper motion analysis: a significant fraction of the halo stars near the Sun are associated with a single large kinematic structure that has slightly retrograde mean motion. These stars dominates the CMD blue sequence revealed in the Gaia data in figure 11.8.

There is a strong similarity between the observations (on left) and the simulation (on right) of the formation of a thick disk via a 20% mass-ratio merger. The retrograde structure could be largely made up of stars originating in an external galaxy that merged with the Milky Way in the past. This feature is called Enceladus-sausage.

Another map derived by DR2 is the parallax map: it is a Galactic map where each star has a color which is representative of its parallax. This is a map of distribution of stars with retrograde motion nearby the Sun.

In figure 11.10 we can see the parallax map. Nearby Gaia-Enceladus stars (with parallaxes > 0.25 mas, darker points, more distant) are distributed over the entire sky. More distant stars are preferentially found in specific regions of the sky. Thirteen GCs can be associated with Gaia Enceladus based on their angular momentum.

Moreover GAIA DR2 detected a large-scale gradient in the radial velocity across the full sky. Such a coherent pattern can only be obtained if stars are moving in the same (retrograde) direction on elongated orbits. This means that this structure (to which all stars belonged) is very large, so the object that merged with MW was very large.

In particular we can infer a more detailed $[\alpha/Fe]$ vs $[Fe/H]$ map and detect the Gaia-Enceladus stars.

In figure 11.11 there this map. Stars with retrograde orbits have a kind of elongated structure.

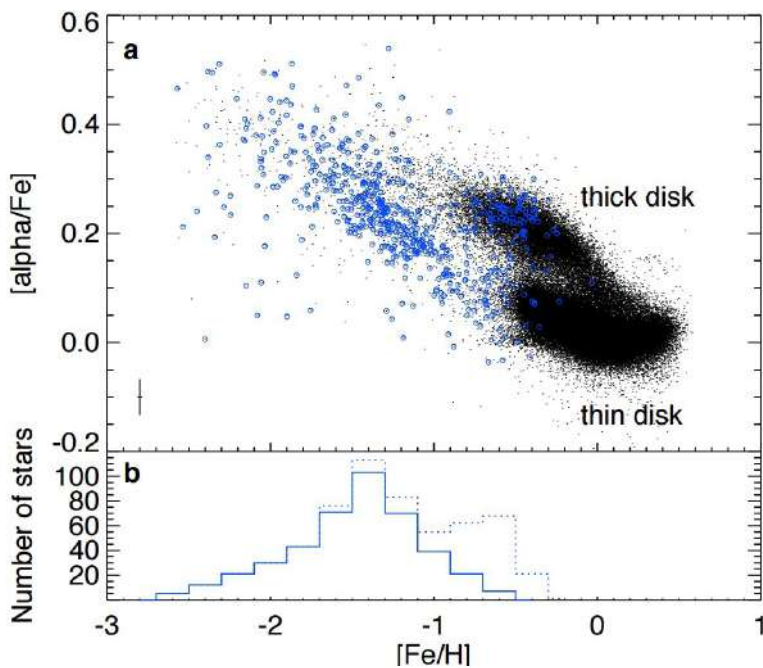
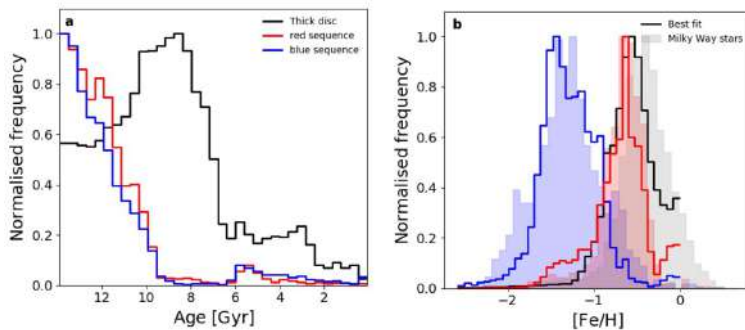
Figure 11.11: Map of $[\alpha/\text{Fe}]$ vs $[\text{Fe}/\text{H}]$.

Figure 11.12: The age distribution of the two component of the halo and of the thick disk stars.

The large metallicity spread of the retrograde structure stars, implies that they did not form in a single burst in a low mass system. The more metal-rich stars have lower $[\alpha/\text{Fe}]$ at the characteristic metallicity of the thick disk ($[\text{Fe}/\text{H}] \sim -0.6$). Hence, they were born in a system with a lower star formation rate than the thick disk.

Based on appropriate chemical-evolution models, the stellar mass for the progenitor system is $\sim 6 \times 10^8 M_\odot$, 1/4 of the primordial Milky Way.

The last step was done in 2019 by Gallart et al. They analysed the age distribution shown in figure 11.12 on left and the iron content distribution on right panel. The red and the blue distributions are stars of the red and blue path of the halo CMD. The age distributions suggest that the stars in the blue and red sequences of the halo CMD are equally old, and older than the bulk of thick disc stars. Look at the right panel: the red sequence would host halo stars, formed within the seed progenitor of our Milky Way. The in-situ halo is naturally more metal rich than the accreted halo population originating in the lower-mass galaxy Gaia-Enceladus whose stars form most of the blue sequence.

There was probably another merging event with the so called Sequoia galaxy. The Sequoia galaxy is responsible for a major accretion episode, distinct from Gaia Enceladus. The Sequoia event is responsible for the bulk of high-energy retrograde stars in the halo. The stellar mass was $5 \times 10^7 M_\odot$, instead the total mass was around $10^{10} M_\odot$, considering also dark matter. This is in contrast with what we found previously: here the two sequences have same age and when Gaia-Enceladus galaxy merged with the Milky Way, MW was already subjected to a merging process.

Chapter 12

The second Parameter problem of the HB morphology

We known that HB is an important zone in the CMD. Stars in this evolutionary phase are burning He in the core in a stable way. We call it horizontal because in a certain filter and with a particular color these stars are located horizontally.

Metallicity is considered the first parameters that determine the HB morphology. Indeed a metal rich population shows a red HB, instead a metal poor population a blue HB.

However the classical second-parameter problem indicates that globular clusters with the same metallicity have different HB morphologies.

In figure 12.1 we can see many GCs: in the upper panels there are CMDs of clusters with different metallicity and different HB while in the bottom panels there are shown two GC with same metallicity but different HB.

The second parameter problem is one of the main open issues of stellar Astrophysics of the last ~ 60 years. Many suggested second parameters include: cluster age, ellipticity, mass, central concentration, binaries, planets or stellar mass loss.

Based on the the difference between the color of RGB at the HB level and the median HB color of HB stars Dotter et al. suggested that age is the second parameter.

On the contrary, based on the maximum temperature of HB, Recio-Blanco et al. suggested that the HB morphology depends on cluster mass.

An alternative approach

Astronomers tried to resolve the second order problem by using two parameters and not only one. A global parameter that varies from GC to GC and a nonglobal parameter that varies within the GC. Moreover they introduced a new metric:

- **L1:** color distance from the RGB and the reddest part of HB;
- **L2:** color extension of the HB.

L1 depends on metallicity, as we can see in figure 12.3. In this plot there are three group of stars, each of them corresponds to one GC, with a different HB. In particular there is a strange correlation between metallicity and L1.

Three groups of clusters are:

- **G1:** Metal rich GCs ($[Fe/H] > -1$). They are not involved in second parameter problem and present red horizontal branch alone;

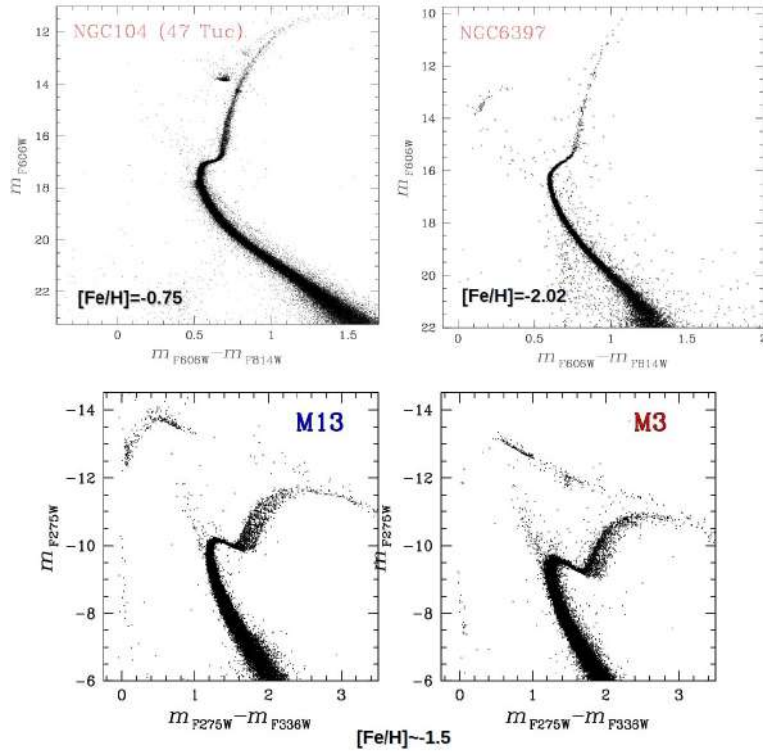


Figure 12.1: Comparison between many GCs to showing the HB morphologies.

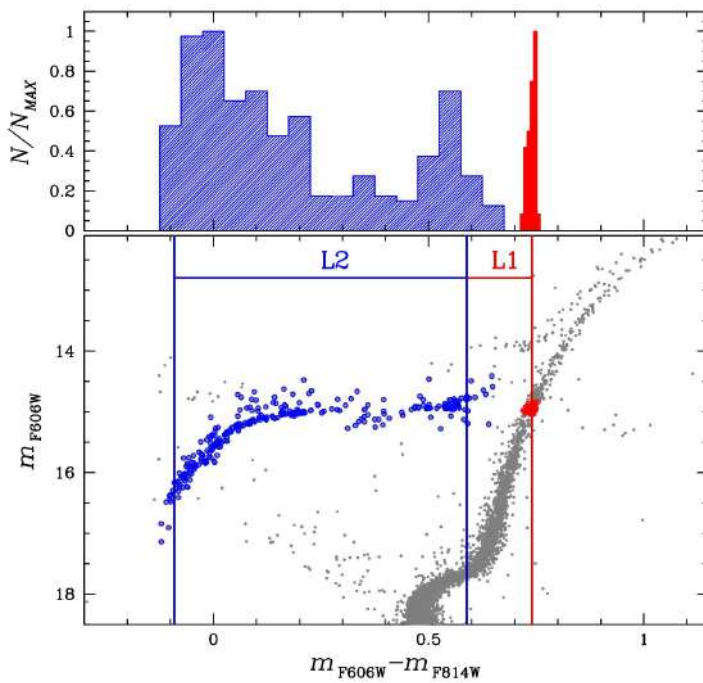


Figure 12.2: CMD that shows graphically L1 and L2 parameters.

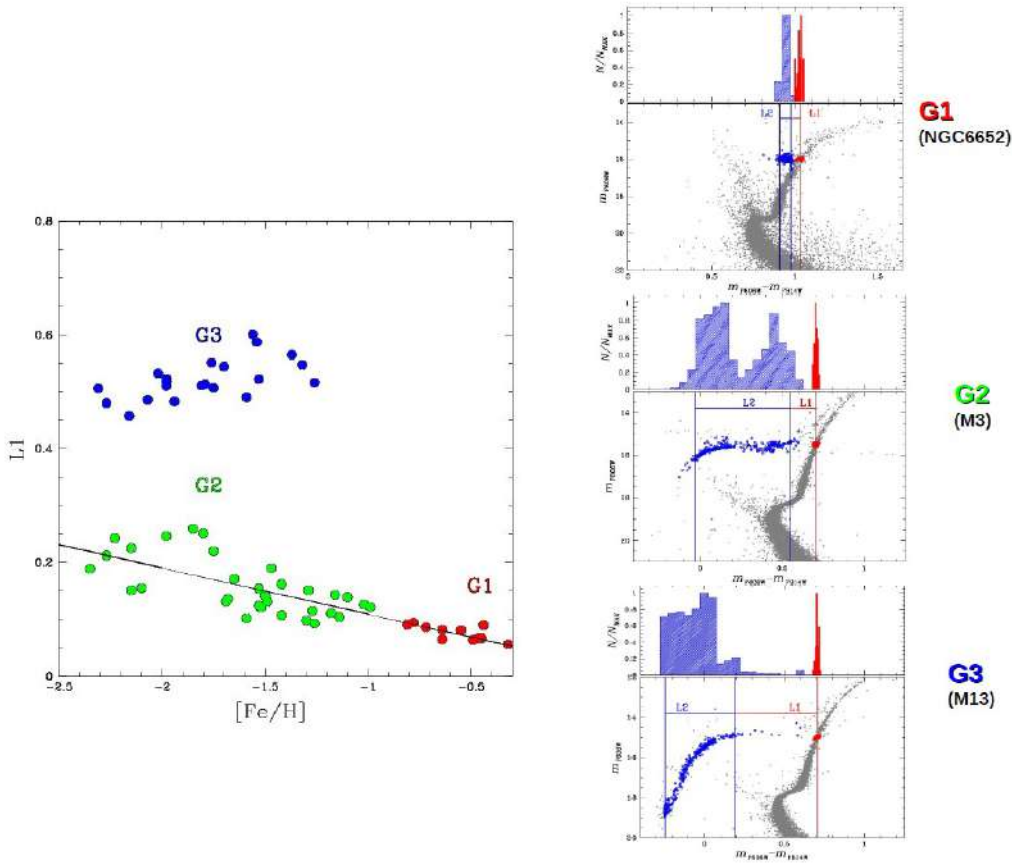


Figure 12.3: On left L1 against the metallicity, on right the CMDs of three clusters.

- **G2:** GCs with $L1 < 0.4$, with red stars close to HB;
- **G3:** GCs with $L2 > 0.4$, with HB distant from RGB.

$L1$ does not correlate with the absolute luminosity. This is apparently in disagreement with Recio Blanco et al. 2006. $L1$ correlates with age, in agreement with Dotter et al. 2010 findings (figure 12.4).

Let's look at the dependencies of $L2$. It does not correlate with metallicity, but does not correlate with age, this latter in apparent disagreement with Dotter et al. 2010. On the contrary, $L2$ correlates with absolute magnitude (i.e. the cluster mass), in agreement with Recio Blanco et al. 2006.

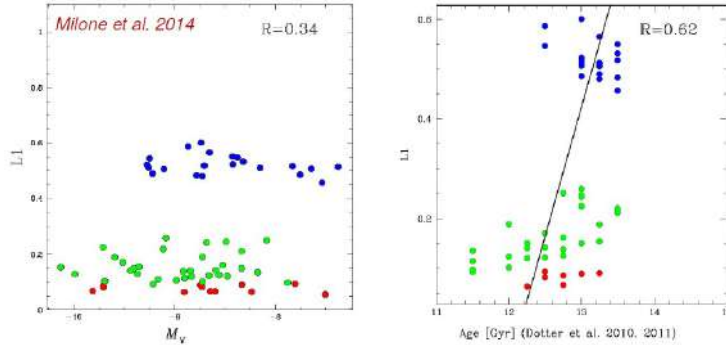


Figure 12.4: On left L1 against the absolute luminosity, on right against the age.

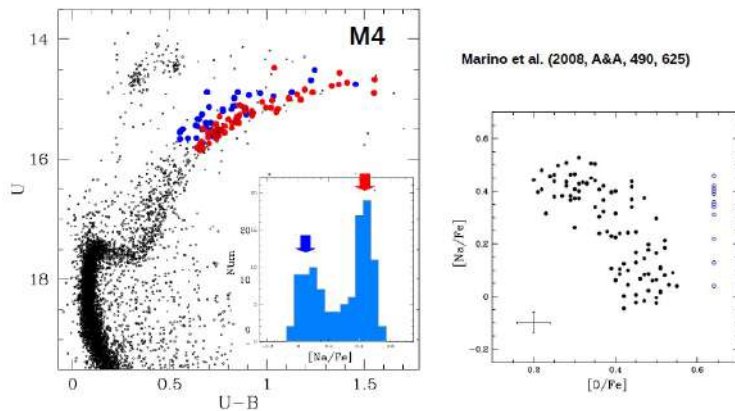


Figure 12.5: CMD of M4, in blue and red are shown two different population with different Na content.

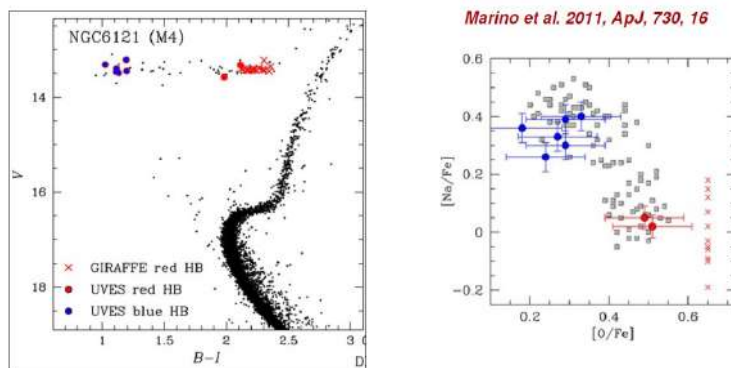


Figure 12.6: CMD of M4 where there are shown two population of stars in the HB.

12.1 Multiple populations and the 2nd parameter of the HB morphology

M4 hosts at two stellar populations with different C , N , O , Na , Al and a bimodal RGB. Na -rich stars define a narrow sequence on the red RGB, while Na -poor stars define a spread bluer RGB (figure 12.5)

In figure 12.6 stellar populations with different Na and O define distinct HB sequences. All star in blue HB have chemical composition similar to second generation stars of GC while stars in red HB are consist with being first population stars. This is the evidence that multi population are connected with morphology of the HB.

One of the element that varies in multi population is Helium. Helium abundance can be inferred from spectroscopy of few stars in few clusters because it is quite difficult to estimate. Analysing a few HB stars, astronomers discovered that these stars present an helium enrichment. We know that the multiple sequences in the CMD correspond to stellar populations with different Helium content. The maximum helium variation correlates with the cluster mass. The incidence and the complexity of multiple populations both increase with cluster mass.

The maximum helium variation correlates with the HB extension. Helium is a second parameter of the HB morphology (figure 12.7).

Summary- The color distance from the RGB and the reddest part of the HB, L1, is governed by metallicity and age. The color extension of the HB, L2, depends on mass. But massive GCs have exhibit large Helium variations. Hence L2 depends on the helium.

Global & non global Parameters of the HB - Age and metallicity are the main global parameters, while the range of helium abundance within a GC is the main nonglobal parameter defining the HB

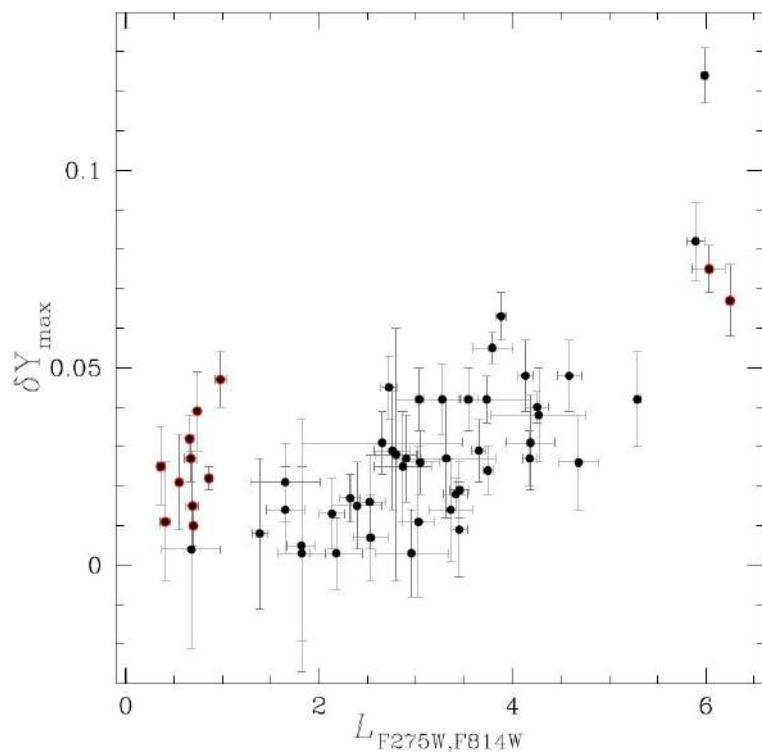


Figure 12.7: Helium content as function of L2.

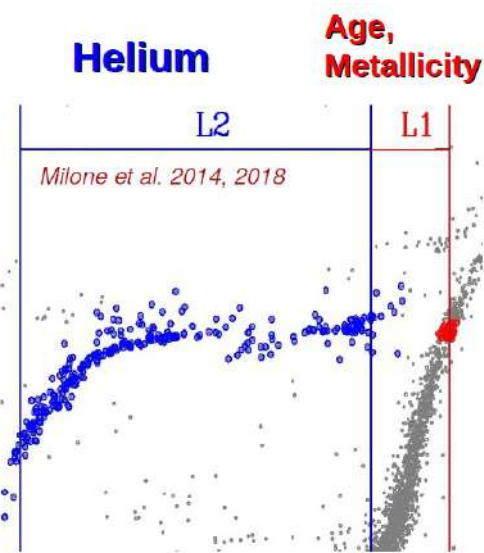


Figure 12.8: CMD that shows L1 and L2 parameters.

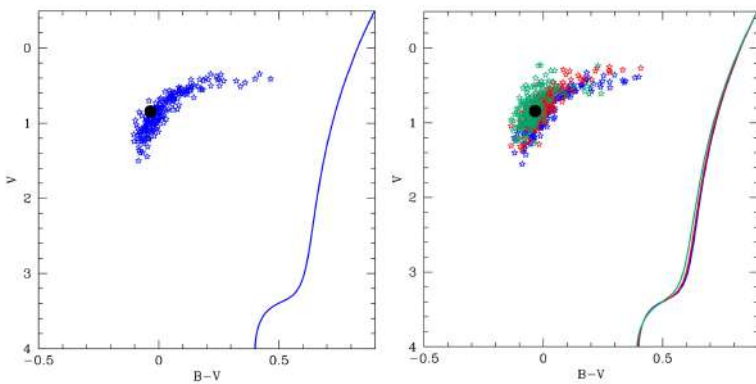


Figure 12.9: CMD with a focus on HB zone. In blue a model that simulated some HB stars.

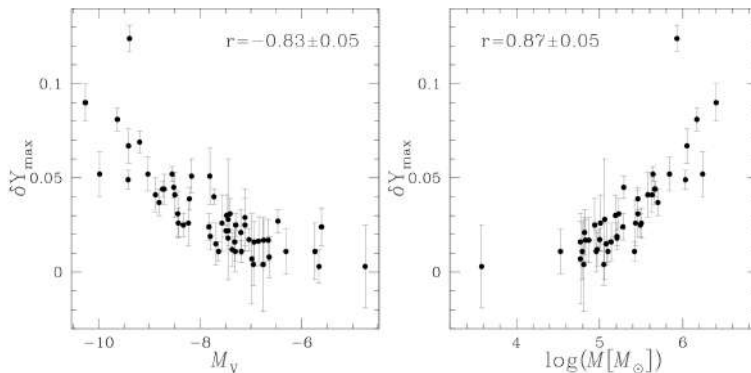


Figure 12.10: Relation between Helium content and absolute magnitude and Mass.

morphology of GCs (figure 12.8).

12.2 The mass loss contribution

We have said that HB star is burning He in the core, it is burning also H in a shell. In pre-HB stars occur many mass loss events. Hence, when the HB phase starts, these stars have lost some mass. The four main parameters which regulate the envelope and the star position are age, metallicity (here as [Fe/H]), helium content (Y) and mass loss. Age and Metallicity can be evaluated from independent sources. Helium and mass loss can not.

Once we know the age and metallicity, the position of a star on the HB depends on helium (Y) and the total mass loss in pre-HB stages

In figure 12.9 a CMD with a model for some HB stars. On right there are shown multiple combination of helium (Y) and mass loss that produce the same HB stars. We need a way to break this parameter degeneracy! Two population with different chemical abundance could be identify via the chromosome map. With the populations identified we can measure the colour difference between them. Combining this with synthetic spectra and stellar evolution models we can find a link with helium, that we can see in figure 12.10. The helium correlates with the mass and the absolute magnitude (a proxy of a stellar mass).

12.2.1 M4 Case

M4 is an ideal target to test the new approach. M4 have two populations well identified in all evolutionary phases. we have strong indication on the nature of the HB stars. In the case of M4 $\delta Y \sim 0.013$. We can now start simulating the HB with a new constraint (The mass loss that changes the Mass and the absolute magnitude). Let us analyse the figure 12.11. We know from spectroscopy that all the first generation stars populate the red HB (first panel). If we add the second generation

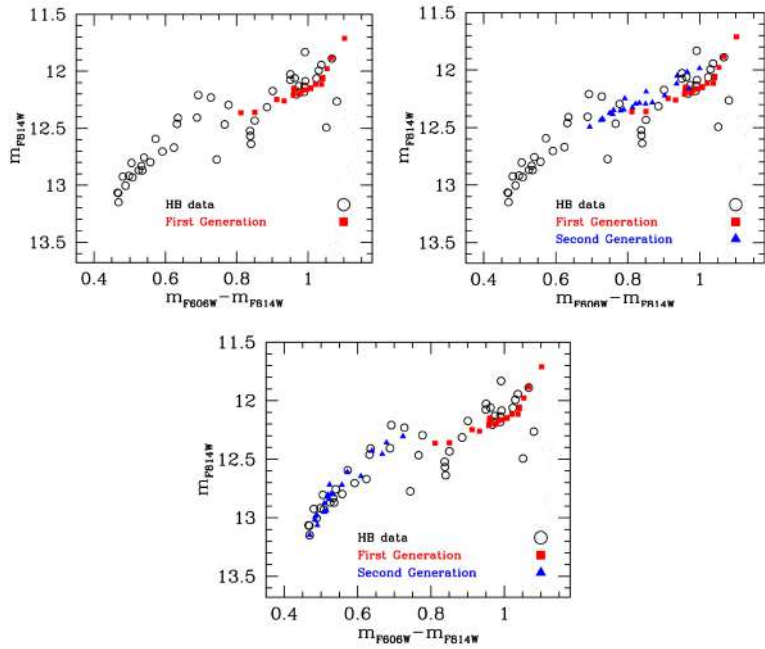


Figure 12.11: CMD of M4 with different simulation models.

stars without changing their mass loss we get a poor fit (second panel). On the contrary, if we change the value of mass loss between the two populations we get a good fit (third panel). The need to increase mass loss (by about 15%) tells us that the situation is more complicated. Now we need to extend this approach to the other clusters. We need to locate (to fit well) the 1st (1G) and the most extreme part of the 2nd generation (2Ge, corresponding to Y_{\max}) of the branch. For most GCs these correspond to the reddest and the bluest (and faintest) group of stars on the HB. Since other parameters are set independently, we need to estimate their total RGB mass loss (μ), and the mass loss difference ($\Delta\mu e$), if any. We apply this to more than 50 GCs. In almost all GCs the extreme part of the 2G needs to lose more mass.

We have two independent parameters: the total RGB mass loss of the 1G (μ_{1G}), and the mass loss difference with the 2Ge ($\Delta\mu e$). We built maps to study these correlations from a wider perspective.

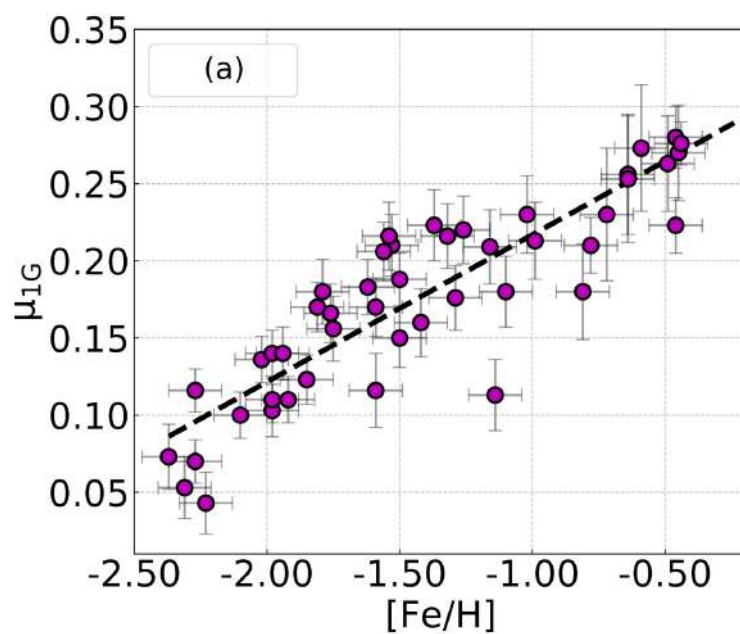
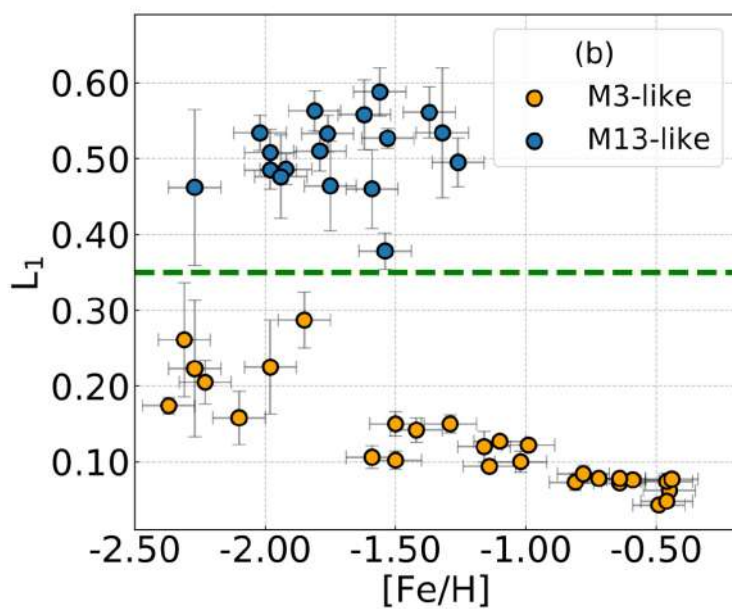
Most important correlation of the 1G

A strong correlation with metallicity (here as $[Fe/H]$) is present in our results. This one is so strong that the other are reflections of it. In figure 12.12 there is the plot of this relation. The best fit line is described by the following: $\mu = 0.095 [Fe/H] + 0.313$. Look at the middle part of the plot: the scatter of these points is larger than their average error. Why the scatter is larger than the errors? To answer this question we need to recall the diagram in figure 12.3 that is shown in a best way in figure 12.13. There are two well defined groups in the L1 vs $[Fe/H]$ plane.

In figure 12.14 we can see the same plot L1 vs. $[Fe/H]$ and the μ_{1G} vs. $[Fe/H]$. With the same color are shown the same population stars. Then, the scatter is so large due the overlap of two population. The groups have different slopes, indeed, large scatter.

Most important correlation of the 2Ge

The strongest correlation in the $\Delta\mu e$ map is with the mass of the host GC. In spite of helium enrichment a mass loss enrichment is still needed. In figure 12.15 we can see that the two groups behave similarly. The best fit line is: $\log(\Delta\mu e) = 0.823 \log(M_i) - 6.268$.

Figure 12.12: Relation between μ_{1G} and $[\text{Fe}/\text{H}]$.Figure 12.13: Relation between L_1 and $[\text{Fe}/\text{H}]$.

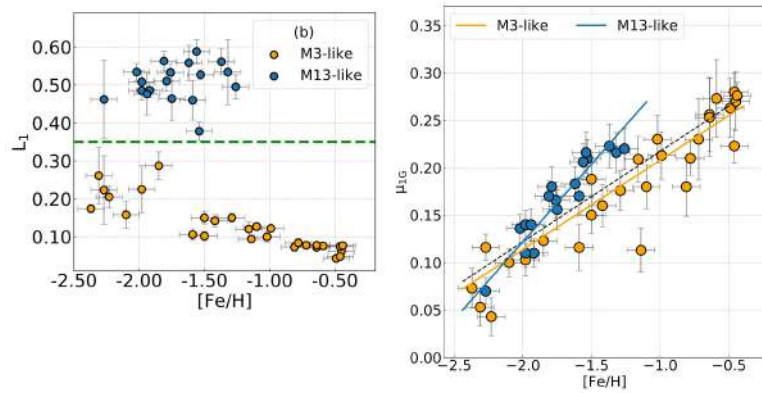


Figure 12.14: Relation between L_1 and $[Fe/H]$ on left and μ_{1G} against $[Fe/H]$ on right.

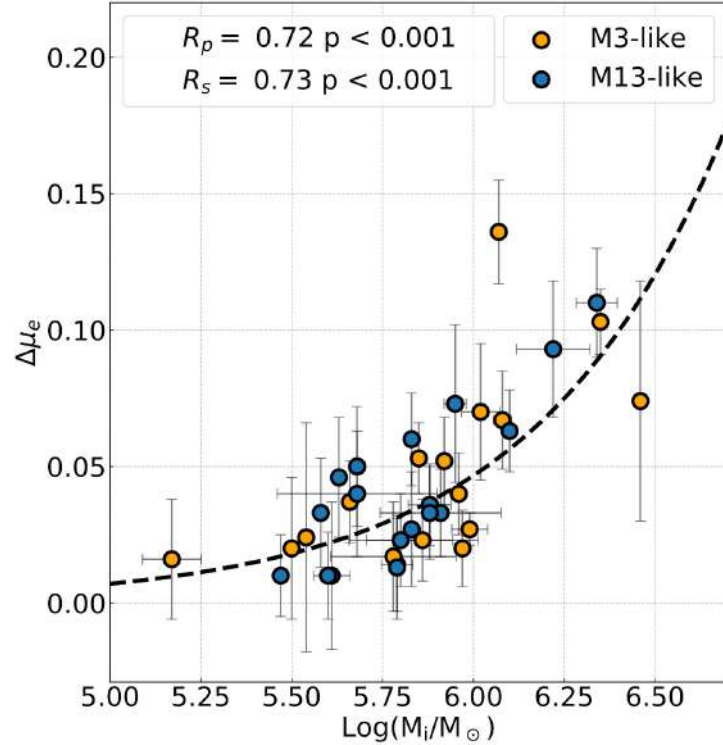


Figure 12.15: Relation between $\Delta\mu_e$ and mass.

Conclusion

- The integrated mass loss of the 1G stars in GCs increases with metallicity.
- A new mass loss law can be defined from the data $\mu = 0.095[Fe/H] + 0.313$
- A group of clusters, classically identified as the second parameter ones, needs larger than average mass loss.
- Additional mass loss is always necessary to describe the 2Ge. A strong correlation is present between cluster mass and additional mass loss.
-

Most of these points are open questions and are known only from the data! No formal theory or unified scenario exists yet!

Chapter 13

Dwarf Galaxies

13.1 What is a dwarf galaxy?

To obtain a clear definition of dwarf galaxy, look at diagram in figure 13.1.

In this graphic there is absolute magnitude M_v on x-axis as proxy of total mass of stellar system while on y-axis there is the logarithm of $r_{1/2}$ which is half-mass radius (the radius that include half mass of the stellar system). In the diagram it is clear that galaxies, dwarfs galaxies or Globular Clusters populate distinct regions.

In particular systems more simple like GCs populate a region of relatively low absolute magnitude and low value of half-mass ratio. Here the luminosity is lower, as the mass and the shape is smaller. These compact objects are not distributed along sequences but they are spread out in a small area.

On the contrary Ultra Faint Dwarfs are distributed along a sequences over GCs region and they are characterized by low luminosity but higher value of half-mass radius, compared with objects of same luminosity.

Then, at higher value of luminosity (smaller value of absolute magnitude) are located Spheroidal Dwarfs Galaxies.

From a historically point of view, structural properties are used to distinguish dwarf galaxies from the other stellar systems. However, still today, there is not a clear distinction between Dwarfs Galaxies and GCs. The presence of dark-matter halo is considered another distinctive feature.

So what is the classification of Dwarfs Galaxies? How they born and evolved? What are their morphological transformations?

13.1.1 Dwarf Spheroidals (dSphs)

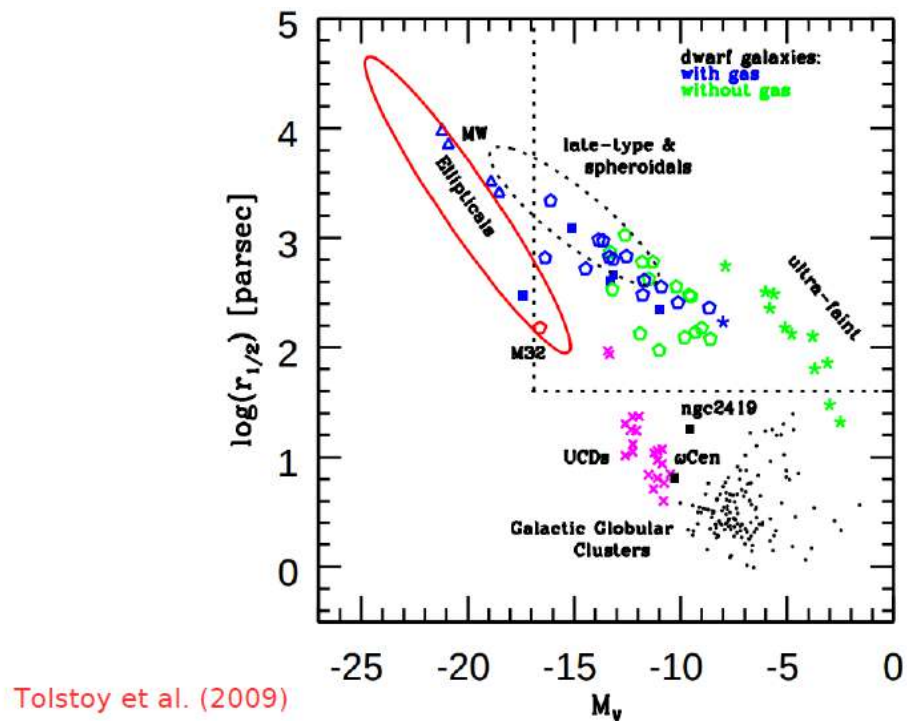
Dwarf Spheroidals are low-luminosity galaxies of the local group. They are devoid of gas and with little to no star formation. While similar to dwarf elliptical galaxies, dSphs are spheroidal in shape, they have lower luminosity. dSphs usually orbit large galaxies (like the Milky Way).

13.1.2 Dwarf Irregulars (dIrrs)

Another class is Dwarfs Irregulars. They are usually gas rich so they are characterized by presence of bluer stars, from resent star formation. They present also other internal structures with redder stars.

13.2 Morphological transformations

Were Dwarfs Galaxies born as we see them now days? Or did they evolve during time? Let us look at menu phenomena that occur in a galaxy.

Figure 13.1: Diagram with $\log(r_{1/2})$ against M_v .

13.2.1 Ram pressure

Ram pressure is a pressure exerted on a body moving through a fluid medium, caused by relative bulk motion of the fluid rather than random thermal motion. It causes a drag force to be exerted on the body.

Within astronomy and astrophysics, galaxies in a galaxy cluster moving through a hot intracluster medium would experience a pressure. In particular, the space between galaxies in a cluster is filled with superheated gas and plasma, which drags and pulls at galaxies as they move through it.

Ram pressure stripping is thought to have profound effects on the evolution of galaxies. As galaxies fall toward the center of a cluster, more and more of their gas is stripped out, including the cool, denser gas that is the source of continued star formation. Spiral galaxies that have fallen at least to the core of both the Virgo and Coma clusters have had their gas (neutral hydrogen) depleted in this way and simulations suggest that this process can happen relatively quickly, with 100% depletion occurring in 100 million years to a more gradual few billion years.

For example, the pressure from the Coma cluster's hot constituent plasma has stripped gas from spiral galaxy D100 and torn it away from the galaxy's main body, and drawing it out into the red plume.

13.2.2 Photo-evaporation

The photo-evaporation phenomenon involves the UV emission by a quasar or other sources. The strong UV radiation from cosmic reionization may suddenly remove the gas from the galaxies. Hence, cosmic reionization may be responsible for the quenching of the star formation.

13.2.3 Stellar evolution

Supernovae and stellar winds can inject kinetic energy in the surrounding gas. If the gas acquires a velocity high enough to overpass the galaxy potential well, it can escape the galaxy.

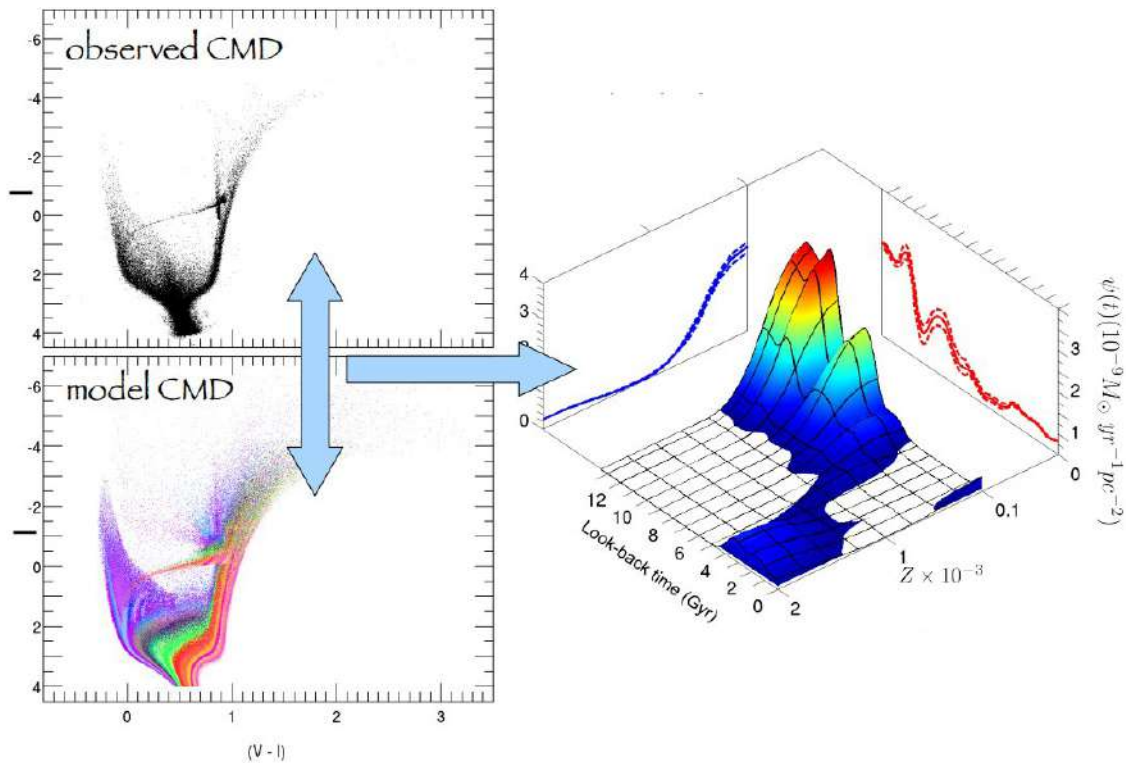


Figure 13.2: On right CMD with best fit by using a lot of isochrones, on left the 3D plot that relates look-back time, Z and $\psi(t)$

13.2.4 Harrassment

Harrassment indicates the tidal interaction exerted by a major galaxy on an orbiting dwarf. It can result in a tidal stirring of the dwarf which, in extreme cases, can also lead to tidal stripping and removal of the gas.

13.2.5 Star formation history

Let's give a look at upper panel on left side of figure 13.2: this is the CMD of a Dwarfs Galaxy. From qualitative point of view, we infer presence of one old stellar population, a bimodal HB with red side well populated. Maybe there is a spread in age and metallicity. There is also a crowded region of blue objects but not all of them are Blue Stragglers: this is a signature of young stellar population or multiple stellar population very young (also about 1 Gyr).

However to confirm, or not, what we see by eyes and constrain better star formation history are necessary more accurate photometric measurements. Indeed deep photometry of MS stars is needed to derive accurate star-formation history (SFH).

A problem in the derivation of the SFH is the completeness of the data. If we take a astronomical image and we count all faint stars we certainly lose some stars, due their faint magnitude. For this reason, from observational point of view, to a CMD astronomers assign a value called **completeness** which indicate the instrumental capability to detect stars. Of course, fainter is the star, smaller is the completeness. For example value around 0.75 means that 25% of stars are lost. For this reason during astrophysical analyses, astronomers use stars for value of completeness quite high.

Of course isochrones provide a first indication of the star-formation history and the metallicity of the stellar populations. Then an approach could be the comparison between an observed CMD and a simulated one. In particular, the observed CMD is compared with a large number of simulated CMDs of simple stellar populations.

Once obtained the best fit, astronomers derive a 3D plot as that we can see in figure 13.2. The com-

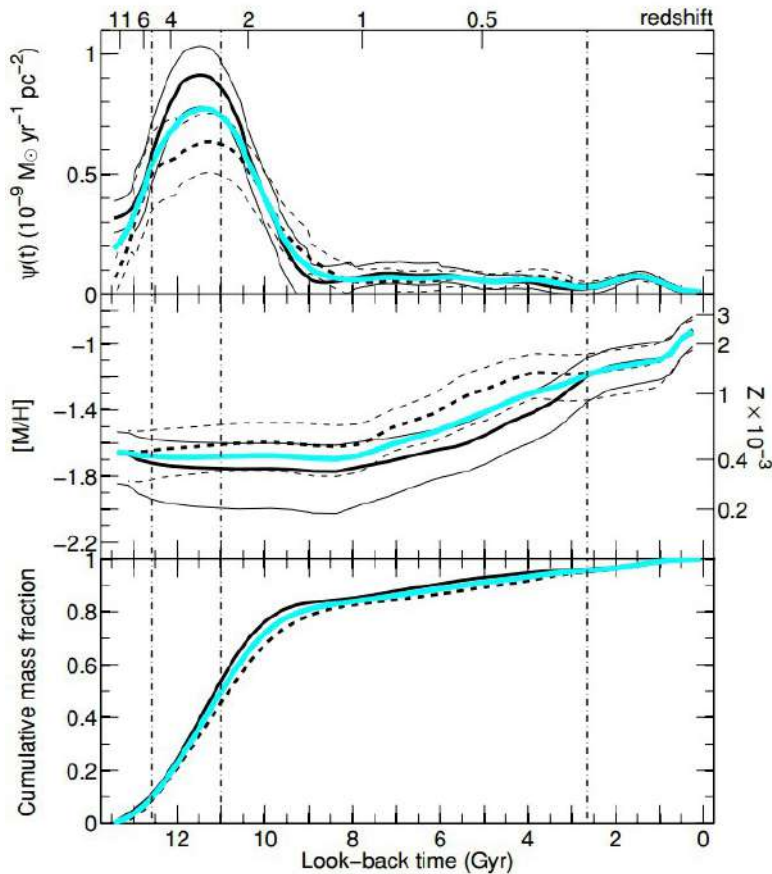


Figure 13.3: Plot of the $\psi(t)$, metallicity and cumulative mass fraction as function of look back time.

bination of stellar populations that better reproduces the observed CMD provides the star-formation history and the chemical evolution with time. Indeed, once the better fit has been found, for data simulated all stellar properties are known.

However only appropriate regions of the CMD are used to compare the observations with the simulated CMDs. From the simple stellar populations that compose the best-fit CMD it is possible to infer star-formation and metallicity at different redshift, as we can see in figure 13.2 on right, where $\psi(t)$ is the star formation as function of the redshift and look-back time.

In figure 13.3 we can see the result of this approach with LGS-3. This galaxy formed $> 80\%$ of stars before 8 Gyr ago. Hence it is similar to dSphs. There is also a residual star formation after 9 Gyr and some stars younger than 1 Gyr.

An important point that we can study by using the SFR is the rule of the cosmic re-ionization and the SNe feedback. To do this the best target are isolated galaxies in the local group.

Let us analyse the CMD of CETUS, TUCANA, LGS-3, PHOENIX, IC1613, LEO-A shown in figure 13.4.

The 3D plots are shown in figure 13.5.

By eyes it is clear the presence of three main groups. Dwarfs Spheroidal Galaxies, transitions ones and Dwarfs Irregular Galaxies.

DSphs have a peck of star formation at higher look-back time. They are characterized by low metallicity and old stellar populations. There is just a tiny fraction of young stars or Blue Stragglers (here not distinguishable). On the contrary transitions galaxies have still some ongoing star formation while irregular galaxies have a strong star formation along the time, also in recent epoch.

Now, let us compare the result of the $\psi(t)$ and of the metallicity as function of look back time to infer

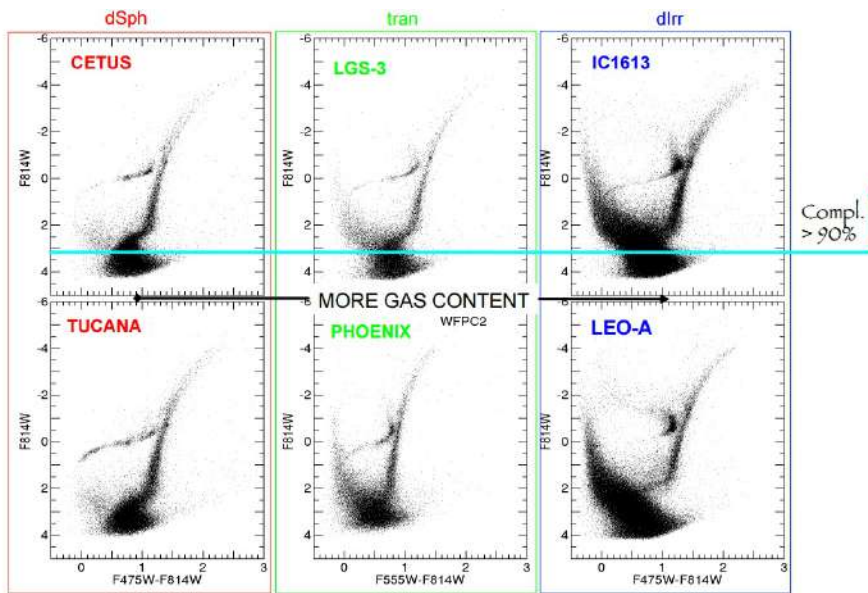


Figure 13.4: CMDs of isolated galaxies in the local group.

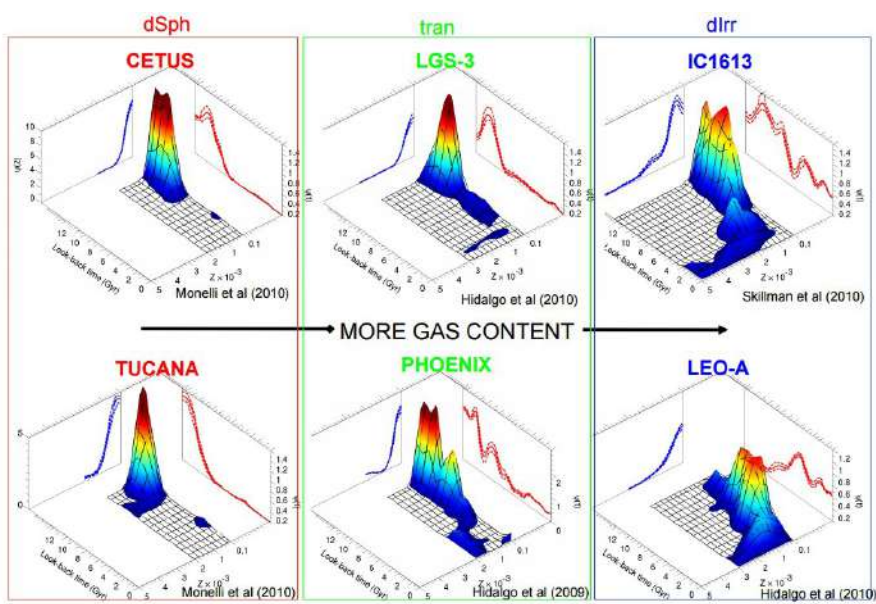


Figure 13.5: 3D plots of isolated galaxies.

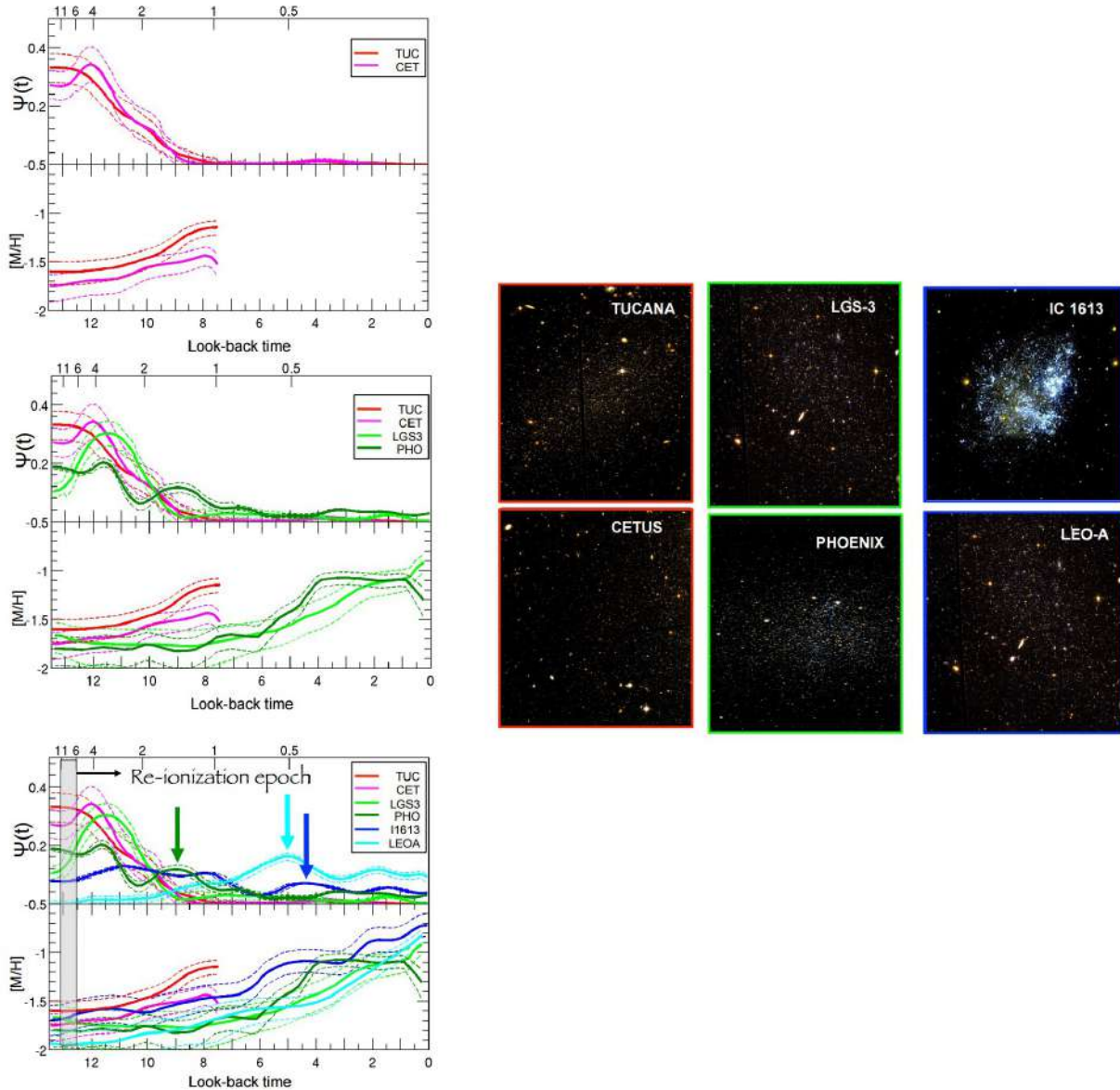


Figure 13.6: Plot of the $\psi(t)$, metallicity and cumulative mass fraction as function of look back time.

more accurate information.

In figure 13.6 is shown the result from these galaxies.

- Cetus-Tucana:
 - they have no gas and very low surface brightness;
 - both formed $> 90\%$ of its stars before 10 Gyr ago;
 - there are 0 stars younger than 8 Gyr;
 - age-metallicity relation has the same behavior. Of course it is not possible to determine age-metallicity relation after 8 Gyr because there are no stars with younger ages;
 - also from optical images, it is clear the absence of gas regions.
- LGS3-Phoenix:
 - SFR remarkably similar to dSph: both formed $> 80\%$ of stars before 9 Gyr ago;
 - there is a residual star formation after around 9 Gyr ago and some stars younger than 1 Gyr (consistent with current low-not null-gas fraction);

- age-metallicity relation has the same behavior (but different than dSph).
- IC1613-LeoA:
 - IC1613 and LeoA contain gas and HII regions;
 - there is an important star formation at intermediate and young ages: both formed $> 60\%$ of their stars after 9 Gyr ago;
 - there is an important star formation in the last 1 Gyr.

In the last panel of the figure 13.6 we can see the result of the comparison.

Re-ionization seems to have not stopped star formation in any of these galaxies. Phoenix, LeoA and IC1613 had a medium-to-high star formation rate clearly when the universe was fully re-ionized.

13.3 Ultra-compact dwarf

Ultra-compact dwarfs (UCDs) are a quite new class of stellar systems discovered in the core regions of nearby galaxy cluster. UCDs are characterised by old stellar populations, are larger, brighter and more massive than the biggest Milky Way GCs, but at the same time significantly more compact than typical dwarf galaxies of comparable luminosity.

The hypothesis of formation are:

1. UCDs are merged stellar super-clusters. Indeed some simulations based on models predict formation of compact objects after merging of super star clusters. In this case, the point is to search for the progenitor. Maybe one progenitor has been found in 2004. It is W3, a supermassive young cluster in NGC7252 with mass around $10^7 M_\odot$, age of $\sim 300 - 500$ Myr and $M_v = -16.2$;
2. UCDs are remnant nuclei of tidally stripped dwarf galaxies, similar to what we expect for GCs;
3. UCDs are the most massive GCs of their host galaxies;
4. UCDs are genuine compact dwarf galaxies formed in the smallest peaks of primordial dark matter fluctuations.

Chapter 14

Dark matter and stellar streams

Dark matter is an important component of our galaxy, indeed visible mass (composed by stars, gas clouds or dust) is about $7 \times 10^{10} M_{\odot}$ while the total mass, counting also dark matter, is $1.5 \times 10^{12} M_{\odot}$. In particular around 90% of the MW is not visible. So it is fundamental to study structure, properties and distributions of dark matter.

In the universe gravitational lensing can be used to detect presence of dark matter at different scales but we need other processes or experiments to infer more information about this type of matter.

In particular the key point is: what is the dark matter?

What we know for sure is that DM interact with ordinary matter via gravity interaction, but we do not know if there are others interactions and what kind of particles form dark matter and their properties. To answer to many questions, in the last few decades many experiments have been created.

The first one is LUX (large underground xenon). It is a DM detector with main goal to understand if and eventually how dark matter interact with ordinary matter. It is located underground in order to minimize contamination but until today we do not have any result.

Does DM interact with itself? To investigate this we use Fermi gamma-ray Space Telescope but today we have no results.

Can DM be produced in laboratory? Physics manage it with an accelerator like LHC in Cern but with no results.

Now, assuming that dark matter is composed by particles, according to size of them, we can simulate different structures.

In the case of some simulations, for particles of small dimensions, we expect a central over-density surrounded by big dark matter halo. On the other side for another simulation, based on different particle size and according to the CDM, there are $\sim 10^4$ subhalos in the Milky Way with masses bigger than $10^7 M_{\odot}$.

14.1 The Hunting

How can we investigate the distribution and the properties of the DM? The key is the tides!

For example the moon causes a deformation of the Earth surface, in particular a gravitational pull of the moon creates tides.

We can talk about tides by using the ratio between the tidal acceleration (Δa) and the Earth's acceleration (a).

In figure 14.1 we can see some calculations of the tidal effect due to the Moon. Knowing that Earth mass $M = 81 \times m$ and the distance $d = 60 \times R$, we calculate a deformation very small, about

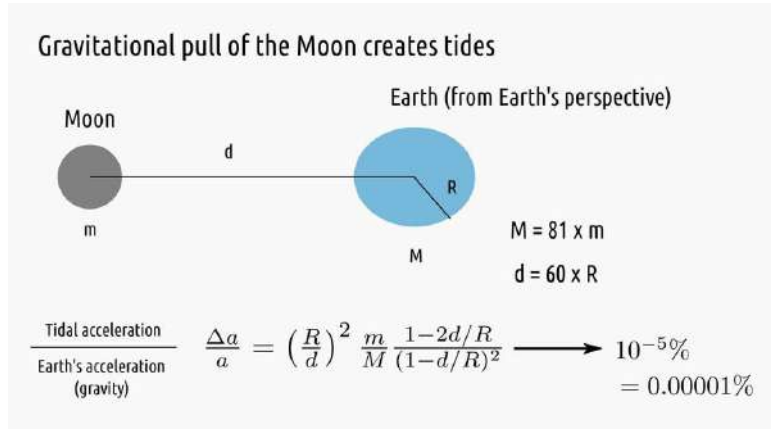


Figure 14.1: Derivation of the gravitational pulling of the Moon. Here R is the radius of Earth, d is the distance between Earth and Moon, m is Moon mass and M is Earth mass.

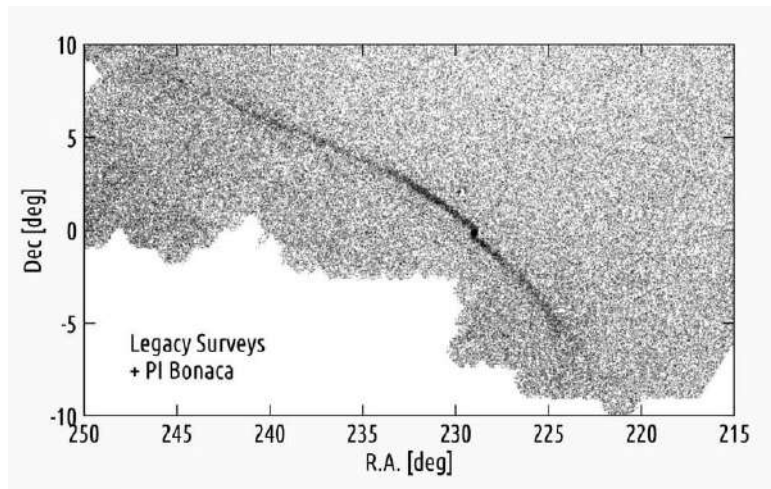


Figure 14.2: Stream of stars of Palomar 5.

$$10^{-5\%} = 0.00001\%.$$

However gravitational pull of the Milky Way creates tides, too! In particular considering a cluster like the Moon and the Galaxy like the Earth, we can make same calculation. If m is cluster mass, M is Galaxy mass, R cluster radius and d distance between Galactic center and the cluster, then we can infer how much is the tidal force. Assuming that for a star cluster close to the Sun $R/d = 5 \times 10^{-4}$ and $m/M = 2 \times 10^8$, for Hyades cluster $\frac{\Delta a}{a} \sim 0.01$ while for Pleiades cluster $\frac{\Delta a}{a} \sim 0.05$.

As consequence of this tidal interaction with the Milky Way, a cluster orbiting the Galaxy makes peculiar orbits and it transforms over a short period (around 800 million years) from a compact object to elongated stream, losing an important fraction of stars during interaction.

In Palomar 5 we could see a tidal stream of stars, as shown in figure 14.2. It is an elongated structure, very extended over the sky indeed this image has very large field of view. There are still residuals visible in the diagram but it is clear the presence of this tidal stream of stars. In general these streams are very important to detect indeed they give information about dark matter content and its distribution around the Galaxy. Indeed a stellar streams preserve a record of all gravitational interactions, also with dark matter.

However not all streams are equal. According to galaxy type and based on simulations, they have a different structure. In the case of a smooth galaxy, stellar stream is a sequence very narrow and well defined while in the case of a clumpy galaxy with dark matter halos stellar streams are elongated along a sequence with more complex structure. In this latter case there are over-densities of stars,

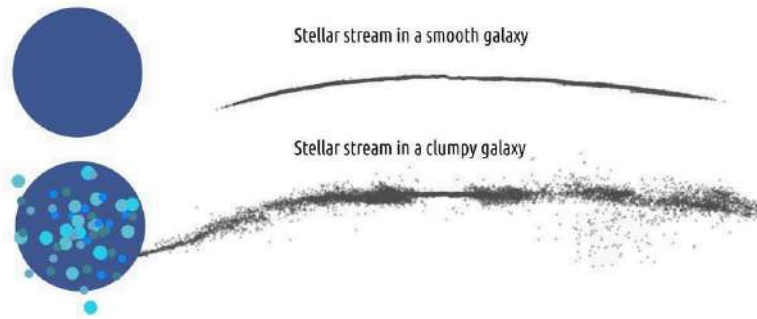


Figure 14.3: Stream of stars of a smooth galaxy and a clumpy galaxy.

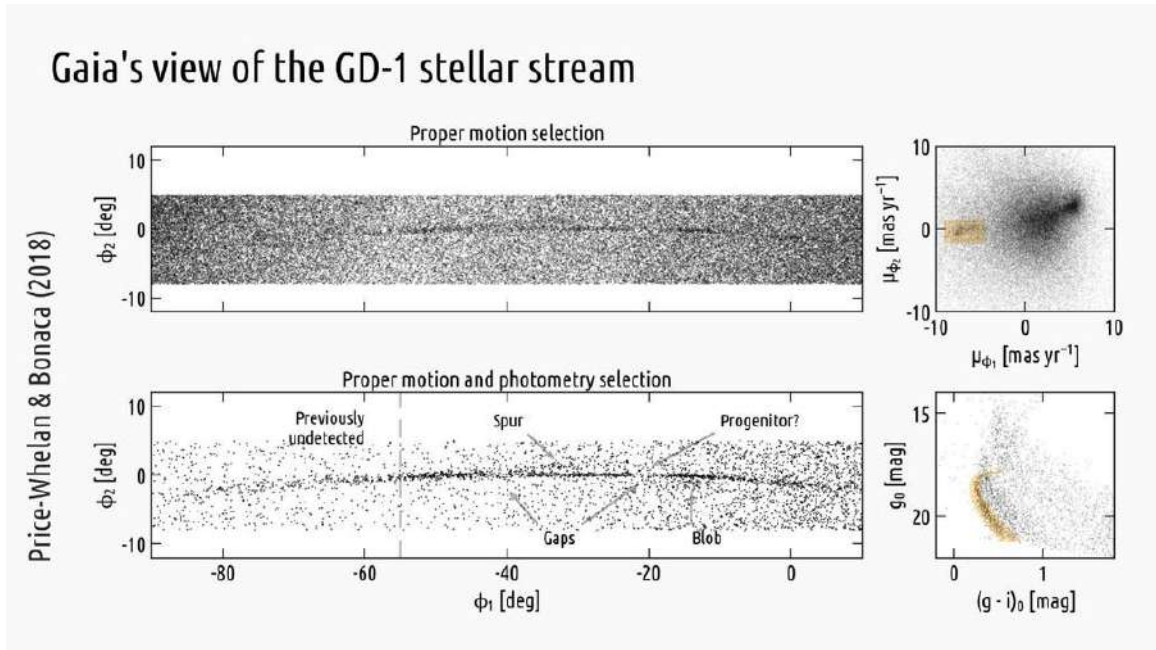


Figure 14.4: Detection of stream's stars.

gaps and points spread out distributed along the sequence given by interaction with MW. What we have to do is compare simulations with observational measurements.

Thank to a wide cameras we can obtain a complete sky map, where we can see these streams. One of the most important stream is GD-1 in the northern sky.

By using proper motion of GAIA and color from CMD astronomers are able to detect the stream stars. Indeed we assume that GCs have old population so analysing the color we can distinguish them from younger stellar populations on the field of view.

In figure 14.4 there is shown the process of selection and detection of stream's stars. As shown in upper diagram, first we plot distribution of stars where it is not possible to detect peculiar structure. So then we plot only stars in over-dense regions: here is clear the presence of some structure like streams. In particular, removing residuals, it is visible a complex structure like one of clumpy galaxies (see figure 14.5): GD-1 stream is very similar to a simulated one for a cluster that interact with another object.

14.2 Candidates

There are some candidates for the perturber of GD-1 like MW's satellites, GCs or dwarf galaxy, dark matter clumps or black holes.

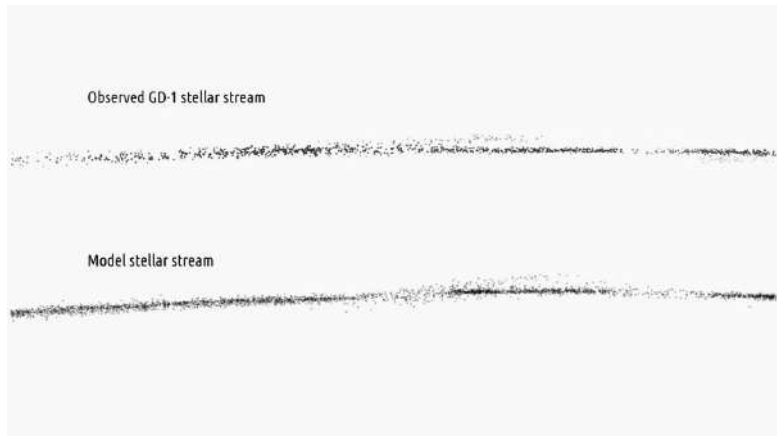


Figure 14.5: GD-1 stream compared with a model, which have interacted with an other object.

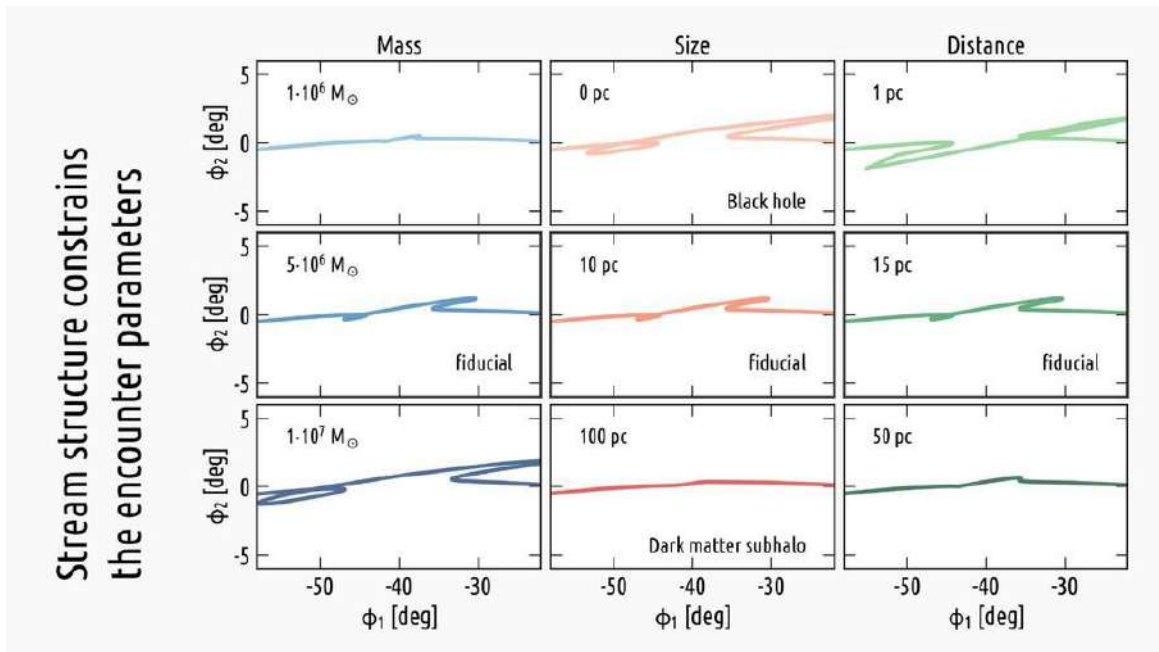


Figure 14.6: Simulation for different values of mass, size and distance.

We have to investigate among these three possibilities. To do this we must derive the properties of the perturber such as mass, size and closest distance.

In figure 14.6 we can see the simulations of different values of mass, size and distances. These quantities are used as constrains for knowing the perturber of GD-1.

Another approach is reconstruct all the orbits of all MW's satellites and of GD-1 stream and investigate if in the past there was an interaction.

In figure 14.7 there are shown the relative distances as functions of the look back time. Thanks to this approach we could exclude all visible candidates.

Excluding this type of perturbers, dark matter subhalo is a plausible one for GD-1.

In figure 14.8 we can see a plot with the possible area of mass-size couple for the GD-1 perturber and for a DM subhalos. Two areas overlap in a small region.

In the future new modern telescopes, mainly in space, will reach fainter magnitude like 27 so they will provide new deeper photometric data in order to detect more stellar streams in the sky. Having more data we will be able to test simulations and scenarios.

The GD-1 perturber is not a known satellite of the Milky Way

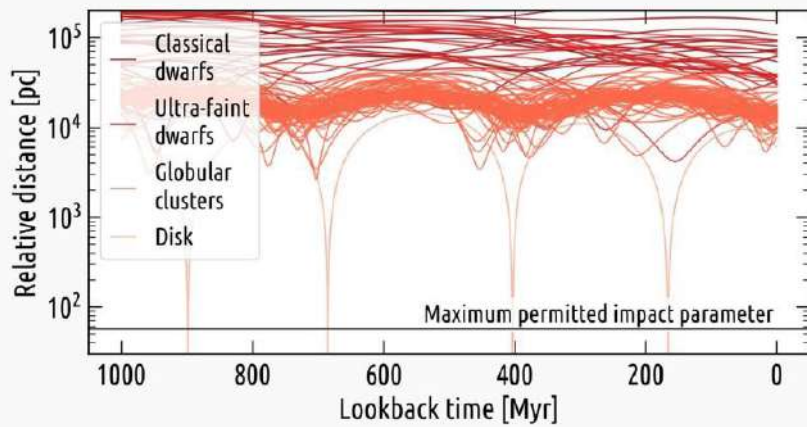


Figure 14.7: Comparison between the GD-1 and MW's satellites orbits.

Dark matter subhalo is a plausible perturber of GD-1

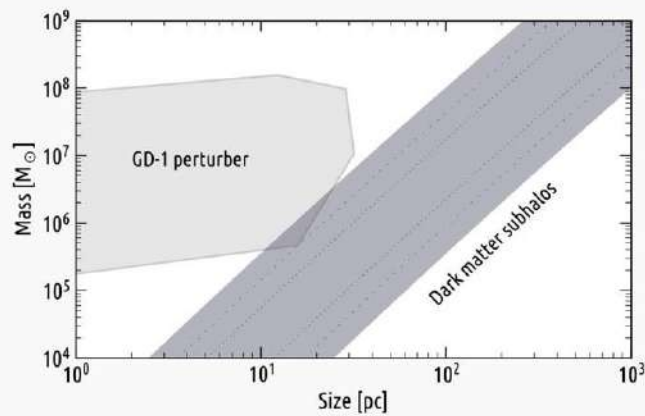


Figure 14.8: A plot of Mass-size of the GD-1 perturber and of DM subhalos.

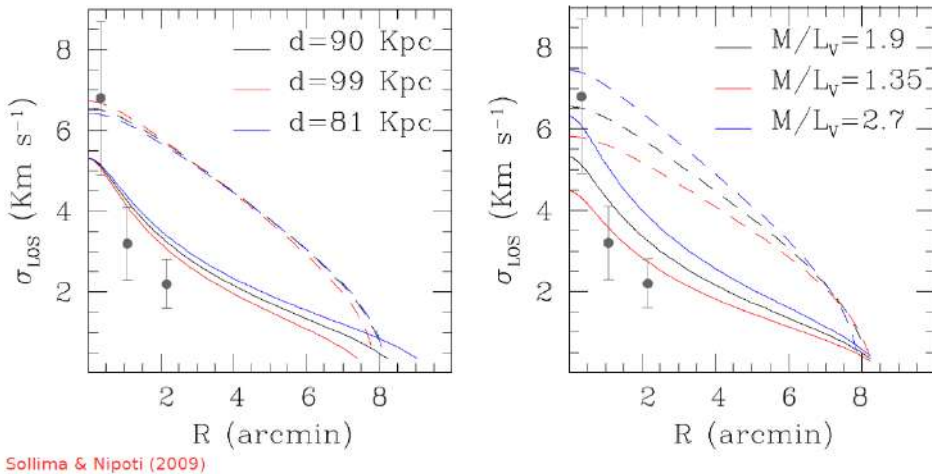


Figure 14.9: Diagram reproducing simulations for different distances and different values of M/L_v ratio.

14.3 Modified Newtonian Dynamics (MOND)

Something connected with dark matter is the velocity distribution of stars in external regions of galaxies. Using spectra we are able to infer the velocity profile of a structure like a galaxy. In particular using 21 cm line of H we detect velocity distribution from the central part up to the external regions. From classical physics we expect a peak of velocity from a certain distance from the center and then a decreasing trend going in the external region. However what we measure is an increasing velocity with higher value in the external part of the galaxy. But the visible mass in galaxies and galaxy clusters is not sufficient to account for their dynamics, when analysed using Newton's laws. This means that we have to search for another explanations.

To solve this discrepancy, Milgrom (1983) suggested that the gravitational force experienced by a star in the outer regions of a galaxy came to vary inversely with radius (as opposed to the inverse square of the radius, as in Newton's law of gravity). In MOND (Modified Newtonian Dynamics), violation of Newton's laws occurs at extremely small accelerations. In this case Milgrom suggested a theory without dark matter content.

We could use GC to investigate this phenomenon because GCs are object without dark matter, so, if dark matter is not real we have to see the same result of galaxy in far away GCs.

NGC2419 is a massive globular cluster in the outer halo of the Milky Way ($d \sim 87\text{ kpc}$). It is one of the GCs with the largest predicted velocity dispersion profile by Newtonian and MOND models. Moreover it is quite distant so stars are poorly affected by gravitational field of our Galaxy so in principle we are able to discriminate between gravitational effect from MOND and Newton's law.

By comparison of predictions and what we observe of NGC2419, the kinematics of GC might be hard to explain in MOND, as visible in figure 14.9.

Chapter 15

Summary of Marco Tailo conference

In this small chapter we will treat issues discussed by Marco Tailo during its conference done for this course. Here there is a short summary.

The outline of the conference is:

- explore the problem of the parameter degeneracy on the Horizontal Branch;
- try to explain how we can break it;
- finally discuss some implications.

15.1 The position of a star on the HB

The Horizontal Branch is the locus of the helium burning stars. They are the product of the Helium flash at the Red Giant Branch tip. After this flash they loss luminosity and reach their position in HB.

These stars have always played a central role in the study of Globular Clusters.

In particular the Horizontal Branch morphology changes with the iron content ($[Fe/H]$) of the host cluster. As seen in figure 15.1, for metal poor clusters we have mainly blue stars, for metal rich only red stars while for intermediate cases are present both blue and red stars.

However not all clusters follow this HB morphology with metallicity. For example clusters M13 and M3 have similar metallicity and age but they present a very different Horizontal Branch, as visible in figure 15.2. This is the **second parameter problem**: this means that metallicity is not the unique parameter that changes HB morphology. In spite of decades of study this is still one of the trickiest problems to solve.

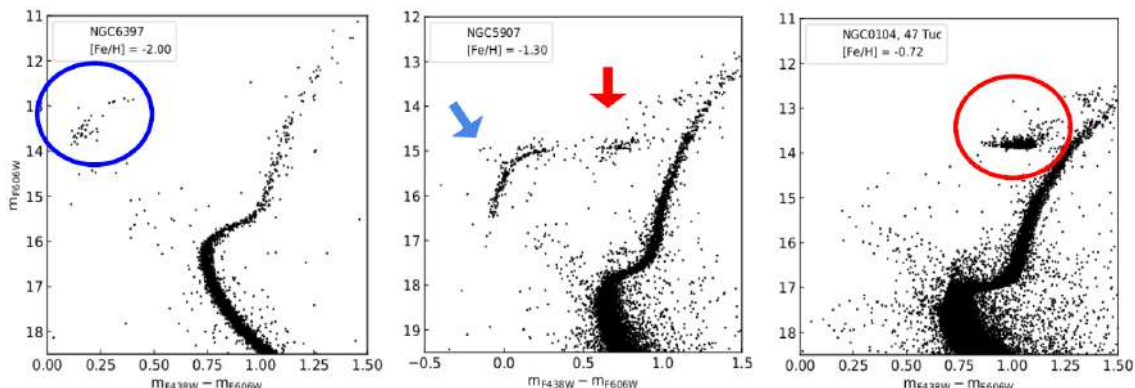


Figure 15.1: Metal poor cluster on left, metal rich on right and intermediate in the center.

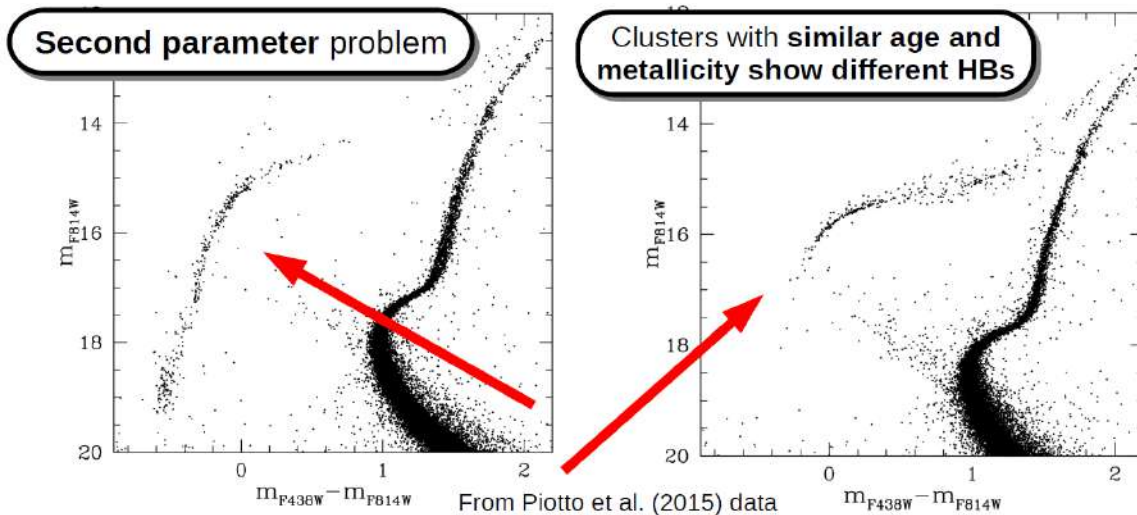


Figure 15.2: CMD of clusters M13 on left and M3 on right.

To understand this problem and to try to resolve it, it is necessary to talk about the astrophysical structure of HB stars. They are stars with active *He* core (they burn *He* into *C* with triple-alpha process) and with an envelope where *H* is burnt in *He* thought CNO cycle.

In particular the core does not change so the evolution is regulated only by envelope. So the less massive is the HB star, the less extended is the envelope, the bluer it is.

In general four main parameters regulate the envelope and the star position: age, metallicity (here as $[Fe/H]$), helium content (Y) and mass loss. What is the problem is that there is no unique combinations of them: there are HB stars with solar Helium content and high mass loss or stars very rich in *He* but with low mass loss. So the challenge is to break this parameter degeneracy.

Age (from asteroseismology or other methods seen during the course) and metallicity (from spectroscopy) can be evaluated from independent sources. On the contrary Helium and mass loss can not. In particular Helium is very difficult to determine from spectra.

Once we know the age and metallicity, the position of a star on the HB depends on Helium and the total mass loss in pre-HB stages. In particular multiple combination of helium and mass loss produce the same HB stars, as shown in figure 15.3. We need a way to break this parameter degeneracy!

15.2 Breaking the degeneracy

To break this degeneracy we can identify the populations via the chromosome map! Inside this type of diagrams there is the clear distinction between first and second generation stars. Then, with the populations identified, we can measure the colour difference between them.

Combining this with synthetic spectra and stellar evolution models we can find a link with Helium content. This is an indirect method to quantify Helium content. Relations between Helium content and absolute magnitude and the logarithm of the mass is shown in figure 15.4.

The next step is to apply what we found to study simple stellar population, like M4 for which we have spectroscopic measurements on HB stars and for which we infer presence of two populations well identified in all evolutionary phases. In this case we have strong indication on the nature of the HB stars. In the case of M4 $\delta Y \sim 0.013$.

We can now start simulating the HB with a new constraint! We know from spectroscopy that all the first generation stars populate the red HB. If we add the second generation stars without changing their mass loss we get a poor fit. On the contrary, if we change the value of mass loss between the two populations we get a good fit, as shown in figure 15.5. The need to increase mass loss (by about

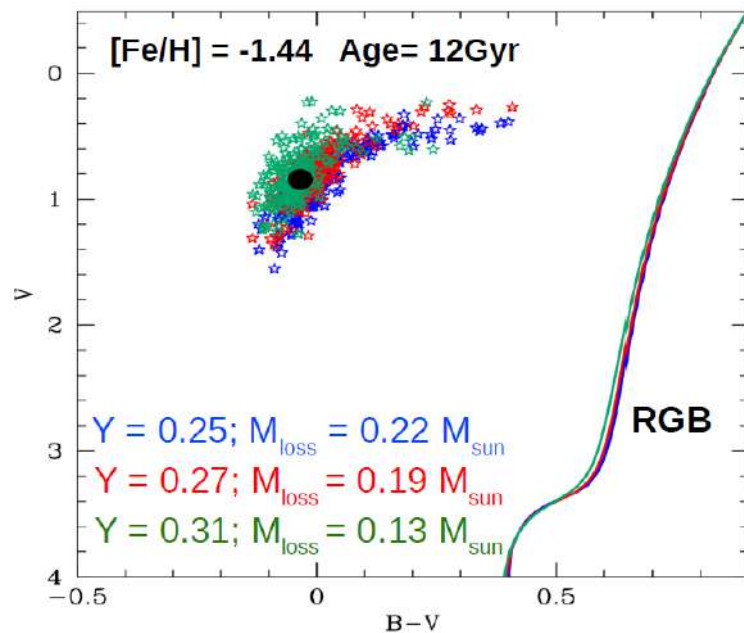


Figure 15.3: HB of stars with different combinations of mass loss and Helium content: they are the same!

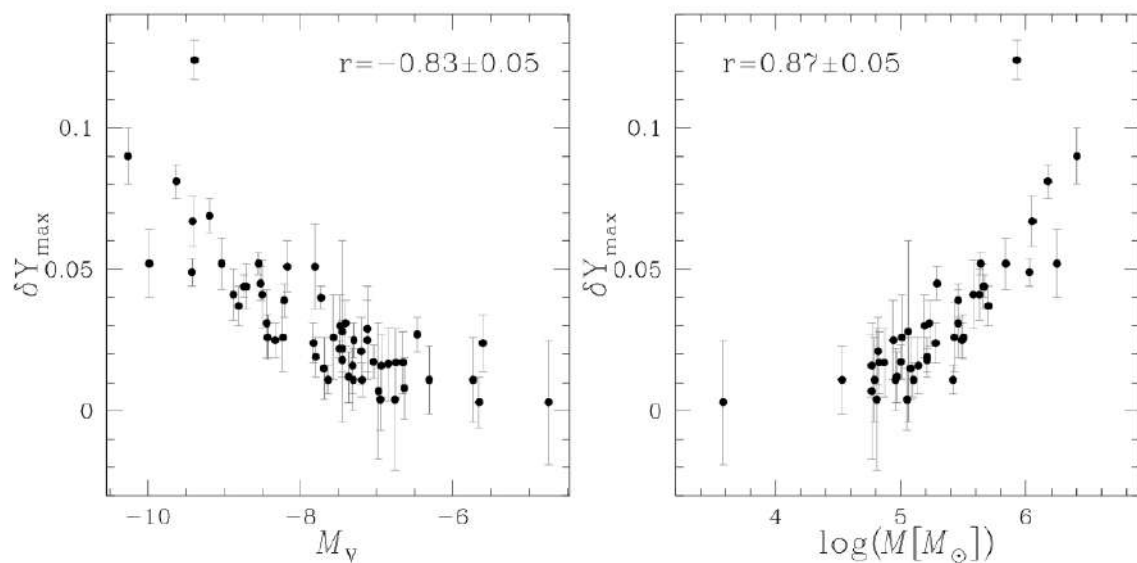


Figure 15.4: Relations between Helium content and absolute magnitude and the logarithm of the mass.

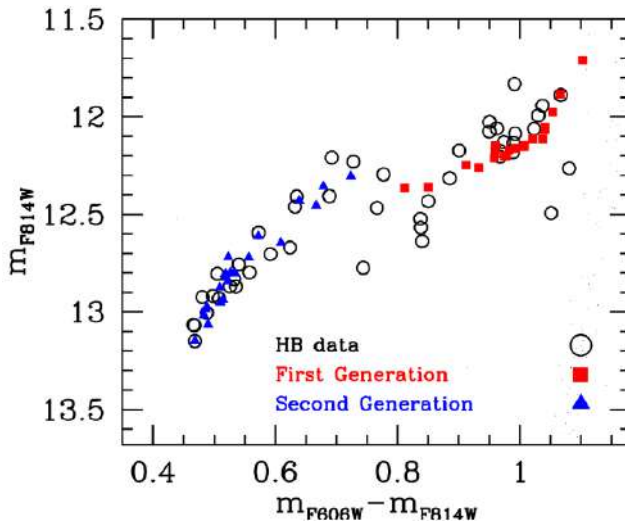
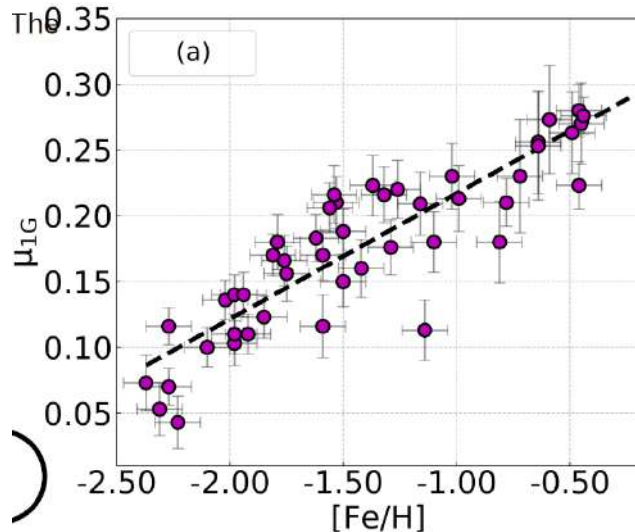


Figure 15.5: Good fit obtained changing the value of mass loss.

Figure 15.6: Diagram with metallicity against μ_{1G} . It is clear that there is a strong relation between them.

15%) tells us that the situation is more complicated.

After this case, it is necessary to extend what we found to other clusters. We need to locate the 1st (1G) and the most extreme part of the 2nd generation (2Ge, corresponding to Y_{max}) of the branch. For most GCs these correspond to the reddest and the bluest (and faintest) group of stars on the HB. Since other parameters are set independently, we need to estimate their total RGB mass loss (μ), and the mass loss difference ($\Delta\mu_e$), if any.

We apply this to more than 50 GCs. In almost all GCs the extreme part of the 2G needs to lose more mass

15.3 Searching for correlations

We have two independent parameters: the total RGB mass loss of the 1G (μ_{1G}), and the mass loss difference with the 2Ge ($\Delta\mu_e$). So we built maps to study these correlations from a wider perspective.

In particular A strong correlation with metallicity (here as $[Fe/H]$) is present in our results. See figure 15.6: it is a straight line.

This one is so strong that the other are reflections of it. In particular the best fit line is described by $\mu = 0.095 [Fe/H] + 0.313$ and the scatter of these points is larger than their average error. Why the

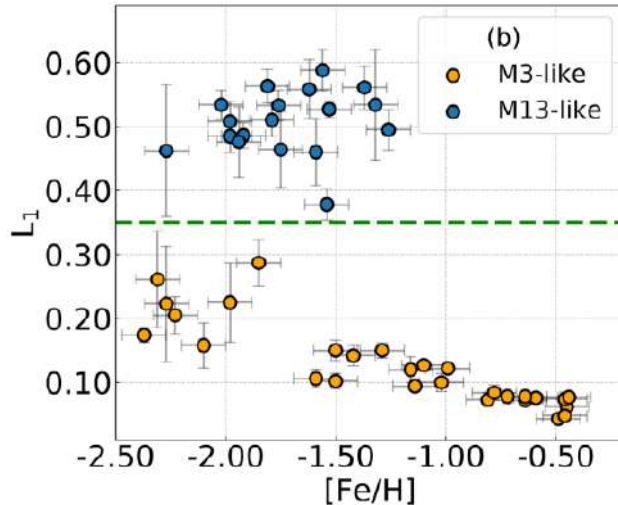
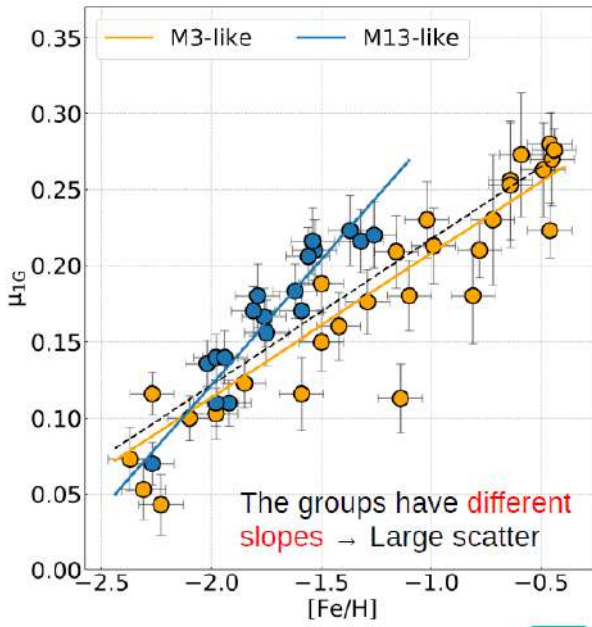
Figure 15.7: Diagram L_1 vs $[Fe/H]$ plane for clusters like M3 and M13.

Figure 15.8: Two groups, as shown here, have different slopes.

scatter is larger than the errors?

15.3.1 Most important correlation of the 1G

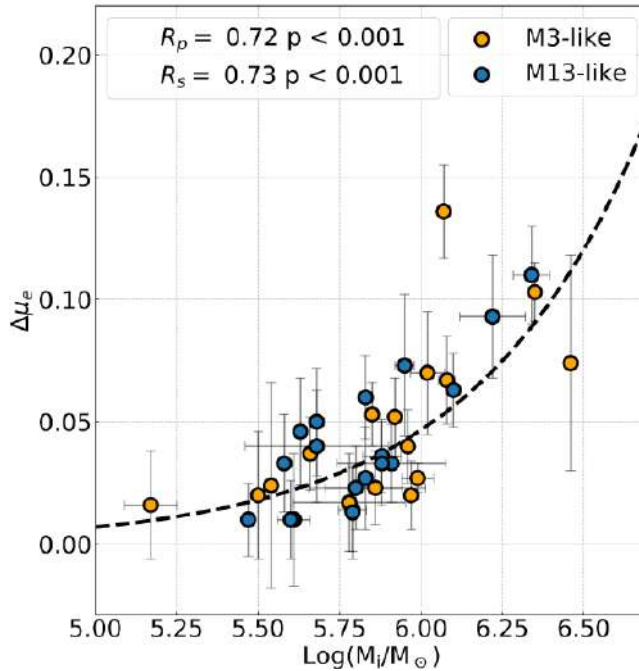
To understand why scatter is larger than the errors, it is important to understand the correlation of the 1G. As shown in figure 15.7, there are two well-defined groups in the L_1^1 vs $[Fe/H]$ plane for clusters like M3 and M13.

In particular, from diagram μ_{1G} against metallicity, the two groups have different slopes. For this reason we measure a large scatter. This is clear from figure 15.8.

15.3.2 Most important correlation of the 2Ge

As shown in figure 15.9, the strongest correlation in the $\Delta\mu_e$ map is with the mass of the host GC. In spite of helium enrichment a mass loss enrichment is still needed. In this case the two groups behave

¹ L_1 is distance between the RGB and the red side of the HB.

Figure 15.9: $\Delta\mu_e$ vs $\log M_i/M_\odot$ diagram.

similarly and the best fit line is $\log(\Delta\mu_e) = 0.823 \times \log(M_i) - 6.268$.

15.4 Conclusions

Conclusions can be summarized in the following points.

- The integrated mass loss of the 1G stars in GCs increases with metallicity.
- A new mass loss law can be defined from the data $\mu = 0.095 [Fe/H] + 0.313$.
- A group of clusters, classically identified as the second parameter ones, needs larger than average mass loss.
- Additional mass loss is always necessary to describe the 2Ge.
- A strong correlation is present between cluster mass and additional mass loss.

Most of these points are open questions and are known only from the data! No formal theory or unified scenario exists yet!

Chapter 16

Exam simulations

In this small chapter are presented two simulations of exam which means two description of CMDs.

16.0.1 Simulation 1

Look ate figure 16.1. Describe this CMD and its visible features.

On left panel is visible a very well defined CMD in optical band. It is visible a well populated sub giant branch and RGB, signatures of an old stellar population. The reason for this is associated to astrophysical explanation: in the case of young population stars evolve very fast so in CMD we found a smaller number of stars in sub giant branch while in case of old population these sequences are more rich in stars.

It is also clear that it is a metal poor cluster, due to the slope of RGB with small angle of inclination and due to the presence of a well defined horizontal branch. On the contrary, in case of metal rich clusters, the angle of inclination of RGB is bigger and above all they are characterized by red HB. Of course there are also other parameters responsible for HB morphology but metallicity is the most important.

In general Red HB and Red Clumps are indicative of young and metal rich population while metal poor clusters have blue Horizontal Branch.

Let's now return to the object. Observing in multi-band photometry (right panel) the diagram splits into different sequences, at least 2 or maybe 3. This occurs due to the presence of different stellar population. According to filter used in this case, like $F336W$, this diagram is sensitive to chemical

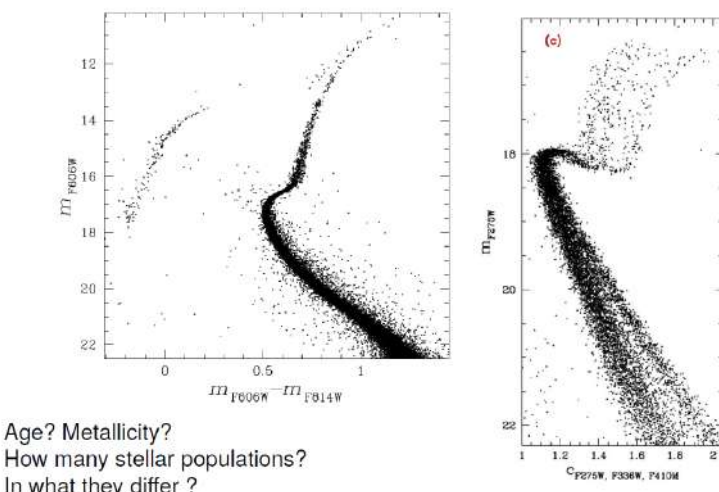


Figure 16.1: CMD number 1.

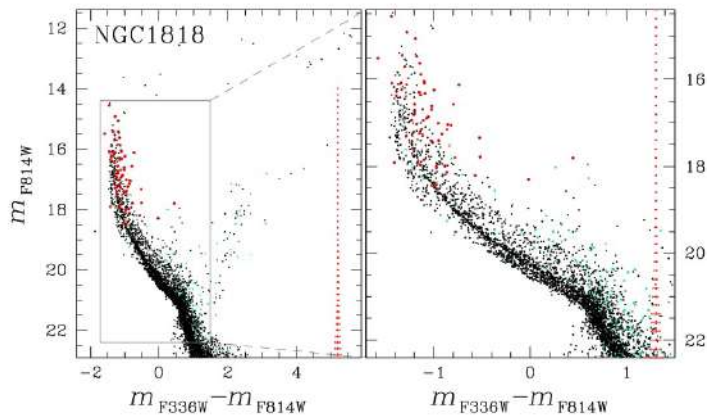


Figure 16.2: CMD number 2.

composition, in particular on Nitrogen. Second population stars are Nitrogen rich so they have deep molecules bands in the corresponding filter. For this reason they appears fainter and redder than population 1. For same reason it is also sensitive to Oxygen.

16.0.2 Simulation 2

Look ate figure 16.2. Describe this CMD and its visible features.

Look at panel on right. First of all it is quite clear the presence of big fraction of binaries stars. There is also a spread out of the point in the bottom part pf the sequence at lower magnitudes due to higher observational errors (as indicated by red point in column on the right of the graphic).

It is a young population indeed there are few stars in RGB. There is also an extended Turn-Off point, possibly associated to stellar population of different age and rotation rate. Moreover inside the diagram are recognizable two sequences associated to two rotation rate (in red part, on right sequence, there are fast rotators and in blue part, on left sequence, there are slow rotators). Then the two sequences merge together at a point corresponding to $1.5 M_{\odot}$: here stars change their structure from convective to radiative.

An important fraction of binaries is visible.

On left panel are visible also some field stars at right of CMD.

16.0.3 Simulation 3

Look ate figure 16.3. Describe this CMD and its visible features.

Look at left figure 16.3: they are CMD of two classical dwarfs galaxies, satellites of Milky Way. Try to infer properties of these objects is fundamental in order to understand what is their contribution to the re-ionization of the Universe.

On left panel there CMD of Tucana. Here Horizontal Branch seems to be more extended to the blue part of the diagram. It also contains a higher fraction of binaries. It is an old stellar population without visible traces of multiple stellar population.

On the other side, in CMD of Cetus, it is evidence the Red Clump. Moreover, due to the slope of RGB it seems to be metal poor however the presence of Red Horizontal Branch (usually associated to metal rich stars) maybe indicate that Cetus is metal rich. More information about metallicity are available with more detailed studies. Then, as visible in the upper part of the diagram, it is quite clear the presence of two multiple stellar populations even if it is poorly populated here.

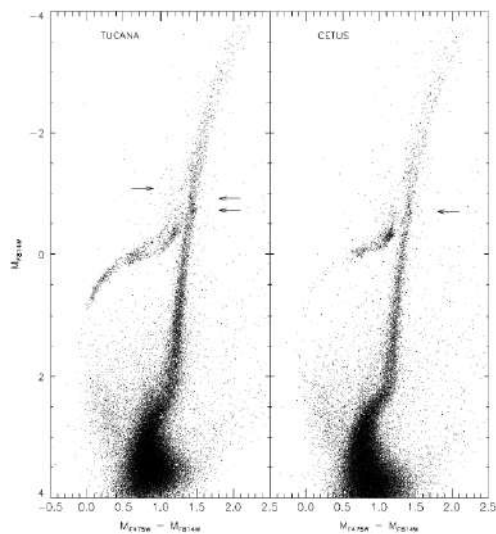


Figure 16.3: CMD number 3.

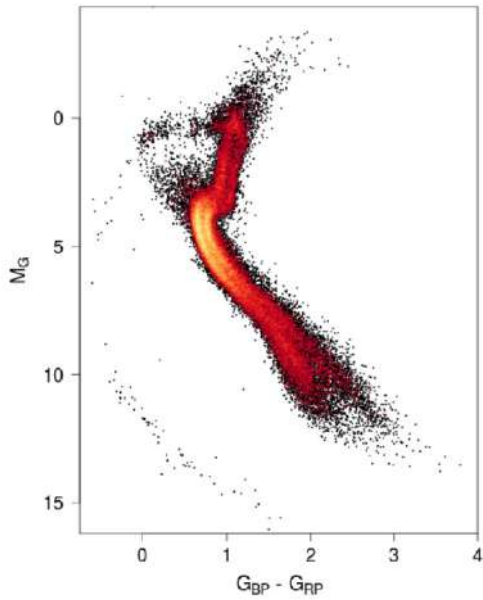


Figure 16.4: CMD number 4.

16.0.4 Simulation 4

Look ate figure 16.4. Describe this CMD and its visible features.

Look at left figure 16.4: this CMD is a very complex one, obtained with high resolution photometry of Gaia Telescope.

In this graphic it is clear the presence of two different populations with different age but same metallicity.